Aus dem Institut für Immunologie des Biomedizinischen Centrums

der Ludwig-Maximilians-Universität München

Vorstand: Prof. Dr. Thomas Brocker

Investigating T cell receptor-dependent post-transcriptional gene regulation by Roquin to characterize lymphocyte fate decisions

Dissertation

zum Erwerb des Doktorgrades der Naturwissenschaften (Dr. rer. nat.)

an der Medizinischen Fakultät der

Ludwig-Maximilians-Universität München

vorgelegt von

Henrik Schmidt

aus Berlin, Deutschland

2021

Mit Genehmigung der Medizinischen Fakultät der
Ludwig-Maximilians-Universität München

Betreuer: Herr Prof. Dr. Vigo Heissmeyer

Zweitgutachterin: Frau Prof. Dr. Alla Skapenko

Dekan: Herr Prof. Dr. Thomas Gudermann

Tag der mündlichen Prüfung: 20.12.2021

I. Eidesstattliche Versicherung

Hiermit versichere ich, Herr Henrik Schmidt, geboren am 23. Juni 1992 in Berlin, an Eides statt, dass ich die vorliegende Dissertation mit dem Titel

„Investigating T cell receptor-dependent post-transcriptional gene regulation by Roquin to characterize lymphocyte fate decisions"

selbstständig verfasst, mich außer der angegebenen keiner weiteren Hilfsmittel bedient und alle Erkenntnisse, die aus dem Schrifttum ganz oder annähernd übernommen sind, als solche kenntlich gemacht und nach ihrer Herkunft unter Bezeichnung der Fundstelle einzeln nachgewiesen habe.

Ich erkläre des Weiteren, dass die hier vorgelegte Dissertation nicht in gleicher oder in ähnlicher Form bei einer anderen Stelle zur Erlangung eines akademischen Grades eingereicht wurde.

Henrik Schmidt

Wien, den 23. Dezember 2021

II. Zusammenfassung

Das adaptive Immunsystem ermöglicht mehrzelligen Organismen feinregulierte, Erreger-spezifische Immunantworten zur Bekämpfung von Infektionen. Eine dynamische zelluläre Anpassung an Pathogene kann durch posttranskriptionelle Genregulation als molekularer Schalter der Aktivierung zellulärer Immunantworten erreicht werden. Die RNA-bindenden Proteine (RBPs) Roquin-1 (*Rc3h1*) und Roquin-2 (*Rc3h2*) sind maßgeblich an der Regulation der T-Zellaktivierung beteiligt und steuern die Differenzierung von Tfh- sowie Th17-Zellen. Mutationen in *Rc3h1* werden mit autoinflammatorischen Erkrankungen und Autoimmunität in Verbindung gebracht und der Funktionsverlust von *Rc3h1* ist mit einer exzessiven Immunaktivierung sowie der Derepression von *Icos*, *Tnfrsf4* (*Ox40*), *Tnf* und *Nfkbid* mRNA-Molekülen verbunden. Hierbei erkennt die essentielle N-terminale ROQ-Domäne hochaffine konstitutive Abbauelemente (engl. *constitutive decay elements*, CDE), die ursprünglich in dem 3'-UTR (engl. *3'-untranslated region*) der *Tnf* mRNA identifiziert wurden und es wird angenommen, dass differenzielle Affinitäten/Aviditäten unterschiedlicher ROQ-CDE-Interaktionen einen präferenziellen Abbau von mRNA koordinieren. In CD4$^+$ T-Zellen spaltet die TCR-induzierbare MALT1-Paracaspase beide Roquin-1 und Roquin-2 Proteine, wobei dadurch die Funktionalität von Roquin beeinträchtigt und T-Zell-Aktivierung sowie die Differenzierung von Effektorfunktionen ausgelöst werden. Extrazelluläre TCR-Signale müssen quantitativ interpretiert werden, doch nur wenig ist darüber bekannt, wie Affinitäten bzw. Aviditäten von Antigen-TCR-Interaktionen sowie die TCR-assoziierte Signaltransduktion in maßgeschneiderte Genexpression umgewandelt werden.

Die vorliegende Dissertation erläutert, wie der posttranskriptionelle Regulator Roquin TCR-Signalstärken integriert, um die Regulation von mRNA-Stabilität und Th17-Differenzierung zu steuern. Transgene Mausmodelle gradueller Deletion der *Rc3h1* und *Rc3h2* Gene, retrovirale Rekonstitutionen unter Verwendung von Roquin-1-Mutanten mit veränderten ROQ-CDE-Affinitäten und Titrationen OVA-Antigen-vermittelter T-Zell-Aktivierung zeigten spezifische dosis-abhängige Kinetiken der Derepression von mRNA-Molekülen, wobei IκB$_{NS}$ (*Nfkbid*) besonders hohe funktionelle Avidität aufwies. Antigen-Signale mit zunehmender Avidität wurden in graduelle Spaltung von Roquin sowie zunehmende Th17-, nicht aber Th1-Differenzierung umgewandelt. Ein mithilfe von CRISPR/Cas9 generiertes MALT1-resistentes Roquin-1-Modell (*Rc3h1*^{Mins}) verdeutlichte die starke Repression von IκB$_{NS}$ während dynamischer T-Zell-Aktivierung, um Th17-Differenzierung zu beeinträchtigen. *Rc3h1*^{Mins} repräsentiert das erste transgene Modell eines MALT1-resistenten Substrats. In diesem Modell wird Roquin-1 trotz MALT1-Aktivierung nicht länger gespalten, es rekapituliert den Phänotypen des Modells inaktivierter MALT1-Paracaspase (*Malt1*$^{PD/PD}$) teilweise und bestätigt die Bedeutung von Roquin für die Tfh- und Th17-Differenzierung. Diese Studie verdeutlicht die notwendige Beteiligung der TCR-abhängigen Spaltung von Roquin-1 und hochaffiner ROQ-CDE-Bindungsstellen an der Prävention der Th17-abhängigen Autoimmun-Enzephalomyelitis (EAE) *in vivo* und die Modulation der NF-κB-Aktivität durch die limitierte Induktion von IκB$_{NS}$. Die Roquin-Spaltung trägt dynamisch zur Interpretation von TCR-Signalen bei und die Verfügbarkeit von Roquin setzt einen quantitativen Schwellenwert

für die *in vitro* und *in vivo* Differenzierung von Th17-Zellen voraus, der durch einen distinkten Signalweg von TCR-MALT1-Roquin-IκB$_{NS}$ reguliert wird. Schließlich unterstützt diese Arbeit die Idee eines Roquin-spezifischen MALT1-Inhibitors. Dieser könnte autoinflammatorische Phänotypen von *Malt1*$^{PD/PD}$-Mäusen oder bereits bekannten MALT1-Inhibitoren umgehen und gleichzeitig die Th17-getriebene Pathogenese bei Autoimmunerkrankungen begrenzen.

III. Summary

Adaptive immunity provides multicellular organisms with fine-tuned pathogen-specific immune responses. Dynamic cellular adaptation to infections can be achieved by post-transcriptional gene regulation as a molecular switch for host defense activation. The RNA-binding proteins (RBPs) Roquin-1 (*Rc3h1*) and Roquin-2 (*Rc3h2*) regulate immune homeostasis by the control of Tfh and Th17 cell differentiation. Mutations in *Rc3h1* are linked to autoimmune or autoinflammatory diseases and its loss-of-function is associated with excessive immune activation next to derepression of its targets *Icos*, *Tnfrsf4 (Ox40)*, *Tnf* and *Nfkbid* mRNA. The unique ROQ domain recognizes high affinity constitutive decay elements (CDE) originally identified in the 3'-UTR of *Tnf* mRNA and differential ROQ-CDE affinities/avidities likely coordinate preferential mRNA degradation. In CD4$^+$ T cells, the TCR-inducible MALT1 paracaspase cleaves Roquin-1/2 proteins to inactivate their function and to mount effector responses during T cell activation. TCR signals require quantitative interpretation, yet only few reports explain how TCR signal transducers and antigen-TCR affinities/avidities are converted into tailored gene expression programs.

This doctoral thesis elucidates how the post-transcriptional regulator Roquin integrates TCR signal strength to guide mRNA and Th17 fate regulation. Transgenic mouse models of graded *Rc3h1* and *Rc3h2* deletion, retroviral reconstitutions using Roquin-1 mutants of altered ROQ-CDE affinities and titrations of OVA antigen-mediated T cell activation revealed distinct dose-response kinetics of target derepression, with IκB$_{NS}$ (*Nfkbid*) having particularly high functional avidity. Antigen signals of increasing avidity were converted into graded cleavage of Roquin and Th17 but not Th1 fates. A CRISPR/Cas9-derived MALT1-insensitive Roquin-1 model (*Rc3h1*^{Mins}) maintained IκB$_{NS}$ repression during T cell activation to impair Th17 differentiation. *Rc3h1*^{Mins} represents the first transgenic knockin model of a MALT1-insensitive substrate that in part phenocopied the MALT1 protease-dead model (*Malt1*$^{PD/PD}$) and proved Roquin function in Tfh and Th17 differentiation. This study emphasizes the crucial involvement of TCR-dependent Roquin-1 cleavage and high affinity binding sites in the prevention of Th17-dependent autoimmune encephalomyelitis (EAE) *in vivo* and the modulation of NF-κB activity by limiting IκB$_{NS}$ expression. Roquin cleavage dynamically contributes to TCR signal interpretation and its expression levels set a quantitative threshold for *in vitro* and *in vivo* Th17 differentiation regulated by the TCR-MALT1-Roquin-IκB$_{NS}$ axis. This work supports the idea of a Roquin-specific MALT1 inhibitor to circumvent autoinflammatory disorders of *Malt1*$^{PD/PD}$ or MALT1 inhibitor-treated mice and to limit Th17 pathogenicity in autoimmune diseases.

IV. Table of Contents

V. Abbreviations

-/-	knockout
α	alpha
β	beta
δ	delta
γ	gamma
κ	kappa
μ	micro
θ	theta
4'OH-tam	4'hydroxy-tamoxifen
A	adenine
A	alanine (Ala)
aa	amino acid
Ab	antibody
ADE	alternative decay element
ANA	anti-nuclear antibody
Amp	ampicillin
APC	allophycocyanin
APC	antigen-presentig cell
APS	ammonium peroxodisulfate
ARE	AU-rich element
Bcl10	B cell lymphoma 10
BCR	B cell receptor
BM	bone marrow
bp	base pair
BSA	bovine serum albumin
BV	brilliant violet
C	cytosine
Carma1	CARD-containing MAGUK protein-1
CARD11	caspase recruitment domain containing protein 11
Cas9	CRISPR-associated endonuclease 9
CBM	Carma1/CARD11-Bcl10-MALT1 complex
CD	cluster of differentiation
CDE	constitutive decay element
CDS	coding sequence
CRISPR	clustered regularly interspaced short palindromic repeat
C-term	carboxy-terminus
CTL	cytotoxic T lymphocyte
DC	dendritic cell

DKO	double knockout
DMEM	Dulbecco's Modified Eagle Medium
DMSO	dimethyl sulfoxide
DN	double negative
DNA	deoxyribonucleic acid
dNTP	deoxyribonucleotide triphosphate
dox	doxycycline
DP	double positive
DTT	dithiothreitol
EC50	half-maximal effective concentration
ECL	enhanced chemiluminescence
E. coli	Escherichia coli
EDTA	ethylenediamine tetra-acetic acid
ELISA	enzyme-linked immunosorbent assay
EMSA	electrophoretic mobility shift assay
Ert2	estrogen receptor type 2
EtOH	ethanol
FACS	fluorescence-assisted cell sorting
FC	flow cytometry
FCS	fetal calf serum
FITC	fluorescein isothiocyanate
FO	follicular
Foxp3	forkhead-box protein P3
FSC	forward scatter
G	guanine
GC	germinal center
GFP	green fluorescent protein
HBS	HEPES-buffered saline
HDR	homology-directed repair
HEK293	human embryonic kidney 293
HEPES	4-(2-hydroxyethyl)-1-piperazineethane sulfonic acid
HRP	horseradish peroxidase
i	induced
I	ionomycin
IFN	interferon
Ig	immunoglobulin
IL	interleukin
IP	immunoprecipitation
IRF	interferon regulatory factor
K	lysine (Lys)
kb	kilo base pair

kDa	kilo Dalton
KO	knockout
LB	Luria-Bertani (lysogeny broth)
LBE	linear binding element
LN	lymph node
M	methionine (Met)
mAb	monoclonal antibody
MCPIP-1	monocyte chemoattractant protein-1-induced protein-1
MEF	mouse embryonic fibroblast
MFI	mean fluorescence intensity
MALT1	mucosa-associated lymphoid tissue lymphoma translocation protein-1
MAGUK	membrane-associated guanylate-like kinases
MHC I/II	Major Histocompatibility Complex I/II
Mins	MALT1-insensitive
mRNA	messenger RNA
MZ	marginal zone
N-term	amino-terminus
NKT	natural killer T cell
NMD	nonsense-mediated decay
nt	nucleotide
p	pobability (value)
PABP	poly(A) binding protein
PAGE	polyacrylamide gel electrophoresis
PAMP	pathogen-associated molecular pattern
PBS	phosphate-buffered saline
PE	phycoerythrin
Pen	penicillin
PI	protease inhibitor
PMA	phorbol myristate acetate
PRR	pattern recognition receptor
PTM	post-translational modification
PVDF	polyvinylidene difluoride
R	arginine (Arg)
RBP	RNA-binding protein
RNA	ribonucleic acid
RT	room temperature
san	*sanroque* (M199R)
SDS	sodium dodecylsulfate
sgRNA	single guide RNA
SL	stem loop
SLE	systemic lupus erythematosus

SP	single positive
SSC	sideward scatter
T	thymine
TBE	tris-borate-EDTA
TBS	tris-buffered saline
TCR	T cell receptor
TEMED	N,N,N',N'-tetramethyl-ethylenediamide
Tfh	follicular T helper cell
Th	T helper cell
TNF	tumor necrosis factor
Treg	regulatory T cell
TRAF	TNF receptor-associated factor
TTP	tristetraproline
Tris	tris(hydroxymethyl)-aminomethane
UTR	untranslated region
UV	ultra violet
WT	wild type
Y	tyrosine (Tyr)

1. Introduction

1.1. The immune system

The immune system prevents multicellular organisms from pathogenic infections and represents the major mediator of host defense. A network of physical barriers including epithelial cells in the skin or mucus layers in the gastrointestinal tract and lymphocytes of the innate and adaptive immune systems account for general health maintenance and pathogen clearance upon encounter. The immune system relies on humoral and cellular immune responses both of which provide host defense strategies to fight bacterial, fungal and viral infections.

1.1.1. Innate immunity

The innate immune response is the early-stage defense mechanism that is rapidly activated upon infection with pathogens which managed to overcome physical barriers. Innate immunity is driven by effector cells that are specialized to recognize foreign antigens and can be classified as macrophages, neutrophils, dendritic cells (DCs), natural killer (NK) cells and NK-like innate lymphoid cells (ILCs). They recognize pathogen-associated molecular patterns (PAMPs) via a diverse repertoire of pattern recognition receptors (PRRs) to direct the clearance and removal of non-self antigens by phagocytosis and opsonization (Akira et al., 2006). Thereby, internalization of antigenic particles triggered by ligand-receptor interactions leads to its uptake into the cell in which early and late endosomes as well as lysosomes are the main intracellular localizations of antigen processing (Dudziak et al., 2007). Besides, the sequential accumulation of PAMP-guided innate effector cells is associated with complement system activation (Dunkelberger and Song, 2010). Cell receptor networks including opsonin molecules such as immunoglobulin (IgG) antibodies or complement proteins recognized by Fcγ receptors (FcγRs) mediate the continuous recruitment of phagocytes to coordinate pathogen lysis via membrane-attack complexes.

1.1.2. Adaptive immunity

1.1.2.1. Central T cell tolerance

Beyond innate immunity, infections with persisting pathogens require the activation of highly specific adaptive immune responses. Adaptive immunity includes humoral and cellular response mechanisms that are based on B and T lymphocytes expressing either unique B cell receptors (BCRs) or T cell receptors (TCRs). Whereas B lymphocytes differentiate into antibody-producing

plasma cells for humoral immune responses, T lymphocytes differentiate into subtypes of effector T cells to mount elaborate CD8+ cytotoxic or CD4+ helper T cell responses (Germain, 2002). Fine-tuned lymphocyte development establishes a functional immune system to act in response to foreign antigens, yet tolerating self-antigens to prevent autoimmunity. Both B and T lymphocytes originate from lymphoid progenitors in the bone marrow. Whereas B cell differentiation includes negative selection of self-reactive BCRs within the bone marrow, T cell precursors migrate to the thymus to undergo positive selection, clonal diversion (agonist selection) or clonal deletion (Moran and Hogquist, 2012). Initial thymic T cell lineage commitment is Notch1 signaling-dependent, involves CD3 complex expression and proceeds towards genetic rearrangements of the TCR. Thymic progenitors are termed double-negative (DN) lacking CD4/CD8 co-receptor expression and TCR β chain gene rearrangements occur in stages DN2-3, while pairing with TCR α chains (pre-TCR) in DN3 is followed by TCR α chain gene rearrangements in stage DN4 thymocytes that begin to express both CD4 and CD8 co-receptors. The creation of conventional αβ or γδ paired TCR chains gives rise to thymocytes from two genetically distinct T cell lineages (Radtke et al., 1999; Kreslavsky et al., 2008; Ciofani and Zúñiga-Pflücker, 2010). The αβ TCR thymocytes acquire CD4 and CD8 co-receptor expression giving rise to double-positive (DP) thymocytes of TCR repertoires with random specificities. DP-intrinsic TCR affinities for self-peptide MHC ligands (peptide:MHC) presented by epithelial cells in the thymic cortex guide the outcome of positive selection according to the quality and strength of the antigen-TCR interaction (Xing et al., 2012). T cells of low to moderate TCR affinities for self-antigens are positively selected. Besides, those that do not react to self-peptide MHC ligands die by neglect. Precursors of too strong TCR and self-antigen interactions are eliminated by clonal deletion in the thymic medulla. This negative selection excludes self-reactive T lymphocytes likely causing autoimmunity. Reinforcing the idea of deterministic TCR affinity in thymic development, increased TCR signal strength and agonist selection (cells responsive to activating ligands) have been shown to guide non-conventional high-affinity αβ TCR thymocytes to commit to regulatory T cell (Treg) or natural killer T cell (NKT) fates (Jordan et al., 2001; Moran et al., 2011). Moreover, the TCR strength model proposes that particularly strong signals rather promote γδ TCR fates, while attenuated TCR signaling diverts thymocytes to promote αβ TCR fates indicating that TCR strength controls thymic αβ versus γδ lineage commitment (Haks et al., 2005; Hayes et al., 2005).

DP αβ TCR thymocytes that survive this developmental process differentiate into CD8+ cytotoxic T lymphocytes (CTLs) when their TCR has recognized self-peptide antigen in the context of MHC class I. In contrast, TCR interactions with self-peptide:MHC class II complexes result in the commitment to CD4+ helper T lymphocytes. Late-stage CD4+ or CD8+ T cell lineage commitment itself has been associated with transcriptional antagonism of Th-POK-mediated CD4+ and Runx-mediated cytotoxic CD8+ T cell fates (He et al., 2005; Egawa and Littman, 2008). After positive selection, mature CD4+ and CD8+ T cells exit the thymus and circulate in the periphery to survey peptide:MHC complexes of antigen presenting cells. In the absence of an immune challenge, self-peptides loaded onto MHC only elicit tonic signaling that does not propagate canonical T cell activation but these minor TCR ligations affect and maintain signaling-responsive gene expression (Bartleson et al., 2020). The mechanisms of naive CD4+ T cell activation by professional antigen

presenting cells (APCs) and the intracellular signaling events driving T cell survival, proliferation and differentiation will be described in the upcoming sections.

1.1.2.2. T cell activation and T cell receptor signaling

The peptide:MHC-TCR ligation represents an antigen-specific response against invading pathogens that is mediated by enhanced antigen processing activity of DCs, the major subset of antigen presenting cells (APCs). Once antigenic cargo is internalized, DCs start to mature and migrate to peripheral lymph nodes where T cells can scan peptide:MHC complexes for their cognate antigen. First described in the 1970's, the two-signal model introduced a mechanism of how naive T lymphocyte stimulation by antigenic peptides (signal-1) induced either full T cell activation and immune responses in the presence or T cell unresponsiveness (anergy) in the absence of the second co-stimulatory signal-2 (Bretscher and Cohn, 1970; Lafferty and Cunningham, 1975). Cognate peptide:MHC confers specificity to T cell receptor activation, yet co-stimulation by an additional CD28 receptor reads out the activation and maturation of DCs according to upregulation of the CD28 ligand B7. Co-stimulation is required to synergize with TCR signaling for productive T cell activation and proliferation (June et al., 1987). The transition of conventional quiescent naive T cells to an activated state is referred to as T cell priming and an increasing number of co-stimulatory receptors of the immunoglobulin (Ig) or tumor necrosis factor receptor (TNFR) superfamilies have been identified to augment and potentiate TCR-CD3 signaling to initiate genuine T cell activation (Chen and Flies, 2013). Importantly, CD28, the major co-stimulatory receptor, has been shown to interact with its CD80 (B7.1) and CD86 (B7.2) ligands expressed by activated APCs to support T cell activation, production of IL-2 and interleukin-2 (IL-2)-dependent proliferation (Fraser et al., 1992). CD28 signals integrate into early signaling events concomitant to antigen-TCR engagement and affect antigenic peptide thresholds needed for T cell-mediated immune activation (Tuosto and Actuo, 1998; Diehn et al., 2002). Antigen recognition by T cells is transduced into the cytoplasm via a cascade of different mechanisms including dynamic transmembrane protein rearrangements, lipid-raft microcluster formations and kinase-mediated post-translational modifications (protein tyrosine kinases, PTKs). Downstream signal transduction eventually regulates gene expression as modulators of transcription and transcription factors itself are activated by combined TCR/CD28-dependent T cell signaling pathways. Intracellular networks of antagonistic factors and signaling cascades ultimately tailor the transcriptional program of stimulated T cells and thus effector differentiation by activation of transcription factors such as AP-1, NFAT and NF-κB (Rincón and Flavell, 1994; Michel et al., 2000; Gosh et al., 1993).

The recognition of antigenic peptides via the TCR and simultaneous co-stimulatory signals orchestrate the formation of an immunological synapse which also recruits T cell CD4 or CD8 co-receptors into the DC-T cell interface (Gunzer et al., 2000; Chen and Flies, 2013). Downstream TCR signaling and co-receptor engagement within the supra-molecular activation cluster (SMAC) activates the tyrosine kinase Lck to phosphorylate immunoreceptor tyrosine-based motifs (ITAMs)

which recruits and activates the SYK family tyrosine kinase ZAP-70 (ζ chain-associated protein kinase of 70 kDa) (Chan et al., 1992; Smith-Garvin et al., 2009). ZAP-70 triggers activation of SLP-76 (SH2 domain containing leukocyte protein of 76 kDa) and the adaptor protein LAT (linker for activation of T cells) that associate with and scaffold the TCR signaling complex (Zhang et al., 1998). Recruitment of the Tec kinase family member ITK (IL-2 inducible T cell kinase) subsequently phosphorylates and activates PLCγ1 which hydrolyzes the phospholipid phosphoinositol-4,5-bisphosphate (PIP2) to both inositol-1,4,5-triphosphate (IP3) and diacylglycerol (DAG) second messengers (Bogin et al., 2007). Proximal to the T cell membrane, DAG activates the protein kinase C θ (PKCθ) whose signaling activity drives transcriptional activation of nuclear factor κB (NF-κB) that will be discussed in section 1.1.2.4 in more detail. Apart from this, DAG also initiates the mitogen-activated protein kinase (MAPK) signaling cascade that depends on the activation of the upstream GTP-exchange factor (GEF) RasGRP (Dower et al., 2000). MAPK signaling eventually orchestrates the formation of the activator protein-1 (AP-1) by c-Fos and c-Jun dimerization that is followed by Jnk-dependent phosphorylation of c-Jun to foster transcriptional activity of AP-1. On the other hand, PLCγ1-dependent IP3 elevates intracellular calcium (Ca^{2+}) concentration by modulating endoplasmatic reticulum (ER) calcium store depletion and CRAC channel permeability to increase extracellular calcium influx (Feske, 2007). Diffusing calcium ions bind calmodulin that in turn activates calcineurin - a phosphatase which enables nuclear translocation of the nuclear factor of activated T cells (NFAT). Together, transcriptional activation of NF-κB, AP-1 and NFAT tailor defined gene expression profiles including IL-2 and T helper cytokines to induce effector T cell differentiation and proliferation.

Despite TCR-specific intracellular signaling cascades, CD28-mediated co-stimulatory pathways crucially affect threshold activities of T cell activation and either distinct qualitative or overlapping quantitative models of CD28-guided support of TCR signaling have been described (Schmitz and Krappmann, 2006). CD28 supports TCR signaling by phosphatidylinositol 3-kinase (PI3K)-dependent and GRB2 (growth factor receptor-bound protein 2) adaptor protein-dependent mechanisms. The cytoplasmic tail YMNM motif of CD28 attracts the p85 subunit of PI3K to establish a functional bridge to the PI3K-Akt pathway (Pagès et al., 1994). The proline-rich region (PRR) of CD28 interacts with ITK to augment TCR-induced activation of PLCγ1 and Ca^{2+} signaling (Marengere et al., 1997; Michel et al., 2001). Additionally, CD28's cytoplasmic PYAP motif associates with the PTK Lck and recruits GRB2 to promote PKCθ activity required for NF-κB activation and IL-2 induction by fostering NFAT translocation (Okkenhaug and Rottapel, 1998; Holdorf et al., 1999; Coudronniere et al., 2000). Interestingly, the inducible co-stimulator ICOS, which represents a gene duplicate of CD28 lacking the PYAP motif fails to recruit both GRB2 and Lck to induce IL-2 expression (Rudd et al., 2003). Together, CD28 co-stimulation facilitates TCR signal integration by multiple layers of interactions with PTKs, i.e. Tec family (ITK) and Src family kinases (Lck), which licences T cells to mount efficient immune responses and to circumvent anergy (Gibson et al., 1998).

Amplifying the magnitude of peptide:MHC-TCR interactions, CD28 co-signaling during early antigen recognition has been associated with tuning the duration required for optimal T cell activation, yet also the density or number of TCRs, its lipid raft-guided SMAC formation and

specific antigen avidity have been involved to determine T cell stimulatory thresholds (Kündig et al., 1996; Viola et al., 1996; Bachmann et al., 1996). The amount of TCR stimulation via the peptide:MHC-TCR interaction at the T cell/APC surface has been linked to different degrees of proportional T cell activation. Apart from stabilizing effects of synapse formation, the strength of specific antigen-TCR ligation is majorly defined by affinities (K_d, dissociation constant), the dwell time or half-life ($t_{1/2}$) of the peptide being bound to the TCR and the aggregate half-life ($t_{1/2*}$) that combines both previous factors and also considers rebinding occuring with peptide:MHC-TCR interactions of particularly high binding rates, i.e. $K_{on} = K_{off}/K_d$ (Aleksic et al., 2010; Govern et al., 2010). Conclusively, TCR interactions have been described to depend on qualitative (affinity) and quantitative (strength) binding properties, although it remains poorly understood how these modular interactions actually drive T cell activation and differentiation *in vivo*. The complexity of this mechanism is furthermore not only restricted to single 3D cell-to-cell interactions but is also macroscopically tailored on 2D surfaces of multiple cells simultaneously interacting with many peptide:MHC complexes. To this extent, unspecific binding partners of encountering DCs and T cells as well as random cell adhesion in fluidic cell environments are considered to exert crucial secondary functions for maintained peptide:MHC-TCR interactions (Gascoigne et al., 2016).

TCR/CD28 signal strength and sustained T cell/APC interactions promote T cell activation and survival, T cell fitness of effector/memory cells and drives their progressive differentiation (Gett et al., 2003). The next section will delineate subsets of T helper cells and highlight how TCR strength has been linked to functional diversification and proliferation of T cells committing to different CD4+ T helper fates.

1.1.2.3. CD4+ T cell differentiation and TCR strength

CD4+ T cells coordinate discrete adaptive immune responses to a diverse array of pathogens. In response to specific pathogens and depending on the milieu conditions under which they receive TCR stimulation, naive CD4+ T cells differentiate into one of the major CD4+ T effector cell subsets. The set of T helper (Th) cells includes Th1, Th2, Th17, iTreg and T follicular helper (Tfh) cells that have specific as well as shared functions within adaptive immune responses initiated by the previous recognition of peptide antigens (**Fig. 1** and Zhu et al., 2010; O'Shea and Paul, 2010).

The Th1 population accounts for adaptive lymphocyte cells of type I immunity. This type I effector module fights and processes intracellular pathogens including viral infections. Th1 cells are well-known IL-12-dependent producers of interferon γ (IFN-γ) and tumor necrosis factor α (TNFα) (Magram et al., 1996). Equipped with this set of cytokines, Th1 cells are able to mediate the activation of macrophages that themselves produce IFN-γ and thus promote inflammatory responses. Due to Th1-specific expression of the heterodimeric receptor complex IL-12Rβ1/ IL-12Rβ2, the corresponding cytokine IL-12 together with IFN-γ stimulate the induction of STAT1/ STAT4 (signal transducer and activator of transcription) signaling and downstream transcriptional activation of the Th1 gene signature (Park et al., 2000; Afkarian et al., 2002). Th1 lineage commitment is spearheaded by the transcriptional master regulator T-bet (gene *Tbx21*) which

directs cellular Th1 identity and function and also represses alternative T cell fates such as Th17 by specific formation of T-bet-Runx1 complexes to inhibit transactivation of Th17 promoting RORγt (gene *Rorc*) expression (Szabo et al., 2000; Lazarevic et al., 2011).

The type II immunity gives rise to the Th2 population that predominantly provides immunity against extracellular parasites, protects from allergic diseases and has been involved in the regulation of IgE antibody production. Th2 cells depend on IL-4-induced STAT6 signaling and mediate the recruitment of granulocytes, e.g. basophils and neutrophils, to accomplish elimination and clearance of parasitic pathogens (Murphy and Reiner, 2002). IL-4, IL-5 and IL-13 are the key Th2 cytokines and their expression is governed by the Th2-specific transcription factor Gata3 (Zhang, et al., 1997; Lee et al., 2000). The function of Gata3 has been linked to direct binding of multiple sites proximal and distal to the *Il4/Il5/Il13* loci (Kanhere et al., 2012). Moreover, the paradigm of lineage-specifying gene silencing or activation was reinfored by antagonistic T-bet- or Gata3-mediated control of alternative pathways with skewing of T cells towards Th2 fates by overexpression of Gata3 or the deletion of an *Il4* gene silencer promoting *Il4* and *Il13* transcription (Ansel et al., 2004; Jenner et al., 2009).
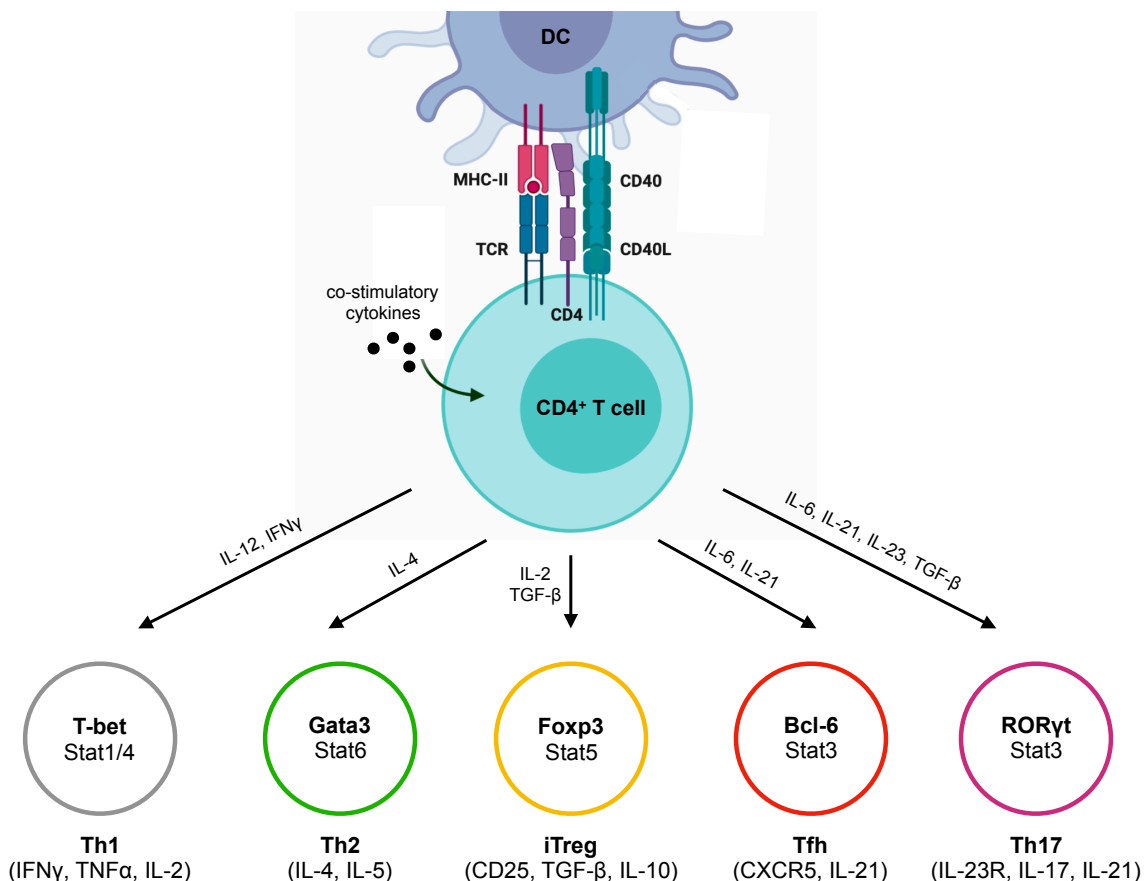
Fig. 1: Overview of CD4+ T cell differentiation pathways. Scheme of naive CD4+ T cell activation in the periphery via antigen-TCR ligation together with co-receptor signaling and co-stimulatory cytokines that leads to multiple trajectories of T effector cell fates. T helper subsets including Th1, Th2 and Th17 are color-coded and annotated with respective transcriptional master regulators (i.e. T-bet, Gata3, RORγt) and their individual cytokine profiles; in part created with BioRender and adapted from Zhou et al., 2010.

Antigen-specific responses against extracellular bacteria and fungi are carried out by Th17 cells which, in addition to Th1 and Th2, represent a third distinct effector lineage (Harrington et al., 2005). The Th17 effector T cell population accounts for the type III immunity, drives the attraction and activation of neutrophils and is profoundly associated with autoimmunity (Iezzi et al., 2009). The transcriptional activator RORγt is the master regulator of Th17 cells that produce and secrete high amounts of IL-17A/IL-17F and IL-21 (Ivanov et al., 2006; Korn et al., 2009). Interestingly, Th17 differentiation has been shown to occur in a stepwise manner wherein STAT3-activating TGF-β, IL-6, IL-21 and IL-1β stimulation of naive T lymphocytes triggers *de novo* Th17 fate decisions (Veldhoen et al., 2006; Ghoreschi et al., 2010). However, pro-inflammatory and cytotoxic Th17 cells require additional IL-23 stimulation to establish intracellular STAT3 signaling and robust transcriptional activation of the Th17 landscape of cytokines including GM-CSF and causing autoreactive neuroinflammation during experimental autoimmune encephalomyelitis (EAE) (Cua et al., 2003; El-Behi et al., 2011; Codarri et al., 2011). IL-23, a heterodimeric protein composed of IL-23 (p19) and the IL-12p40 subunit, not only shares the p40 subunit with IL-12 (Oppmann et al., 2000). Additionally, the T cell-specific receptor subunit IL-12Rβ2 is necessary for both IL-12 (IL-12p70) and IL-23 transmembrane signaling as it binds the shared p40 monomer to induce STAT3/STAT4 signaling (Lee et al., 2009; Teng et al., 2015). Th17 and Th1 cells show a remarkable overlap in their network of stimulatory cytokines and receptor-associated STAT signals that are likely in charge of Th1/Th17 cell plasticity, yet the dynamic landscape of transcriptional regulators of STAT3-induced Th17 fates including IRF4-BATF transcription factor complex activities remains to be fully described (Brüstle et al., 2007; Ciofani et al., 2012).

In 2008, multiple reports described the antagonistic modulation of Th17 and regulatory T cell (Treg) fates by interactions among lineage-specifying transcription factors RORγt and Foxp3 with Runx1 or TGF-β (Betelli et al., 2006; Yang et al., 2008; Zhang et al., 2008). Treg cells are critical for maintaining immune homeostasis by controlling effector T cell function and rather reduce than amplify inflammatory immune responses in favor of T cell tolerance. Runx transcription factors promote Foxp3 expression to induce or maintain Treg programs and ambivalent TGF-β signals for Foxp3 and RORγt induction are contextualized by absence of inflammatory IL-6 in which Foxp3 dominantly antagonizes RORγt to skew balances in favor of Treg over Th17 fates (Zhou et al., 2008; Bruno et al., 2009). Consequences of Treg-deficiency or mutations in their hallmark transcription factor Foxp3 have been described for s*curfy* mice suffering from fatal multiorgan autoimmune disease that resembles symptoms observed for the human autoimmune disorder IPEX (Immune-dysregulation Polyendocrinopathy Enteropathy X-linked) (Brunkow et al., 2001; Fontenot et al., 2003; Hori et al., 2003). Whereas conventional T cells acquire distinct effector functions in response to cytokines and co-stimulation, Treg cells dampen effector T cell activities by expressing co-inhibitory molecules, i.e. CTLA-4, PD-1 and TIGIT, or secreting anti-inflammatory cytokines, i.e. TGF-β and IL-10, to prevent exaggerated immune responses (Joller et al., 2014). Treg-specific expression of CTLA-4 attenuates effector T cell activity as it competes with CD28 for binding to CD80 (B7.1) and CD86 (B7.2) on DCs decreasing the degree of co-stimulation (Wing et al., 2008). Additionally, PD-L1/PD-1 signaling synergizing with TGF-β is involved in Foxp3 induction while enhancing iTreg cell-mediated suppression and the co-inhibitor TIGIT promote the production

of IL-10 whose anti-inflammatory function has been reported essential for Treg-specific IL-10R-induced STAT3 phosphorylation and suppression of Th17 cell responses (Francisco et al., 2009; Yu et al., 2009; Chaudhry et al., 2011). Treg cells are highly responsive to IL-2 levels and consequently show high expression of CD25, i.e. IL-2Rα, which allows Treg cells to sense minimum concentrations of IL-2 to outcompete other effector T helper cells via cytokine deprivation (Pandiyan et al., 2007). Moreover, IL-10-mediated suppressive capacities of Treg cells have been reported to require both IRF4 and Blimp-1 transcriptional activities. IL-2-responsive IRF4 induction is directly involved in binding to exons 5 and 6 of Blimp1 (*Prdm1*) which, together with IRF4, induces active chromatin remodeling within the first introns of the *Il10* locus (Cretney et al., 2011). TCR/CD28-dependent signals crucially affect the *de novo* generation of iTreg cells and CD28-mediated activation of the tyrosine kinase Lck supports both IL-2 cytokine production, the induction of Foxp3 and the Treg-associated co-stimulatory receptors GITR as well as CTLA-4 (Tai et al., 2005). Despite its central dependency on TCR- and CD28-mediated stimulation, thymic Foxp3^{+} Treg cell differentiation has been associated with controversial effects of IL-2 signaling utilizing either IL-2Rβ- or IL-2Rα-deficient mice (Malek et al., 2002; D'Cruz and Klein, 2005). In fact, several studies have rather concluded an involvement of IL-2 signals for maintaining homeostasis and competitive fitness of Treg cells *in vivo* with non-regulatory T cells providing external IL-2 (Fontenot et al., 2005; Setoguchi et al., 2005). IL-2-induced STAT5 signaling is essential for Treg development, restores Treg cell numbers in CD28-deficient mice and ectopic STAT5 activation drives Foxp3 expression for Treg survival, proliferation and suppressive function (Burchill et al., 2008; Chinen et al., 2016). Its proliferative capacity increases Treg cell numbers to an equilibrium to effector T cells and thus ensures an anti-inflammatory environment when there is no pathogenic signal to be fought. Conclusively, Treg cells limit immune responses by providing a framework of immune tolerance.

Follicular T helper cells (Tfh cells) interconnect cellular and humoral immunity as they promote B cell maturation and antibody production via direct cell-to-cell interactions and paracrine cytokine signals in GCs (germinal centers) (Schaerli et al., 2000; Crotty, 2011). Guided by extrinsic IL-6 and IL-21 signals and STAT3-induced transcriptional activity of Bcl6, naive CD4^{+} T cells differentiate to Tfh cells to mediate T cell-dependent B cell responses and to initiate GC reactions, supplying GC B cells with cytokines and co-stimulation for somatic hypermutation and affinity maturation of antibodies (Lee et al., 2011; Nakayamada et al., 2011; Crotty, 2019). The IL-2-dependent bifurcation of CD4^{+} T cells into Tfh instead of effector T cells can be detected as soon as 8 hours post-activation *in vitro* and Tfh commitment is tightly regulated by reciprocal antagonism of Bcl6 and Blimp-1 transcription factors (Johnston et al., 2009; DiToro et al., 2018). Upregulation of Bcl6 facilitates expression of the Tfh-characteristic chemokine receptor CXCR5 and both co-inhibitory/co-stimulatory receptors PD-1 (*Pdcd1*) and ICOS, the latter of which also being involved in c-Maf-dependent upregulation of IL-21 and supporting Bcl6 induction (Bauquet et al., 2009; Choi et al., 2011). CXCR5 surface expression fosters Tfh cell migration to the T-B border (B cell follicle) which reciprocally requires repression of the chemokine receptor CCR7 (Hardtke et al., 2005; Crotty et al., 2019). While Bcl6 is necessary for Tfh differentiation and maintenance of the GC Tfh phenotype *in vivo*, ablation of CXCR5 only marginally affects Tfh function. Importantly, loss of Bcl6

has been recently reported to allow trans-differentiation of ex-Tfh to Th1 cells and the plasticity of Th1/Tfh cells has been associated with opposing signals from IL-2R promoting T-bet and Blimp-1 versus Tfh-specific Bcl6 activities (Nakayamada et al., 2011; Pepper et al., 2011; Alterauge et al., 2020). Another comprehensive analysis of competing transcription factors downstream of Bcl6 that repress positive features of Tfh biology, including Id2 regulating *Cxcr5* or Runx2/3, Gata3 and Klf2 repressing *Pdcd1*, *Icos*, *Il6ra* and *Il21*, supports the idea of gene regulatory networks of repressor-of-repressor circuits with Bcl6 as the nexus factor determining Tfh fates (Choi et al., 2020).

Noteworthy, dysregulated GC-Tfh pathways leading to SLE-like autoimmune diseases have been associated with the *sanroque* (M199R) mutant of the RNA-binding protein Roquin-1 (*Rc3h1*) linking post-transcriptional gene expression to Tfh phenotypes. In more detail, *Rc3h1*[san/san]-associated spontaneous GC formation in absence of antigen was partially caused by enhanced Tfh inducing ICOS expression, yet knockout of *Icos* in *Rc3h1*[san/san] mice did not completely rescue the Tfh phenotype (Lee et al., 2012). However, halving the gene dose of Bcl6 ameliorated lupus pathology and reduced GC formation in *Rc3h1*[san/san] mice (Linterman et al., 2009). Within this thesis, differential effects of Roquin-mediated regulation of mRNA stability will be deciphered in view of T helper cell fate decisions since TCR-induced depletion of Roquin proteins plays pivotal roles for Th17 and Tfh commitment.

Initial commitment to the Tfh cell lineage is determined during the naive T cell priming event and the immediate Tfh versus T effector (Teff) fate polarization post-activation implies a dominant role for cell-intrinsic factors determining the Tfh/Teff cell outcome (Bartleson et al., 2020). T cell differentiation has been linked to TCR signal strength which directs signal transduction and transcriptional activation to instruct specific T helper differentiation programs. Depending on antigenic TCR signal quality (single affinity/avidity) or quantity (TCR strength) and supported by co-receptors and co-stimulation, immunological synapse formation together with peptide:MHC-TCR interaction dwell times help to orchestrate the recruitment of intracellular adaptor proteins and PTKs for multiplexed channeling of TCR signals guiding transcriptional gene signatures (Kim et al., 2013). Multiple TCR-focused studies in the late 1990's have highlighted that the duration of TCR stimulation, the amount of TCRs interacting (TCR occupancy) with peptide:MHC, the requirement of CD28-mediated co-stimulation and single antigen potency crucially determine T cell activation and differentiation (Valitutti et al., 1995; Viola et al., 1996; Leitenberg et al., 1998; Rogers and Croft, 2000). In fact, first ideas on TCR-guided Th1 or Th2 cell fates have been derived from analyses of TCR complex aggregates at sites of lipid raft-dependent peptide:MHC contacts and pronounced Ca^{2+} signaling in Th1 but not Th2 cells which were less responsive at reduced peptide dose (Constant et al., 1995; Balamuth et al., 2001).

Naive $CD4^+$ T cell stimulation triggers the expression of the IL-2 receptor α (CD25) and its induction is proportionate to other markers of TCR strength and T cell activation, i.e. Ca^{2+} flux, Nur77 and CD69 (Wülfing et al., 1997; Moran et al., 2011). IL-2Rα induction is accompanied by upregulation of IRF4 (interferon-regulatory factor 4) that additionally recruits BATF to form transcription factor complexes promoting effector T cell differentiation by transcriptional activation of Blimp-1 (*Prdm1*) (Krishnamoorthy et al., 2017). A well-known paradigm supports the idea that

TCR strength instructs upregulation of both antagonistic transcription factors Bcl6 and Blimp-1, although Bcl6 has been associated with low signal strength and Tfh commitment, while increasing TCR signal strength promotes Blimp-1 outcompeting repressive effects of Bcl6. Thus, this mechanism of TCR-tuned transcriptional activation separates T cells differentiating towards either the Tfh lineage (Bcl6^{high}) or towards the effector-like T cell lineage (Blimp-1^{high}) including Th1, Th2 and Th17 cells (Krishnamoorthy et al., 2017; Snook et al., 2018). Among all subsets of effector T helper cells, fate choice analyses suggest Th2 commitment at low TCR signal strength whereas both Th1 and Th17 are considered as TCR strength-dependent requiring particularly high signal thresholds. Importantly, quantitative differences in TCR strength have been reported to outcompete qualitative effects of adjuvants/cytokines in polarizing T cell differentiation (van Panhuys et al., 2016). However, only little is known about the specific requirements of Th1 or Th17 fate choices at high TCR strength and models of antigen-derived TCR strength have rather focused on ratios of general Tfh/Teff commitment, Th1/Th2 and Th17/iTreg cell fates. Strong TCR signals are assumed to promote Th1 over Th2 (Hosken et al., 1995; Jorritsma et al., 2003; Milner et al., 2010; van Panhuys et al., 2014). Studies focusing on the Tec family kinase ITK (*Itk*) indicate that its activity is a pivotal positive regulator of Th17 commitment and thus, efficient TCR strength integration has been associated with commitment to Th17 rather than iTreg fates (Gomez-Rodriguez et al., 2009; Gomez-Rodriguez et al., 2014). Besides, Th17 fate choice critically requires additional DC-T cell cross-talk via CD40-CD40L interactions to transmit strong TCR signals for productive Th17 fate programs at high antigen dose (Iezzi et al., 2009). Finally, conflicting data suggested either Th1 over Tfh commitment at strong TCR signals or pronounced Tfh accumulation due to persistent TCR-antigen interactions. The field has been contentious in its findings since some studies suggest that increased TCR avidity for antigenic peptide:MHC or sustained interactions and IL-2 production promote Tfh cell development, while others have concluded the opposite or could not find any effects on Tfh cell fates (Fazilleau et al., 2009; Deenick et al., 2010; Ploquin et al., 2011; Baumjohann et al., 2013; Tubo et al., 2013; Keck et al., 2014; Krishnamoorthy et al., 2017; Kotov et al., 2018; Bartleson et al., 2020).

However, despite global transcriptional activators or repressors of alternative fates not much is known about the genuine molecular switches and regulatory transcriptional programs that directly link TCR signal strength in an integrative network to specific T cell fate decisions. A central aspect of this doctoral thesis was to extend the concept of TCR strength-dependent post-transcriptional regulation of T cell fates by genetic manipulation of the RNA-binding protein paralogs Roquin-1 (*Rc3h1*) and Roquin-2 (*Rc3h2*) which will be introduced in more detail in section 1.3.

1.1.2.4. The CBM complex in T cell activation and differentiation

Antigen-dependent and TCR-induced NF-κB signaling is mediated by the Carma1/CARD11-Bcl10-MALT1 (CBM) signalosome complex to tailor various T and B lymphocyte functions (Hara et al., 2003; Ruland et al., 2003). Likewise, CBM components are involved in innate immune responses since C-type lectin receptor pathways, i.e. Dectin-1/2 or Mincle, and RIG-I receptors involve analogous CARD9 activities in myeloid cells (Strasser et al., 2012). Various missense mutations and chromosomal translocations involved the genes encoding *Carma1* (CARD11), *Bcl10* and *Malt1* as *bona fide* oncogenes associated with lymphomas, i.e. non-Hodgkin's MALT lymphoma and diffuse large B cell lymphoma (DLBCL). Mechanistically, mutations in *Carma1* have been shown to overcome its autoinhibition in absence of TCR signals and translocations in both *Bcl10* and *Malt1* genes lead to constitutive NF-κB activation (Uren et al., 2000; Lenz et al., 2008; Hailfinger et al., 2009). The filamentous assembly of the CBM signalosome is induced by TCR/ZAP-70-stimulated PKCθ- and PI3K (PDK1)-dependent Carma1 phosphorylation. Of note, Carma1 is synonymous to CARD11 which contains additional PDZ, SH3 and GUK domains defined as membrane-associated guanylate kinase (MAGUK) region (Ruland et al., 2018). Nucleation of phosphorylated Carma1 (Carma1 seed) releases its intramolecular autoinhibition and allows binding of Bcl10 to drive its helical filament formation. Both Carma1 and Bcl10 comprise caspase recruitment domains (CARD) to interact and the C-terminal Ser/Thr-rich domain of Bcl10 associates with the N-terminal Ig domains of MALT1 which additionally employs a C-terminal paracaspase domain to cleave protein substrates in an arginine-specific manner (**Fig. 2** and Qiao et al., 2013). Phosphorylation of Carma1 at serine residues (S564, S649, S657) has been described as a PKCθ-dependent switch for NF-κB activation, and the cooperative mechanism of CBM complex assembly via Bcl10 reflects PKCθ/Carma1-sensitive threshold responses in TCR and BCR signaling (Wang et al., 2002; Sommer et al., 2005; Matsumoto et al., 2005).
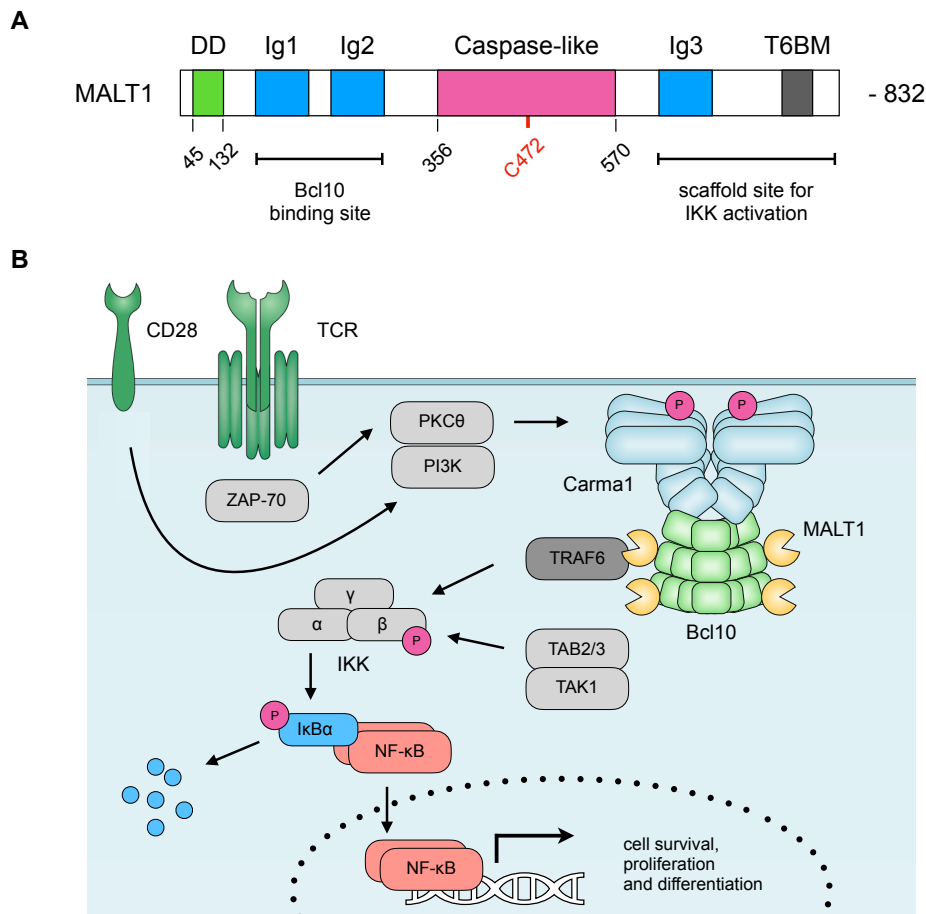
A

DD | Ig1 | Ig2 | Caspase-like | Ig3 | T6BM

MALT1 — 832

45 | 132 | 356 | C472 | 570

Bcl10 binding site

scaffold site for IKK activation

B

CD28   TCR

PKCθ
PI3K
ZAP-70

Carma1
MALT1
TRAF6
Bcl10

γ
α | β
IKK

TAB2/3
TAK1

IκBα
NF-κB

NF-κB

cell survival, proliferation and differentiation

Fig. 2: Domain organization of the MALT1 paracaspase and TCR-induced and Carma1-Bcl10-MALT1 (CBM) complex-driven NF-κB signaling pathways. (**A**) Representative scheme of the domain organization of MALT1 (832 aa) comprising a DD (death domain), three individual Ig (immunoglobulin 1-3) and the Caspase-like domains as well as a TRAF6-binding motif (T6BM). (**B**) Scheme illustrating TCR-induced CBM activation and scaffold function of MALT1 to link antigen-TCR interactions to NF-κB activation. Briefly, upon TCR ligation and co-stimulation, protein kinase C θ (PKCθ) and PI3K activate Carma1 via phosphorylation to oligomerize with preformed Bcl10-MALT1 units. As a result, CBM filaments form and recruit E3 ubiquitin ligases such as TRAF6 and the IKK complex is activated by TAK1 and TAB2/3 proteins. IKK-driven phosphorylation of IκBα induces its proteasomal decay and releases NF-κB dimers to translocate into the nucleus for transcriptional activation. Signaling cascade design was adapted and derived from Thome et al., 2010; Schlauderer et al., 2018; Ruland et al., 2018.

CBM function is crucial for TRAF6-mediated scaffolding to direct canonical NF-κB activation via the IκB kinase (IKKα/β/γ). This kinase complex becomes activated by concerted TRAF6 ubiquitin ligase and TAK1 kinase activity guided by oligomerized Bcl10 and MALT1 to induce IκBα inhibitor degradation and transcriptional NF-κB activation (**Fig. 2** and Sun et al., 2004). IκBα becomes ubiquitinylated and dissociates from NF-κB. Release of NF-κB from its canonical inhibitor allows its translocation into the nucleus where members of the NF-κB family act as *trans*-factors promoting DNA transcription. Likewise, Bcl10 signalosomes control JNK and p38 MAPK signaling which feeds into the progression of T cell activation, survival and proliferation (Blonska et al., 2007; Gross et al., 2008).

In addition, MALT1 paracaspase activity is required for proteolytic cleavage of substrates involved in either mRNA decay, i.e. Roquin-1, Roquin-2, the endonucleases Regnase-1 and N4BP1 (Jeltsch et al., 2014; Uehata et al., 2013; Yamasoba et al., 2019), or the modulation of the NF-κB pathway including CYLD, Bcl10, A20, HOIL1, RelB and MALT1 itself (Coornaert et al., 2008; Rebeaud et al., 2008; Düwel et al., 2009; Staal et al., 2011; Hailfinger et al., 2011). Substoichiometric Carma1 nucleates Bcl10 to form filamentous structures which are constitutively associated with MALT1 paracaspase units at a 1-to-1 ratio. The Carma1 seed serves as a central signaling hub for the assembly of star-shaped Bcl10 filaments that become cooperatively decorated with dimerized MALT1 and bridge Carma1 phosphorylation to immune activation (David et al., 2018; Gehring et al., 2018). Moreover, cyro-EM structures indicate that TRAF6 assembles with CBM filaments creating diameters of approx. 40 nm and providing mechanistic ideas on how TRAF6 directs its ubiquitin ligase activity to mediate K63-linked mono- and polyubiquitination of MALT1 (David et al., 2018). MALT1 dimerization and its TRAF6-mediated monoubiquitination at lysine 644 in the C-terminal Ig3 domain are necessary for structural rearrangements of MALT1 to achieve its catalytically active conformation (Pelzer et al., 2013; Schlauderer et al., 2013). Macroscopically, both Ig3 and paracaspase domains of MALT1 protrude from the MALT1 death domain (DD) and Bcl10 CARD interface to accomplish intramolecular modifications allowing substrate recognition and cleavage at the filament periphery (Schlauderer et al., 2018). In 2011, the crystal structure of an inhibitor-bound MALT1 fragment (residues 339-719) containing the paracaspase and an Ig-like domain has uncovered the MALT1 cleavage motif of VRPR (z-VRPR-fmk) which was later confirmed by mutagenesis studies determining optimal catalytic efficiencies of MALT1 for LVSR motifs, although the number and precise sequence motifs of cleavage sites varies across substrates (Yu et al., 2011; Hachmann et al., 2012; Demeyer et al., 2016). MALT1 autoproteolysis, Bcl10, A20 and HOIL1 cleavage may provide negative feedback after the initial pulse of CBM-mediated activation of NF-κB and IL-2 expression, while cleavage of CYLD and RelB presumably amplify and prolong IKK-dependent NF-κB or JNK signaling (Ruland et al., 2018). HOIL1 (heme-oxidized IRP2 ubiquitin ligase) is required for its interacting protein HOIP which forms a linear ubiquitin chain assembly complex (LUBAC) to ubiquitinate IKKγ (NEMO); however, MALT1-mediated cleavage of HOIL1 disassembles LUBAC and thus reduces linear ubiquitination to autoinhibit further canonical NF-κB signaling (Klein et al., 2015). Similarly, A20 cleavage has been associated with limiting the degree of MALT1-IKK interactions by removing K63-linked ubiquitin chains from MALT1 (Düwel et al., 2009).

Mouse models of germline CBM component deficiencies show severe defects in conventional lymphocyte activation and consequently fail to provide genuine adaptive immunity as evidenced by increased susceptibilities of *Bcl10*^{-/-} and *Malt1*^{-/-} mice to viral infections (Ruland et al., 2001; Thome et al., 2010). In humans, MALT1 point mutations (i.e. S89I, T580S or Y353fs*18) have been as well reported to cause severe combined immunodeficiency (CID) syndromes (Jabara et al., 2013; McKinnon et al. 2014; Punwani et al., 2015). Therein, mutations in *Malt1* majorly caused altered expression levels of functional MALT1 and patients with loss-of-function (LOF) *Malt1* mutations developed autoimmunity or autoinflammation possibly caused by dysregulated immune homeostasis due to reduced numbers of Treg cells. Constitutive NF-κB activation due to mutations,

chromosomal translocations or overexpression of CBM components is a well-known primary driver of MALT-associated lymphomas. Conversely, allosteric inhibition of the MALT1 paracaspase using small molecule inhibitors and the genetic inactivation of MALT1 protease activity (protease dead *Malt1*[PD/PD] mutant, C472A) were associated with improved anti-tumor immunity at the expense of suffering from autoimmune phenotypes (Martin et al., 2019; Martin et al., 2020).

Indeed, MALT1 function is particularly critical for Treg development and Th17 differentiation, and *Malt1*-deficient, *Malt1*[PD/PD] (C472A) as well as MALT1 inhibitor-treated mice are resistant or less susceptible to experimentally induced autoimmune encephalomyelitis (EAE) (Brüstle et al., 2012; Bornancin et al., 2015; Gewies et al., 2015). Models of MALT1 deficiency (*Malt1*^{-/-}) and protease inactivation (*Malt1*[PD/PD]) demonstrated that MALT1 modulates transcriptional programs downstream of antigen/TCR ligation and its function was reported essential for the development of thymic/peripheral Treg cells, B1 B cells as well as MZ B cells and the induction of pathogenic Th17 cells (Ruland et al., 2003; Jaworski et al., 2014). Surprisingly, mutant *Malt1*[PD/PD] but not *Malt1*^{-/-} mice suffer from spontaneous IFN-γ-mediated autoinflammation as well as an IPEX-like imbalance of increased T effector (Teff) to Treg cell ratios, and loss of CBM assembly by deletion of *Bcl10* or *Carma1* in Treg cells and MALT1 paracaspase inhibition improved anti-tumor responses (Cheng et al., 2019; Rosenbaum et al., 2019; Di Pilato et al., 2019).

1.1.2.5. Atypical inhibitors of NF-κB activation

TCR-dependent NF-κB signaling is a major determinant of lymphocyte activation and expansion that needs to be tightly controlled in naive and activated T cells to prevent excessive transcriptional activity. The NF-κB transcription factor family comprises multiple Rel homology domain (RHD)-containing members including c-Rel, p65 (RelA), RelB and p50/105 as well as p52/100 which associate and dimerize, e.g. p50/RelA and p50/c-Rel, to induce target gene expression via κB DNA binding sites (Wang et al., 2012). Classical control mechanisms of NF-κB signaling encompass binding of Rel homolgy domains by inhibitor proteins, i.e. IκBα, IκBβ and IκBε, which covers nuclear localization signals (NLS) and prevents nuclear NF-κB translocation (Huxford et al., 1998). Upon T cell activation and co-stimulation, however, inhibitors bound to NF-κB are phosphorylated by the IκB kinase (IKK) complex to drive dissociation and proteasomal degradation of IκBs releasing NF-κB factors for translocation into the nucleus. In contrast, atypical IκBs, i.e. Bcl-3, IκB[NS], IκBζ, IκBη, become activated during T cell stimulation and add another layer of complexity to the dynamic modulation of NF-κB when classical inhibition is turned off due to proteasomal degradation (Hayden and Gosh, 2012; Schuster et al., 2013). Atypical IκBs are localized in the nucleus and do not exclusively act as inhibitors but also activate secondary responses as transcriptional inducers (Hörber et al., 2016). In more detail, IκB[NS] (encoded by the *Nfkbid* gene) interacts with p50 and/or c-Rel to induce the Treg-specific transcription factor Foxp3 and directly binds to the IL-10 gene locus. Thus, deficiency in IκB[NS] is associated with impaired thymic and peripheral Treg development, yet it remains elusive how IκB[NS] elicits its transcriptional activity lacking DNA-binding domains (Schuster et al., 2012; Annemann et al., 2015). Both IκB[NS] and IκBζ

(*Nfkbiz* gene) share an involvement in Th17 fate decisions as IκB-deficient models revealed impaired production of IL-17A and/or RORγt which was further confirmed by protection from experimental autoimmune encephalomyelitis (EAE) (Okamoto et al., 2010; Kobayashi et al., 2014). Importantly, atypical inhibitors such as IκB$_{NS}$ and IκBζ need to be tightly regulated in absence of antigen exposure and the RNA-binding proteins Regnase-1 (*Zc3h12a*) and Roquin-1/2 (*Rc3h1/2*) are pivotal post-transcriptional regulators of *Nfkbid* and *Nfkbiz* induction. Post-transcriptional gene regulation is essential for innate and adaptive immunity (Kafasla et al., 2014) and its fundamental concepts will be described in the upcoming section.

1.2. Post-transcriptional gene regulation

The central three-step biomolecular dogma of gene expression was first described in 1961 when Meselson and colleagues introduced messenger RNAs (mRNA) as unstable intermediates between the gene encoding DNA and protein synthesizing ribosomes (Brenner et al., 1961). The cellular pool of ribonucleic acids (RNAs) consists of approximately 4% mRNA, 15% transfer RNA (tRNA) and 80% ribosomal RNA (rRNA) which account for general protein biosynthesis. Moreover, non-coding microRNAs (miRNA) and small nuclear RNAs (snRNA) have been found to play pivotal roles in post-transcriptional gene regulation and mRNA splicing, respectively.

The plethora of extra- and intracellular pathogens as well as inter-species molecular interactions requires a robust and rapid defense strategy of multicellular organisms. Indeed, eukaryotic post-transcriptional gene regulation provides fast adaptation of immune responses as dynamic alterations in gene expression and proteome diversity allow to prioritize on genes particularly important for initial host defense actions. The subcellular localization of mRNA varies within cytoplasmic foci as specialized compartments termed P-bodies and stress granules have been reported to contain mRNA decay factors along with translationally repressed mRNA targets or to store and protect mRNA transcripts during changes in cellular microenvironments and upon general cellular stress. Thus, gene regulation via post-transcriptional control of mRNA decay or stability represents a crucial and tightly regulated component of immunological reactivity guiding adaptive immune cell plasticity (Kafasla et al., 2014).

The level of mRNA expression is controlled by two opposing pathways: (i) DNA transcription by RNA synthesizing RNA polymerases in the nucleus and (ii) mRNA degradation and breakdown into nucleotides within the cytoplasm. Imbalance of mRNA homeostasis is generally associated with diseases including tumor progression, autoimmune or inflammatory disorders due to uncontrolled proto-oncogene or immune-related cytokine expression as well as cancer metastasis as a result of non-stop expression of proteins involved in cell cycle progression. Regulation of mRNA stability is majorly governed by *cis*-regulatory elements and *trans*-acting factors binding to mRNA sequences or secondary structures (*cis*-elements) either in the 5'- or 3'-UTRs (untranslated regions) of mRNA. Many *trans*-acting factors mediate degradation of specific mRNA targets by recruiting enzymes and factors that orchestrate mRNA breakdown (Schuster and Hsieh, 2019).

Hence, the following sections will focus on (i) detailed mechanisms of mRNA decay and (ii) examples of *trans*-acting factors including the RNA-binding protein paralogs Roquin-1/2 that post-transcriptionally tailor gene expression in immune cells to determine lymphocyte fate decisions.

1.2.1. Mechanisms of eukaryotic mRNA decay

Post-transcriptional regulation (PTR) predominantly features three pathways of mRNA decay: (i) exonucleolytic decay via deadenylation/decapping, (ii) endonucleolytic decay driven by site-specific RNases and (iii) nonsense-mediated decay (NMD) as a surveillance or quality control mechanism. Notably, mRNA decay involves a complex network of factors contributing to RNA recognition and degradation and functional units of RNA-bound proteins are referred to as regulatory ribonucleoprotein (RNP) complexes orchestrating the recruitment of factors for mRNA degradation. Eukaryotic single-stranded mRNA structures can be categorized into three major sequences including (i) the 5'-UTR, (ii) the gene coding sequence (CDS) and (iii) the 3'-UTR. The 7-methyl guanosine cap (abbreviated "m7Gppp" or "5'-cap") protects mRNA at the 5' end from degradation by 5'-3'-exonucleases, while a poly(A) tail (abbreviated AAA_n) covers and protects mRNA at the 3' end (**Fig. 3**). Mammalian 3'-UTR Poly(A) tails can encompass up to 250 nucleotides (n ~ 250) and are bound by multiple poly(A)-binding proteins (PABP). At the 5'-UTR, the multi-protein complex eIF4F binds the 5'-cap to promote translation initiation. These messenger RNPs can be organized in a linear fashion or circularize via protein-protein-interactions of the 5'-eIF4F and the 3'-PABP (Tarun and Sachs, 1996).

Studies in yeast (*S. cerevisiae*) have unraveled the complex network of enzymes mediating degradation of mRNA and factors involved are subdivided in 5'-cap-relevant decapping enzymes or 3'-poly(A) tail-relevant deadenylases (**Fig. 3** and Parker and Song, 2004). However, onset of decay at the 3' end of mRNAs influences decay mechanisms at the 5' end as the initial recruitment of the poly(A) nuclease (PAN2-PAN3) shortens the poly(A) tail until PABPs can no longer bind and protect the 3' end from non-specific nucleases (Decker and Parker, 1993). Hence, de-circularization starts by loss of 3' end PABP-binding and subsequent activation of the Ccr4-Not complex finalizes detachment of the poly(A) tail. Following deadenylation, 3'-5' exonucleolytic decay by the exosome complex irreversibly processes and cleaves off deadenylated mRNA nucleotides (Mitchell et al., 1997; Jacobs Anderson and Parker, 1998). Next, post rate-limiting deadenylation, the 5'-cap (m7G) is targeted by the decapping enzymes DCP removing accessible m7G-cap structures which triggers 5'-3' exonucleolytic decay executed by the Xrn1 exonuclease (Muhlrad et al., 1994). In more detail, decapping by DCP1/DCP2 is initiated by concerted action of a Pat1-Lsm1-7 complex that - together with the ATP-dependent RNA helicase DHH1/RCKp54 - removes the eIF4F complex protecting the 5' end of mRNAs (Beelman et al., 1996; Tharun and Parker, 2001). Moreover, enhancer/activator proteins including enhancers of decapping (Edc) and DCP1 stimulate DCP2-driven m7G-decapping which results in 5'-monophosphate groups targeted by Xrn1 (**Fig. 3**).
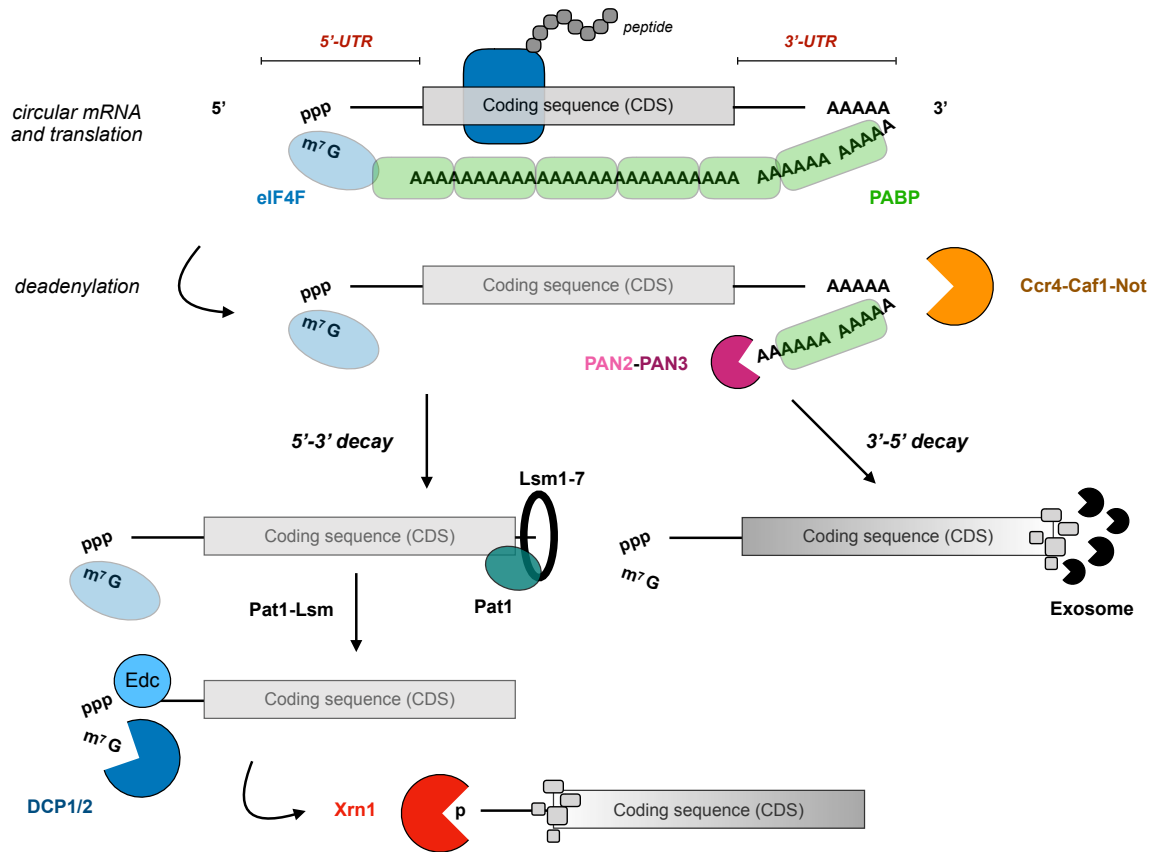
Fig. 3: Eukaryotic mechanisms of exonucleolytic mRNA decay. Scheme illustrating exonucleolytic mechanisms of mRNA degradation (5'-3' or 3'-5' orientation) at 5'- and 3'-UTRs. 3'-5' decay: Rate-limiting deadenylation is carried out by PAN2-PAN3 ribonucleases together with the Ccr4-Caf1-Not complex followed by exonucleolytic decay via the 9-subunit exosome complex. 5'-3': Post deadenylation, m⁷G is removed (decapping) by DCP1/2 proteins and the Xrn1 exonuclease digests mRNA in 5'-3' orientation. Abbreviations: eIF4F, eukaryotic initiation factor 4F; PABP, polyadenylate-binding protein; PAN2/3, PAB-specific ribonuclease 2 and 3; Edc, enhancer of decapping; Xrn1, exoribonuclease 1; Lsm, Sm-like protein 1-7.

Endonucleolytic activity has been shown to play rather small roles for general mRNA turnover but it especially affects specific pathways of mRNA decay: Firstly, RNA interference (RNAi) pathways in which Argonaute (Ago) proteins cleave mRNA perfectly bound by complementary microRNA (miRNAs) and secondly, mRNA surveillance pathways employ the endonuclease SMG6 which cleaves nonsense mRNA targets bearing premature termination codons (PTC) (Liu et al., 2004; Eberle et al., 2009).

1.2.2. Co- and *trans*-acting factors of mRNA turnover

3'-5'-exonucleolytic mRNA turnover by exosome complexes is dependent on linearized single-stranded RNA substrates. Co-factors such as RNA helicases and polymerases generate segments of single-stranded RNA which can then be targeted by exonucleolytic breakdown. Herein, conserved RecA domains of ATP hydrolysis-driven RNA helicases such as Dbp5 and UPF1 facilitate unwinding of secondary mRNA structures or remodelling of mRNPs to provide accessible RNA targets (von Möller et al., 2009; Chakrabarti et al., 2011). Moreover, many RNA helicases complex with exo- or endonucleases to turn RNA decay into a rapid two-step process of mRNA unwinding followed by targeted degradation (including SKI/exosome and UPF1/SMG6 complexes; Halbach et al., 2013; Falk et al., 2014). In more detail, mRNA surveillance and turnover are as well dependent on *trans*-factors that recognize, bind and process mRNA targets identified via their unique *cis*-regulatory elements within mRNA 3'-UTRs.

Surveillance pathways resemble quality control mechanisms in mRNA regulation and include nonsense-mediated mRNA decay (NMD) which is triggered by insertion of PTCs creating false 3'-UTRs as primary *cis*-regulatory elements. In eukaryotes, the NMD machinery is mRNA splicing-dependent as exon junction complexes (EJC) deposited after stop codons signal for genuine PTCs. *Trans*-acting NMD factors include UPF1, UPF2 and UPF3 that assemble the decay inducing complex (DECID) recruiting SMG6 to endonucleolytically cleave mRNA between the PTC and the EJC. Turnover pathways include microRNA-mediated gene silencing as well as ARE- and CDE-mediated mRNA decay. Gene silencing by miRNAs is based on complementary base-pairing within mRNA 3'-UTRs that can cause translational mRNA inhibiton or RNA-induced silencing complex (RISC)-dependent degradation (Huntzinger and Izaurralde, 2011; Winter et al., 2009).

RNA-binding proteins (RBPs) and miRNAs represent the most versatile and important *trans*-factors recognizing *cis*-elements as linear sequence motifs and/or folded secondary structures in 3'-UTRs of mRNA. With this, RBPs regulate mRNA decay and translational output, while *trans*-acting factors at the 5'-end of mRNA have been associated with initiation of translation.

Immune responses combating infections are precisely controlled and inappropriate responses can lead to inflammatory or autoimmune diseases. Immune cell activation, immune homeostasis and antiviral responses are crucially regulated by RNA-binding CCCH zinc finger proteins which impose anti-inflammatory control through the regulation of cytokine production (Fu and Blackshear, 2016). By mediating mRNA decay, CCCH zinc finger proteins such as TTP, Roquin and Regnase-1 (MCPIP1) promote the resolution of inflammation, control the magnitude of adaptive immune responses and ensure immunological homeostasis.

Among CCCH zinc finger proteins, AU-rich elements (AREs) within 3'-UTRs are bound by AU-binding proteins (AUBPs) that either activate or repress mRNA decay. A prominent example of a *trans*-acting AUBP is the tandem CCCH zinc finger protein Tristetraprolin (TTP; *Zfp36* gene) that regulates *Ifng* and *Tnfa* mRNA stabilities. As for TTP, many RNA-binding *trans*-acting factors recognize elements within 3'-UTRs and function by recruiting mRNA decay enzymes, including Ccr4-Not by TTP that is regulated by Toll-like receptor (TLR)-induced p38-MAPK/MK2 signaling

(Stoecklin et al., 2004). TTP phosphorylation by the MK2 kinase may change the RNA affinity of TTP and promotes its sequestration by 14-3-3 protein-protein interaction which diminishes mRNA decay as measured by decreased deadenylation of target transcripts (Clement et al., 2011; Tiedje et al., 2016).

Despite sequence-specific linear binding of *cis*-elements, secondary structures of mRNA have been classified as constitutive/alternative decay elements (CDE or ADE) with the first CDE identified within the 3'-UTR of *Tnfa* mRNA in 2003 (Stoecklin et al., 2003). These secondary CDE structures encompass conserved stem-loop motifs including a tri-loop hairpin (pyrimidine-purine-pyrimidine) sequence attached to a base-pairing stem-loop of 7 nucleotides (Tan et al., 2014; Schlundt et al., 2014). RNA-immunoprecipitation assays (RNA-IP) including mass spectrometry, nuclear magnetic resonance (NMR) studies and X-ray crystal structures identified Roquin proteins as potent RNA-binding *trans*-factors destabilizing *Tnfa* mRNA (Leppek et al., 2013; Schlundt et al., 2014). Signal-induced immunological gene expression programs are guided by RBP function and thus, TTP-, Roquin- and Regnase-dependent mRNA expression is silenced prior to T cell activation. The regulatory network of RBPs shares overlapping transcript targets, e.g. *Tnf* mRNA repression by TTP or Roquin and *Il2* mRNA repression by TTP or Regnase, and also antagonistic functions of Regnase-1 and Arid5a have been described for the balanced regulation of *Il6* mRNA stability (Masuda et al., 2013; Fu and Blackshear, 2016). Maintaining balanced cytokine conditions or even modulating the degree of transcriptional activation by limiting inducible factors involved in T cell activation, CCCH zinc finger type RNA-binding proteins highlight the central role of mRNA *trans*-acting factors in translating cellular context into appropriate transcriptional responses.

Finally, PTRs affect processes involved in lymphocyte maturation, peripheral activation and control of T cell tolerance which as well comprises specialized functions of immunoglobulin secretion and affinity maturation guided by B follicular helper T cells (Jiang et al., 2015). The following sections will focus on the specific roles of Roquin-1/2 protein paralogs in mediating post-transcriptional regulation of immune-relevant mRNA targets and its implications for immune homeostasis and the development of autoimmunity.

1.3. The RNA-binding protein Roquin

1.3.1. The Roquin family of *trans*-acting factors

The Roquin protein was first described in 2005 when Vinuesa and colleagues introduced Roquin as a member of the RING-type ubiquitin ligase protein family (Vinuesa et al., 2005). In fact, an ethylnitrosurea mutagenesis screening for autoimmune regulators has unraveled the murine point-mutation M199R in Roquin-1 and these homozygous *sanroque* mice (*Rc3h1*[san/san]) were associated with features of typical systemic lupus erythematosus (SLE) including antinuclear auto-antibodies (ANAs) and increased accumulations of both follicular helper T and GC B cells. Subsequent studies have highlighted critical contributions of Roquin to post-transcriptional control

of autoimmunity and T lymphocyte plasticity as it was identified as an RNA-binding protein destabilizing *Icos* mRNA (Yu et al., 2007).

1.3.2. Molecular function and domain organization of Roquin

Two paralogs, Roquin-1, encoded by the gene *Rc3h1*, and Roquin-2 (also known as membrane-associated nucleic acid-binding protein, Mnab), encoded by *Rc3h2*, are members of the Roquin family. Both paralogs redundantly recognize and bind specific secondary mRNA structures within the 3' end (3'-UTR) of mRNA targets. In general, Roquin activity is considered to repress target mRNA translation as it negatively regulates mRNA stability and promotes mRNA decay. Roquin proteins are ubiquitously expressed; however, Roquin-1 outcompetes Roquin-2 expression by approx. 5-fold in murine T lymphocytes (Vogel et al., 2013). Within cells, Roquin family members accumulate in cytoplasmic processing bodies (P-bodies) or stress granules to dynamically shape post-transcriptional control of gene expression (Athanasopoulos et al., 2010; Glasmacher et al., 2010).

Three different mRNA structure motifs enable Roquin to recognize and bind mRNA 3'-UTRs: (i) the constitutive decay element (CDE), (ii) the alternative decay element (ADE) that was observed in SELEX experiments (Systematic Evolution of Ligands by EXponential Enrichment) and (iii) the linear binding element (LBE) (Schlundt et al., 2014; Janowski et al., 2016; Braun et al., 2018; Essig et al, 2018). Roquin-2 activity can compensate for loss of Roquin-1 and strong similarities in their domain organization suggest functional redundancy (Vogel et al., 2013). Indeed, both proteins comprise 1,130 (Roquin-1) to 1,187 (Roquin-2) amino acids, respectively, and share almost identical domains at their N-terminus (**Fig. 4**). The N-terminal RING finger (really new interesting gene), ROQ and CCCH-type zinc-finger (ZF) domains are of 81-99% sequence similarities and conserved among metazoans (Tan et al., 2014; Pratama et al., 2013). The ROQ domain is unique as it does not share sequence conservation with other proteins and it is required for CDE-binding which was shown in a ROQ domain crystal structure (residues 174-325) complexed with *Tnf* CDE stem-loop RNA (Schlundt et al., 2014). The predominantly α-helical ROQ domain is flanked by HEPN$_N$ and HEPN$_C$ domains (higher eukaryotes and prokaryotes nucleotide-binding domain) and the C-terminal segment following the CCCH ZF domain appears to be poorly conserved among Roquin paralogs containing proline-rich regions (PRRs) and either a coiled-coil domain (Roquin-1) or a hydrophobic region (Roquin-2) (Srivastava et al., 2015; Pratama et al., 2013).
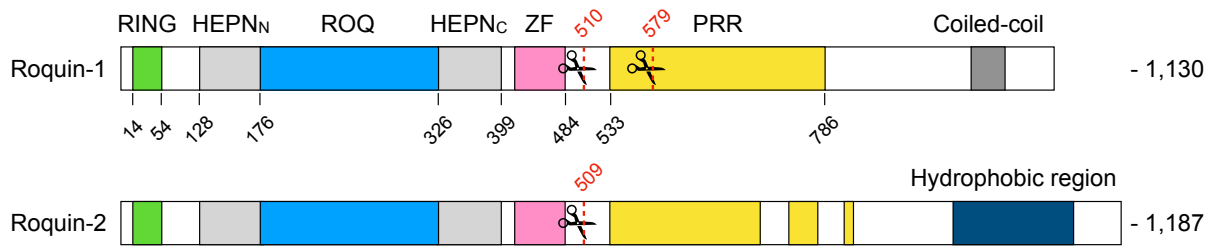
Fig. 4: Domain organization of the Roquin-1 and Roquin-2 paralogs. Representative scheme of the domain organization of Roquin-1 (1,130 aa) and Roquin-2 (1,187 aa) proteins including N-terminal RING (really interesting new gene), HEPN (higher eukaryotes and prokaryotes nucleotide-binding domain), ROQ and ZF (zinc finger, CCCH) domains that share high sequence similarities among paralogs. At the C-terminus, Roquin paralogs harbor PRRs (proline-rich regions) and either a coiled-coil (Roquin-1) or hydrophobic region (Roquin-2). Scissors indicate MALT1 cleavage sites within Roquin-1 (arginines 510 and 579) and Roquin-2 (arginine 509) and structural information was derived from Pratama et al., 2013; Schlundt et al., 2014; Srivastava et al., 2015.

Moreover, helix-turn-helix (HTH) and winged-helix (WH) motifs of ROQ subdomains II and III create dual binding sites termed A (binding to RNA loops) and B (binding to double-stranded RNA) (Schütz et al., 2014; Tan et al., 2014). The set of mRNA targets is considerably large and Roquin has been shown to regulate mRNA transcripts of activation-induced co-stimulatory/inhibitory receptors *Icos*, *Ox40* and *Ctla-4*, transcription factors such as *c-Rel* and *Irf4* as well as modulators of transcription including *Nfkbid* (IκB$_{NS}$) and *Nfkbiz* (IκBζ) of the NF-κB signaling pathway (Yu et al., 2007; Janowski et al., 2016; Jeltsch et al., 2014). In T cells, Roquin-derived RNPs resemble central units of mRNA stability regulation that control peripheral T cell tolerance. Especially, the regulation of co-stimulatory or co-inhibitory mRNAs (i.e. *Icos*, *Ox40*, *Ctla-4*) render Roquin-mediated decay mechanisms to be crucial contributors to the systemic control peripheral T cell activation and tolerance, while repression of *c-Rel*, *Irf4* and *Nfkbid* (IκB$_{NS}$) mRNA targets is strongly associated with the regulation of helper T cell differentiation.

Mutational and electrophoretic mobility shift assay (EMSA) analyses uncovered conserved lysine residues K220A, K239A and K259A to be important for ROQ-*Tnf* CDE RNA interactions. Yet another mutated arginine residue, R260A, has been annotated with largest chemical shift perturbations (CSPs) in HSQC NMR studies which diminishes CDE-specific binding by the ROQ domain and underscores its essential contributions to mRNA recognition (Schlundt et al., 2014). Besides the analysis of ROQ binding to the canonical *Tnf* CDE RNA, *Icos* and *Ox40* mRNAs were as well tested by EMSA and/or crystallization providing evidence of ROQ domain recognition patterns based on mRNA secondary structures. Moreover, SELEX-derived ADE and ADE-like hexa-loop motifs have been reported for the 3'-UTR of *Ox40* mRNA involving another tyrosine Y250A mutation in additional target-specific interactions with the ROQ domain (Janowski et al., 2016). Surface-plasmon resonance (SPR) and isothermal titration calorimetry (ITC) analyses have confirmed binding affinities/kinetics yielding dissociation constants (K_d) in the micro- to nanomolar

range for ROQ-*Nfkbiz* LBE (3.6 µM), ROQ-*Ox40* CDE-like (1.46 µM), ROQ-*Ox40* ADE-like (0.081 µM) and ROQ-*Tnf* CDE (0.042 µM) interactions (Janowski et al., 2016; Essig et al., 2018). Interestingly, Roquin has also been reported to bind its own 3'-UTR suggesting autoregulatory negative feedback (Leppek et al., 2013; Cui et al., 2017). The RNase Regnase-1, encoded by the gene *Zc3h12a*, has been as well described as a target of Roquin-mediated mRNA decay (Jeltsch et al., 2014), whose own set of destabilized targets includes Th17-associated transcripts of *Il6*, *Il12b* and *c-Rel* and *Nfkbiz* mRNAs (Garg et al., 2015; Cui et al., 2017; Uehata et al., 2013). Regnase-1 endonucleolytic activity is linked to UPF1 helicase-dependent unwinding of structured mRNA targets and thus exemplifies an important immune-relevant helicase-endonuclease complex as described for NMD of nonsense RNAs by UPF1/SMG6 (Mino et al., 2015). Both Roquin and Regnase share overlapping sets of mRNA targets and interconnected mechanisms of Roquin-mediated *Zc3h12a* mRNA destabilization and their individual contributions to cooperative or exclusive mRNA repression are currently becoming explored. However, previous studies by Takeuchi and colleagues suggest spatio-temporally distinct mechanisms of mRNA regulation that involved co-localization of Regnase-1 at ribosomes suppressing translation of active mRNAs instead of destabilization of inactive mRNA by Roquin-1 and Roquin-2 in P-bodies or stress granules (Mino et al., 2015).

Roquin-1/2 proteins are post-transcriptional regulators of inflammatory mRNA stability and the mechanism of mRNA decay initiation has been linked to miRNA-independent Rck helicase and Edc4 recruitment indicating facilitated 5' decapping of mRNA (Glasmacher et al., 2010). Likewise, later studies focusing on ROQ-CDE *Tnf* RNA interactions in macrophages have reported on direct interactions with the Ccr4-Caf1-Not deadenylase complex highlighting the association of Not1 scaffold subunits with redundant Roquin-1 and Roquin-2 paralogs (Leppek et al., 2013). Besides downstream recruitment of factors involved in mRNA decay, initial binding of target mRNAs has been shown to become strengthened in a complex with NUFIP2 (nuclear fragile X mental retardation-interacting protein 2). In more detail, NUFIP2 protein functionally contributed to high-affinity mRNA recognition as both proteins physically interact to cooperatively repress tandem stem-loop motifs within 3'-UTRs of *Icos* and *Ox40* mRNA (Rehage et al., 2018). In contrast to decay-promoting co-factor interactions, Roquin antagonizes functions of miRNA-17~92 as both compete for binding of *cis*-elements in the *Pten* 3'-UTR (Phosphatase and tensin homolog). Interestingly, conventional T helper and Treg cell-specific stabilization of *Pten* mRNA thus extends the regulatory network of Roquin and link its post-transcriptional function to T cell metabolism by inhibiting the PI3K/Akt/mTOR signaling pathway (Essig et al., 2017).

Roquin-mediated mRNA destabilization of factors important for T cell co-stimulation, metabolism and transcriptional programs suggests its crucial involvement in T lymphocyte activation and differentiation decisions; hence, the following section will elaborate on *in vivo* models of hypomorphic Roquin-1 *sanroque* mice (i.e. M199R), systemic and conditional knockouts of Roquin-1/2 (i.e. Roquin-1 single KO, double KO) and a single nucleotide polymorphism (SNP) in the *Rc3h1* gene which creates a premature stop codon (TGA) and translates Roquin-1 function to human lymphocyte homeostasis.

1.3.3. *In vivo* models of Roquin

The systemic *sanroque* M199R Roquin-1 mutant has revealed Roquin as an E3 ubiquitin ligase family member protecting against autoimmune disease. Homozygous *Rc3h1*san/san mice are characterized by severe symptoms of SLE-like autoimmunity which includes splenomegaly, lymphadenopathy, plasmacytic infiltrates in kidneys, livers and lungs as well as antinuclear auto-antibodies (ANAs) and hypergamma-globulinemia starting at 8 weeks of age (Vinuesa et al., 2005). Next to elevated peripheral effector-memory like CD4+ and CD8+ T cells (CD44high CD62Llow), *Rc3h1*san/san CD4+ T cells express increased levels of the ICOS receptor, cytokines such as IL-5 and IFN-γ and accumulate germinal-center B cells within splenic PNA+ GCs. Additionally, an unrestrained formation of CXRC5+ PD-1+ IL-21+ follicular T helper cells has been associated with excessive upregulation of ICOS that has been identified as a direct target mRNA of the Roquin family. However, reducing ICOS expression to 70% in *Rc3h1*san/san *Icos*+/- mice or complete ICOS deficiency in *Rc3h1*san/san *Icos*-/- mice fail to reduce autoimmune phenotypes of *Rc3h1*san/san *Icos*+/+ mice (Yu et al., 2007; Lee et al., 2012). Representing a CD28 paralogue, ICOS has thus gained broad attention as an evolutionarily conserved mechanism of additional inducible co-stimulation that critically shapes effector or follicular helper T cell responses and is post-transcriptionally repressed by Roquin (Tafuri et al., 2001; Linterman et al., 2009). Likewise, elevated ICOS expression on T cells has been observed in mice lacking Roquin-1 in T cells (*Cd4-Cre*) or in the hematopoietic system (*Vav-Cre*), yet these Roquin-1 knockouts fail to elicit unrestrained numbers of Tfh cells, spontaneous GC formation or antinuclear auto-antibodies. The *Cd4-Cre* knockout of Roquin-1 additionally shows an expansion of CD8+ effector-like phenotypes, while the B cell-specific *Cd19-Cre* knockout of Roquin-1 is characterized by expanded B cells, Treg cells and enlarged spleens with insignificantly more GC formation. Strikingly, however, the constitutive knockout of Roquin-1, exons 4-6 of *Rc3h1* flanked by loxP sites and crossed with germline Cre recombinase, causes perinatal lethality within a few hours after birth that has been related to impaired alveolar function in the lung (Bertossi et al., 2011).

Subsequent studies on aberrant Tfh cell formation in *sanroque* mice have uncovered a direct link to IFN-γ signaling since increased IFN-γR signals caused upregulation of the Tfh-specific transcriptional activator Bcl6 (Lee et al., 2012). Yet, the *sanroque* mutant causes disruptive autoimmune perturbations not recapitulated by Roquin-1 knockouts creating a scenario in which the paralog Roquin-2, known as Mnab, may compensate for loss of Roquin-1 expression, a mechanism not assumed to be valid for Roquin-1san/san inhibiting Roquin-2 function (Heissmeyer & Vogel, 2013). The "Tfh paradoxon" has been addressed by additional mutants of either Roquin-1 or Roquin-2 introducing RING-deficient (*Rc3h1/2*rin/rin) mice as well as combinations of *Rc3h1*san/san; *Rc3h2*rin/rin genotypes, all of which indicate that Roquin-2 function compensates for loss-of-function mutations of Roquin-1 (Pratama et al., 2013). These findings are complemented by analyses of post-transcriptional contributions of *Rc3h1* or *Rc3h2* genes showing that excessive peripheral T cell activation or ICOS-promoted Tfh commitment as observed in mice deficient in both paralogs in T cells (*Rc3h1/2*fl/fl; *Cd4-Cre*) are quenched by single Roquin-2 activity in mice lacking only Roquin-1 expression (Vogel et al., 2013). Importantly, mice deficient in *Rc3h1* and *Rc3h2* genes as

well show increased frequencies or numbers of Th17 cells and a distinct Th17 infiltration-driven lung pathology and autoinflammation has been linked to the cooperative derepression of Th17 promoting mRNAs by both Regnase-1 and Roquin proteins regulating transcripts such as *c-Rel*, *Icos*, *Irf4*, *Nfkbiz* and *Nfkbid* mRNAs (Jeltsch et al., 2014).

Observations based on murine manipulations of *Rc3h1* and *Rc3h2* genes appear to translate to the human homolog of Roquin-1 since a homozygous R688* nonsense mutation in the proline-rich region of *Rc3h1* has been extensively characterized for a human patient in 2019 (Tavernier et al., 2019). In fact, the R688* point mutation which leads to a truncated version and a functional impairment of Roquin-1 is associated with an hyperinflammatory syndrome characterized by relapsing hemophagocytic lymphohistiocytosis (HLH) and the heritable genetic disorder in *Rc3h1* systematically causes dysbalanced immune activation and cytokine release (hypercytokinemia) comparable to the M199R *sanroque* mutation in murine *Rc3h1*. Truncated R688* Roquin-1 fails to colocalize in P-bodies and to interact with mRNA decay promoting CNOT1 which presumably accompanied differential effects on mRNA decay. Among patient-derived PBMCs, the hypomorphic *Rc3h1* R688* mutant causes upregulation of ICOS and OX40 receptors as well as increased cytotoxic CD8$^+$ T and pathogenic Th17 cell accumulation, yet also defects in B cell maturation and no autoimmune-related increases in circulating Tfh cells. Noteworthy, the human patient's parents, both classified as heterozygous carriers of the R688* mutation, have been reported to suffer from either lupus (SLE) or rheumatoid arthritis (RA) indicating that homozygosity in R688* is a major driver of the severe pathogenesis (Tavernier et al., 2019). Thus, both well-characterized mutations in *Rc3h1* are associated with shared or distinct phenotypic consequences generally linked to systemic dysregulation of immune homeostasis and the precise contributions of both mRNA binding and the recruitment of mRNA decay inducing factors by Roquin proteins appear to account for the differential post-transcriptional repression of immune modulators specifying helper T cell fate decisions.

1.3.4. TCR-dependent regulation of Roquin

Previous sections have described the mode-of-action and function of Roquin proteins to post-transcriptionally regulate CD4$^+$ T helper cell fates. For this, Roquin represses immune-relevant factors implicated in T cell activation, differentiation and inflammatory cytokine production to quench unlicensed immune activation in the absence of antigenic stimuli or TCR ligation. Along with T cell activation, however, MALT1 paracaspase activity has been reported to cleave and inactivate both Roquin paralogs - a mechanism that has evolved to ensure release of mRNA targets from repression to allow induction of the T cell factors necessary for an immune response (**Fig. 5** and Jeltsch et al., 2014). Thus, the control of Roquin abundance is tightly regulated by TCR- and co-stimulation-dependent MALT1 and directly linked to antigen recognition. Roquin-1 comprises two individual cleavage sites at arginines R510 and R579, while its paralog Roquin-2 only contains the R509 site. Both cleavage sites LISR$_{509}$ or LIPR$_{510}$, respectively, and MVPR$_{579}$ align well with peptide library screenings and structural modeling analyses that suggest a preferred

consensus sequence of LVSR across all known MALT1 substrates (Hachmann et al., 2012; Demeyer et al., 2016). In T cells, MALT1-executed regulation of Roquin has been tested in MALT1-deficient, mutant *Malt1*[PD/PD] and MALT1 mepazine inhibitor-treated CD4^{+} T cells (Gewies et al., 2014; Jeltsch et al., 2014).
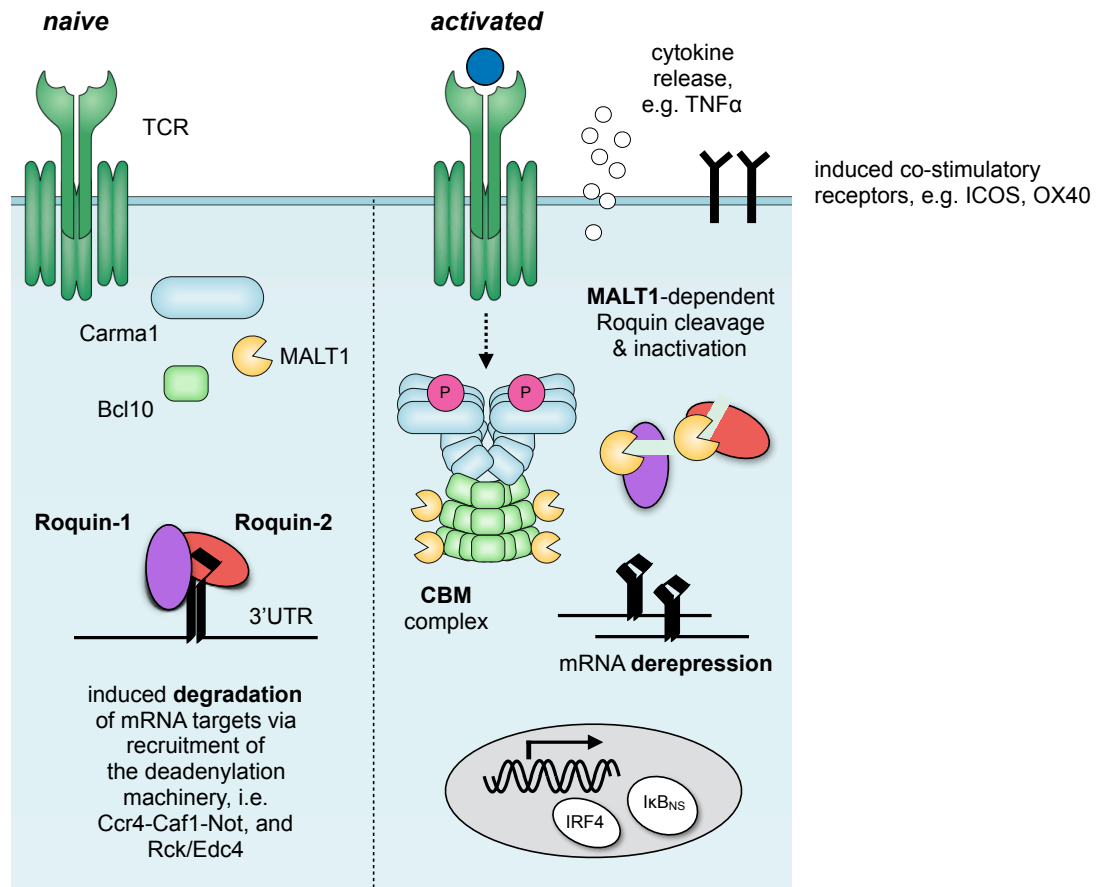

Fig. 5: TCR- and MALT1-dependent regulation of Roquin-1/2 in CD4^{+} T cells. Scheme illustrating TCR-induced CBM complex formation and MALT1 paracaspase activation that leads to cleavage of both Roquin paralogs and drives gene expression upon T cell activation. In resting naive CD4^{+} T cells, Roquin-1/2 bind to CDE/ADE-specific stem loops in mRNA target 3'-UTRs to mediate mRNA degradation and restrict T cell activation/differentiation. Upon TCR ligation and T cell activation, PKCθ-driven phosphorylation of Carma1 triggers CBM complex formation and MALT1 activity. MALT1 proteolytically cleaves Roquin-1 and Roquin-2 at LISR/LIPR or MVPR motifs and mRNA targets become derepressed (incl. transcriptional activators/modulators, cytokines and stimulatory receptors); scheme was adapted from Jaworski et al., 2016; Jeltsch and Heissmeyer, 2016; Ruland et al., 2018.

Moreover, cleavage of both paralogs leads to accumulation of its N-terminal fragments aa1-510/509 and aa1-579 (monoclonal antibody detection) as well as its C-terminal fragments detected by polyclonal immunoblot analyses (Jeltsch et al., 2014), yet it remains unclear to which extent N-terminal cleavage products might remain functional since both include ROQ domains approximately spanning the residues 174-325 (Schlundt et al., 2014). Reminiscent of the Carma1 switch triggered by PKCθ-mediated Carma1 seed phosphorylation, the dynamic inactivation of

Roquin by arginine-specific cleavage switches on gene products that are required for immunological reactivity, T cell activation and its functional differentiation. TCR-dependent and MALT1-executed cleavage of Roquin and regulation of Roquin abundance in T cells delineate a pivotal process in TCR signal interpretation to mediate T cell fate decisions and thus, it will be a major aim of this doctoral thesis described in the following section.

1.4. Hypothesis and aim of the thesis

The involvement of Roquin-mediated destabilization of mRNA targets in autoimmune dysregulation and T lymphocyte differentiation has been described for Roquin-1 mutant variants as well as murine models of *Rc3h1* and *Rc3h2* deficiencies (Tavernier et al., 2019; Vinuesa et al., 2005; Jeltsch et al., 2014). In particular, accumulations of follicular helper T or Th17 cells in Roquin-deficient murine models have been linked to derepressed *Tnfrsf4* (*Ox40*) and *Icos* or *Irf4*, *Nfkbiz* (IκBζ) and *Nfkbid* (IκB$_{NS}$) mRNAs (Yu et al., 2007; Glasmacher et al., 2010; Vogel et al., 2013; Jeltsch et al., 2014). The 3'-UTRs of mRNA targets share distinct CDE, CDE-like and ADE binding motifs of differential ROQ-mRNA affinities/avidities assumed to mediate preferential mRNA decay (Leppek et al., 2013; Tan et al., 2014; Schlundt et al., 2014; Janowski et al., 2016). However, it has remained enigmatic to which extent TCR-induced cleavage of Roquin by MALT1 indeed guides differential derepression of either low or high affinity/avidity mRNAs to direct T cell fates. Conversely, rendering Roquin paralogs insensitive to MALT1-mediated cleavage will help to decipher substrate-specific contributions of Roquin cleavage to dysregulated immune phenotypes observed for genetic and pharmacological manipulation of MALT1 paracaspase function (Bornancin et al., 2015; Martin et al., 2020).

This doctoral thesis tested the hypothesis that quantitative TCR signal strength and proteolytic MALT1 activity are the major physiologic determinants of Roquin-1/2 function in T cells to mediate immune-relevant mRNA derepression and to allow T cell activation and differentiation.

Multiple aspects of Roquin biology will be addressed to answer the question of how T cell stimulation affects Roquin abundance to set thresholds for distinct mRNA derepression that integrate into T cell fate decisions: In **aim 1**, graded deletion of *Rc3h1* and *Rc3h2* alleles and reduced Roquin abundance are utilized to characterize sets of targets of particular quantitative sensitivity to repression. In contrast, in **aim 2**, qualitative Roquin affinity changes due to single or combined mutations within the ROQ domain are analyzed to identify low, intermediate or high affinity/avidity targets according to attenuated ROQ-mRNA interactions. Next, **aim 3** employs antigen-guided TCR signal strength to analyze Roquin inactivation by MALT1-dependent cleavage and defines TCR-induced target derepression/upregulation as well as antigen dose-specific T cell fate commitment. Finally, a CRISPR/Cas9-based model of *Rc3h1*^{Mins} is established in **aim 4** to uncouple Roquin function from TCR signals or MALT1 activity, respectively, and to summarize factors addressed in aims 1-3 as essential contributors guiding *in vitro* and *in vivo* Th17 differentiation.

2. Materials and Methods

2.1. Materials

Unless otherwise indicated all buffers and chemicals used within this project were purchased from Sigma-Aldrich (St. Louis, MO, USA) or Carl Roth (Karlsruhe, Germany). Aqueous solutions and buffers were prepared with filtered and autoclaved MilliQ water derived from a Merck Millipore system. The purification of either plasmid DNA or DNA PCR products was carried out with the PureYield Plasmid Miniprep System (Promega) or the NucleoSpin Gel and PCR Clean Up Kit (Macherey-Nagel). Molecular cloning reactions were performed with the In-Fusion HD Cloning Kit (Takara Clontech), the QuikChange II XL Site-Directed Mutagenesis Kit (Agilent Technologies) or the Golden Gate Assembly kit (NEB, Ipswitch, MA, USA). All DNA oligonucleotide primers were ordered from and synthesized by Eurofins Genomics (Ebersberg, Germany). General sequence identity controls were verified by Sanger sequencing performed by Eurofins Genomics. All RNA isolations were carried out by TRIzol extraction (Ambion) and the generation of cDNA was performed with the Quantitect Reverse Transcription Kit (Qiagen) using the RevertAid Reverse Transcriptase. All quantitative PCRs including High Resolution Melting (HRM) analyses were conducted with the Light Cycler 480 (Roche) using the Universal Probe Library or the HRM Master systems, respectively (Roche). All measurements of protein or DNA concentrations were obtained using a photometer (Eppendorf) or NanoDrop ND100 spectrophotometer (Peqlab), respectively. All Western blot analyses were conducted with X-ray film casettes (VWR) and developed with the Optimax X-ray processor (PROTEC). All flow cytometry-based single cell data was obtained using the Cytoflex S (Beckmann Coulter), Canto or LSR Fortessa (BD) flow cytometers. Data derived from cell-based experiments was processed with the Single Cell Analysis Software FlowJo V10.6 (FlowJo, LLC, OR, USA). Data and statistical analysis was performed with GraphPad Prism Version 5.0b (CA, USA).

2.1.1. Buffers and solutions

Blocking buffer (Western blotting)	5% milk powder in Tris-buffered saline (TBS)
Cryo-conservation solution	10% DMSO in FCS
FACS buffer	2% FCS in Phosphate-buffered saline (PBS)
HBS	280 mM NaCl, 50 mM HEPES, 1.5 mM Na_2HPO_4 2x, pH 6.95 - 7.05
Isolation buffer	2% FCS, 1 mM EDTA, PBS, pH 7.4
Laemmli (loading buffer, 5x)	314 mM Tris, 50% Glycerin, 5% SDS, 10% ß-ME, 0.01% Bromphenol blue, pH 6.8
LB agar	1.5% Bacto agar in LB medium
LB medium	0.5% yeast extract, 1% Tryptone, 1% NaCl

Meister Lysis buffer	20 mM Tris-HCl, 150 mM NaCl, 0.25% NP-40, 1.5 mM $MgCl_2$, pH 7,5
PBS	137 mM NaCl, 2.7 mM KCl, 10 mM $NaHPO_4$, pH 7.4
Permeabilization buffer	0.5% Saponin powder, 1% BSA in PBS
SDS buffer	20 mM Tris, 200 mM Glycine, 0.1% SDS
TAC lysis buffer	13 mM Tris, 140 mM NH_4Cl, pH 7.2
TBE	89 mM Tris-borate, 2 mM EDTA, pH 8.0
TBS	50 mM Tris-HCl, 150 mM NaCl, pH 8.0
TBS-Tween	TBS, 0.05% Tween-20
Western blot transfer buffer	25 mM Tris, 39 mM Glycine, 20% Methanol

2.1.2. Chemicals, media and supplements

2-propanol (Isopronal)	Roth
4'-OH-tamoxifen (1 µM)	Sigma-Aldrich
Acrylamide (30%) 4K	AppliChem
Agarose	Biozym
Ammonium chloride	Sigma
Ammonium peroxide sulfate (APC)	Roth
Ampicillin	AppliChem
β-mercaptoethanol (β-ME, 50 mM)	Roth, Invitrogen
Brefeldin A (BrfA)	Sigma-Aldrich
Bovine serum albumin (BSA)	Sigma-Aldrich
Calcium chloride	Roth
CFA (killed *M. tubercolosis* H37 Ra)	BD Difco™ Adjuvants
Chloroquine	Sigma-Aldrich
Collagenase D	Sigma-Aldrich
cOmplete, EDTA-free Protease Inhibitor Cocktail	Roche
Dimethyl sulfoxide (DMSO)	Sigma-Aldrich
DNase I	Sigma-Aldrich
Dulbecco's Modified Eagle Medium (low glucose)	Invitrogen (Gibco)
dNTP	Fermentas
Dithiothreitol (DTT)	AppliChem
Doxycycline hyclate	Sigma-Aldrich
ECL reagents	Novex® HRP kit, Invitrogen Amersham™, Prime, GE Healthcare
EDTA	Roth
Ethanol	Roth

Ethidium bromide (EtBr)	Roth
Fetal calf serum (FCS)	Invitrogen (Gibco)
Fixation/development solution	Agfa
Formaldehyde (37%)	VWR
Glycerol	Roth
HEPES (1 M)	Invitrogen (Gibco)
Ionomycin	Calbiochem
Kanamycin	Roth
LB agar	AppliChem
LB (Luria broth) medium	Roth
Lipopolysaccharide (LPS)	Sigma-Aldrich
Mepazine (MALT1 inhibitor)	Merck Millipore
Methanol	Roth
Milk powder	Roth
MilliQ water	Merck Millipore
Myelin Oligodendrocyte Glycoprotein (MOG_{35-55})	Auspep Pty Ltd
Non-essential amino acids (MEM NEAA, 100X)	Invitrogen (Gibco)
NP-40	Sigma-Aldrich
$OVA_{323-339}$ peptides	BIO TREND
Penicillin	Thermo Fisher
Percoll	GE Healthcare
Pertussis toxin (PTX, *B. pertussis*)	Sigma-Aldrich
Phorbol-12-myristate-13-acetate (PMA)	Calbiochem
Protein Assay Dye Reagent (Bradford, 5X)	Bio-Rad
Polybrene	Sigma-Aldrich
Proteinase K	Sigma-Aldrich
Saponin	VWR
Sodium azide	Roth
Sodium dodecyl sulfate (SDS)	Roth
Streptomycin	Thermo Fisher
TEMED	Roth
Tris-HCl	Invitrogen
TRIzol® reagent	Ambion (Life Technologies)
Trypan blue	Roth
Trypsin-EDTA (1X, 0.05%)	Invitrogen (Gibco)
Tween-20	AppliChem

2.1.3. Instruments, materials and software

1.5 mL, 2.0 mL tubes	Eppendorf, Beckmann
5.0 mL tubes (FACS)	FALCON, VWR
15 mL, 50 mL tubes	FALCON, Greiner-Bio-One
6-well cell culture plate	Omnilab, Sarstedt
96-well flat-bottom cell culture plate	Sarstedt
96-well V-bottom plate	Roth
90 mm cell tissue culture dish	FALCON, BD
90 mm cell culture dish (non-adherent)	Gosselin
150 mm cell tissue culture dish	VWR
25 cm^2 cell culture flask	BD
75 cm^2 cell culture flask	BD
175 cm^2 cell culture flask	BD
Agarose gel electrophoresis	Bio-Rad
Capillary gel electrophoresis	QIAxcel Advanced (QIAGEN)
Centrifuges	Eppendorf Centrifuge 5424 R
	Hettich Rotanda 460 R
	Thermo Scientific Heraeus Multifuge X3R
Cell counting	Neubauer chamber (Marienfeld)
	CASY cell counter (Innovartis)
Cell culture hood	BERNER FlowSafe® B-[MaxPro]^2-190
Cell incubator (eukaryotic)	37°C, New Brunswick Galaxy 170 S/R
Cell incubator (prokaryotic)	37°C, Memmert
Compensation beads	Thermo Fisher
Cuvettes (UV-transparent)	halbmikro (Brand)
Data and image processing	FlowJo V10.6
	Microsoft Excel
	Apple Mactintosh Numbers
	GraphPad Prism 5
	ApE - A plasmid Editor
	Affinity Designer
Developer (Western blot)	Optimax X-ray processor (PROTEC)
Filtration	100 µm nylon cell strainer (FALCON)
	40 µm nylon cell strainer (FALCON)
	0.45 µm syringe filter Supor® (PALL)
	Acrodisc®
Flow cytometers	Cytoflex S (Beckmann Coulter)
	BD FACSCanto™ (Becton, Dickinson)
	BD LSRFortessa™ (Becton, Dickinson)
Freezer	-80°C (Thermo Scientific), -20°C (Liebherr)

Fridge	4°C (Liebherr)
Gel UV documentation (illuminator)	Bio-Rad
Gel electrophoresis system	PowerPac HC (Bio-Rad)
Gel electrophoresis chamber/casettes	Mini-Protean Tetra System (Bio-Rad)
Heat block	Thermomixer compact (Eppendorf)
Ice machine	Scotsman
Magnetic stirrer	C-MAG HS 7 (IKA)
Medical X-ray film	DV-B, EncapSulite, R20, Typon Röntgen
Medical X-ray film casette	VWR
Microscopy	Zeiss (47 12 02)
	Leica DFC3000G, CoolLED pE-300
Microwave	LG
Needles	26G, 30G (Fine-Ject, VWR)
PCR cycler	GeneTouch (BIOER)
PCR tubes	Nippon Genetics
pH calibration	Schott pH-METER, InoLab pH 720
Photometer	Eppendorf
Pipettes	Rainin, Biozym
PVDF membrane	Merck Millipore
Spectrophotometer	NanoDrop ND100 (Peqlab)
Sterilization	Varioklav (H+R)
Syringes	Omnifix (5 mL, 30 mL)
Ultrapure water	MilliQ (Merck Millipore)
Water bath	GFL
Whatmann paper	VWR
Weighing scale	PFB 1200-2 (Kern)

2.1.4. Kits, antibodies, dyes and cytokines

Multiple commercially available kits were used for molecular and cell biology techniques to perform primary lymphocyte and CD4$^+$ T cell isolation, cell-based intracellular stainings for flow cytometric measurements or cloning and quantitaive PCR experiments:

BD Cytofix/Cytoperm	BD Biosciences
EasySep™ Mouse CD4$^+$ T Cell Isolation Kit	STEMCELL Technologies
EasySep™ Mouse Naive CD4$^+$ T Cell Isolation Kit	STEMCELL Technologies
Foxp3 staining buffer kit	Invitrogen (eBioscience)
In-Fusion® HD cloning kit	Takara Clontech
Light Cycler 480 probes master	Roche
Nucleobond Xtra Midi/Maxi	Macherey-Nagel (MN)

NucleoSpin Gel and PCR Clean Up Kit	Macherey-Nagel (MN)
PureYield Plasmid Miniprep System	Promega
QuantiTect Reverse Transcription Kit	Qiagen
QuikChange II XL Site-Directed Mutagenesis kit	Agilent Technologies
Universal Probe Library	Roche

All antibodies used for flow cytometric analysis of lymphocyte cells are listed including clone identifiers and specific fluorophore conjugates (**Table 1**). Antibodies were used at dilutions according to manufacturer's protocols or previous antibody-conjugate titrations and fluorophore-conjugated secondary antibodies (anti-rat/anti-mouse) were used for visualization of signals of primary mAbs without direct fluorophore conjugation.

Table 1: Antibodies for flow cytometry.

Target	Clone	Conjugate	Origin
Cas9	7A9-3A3	primary mAb	CST
CD3	17A2	eF450	Invitrogen (eB)
CD4	GK1.5	APC, FITC, PE, eF450	Biolegend, eB, Invitrogen
CD8α	53-6.7	APC, FITC	Biolegend, Invitrogen (eB)
CD11c	N418	PE, FITC	Invitrogen (eB)
CD19	MB19-1	FITC	Invitrogen (eB)
CD21/35	7G6	PE	BD Pharminogen
CD23	B3B4	Pacific Blue (eF450)	Biolegend
CD25 (IL-2Rα)	PC61.5; eB704	PE, FITC, APC	Invitrogen (eB)
CD27	LG.3A10	PE-Cy7	Biolegend
CD44	IM7	APC, FITC, BV510	eB, Biolegend
CD45R (B220)	RA3-6B2	PE, PerCP-Cy5.5	Invitrogen (eB)
CD62L	MEL-14	APC, FITC, PE	Invitrogen (eB)
CD69	H1.2F3	PE	Invitrogen (eB)
CD86	GL1	PE	eB
CD95	15A7	APC	eB
CD122 (IL-2Rβ)	5H4	PE	eB
CD134 (OX40)	OX-86	APC, PE	eB
CD152 (CTLA-4)	UC10-4B9; -4F10-11	APC, PE	eB, BP Pharminogen
CD185 (CXCR5)	L138D7	APC	Biolegend

CD278 (ICOS)	C398.4A; 7E.17G9	APC, PE	Biolegend, eB
CD279 (PD-1)	J43	FITC, PE	eB
c-Rel	1RELAH5	PE	Invitrogen (eB)
Fc block		primary	in-house
Foxp3	FJK-16s	FITC, PE	Invitrogen (eB)
GL-7	GL-7	AF488, FITC	eB, BD Pharminogen
IFNγ	XMG1.2	APC	Invitrogen (eB)
IL-17A	eBio17B1; TC11-18H10.1	PE, BV785	Invitrogen (eB), Biolegend
IRF4	3E4	eF660	Invitrogen (eB)
IκB$_{NS}$	4C1	primary	in-house
MHCII	M5/114.15.2	FITC	eB
PLZF	9E12	PE, PE-Cy7	Biolegend
p-S6 (235/236)	D57.2.2E	PE-Cy7	Invitrogen (eB)
Regnase-1	15D11	primary	in-house
Roquin-1/2	3F12	primary	in-house
Roquin-1 1-510	5F6	primary	in-house
RORγt	Q31-378	AF647, BV421	BD Pharminogen, BD Horizon
T-bet	eBio4B10	eF660, PE	eB
TCRβ	H57-597	FITC	Invitrogen (eB)
TCRγδ	GL-3	APC	Invitrogen (eB)
TCR Vα2	B20.1	FITC	Invitrogen (eB)
TCR Vβ5.1/5.2	MR9-4	eF450	Invitrogen (eB)
Thy1.1	HIS51	APC	eB
TNFα	MP6-XT22	PerCP-eF710	Invitrogen (eB)
2nd goat a-rat/mouse	Poly4054; MRG2a-83	AF647, FITC	Biolegend, Invitrogen (eB)
PBS57-CD1d tetramer	iNKT (mCD1d)	PE	NIH
Fixable Viability Dye		eF780	Invitrogen (eB)
Fixable Blue		UV (DAPI)	Invitrogen

Primary antibody incubations for Western blots were carried out at 4°C for at least 16 hours over night and protein expression was detected using secondary HRP-coupled antibodies (anti-rat/anti-rabbit/anti-mouse) and ECL substrates. Specific antibody clones of both primary and secondary antibodies are shown (**Table 2**).

Table 2: Antibodies for Western blotting.

Target	Clone	Specification	Origin
GAPDH	6C5	primary mAb, mouse	EMD Merck Millipore
IRF4	P173	primary mAb, rabbit	Invitrogen (eB)
IκB$_{NS}$	4C1	primary, rat	in-house
Regnase-1	15D11	primary, rat	in-house
Roquin-1/2	3F12	primary, rat	in-house
2nd a-rat	7077S	HRP-coupled	CST
2nd a-rabbit	7074S	HRP-coupled	CST
2nd a-mouse	7076S	HRP-coupled	CST

Primary CD4$^+$ T cell cultures were performed using different antibodies and cytokines according to T helper subset differentiation (Th0, Th1, Th17 and iTreg). All antibodies used for *in vitro* T cell activation and differentiation assays including specific clones and effective concentrations are listed (**Table 3**).

Table 3: Antibodies and cytokines for *in vitro* T cell culture.

Antibody/Cytokine	Clone	Differentiation	Origin	Concentration
Anti-CD3	2C11	-	in-house	0.25 µg/mL
Anti-CD28	37.5N	-	in-house	2.5 µg/mL
Anti-IL4	11B11	Th1, Th17	in-house	10 µg/mL
Anti-IL12	C17.8	Th17, Treg	in-house	10 µg/mL
Anti-IFNγ	XMG1.2.1	Th17, Treg	in-house	5 µg/mL
Anti-hamster IgG	polyclonal	-	MP Biomedicals, # 56984	2.5 mg/mL
hIL-2	-	-	Novartis	200 units/mL

rmIL-6	-	Th17	STEMCELL	60 ng/mL
rmIL-12	-	Th1	STEMCELL	10 ng/mL
rhTGF-β1	-	Th17, Treg	R&D System	10 ng/mL
rmGM-CSF	-	BMDC	CST	20 ng/mL

2.1.5. Enzymes and markers for molecular biology

Agarose gel analyses, Western blotting, restriction analyses and genotyping experiments required various enzymes and markers for molecular biology methods and relevant components needed along with molecular biology kits are listed:

2-log DNA ladder	Biolabs
Protein Marker VI (10-245 kDa)	AppliChem
RevertAid Reverse Transcriptase	Qiagen
Pfu Ultra (Quik Change)	Agilent Technologies
T4 PNK	Promega
T4 DNA ligase	NEB
BbsI, restiction enzyme	NEB
Taq polymerase(s)	Invivogen, NEB, recombinant in-house
NaeI, restriction enzyme	NEB
Crf10I, restriction enzyme	Thermo Scientific
EcoRI, restriction enzyme	NEB

2.1.6. Plasmid constructs and primer sequences

Both CRISPR/Cas9-based targeting of *Rc3h1* and retroviral reconstitutions of iDKO CD4+ T cells required uniquely designed bacterial plasmids/vectors. The vector *MSCVpuro* was used for Golden Gate assembly and cloning of sgRNA sequences which was performed via T4 PNK and T4 DNA ligase reactions. The HDR template for the *Rc3h1*Mins transgene was based on the vector *pCR-Blunt II-TOPO* (Invitrogen) and the design of the *Rc3h1* repair template required In-Fusion HD cloning from gDNA and site-directed QuikChange mutagenesis to insert relevant point mutations at codons of arginines 510 and 579. HEK293 cell transfections were used for virus production of pRetroXtight vectors encoding fused GFP-Roquin-1 proteins and specific primers used for site-directed mutagenesis cloning of both GFP-Roquin-1 variants and the HDR template for *Rc3h1*Mins are shown (**Table 4**).

Table 4: Primers for cloning.

Primer	Sequence (5'-3')	Purpose
K220A	cgcgctgagccgcgcagtgctggtgctg	QC XL II (pRetro)
K239A	atggccaatgctggttgcgctcgcctgcggaaag	QC XL II (pRetro)
Y250A	ggtgcagctgctggctcgcgcgagctgc	QC XL II (pRetro)
R260A	gctgctttaaagtgaccaaagccgatgaagatagcagcc	QC XL II (pRetro)
R510A	cacagtgacacaactgattccagccggcacagaccccagctttg	QC XL II (pCRII TOPO)
R579A	caattcagatggtccctgccggttctcagctatatcc	QC XL II (pCRII TOPO)

Primer sequences used for the initial identification of *Rc3h1*[Mins] alleles from purified gDNA samples are listed in **Table 5** (High Resolution Melting (HRM) primers) and **Table 6** (established genotyping strategy for *Rc3h1* R510A). Of note, HRM was used to identify *Rc3h1*[Mins] founder gDNA heterozygous for the knockin transgene (*Rc3h1*[Mins/+]) and characterized by reduced melting temperatures compared to homozygous *Rc3h1*^{+/+} (wildtype) sequence controls.

Table 5: High Resolution Melting primers.

Primer	Sequence (5'-3')	Purpose
R510A fw	acctcctgcactcccaaatg	HRM (*Rc3h1*[Mins])
R510A rv	aggcggctcagatgttcaaa	HRM (*Rc3h1*[Mins])
R579A fw	ctggaatctgcccctaagag	HRM (*Rc3h1*[Mins])
R579A rv	gctggtaaggtgctgtctca	HRM (*Rc3h1*[Mins])

Table 6: *Rc3h1*[Mins] genotyping primers.

Primer	Sequence (5'-3')	Purpose
R510 common fw	gacccttgagtgcctctttgg	gDNA (*Rc3h1*[Mins])
R510A mut rv	ctggtttcagagaagaatcaaagctggggtctgtgccggc	gDNA (*Rc3h1*[Mins])
R510 wt rv	aagctggggtctgtcccacg	gDNA (*Rc3h1*[Mins])

All relevant primers used for quantitative PCR analyses of RNA levels in *Rc3h1*[Mins] or wildtype control CD4^{+} T cells are shown together with specific identifiers of the UPL probe library system (**Table 7**).

Table 7: Quantitative (q)PCR primer sequences and UPL probes (Roche).

Gene of interest	Primer sequence (5'-3')	# of UPL probe
Hprt for	TCCTCCTCAGACCGCTTTT	95
Hprt rv	CCTGGTTCATCATCGCTAATC	95
Nfkbid for	TTTCTACCCTCCGTCAGACC	9
Nfkbid rv	TACAGCCGGGTATCCAGAGA	9
Tnf for	TCTTCTCATTCCTGCTTGTGG	49
Tnf rv	GGTCTGGGCCATAGAACTGA	49
Tnfrsf4 for	GCTTGGAGTTGACTGTGTTCC	79
Tnfrsf4 rv	GGGTCTGCTTTCCAGATAAGG	79
Ywhaz for	CGCTAATAATGCAGTTACTGAGAGA	2
Ywhaz rv	TTGGAAGGCCGGTTAATTTT	2

2.2. Methods

2.2.1. Mouse models

This work focuses on the analysis of murine primary lymphocytes isolated from different transgenic mouse models (**Table 8**). All mice analyzed were of C57BL/6J genetic background and mice were bred and housed in specific pathogen-free (SPF) barrier facilities in accordance with the respective institutional, state and federal guidelines at the Helmholtz Zentrum München or at the Biomedical Center (BMC) of the Ludwig-Maximilians-Universität München (LMU). All experiments involving mice were performed in accordance with the regulations of and with approval by the local government (Regierung von Oberbayern, ROB). Mice were housed in standard cages on a 12-hour light/dark cycle with *ad libitum* access to food and water.

Transgenic *Rc3h1*^fl/fl and *Rc3h2*^fl/fl mice harbor loxP-sites flanking exon 4 to 6 of the Roquin-1 encoding *Rc3h1* (Bertossi et al., 2011) and loxP-sites flanking exon 4 of the Roquin-2 encoding *Rc3h2* gene (Vogel et al., 2013). *Rc3h1*^fl/fl; *Rc3h2*^fl/fl mice were crossed to *Rc3h1*^+/+; *Rc3h2*^+/+ wildtype mice in different combinations to reach the final set of seven genotypes characterized as the genetic *in vivo* titration of *Rc3h1* and *Rc3h2* alleles. Moreover, mice with loxP-flanked genes were crossed to *Cd4-Cre* (Lee et al., 2001; Sawada et al., 1994). The *Cd4-Cre* transgene drives Cre recombinase expression under control of the *Cd4* promoter and thus conditional deletion of *Rc3h1/2* alleles in the CD4+ and CD8+ T cell lineages. Furthermore, *Rc3h1/2*^fl/fl mice were crossed to *Cd4-Cre-Ert2* mice (Sledzinska et al., 2013) in which Cre recombinase is fused to the estrogen-receptor 2 (ERT2). This transgenic system was used in retroviral reconstitution experiments and allows to induce deletion of loxP-flanked genes in an exclusive CD4+ T cell-specific manner by *in*

vitro treatment with 4'OH-tamoxifen. Transgenic *Rc3h1/2*^{fl/fl}; *Cd4-Cre-Ert2*; *rtTA* mice provided CD4$^+$ T cells for 4'OH-tam-inducible double knockouts (iDKO) of Roquin-1/2 in reconstitution experiments. For this, *Rc3h1/2*^{fl/fl}; *Cd4-Cre-Ert2* mice were crossed with *Gt(ROSA)26*^{Sortm1(rtTA*M2)Jae}, also known as *R26-M2rtTA* knockin, which enables doxycycline-inducible studies utilizing rtTA/tet-ON models (Hochedlinger et al., 2005). The expression of the reverse tetracycline-controlled transactivator (rtTA) allows to perform retroviral overexpression of pRetroX-Tight-Pur vectors (Takara Clontech) encoding for different mutants of GFP-Roquin-1. Here, *in vitro* administration of doxycycline triggers plasmid gene expression controlled by the Tet-responsive promoter in pRetroX-Tight.

Additionally, *Nfkbid*^{fl/fl}; *Cd4-Cre* mice were generated by crossing *Nfkbid*^{fl/fl} with *Cd4-Cre* mice (Lee et al., 2001; Frentzel et al., 2019). A detailed characterization of these mice is described elsewhere. *Nfkbid* mutant mice were bred and maintained under specific pathogen-free conditions at the animal facility of the Helmholtz Centre for Infection Research (Braunschweig, Germany).

2.2.1.1. Targeting strategy of MALT1-insensitive *Rc3h1*^{Mins}

Gene-specific single guide RNAs (sgRNAs) targeting the gene *Rc3h1* (Roquin-1) at sites of R510 or R579 codons, respectively, were *in vitro* tested for efficiency using Cas9$^+$ MEF cell clones. For the generation of the *Rc3h1*^{Mins/Mins} mouse line and in collaboration with Dr. Florian Giesert from the Helmholtz Zentrum München, two functional sgRNAs (i.e. sgRNA_R510: 5'-TGACACAACTGATTCCACGT-3' and sgRNA_R579: 5'-CCAATTCAGATGGTACCTCG-3') were generated from DNA oligonucleotides (Metabion, Planegg/Steinkirchen, Germany) by *in vitro* transcription utilizing the EnGen® sgRNA Synthesis Kit, *S. pyogenes* (New England Biolabs, Ipswich, USA) following manufacturer's instructions. Additionally, a specific targeting template (pCR-Blunt II-TOPO vector; Invitrogen) coding for the two R510A and R579A mutations spanning the genomic region of exon 10, intron 10 and exon 11 was used to perform homology-directed repair (HDR). Prior to pro-nuclear injection, sgRNAs, recombinant Cas9 protein (IDT, Coralville, USA) and the targeting vector were diluted in micro-injection buffer (5 mM Tris, 0.1 mM EDTA, pH 7.2) to reach effective concentrations of 20 ng/µL for each sgRNA, 50 ng/µL for Cas9 and 50 ng/µL for the targeting vector. One-cell embryos were obtained by mating of C57BL/6N males (obtained from Charles River, Sulzbach, Germany) with C57BL/6N females super-ovulated with 5 units of PMSG (Pregnant Mare`s Serum Gonadotropin) and 5 units of HCG (Human Chorionic Gonadotropin). Following pro-nuclear micro-injection, zygotes were transferred into pseudo-pregnant CD1 female mice to obtain live pups. All mice showed normal development and appeared healthy. Handling of animals was performed in accordance to institutional guidelines and approved by the animal welfare committee of the local government (Regierung von Oberbayern). Analysis of gene editing events was performed on genomic DNA isolated from tail or ear biopsies of founder mice and the F1 progeny using the Wizard Genomic DNA Purification Kit (Promega, Mannheim, Germany) following manufacturer's instructions.

Genomic DNA was amplified by High Resolution Melting (HRM) to dissect homozygous wild types (+/+) from heterozygous (Mins/+) Crispr/Cas9 knockins (Light Cycler 480, Roche). Consequently, amplified PCR products were analyzed by agarose gel separation and restriction using NaeI (R510A; NEB) and Cfr10I (R579A; Thermo Scientific) enzymes that specifically targeted base pairs of the introduced repair template but not the wildtype sequence. Heterozygous *Rc3h1*^{Mins/+} knock-in mice were used for interbreedings to generate heterozygous (*Rc3h1*^{Mins/+}) and homozygous (*Rc3h1*^{Mins/Mins}) mice next to WT (*Rc3h1*^{+/+}) littermates.

Table 8: Transgenic mouse lines for *in vitro* and *in vivo* studies.

Mouse line (genotype)	Abbreviation
Cd4-Cre	WT
Cd4-Cre-Ert2	WT
Rc3h1^{fl/fl}; *Rc3h2*^{fl/fl}; *Cd4-Cre*	DKO
Rc3h1^{fl/fl}; *Rc3h2*^{+/+}; *Cd4-Cre*	Roquin-1 KO
Rc3h1^{+/+}; *Rc3h2*^{fl/fl}; *Cd4-Cre*	Roquin-2 KO
Rc3h1^{fl/+}; *Rc3h2*^{fl/fl}; *Cd4-Cre*	Roquin-1 het-KO
Rc3h1^{fl/fl}; *Rc3h2*^{fl/+}; *Cd4-Cre*	Roquin-2 het-KO
Rc3h1^{fl/+}; *Rc3h2*^{fl/+}; *Cd4-Cre*	het-DKO
Rc3h1^{fl/fl}; *Rc3h2*^{fl/fl}; *Cd4-Cre-Ert2*; *rtTA*	iDKO-rtTA
Rc3h1^{+/+}	WT
Rc3h1^{Mins/+}	Mins/+
Rc3h1^{Mins/Mins}	Mins/Mins
Nfkbid^{fl/+}; *Cd4-Cre*	*Nfkbid*^{fl/+}
Nfkbid^{fl/fl}; *Cd4-Cre*	*Nfkbid*^{fl/fl}
OT-II Tcr^{+/-}	WT OT-II
Rc3h1^{Mins/Mins}; *OT-II Tcr*^{+/-}	Mins/Mins OT-II
Nfkbid^{-/-}; *OT-II Tcr*^{+/-}	*Nfkbid*^{-/-} OT-II
Nr4a1-GFP^{+/-}	Nur77

2.2.1.2. Experimental Autoimmune Encephalomyelitis (EAE)

The active EAE disease model was induced on day 0 by subcutaneous (s.c.) injection of 200 µg MOG peptide (Auspep Pty Ltd) emulsified in CFA (BD Difco™ Adjuvants) at the tail base of age-matched mice (Miller et al., 2010). 100 ng of pertussis toxin (PTX, in PBS; Sigma) was intravenously (i.v.) injected on day 0 and on day 2 (200 ng total dose). Mice (9 per group) were checked on a daily basis and scored starting at day 9 after MOG/CFA and PTX injections. Clinical scores were documented up until day 15 after induction resembling the peak of disease scores in wildtype counterparts. On day 15 post immunization, mice were sacrificed by isofluran inhalation, perfused with PBS and CNS samples from spinal cords and brains were isolated for *ex vivo* cell subset analysis. CNS tissue was cut into small pieces and digested by incubation with 1 mg/mL DNase I (Sigma) and 2.5 mg/mL Collagenase D (Sigma) in DMEM medium supplemented with 10% FCS, 100 units/mL penicillin, 100 µg/mL streptomycin, 10 mM HEPES, 50 µM ß-ME, 1x NEAAs for 90 min at 37°C. CNS-infiltrating mononuclear cells were isolated by percoll gradient centrifugation (37%, 70% Percoll in PBS buffer; GE Healthcare). Mononuclear cells were counted, distributed to 96-wells, stimulated with 20 nM PMA and 1 µM ionomycin followed by BrfA treatment (10 µg/mL) for a total of 4 hours and subsequently stained for CD4$^+$ T cell infiltrates and cytokine production using the Foxp3 fixation/permeabilization kit. Flow cytometric analysis was performed with a BD LSR Fortessa (BD) cytometer.

2.2.2. Molecular biology

2.2.2.1. PCR cloning and genotyping

The polymerase chain reaction, abbreviated "PCR", enables exponential amplification of DNA fragments from plasmid or genomic DNA (gDNA) templates. Sequence-specific forward and reverse primers anneal to template DNA at low temperatures, while heat-stable DNA polymerases become activated at elevated cycling temperatures to amplify DNA fragments in a primer-dependent manner. A standard PCR reaction contains approx. 1-100 ng of template DNA, 1x reaction buffer, 1 µL dNTP mix (10 mM stock solution), 1 µL MgCl$_2$ (50 mM), 1-2 µL forward and reverse primer (10 mM each) as well as 1 µL of a DNA polymerase enzyme. In general, PCRs were performed for 25-35 cycles with denaturation at 95°C for 30 seconds, annealing of primers at 50-60°C for 30 seconds and elongation at 70-75°C for 45 seconds.

For cloning of retroviral plasmids, PCR products were size separated by 1% (w/v) agarose gel electrophoresis in 1x TBE buffer and visualized by UV light (Bio-Rad). Correct band sizes for cloning experiments were cut out of agarose gels and DNA amplicons were purified using the QIAGEN gel extraction Kit. Additionally, PCR products of gDNA amplification for genotyping were analyzed using a capillary gel electrophoresis system (QIAxcel).

QuikChange II XL Site-Directed mutagenesis (Agilent Technologies) was used to introduce point mutations within retroviral plasmids (pRetroX-Tight) encoding for GFP-fused Roquin-1 (*Rc3h1*). PCR amplification was conducted with primers containing the mutated sequence flanked by gene-specific sequences 5' and 3' of the mutation and a high-quality proof-reading *Pfu* Ultra Polymerase (supplied with the kit). All mutations in the Roquin-1 sequence of the pRetro-GFP-Roquin-1 reconstitution constructs were generated using step-wise and site-directed mutagenesis reactions.

2.2.2.2. Transformation and bacterial expression plasmids

The chemically competent *E. coli* DH5α strain was used to generate plasmid DNA of all constructs for downstream cell biology applications. For transformation, 50 µL of thawed bacteria suspensions were gently mixed with 2 µL of plasmid DNA and stored on ice for 30 minutes. Subsequently, heat shock transformation (HST) was conducted at 42°C for 30 seconds followed by another incubation on ice for 2 minutes. 100 µL of LB medium were added and *E. coli* DH5α cells were further incubated for 1 hour at 37°C. Finally, *E. coli* DH5α cells were plated onto antibiotic-loaded (100 µg/mL) LB plates over night at 37°C and antibiotic selection of transformed DH5α cells was performed according to plasmid-specific resistance genes.

Small- or large scale *E. coli* DH5α cultures (4 or 250 mL, respectively) in LB medium supplemented with the appropriate antibiotics (e.g. 100 µg/mL ampicillin) were incubated over night at 37°C and shaking at 160 rpm. *E. coli* DH5α cultures were harvested by centrifugation at 4.122 x*g*, 4°C, and plasmids were isolated using either the PureYield Plasmid Miniprep System (Promega) or the Nucleobond Xtra Maxi kit for DNA isolation (Macherey Nagel). Analysis of plasmid DNA fragments was performed by agarose gel electrophoresis (1% w/v agarose in TBE buffer) containing 0.5 µg/mL ethidium bromide. Size-separated DNA bands were visualized under UV light (254 – 366 nm, Bio-Rad).

Retroviral pRetroX-Tight expression plasmids (Takara Clontech) have been utilized for murine CD4^{+} T cell reconstitution experiments. The single GFP coding sequence (CDS) or the murine CDS of Roquin-1 N-terminally fused to GFP were previously inserted into pRetroX-Tight vectors allowing gene expression under the control of a Tet-responsive promotor (Tet-On). Single, double or triple mutations in the CDS of Roquin-1 (e.g. K220A, K239A, R260A) were step-wise inserted by site-directed QuikChange XL II mutagenesis (Agilent Technologies). Retrovirus was generated according to section 2.2.3.7.

2.2.3. Cell biology

2.2.3.1. Cultivation of mammalian cell lines

Two different immortalized and adherent mammalian model cell lines, human embryonic kidney (HEK293) and mouse embryonic fibroblasts (MEF), were cultured in round flat-bottom culture dishes at 37°C and constant 10% CO_2 levels to maintain pH 7.0 conditions and humidity within the cell incubator. The HEK293 cell line was originally established from a human primary embryonal kidney transformed by adenovirus type 5 (Ad 5). Adherent cell lines were cultivated in DMEM medium containing 10% fetal calf serum (FCS), 100 units/mL penicillin, 100 µg/mL streptomycin (Pen-Strep) and 1% HEPES buffer. Splitting of adherent cells was carried out by discarding old medium by vacuum, washing cells with 1x PBS buffer and resuspending cells in DMEM after detachment by Trypsin-EDTA incubation. Given an estimated doubling time of 24-30 hours, confluent HEK293 cells were regularly split every 3-4 days with maximum densities up to 3 x10^6 cells/mL.

Table 9: Immortalized cell lines for *in vitro* studies.

Mammalian cell line	Abbreviation
Human embryonic kidney cells 293	HEK293
Mouse embryonic fibroblast cells	MEF (Cas9+)

Eukaryotic cell suspensions of either organ-isolated murine lymphocytes or of immortalized adherent cell lines (HEK, MEF) were counted with the CASY cell counter or a Neubauer counting chamber. Automatic identification of viable cells (CASY) or a cell suspension mixture with Trypan blue (Neubauer) allowed to calculate absolute cell numbers and cell concentrations (e.g. 1-10 x10^6 cells/mL). For freezing of immortalized mammalian cells, ideal cell numbers were centrifuged (500 *xg*, 5 minutes) and washed once with ice-cold PBS. Cell pellets were resuspended in 1 mL of 10% DMSO in FCS and stored over night at -80°C in a 2-propanol freezing container. For prolonged storage, frozen cell tubes were transferred to a liquid nitrogen tank (-150°C, Thermo Scientific).

2.2.3.2. Isolation and cultivation of primary CD4+ T cells

Primary CD4+ T cells were derived from mice sacrificed at ages of 8-12 weeks by gradual CO_2 euthanasia and spleens as well as axillary, cervical, inguinal and mesenteric lymph nodes were surgically prepared for downstream lymphocyte isolation on ice. For lymphocyte phenotyping by flow cytometry, individual organs including spleen, thymus, lymph nodes, Peyer's Patches or CNS (brain, spinal cord) were separately prepared to isolate single cell suspensions for antibody

stainings in 96-wells. For *in vitro* cultivation, squished organs were passed through 100 µm nylon filters while rinsing with T cell isolation buffer (PBS supplemented with 2% FCS and 1 mM EDTA) and erythrocytes were lysed by Tris ammonium chloride (TAC) lysis buffer incubation for 5 minutes at room temperature. Following centrifugation (500 xg, 5 minutes, 4°C) and resuspension in isolation buffer, cells were again passed through 40 µm filters to ensure homogeneous cell suspensions. Lymphocytes were either counted and directly used for flow cytometric analysis or CD4+ T cells were bead-isolated by negative selection according to the EasySep™ Mouse CD4+ T Cell Isolation Kit protocol (STEMCELL). 4-5 x10^6 CD4+ T cells were activated in 6-wells *in vitro* by plate-bound and goat anti-hamster IgG-crosslinked (MP Biomedicals, #56984) anti-CD3 (0.25 µg/mL; clone 2C11) and anti-CD28 antibodies (2.5 µg/mL; clone 37.5N). Cells were cultivated in Th1-polarizing DMEM medium (Gibco) supplemented with 10% FCS, 100 units/mL penicillin, 100 µg/mL streptomycin, 10 mM HEPES, 50 µM β-mercaptoethanol (β-ME), 1x non-essential amino acids (NEAAs) as well as 10 µg/mL anti-IL-4 and 10 ng/mL IL-12. After 40-48 hours of activation, cells were resuspend in DMEM medium containing 200 units/mL IL-2 to expand Th1 cultures at cell desities of 1 x10^6 cells/mL. On day 6 of CD4+ Th1 cell culture for the *Rc3h1* and *Rc3h2 in vivo* titration, cells were either prepared for flow cytometric target analysis by antibody stainings or flash-frozen in equal numbers to collect samples for bulk protein detection by Western blotting.

2.2.3.3. *In vitro* differentiation and CD4+ T cell stimulation

200,000 naive CD4+ T cells from spleens and peripheral lymph nodes of indicated genotypes were activated in 96-wells *in vitro* by plate-bound and IgG-crosslinked anti-CD3 (0.25 µg/mL) and anti-CD28 (2.5 µg/mL) antibodies. Naive CD4+ T cells were cultivated for 3.5 days upon Th0 (no cytokines, no blocking antibodies), Th1 (10 µg/mL anti-IL-4, 10 ng/mL IL-12), Th17 (10 µg/mL anti-IL-4, 10 µg/mL anti-IL-12, 10 ng/mL TGF-β, 60 ng/mL IL-6, 5 µg/mL anti-IFN-γ) or iTreg (10 ng/mL TGF-β, 10 µg/mL anti-IL-4, 5 µg/mL anti-IFN-γ) polarizing conditions in DMEM medium supplemented with 10% FCS, 100 units/mL penicillin, 100 µg/mL streptomycin, 10 mM HEPES, 50 µM β-ME and 1x NEAAs. On day 2 of differentiation, cells were split 1:2 by adding DMEM medium without additional cytokines. Differentiated cells were washed with cold PBS and subsequently stimulated for 2.5 hours with 20 nM PMA and 1 µM ionomycin (250 µL per well) followed by another 2.5 hours of incubation with additional 10 µg/mL BrfA (300 µL per well) to stall cytokines within T cells. After restimulation, cells were washed in PBS and stained according to section 2.2.3.11. In contrast, iTreg differentiation was analyzed without restimulation. Inhibition of MALT1 protease activity was achieved by mepazine treatment (20 µM, EMD Millipore (Merck)) of CD4+ T cells for 180 min at 37°C before stimulation with PMA/ionomycin for 2 hours (target analysis).

2.2.3.4. OT-II co-culture

Bone marrow (BM) cells from tibia and femur of wildtype mice were differentiated to mature BM-derived dendritic cells (BMDCs) for 6 days in DMEM medium supplemented with 10% FCS, 100 units/mL penicillin, 100 µg/mL streptomycin, 10 mM HEPES, 50 µM ß-ME, 1x NEAAs and 20 ng/mL GM-CSF (Cell Signaling Technologies) at 37°C 5% CO_2 (Madaan et al., 2014). On day 6 of differentiation, lipopolysaccharide (LPS, 100 ng/mL, Sigma) was added for a 24-hour incubation. Mature BMDCs were washed twice in medium, analyzed for DC surface markers incl. CD11c as well as MHC II and subsequently loaded at 1 x10^6 cells/mL with different concentrations of ovalbumin peptides, $OVA_{323-339}$ (wild type or R9 mutant; BIO TREND), for 2-3 hours at 37°C 5% CO_2. Afterwards, BMDCs were washed twice in 10 mL medium and used for co-cultures with magnetic bead-isolated naive CD4$^+$ OT-II T cells at cell-to-cell ratios of 1:1 using 50,000 cells each in 100 µL cultures of flat-bottom 96-wells. Target analysis was conducted after 18 hours of co-culture in medium without any cytokine supplementation (Th0 conditions), while differentiation was analyzed after 3.5 days of co-culture including *in vitro* incubation with or without Th1 (10 µg/mL anti-IL-4, 10 ng/mL IL-12) or Th17 (10 µg/mL anti-IL-4, 10 µg/mL anti-IL-12, 10 ng/mL TGF-β, 60 ng/mL IL-6, 5 µg/mL anti-IFN-γ) antibody/cytokine mixtures to stimulate T helper polarization. Differentiated cells were washed with cold PBS and subsequently stimulated for 2.5 hours with 20 nM PMA and 1 µM ionomycin (250 µL per well) followed by another 2.5 hours of incubation with additional 10 µg/mL Brefeldin A (BrfA, 300 µL per well) to stall cytokines within T cells. After restimulation, OT-II T cells were washed in PBS and stained according to section 2.2.3.11. using anti-TCR Vα2 and anti-TCR Vβ5 surface expression to identify OT-II T cells. Transcription factor analysis was carried out without restimulation and using the Foxp3 kit for fixation and permeabilization of OT-II T cells.

2.2.3.5. Transfection of HEK cells and virus production

Integration of transgenes into adherent MEF cells or primary CD4$^+$ T cells was conducted by retroviral transduction of *E. coli* DH5α-derived plasmids (S1). Retrovirus was produced by calcium-phosphate ($CaPO_4$) transfection of HEK293 cells using MSCV or pRetroX-Tight plasmids containing SV40 promoters and the transgene (sgRNAs or GFP-Roquin-1, respectively) flanked by long terminal repeat (LTR) sequences. Cells were co-transfected with a viral pCl-Eco vector expressing packaging and envelope genes (*gag-pol* and *env*). 8 x10^6 HEK293 cells were seeded into flat-bottom culture dishes for 18 hours before transfection. Next, medium was replaced by 17 ml DMEM supplemented with chloroquine (100 µM) and incubated for 1 hour at 37°C, 10% CO_2. In parallel, transfection mixtures were prepared by mixing 50 µg of plasmid DNA with 5 µg of the packaging vector pCl-Eco, 125 µL of a $CaCl_2$ stock and autoclaved H_2O (1250 µL in total). The plasmid DNA and $CaCl_2$ mixture was then homogenized with 1250 µl HBS (pH 6.95 - 7.05) while constantly vortexing. DNA precipitates were added dropwise to HEK cells after a 20-minute

incubation at RT and DMEM medium exchange was performed 5-6 hours post addition of DNA precipitates. After 48 hours, HEK cell supernatants containing retrovirus particles were syringe-harvested and passed through 0.45 µm syringe filters to be directly used to transduce MEF or CD4+ T cells.

2.2.3.9. Retroviral reconstitution with GFP-Roquin-1

CD4+ T cells derived from *Rc3h1*fl/fl; *Rc3h2*fl/fl; *Cd4-Cre-Ert2*; *rtTA* mice (iDKO, rtTA) were treated on day 0 with 1 µM 4'-OH-tamoxifen for 24 hours at 37°C 5% CO_2 to induce deletion of loxP-flanked *Rc3h1* and *Rc3h2* genes. Subsequently, cells were washed once with medium and *in vitro* activated on day 1 with plate-bound IgG-crosslinked anti-CD3 (0.25 µg/mL) and anti-CD28 antibodies (2.5 µg/mL) upon Th1-polarizing conditions in 6-wells for 40 hours. Retroviral transduction of CD4+ T cells was performed during T cell activation. In parallel, HEK293 cell transfections were used for virus production (see section 2.2.3.5.) of pRetroX-Tight vectors encoding GFP-Roquin-1 proteins (wildtype control or ROQ mutants).

On day 3, virus particles were harvested from HEK293 cell supernatants by 0.45 µm-filtration, mixed with with 10 µg/mL polybrene and applied to iDKO CD4+ T cells. After spin-inoculation for 1 hour at 2,000 rpm 18°C, CD4+ T cells were incubated for approx. 5-7 hours at 37°C 5% CO_2 and then supplied with fresh DMEM medium containing 200 units/mL IL-2. On day 4, T cells were treated with 1 µg/mL doxycycline (DOX) for 16 hours at 37°C 5% CO_2 to induce GFP-Roquin-1 expression via the plasmid-encoded Tet promoter and reverse tetracycline-dependent transactivator (rtTA) activity. On day 5, DOX-induced GFP-Roquin-1 reconstitution was checked by microscopy and Roquin target stainings were performed using APC/AF647-conjugated antibodies to reduce technical variations. Gate slices reflecting graded GFP-Roquin-1 reconstitution levels were separately applied for each replicate experiment and are shown as exemplified in **Figure 6**. Flow cytometric analyses were performed with a BD FACSCanto (BD) cytometer.

2.2.3.10. Screening of sgRNA efficiencies in MEF cells

5 x10^4 MEF cells stably expressing the Cas9 endonuclease were seeded in 6-wells and incubated for 18 hours at 37°C, 5% CO_2. Next, cells were spin-infected at 300 *xg* at 32°C for 2 hours with MSCV retrovirus supernatants of the respective sgRNA oligos and cells were simultaneously treated with 5 µg/mL polybrene. After 6 hours of incubation at 37°C, 5% CO_2, virus supernatant was exchanged with standard DMEM medium. Transduction efficiency and sgRNA abundance was evaluated by flow cytometric detection of the congenic plasmid marker Thy1.1 (MSCV reporter). Downstream testing for Cas9/sgRNA activities as measured by deletion of Roquin-1 was performed via Western blot detection of Roquin-1/2 proteins using the in-house Roquin primary antibody, clone 3F12 (isotype IgG2a).

2.2.3.11. Antibody stainings for flow cytometry

For flow cytometric immunophenotyping, organs and lymph nodes from sacrificed mice were prepared and squished through 100 µm filters while rinsing with FACS buffer (PBS supplemented with 2% FCS, 2 mM EDTA and 0.01% NaN_3) and erythrocytes were removed by incubation with TAC-lysis buffer (13 mM Tris, 140 mM NH_4Cl, pH 7.2). All cell stainings with fluorophore-conjugated antibodies, tetramers or viability dyes were performed in 96-well v-bottom plates with effective staining volumes inbetween 50-100 µL per well. Single cell suspensions of isolated lymphocytes were washed in PBS and stained for viability for 20 minutes protected from light at 4°C (Fixable Viability dye (eF780), LIVE/DEAD Fixable Blue (Invitrogen)). Viability dyes were washed off the cells once by addition of PBS and cell suspensions were subsequently stained with fluorophore-conjugated antibodies or tetramers (50 µL FACS buffer per well) to detect surface proteins. Fixation of cells was realized by either adding 100 µL of 2% formaldehyde (FA) or 100 µL of the Foxp3 Fix/Perm buffer (Invivogen) for 20 minutes at 4°C.

Intracellular stainings with in-house hybridoma supernatant antibodies or directly conjugated commercial antibodies were performed after permeabilization in 0.5% Saponin and 1% BSA in PBS or Foxp3 staining kit permeabilization buffer (Invivogen) for 40 minutes at 4°C. Stained cells were once more pelleted by centrifugation and washed with FACS buffer. Stained cell suspensions of approx. 150 µL in FACS buffer were acquired at either the BD LSRFortessa (5-laser), the BD FACSCanto (3-laser) or the Cytoflex S (4-laser, Beckman Coulter) flow cytometers. Repeated experiments and replicates of different days were acquired at standardized laser settings for FSC, SSC and compensation channels to minimize technical variabilities. Data derived from the descibed cell-based experiments was processed with the Single Cell Analysis Software FlowJo V10.6 (FlowJo, LLC, OR, USA). All antibodies or tetramers used for immunophenotyping and flow cytometric analysis are listed in section 2.1.4. (**Table 1**). Of note, all lymphocyte populations analyzed by flow cytometry were gated according to standardized strategies which included (i) initial SSC-A vs. FSC-A gates, (ii) single cell FSC-W vs. FSC-H gates, (iii) single cell SSC-W vs. SSC-H and (iv) live/dead staining gates to only select viable single cells for downstream phenotypic analyses.

2.2.4. Biochemical methods

2.2.4.1. Cell lysis, SDS-PAGE and Western blotting

T cell lysis was performed with PBS-washed pellets in Meister lysis buffer just-in-time supplemented with 1x cOmplete, EDTA-free protease inhibitor cocktail (Roche) and dithiothreitol (DTT). Lysis buffer exceeded pellet sizes by 2-fold to ensure homogeneous resuspension of cells. After 15 minutes on ice (4°C) with repeated vortexing to mix the suspension, cells were centrifuged at 10,000 x*g* for 15 minutes at 4°C to extract protein lysate supernatants from cellular debris.

Supernatant protein concentration was photometrically determined using a Bio-Rad protein assay (Bradford reagent) according to the Lambert-Beer law and a BSA protein standard.

Equal amounts of protein lysates (30-50 µg) were analyzed by SDS-PAGE (sodium dodecyl sulfate - polyacrylamide gel electrophoresis) in which denatured proteins are passively separated via SDS-induced negative charge. For this, lysates were denatured at 95°C for 5 minutes in 1x laemmli loading buffer (incl. 10% β-ME), loaded onto 10% acrylamide gels and size-separated next to the pre-stained protein marker VI (10-245 kDa, AppliChem). Gels were run at 120 V for approx. 40 minutes and size-separated proteins were electrophoretically transferred onto MeOH-activated PVDF membranes by wet-blotting over night at 40 V and 4°C (Bio-Rad transfer system). After 2 hours of membrane blocking in 5% milk powder in TBS, primary antibodies were applied in either 1% milk powder in TBS-T (e.g. clones 3F12, 15D11, 4C1) or 5% BSA in TBS-T (e.g. GAPDH, IRF4 P173) for over night immuno-blot incubation at 4°C. Before adding secondary HRP-conjugated antibodies (anti-rat, anti-rabbit or anti-mouse) diluted in 1% milk powder in TBS-T for 1.5 hours at RT, membranes were washed three times for approx. 10 minutes with TBS-T containing 1% milk powder. Finally, PVDF membranes were washed three times with TBS-T and immuno-blot signals were analyzed by incubation with different ECL Western blotting reagents (Novex Invitrogen, Amersham GE Healthcare) for HRP-dependent chemiluminescence visualized by exposure to medical X-ray films (DV-B) while proteced from external light. X-ray films were developed using the Optimax X-ray processor (PROTEC). All antibodies used for Western blotting are listed in section 2.1.4. (**Table 2**).

2.2.4.2. RNA isolation and qPCR

Isolation of RNA from pelleted CD4$^+$ T cells was performed by phenol-chloroform extraction using TRIzol (Ambion). RNA quality and yield was measured by spectrophotometry and RNA was then reverse transcribed into cDNA utilizing a reverse transcriptase and the QuantiTect Reverse Transcription Kit (Qiagen) that as well removes trace-amounts of genomic DNA. Probe-based quantitative real-time gene expression (RT-qPCR) was performed with the Universal Probe Library (UPL) system using the Light Cycler® 480 II device (Roche) and intron spanning assays correcting for primer efficiency. Gene-specific amplification of short oligonucleotides corresponds to binding of individual fluorescent probes. Fluorescent signals increase with amplicon abundance and thus reflect expression levels of targeted cDNAs or mRNAs, respectively. In collaboration with Dr. Kai Höfig, Helmholtz Zentrum München, target gene results were normalized to two different house-keeping reference genes *Ywhaz* or *Hprt*, respectively. Target-specific primer sequences and the appropriate UPL probe numbers are shown in section 2.1.6. (**Table 7**).

2.2.4.3. Generation of antibodies

For the generation of the 5F6 anti-Roquin-1 aa1-510 antibody and in collaboration with Dr. Regina Feederle at the Helmholtz Zentrum München, rats were immunized with an ovalbumin-coupled peptide representing the free carboxy-terminus at arginine R510 which results from MALT1 cleavage of Roquin-1 (i.e. OVA-TVTQLIPR). Monoclonal antibodies from hybridoma supernatants were screened by flow cytometry for antibodies recognizing bead-coupled peptides with a free carboxy-terminus (biot-TVTQLIPR) but not a hexa-histidine-conjugated carboxy terminus (biot-TVTQLIPRHHHHHH). Validation of candidates was achieved by testing recognition of ectopic expression of Roquin-1 aa1-510 but not Roquin-1 full-length in transfected HEK293 cells. Endogenous antibody activity was tested using PMA/ionomycin-treated CD4$^+$ T cells of wildtype or Roquin-deficient DKO^T mice. All cleavage experiments were performed with 5F6 hybridoma supernatant (rat IgG2a/k, 1:2 dilution). For the generation of the 4C1 anti-IκB$_{NS}$ antibody, rats were immunized with a GST-fused version of murine IκB$_{NS}$ (*Nfkbid*). Monoclonal antibodies from hybridoma supernatants were screened for antibodies recognizing purified protein in ELISA and ectopic expression of IκB$_{NS}$ in transfected HEK293 cells using a LZRSp-Nfkbid-IRES-GFP construct (Fiorini et al., 2002). Monoclonal antibodies were tested for application in Western blotting and flow cytometry. Experiments were performed with supernatants containing the IκB$_{NS}$ 4C1 antibody (rat IgG2a/k).

3. Results

3.1. Roquin function and TCR signal strength

Hypomorphic mutations in the *Rc3h1* gene and deficiency in both Roquin-1/2 proteins are associated with the development of severe autoimmune or autoinflammatory diseases. The dysregulation of immune homeostasis has been attributed to derepression of mRNA targets leading to excessive T cell activation and differentiation towards Tfh and either Th1 or Th17 cells. The first section of this chapter will highlight how loss of Roquin expression or mutations in its ROQ domain as well as antigen-induced TCR signals and Roquin-1 cleavage determine preferential mRNA target derepression that is linked to the specific differentiation of Th17 cells.

3.1.1. Titration of *Rc3h1* and *Rc3h2* genes affects target regulation

Roquin-1/2 cleavage by MALT1 activity has been linked to TCR signaling, thus amounts of full-length Roquin are believed to decrease in expression levels as T cell activation proceeds. To test the hypothesis that graded inactivation of the system by conditional gene targeting would differentially affect Th17-specific mRNA target regulation, the *Cd4-Cre* transgene was combined with different floxed (fl) or wildtype alleles of *Rc3h1* and *Rc3h2*. Increasingly inactivating redundant Roquin paralog function, the genetic titration of Roquin alleles mimicked graded loss of Roquin availability in CD4$^+$ T cells.

Different combinations of mono-allelic deletions allowed to encompass a spectrum of seven genotypes resembling an *in vivo* titration of Roquin. Indeed, Roquin protein levels were reduced with increased introduction of allelic deletion and immunoblots of Roquin-1 knockout CD4$^+$ T cells still expressed Roquin-2 to levels similar to wildtype counterparts (**Fig. 1A**). Herein, Roquin-1 outcompeted Roquin-2 expression by at least 5-fold (Vogel et al., 2013; Heissmeyer and Vogel, 2013). More importantly, graded loss of Roquin expression in *in vitro* cultured Th1 cells was accompanied by endogenous target derepression of Regnase-1, IκB$_{NS}$ and IRF4 (**Fig. 1A**). Herein, heterozygous deletion of Roquin alleles did not sufficiently induce direct targets, but homozygous deletion of both Roquin-1 alleles and additional inactivation of Roquin-2 alleles accompanied gradual target derepression (**Fig. 1A**).
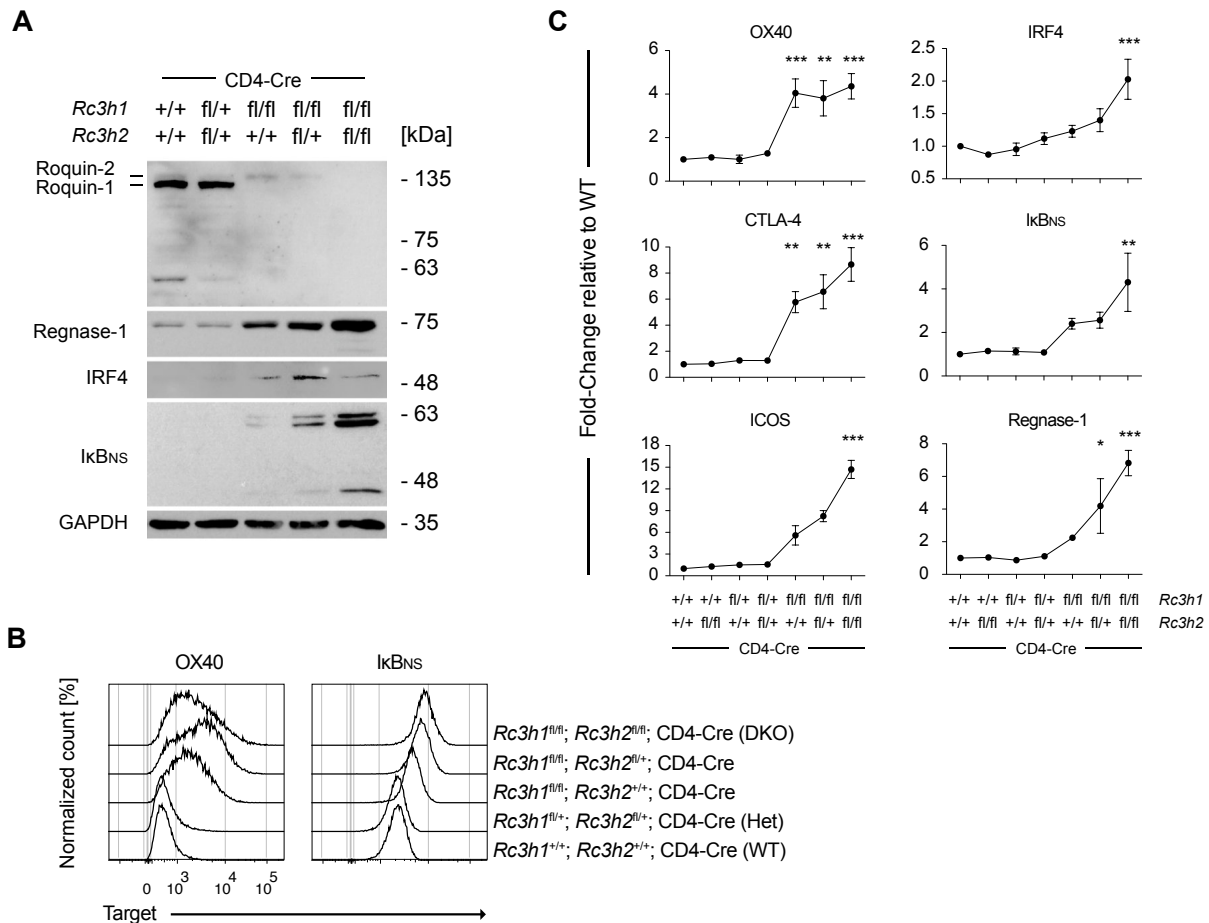
Fig. 1: Graded genetic inactivation of Roquin-1/2 in CD4$^+$ T cells has differential effects on derepression of target mRNAs. (**A**) Western blot analysis for Roquin-1/2, Regnase-1, IRF4 and IκB$_{NS}$ from Th1-polarized CD4$^+$ T cells after a 6-day *in vitro* culture of indicated genotypes including WT (*Rc3h1$^{+/+}$*; *Rc3h2$^{+/+}$*) and Roquin-1/2-deficient (*Rc3h1$^{fl/fl}$*; *Rc3h2$^{fl/fl}$*). A representative of 3 individual experiments is shown. (**B**) Flow cytometry histograms for OX40 and IκB$_{NS}$ expression in Th1-polarized CD4$^+$ T cells of indicated genotypes from day 6 *in vitro* cultures as described in (A), a representative of 5 experiments is shown. (**C**) Fold-change quantification of geometric mean fluorescence intensities (gMFI) of indicated Roquin target proteins as in (A, B). Error bars represent ± SEM of 3-5 replicates per group and statistical analysis was performed by One-Way ANOVA and Dunnett's Multiple Comparison test; *p* values *< 0.05, **< 0.01, ***< 0.001.

On the cellular level, OX40 and IκB$_{NS}$ revealed differential kinetics of binary or graded derepression with increased deletion of Roquin expression (**Fig. 1B**). In general, ICOS, IRF4, IκB$_{NS}$ and Regnase-1 showed regulatory profiles different from OX40 and CTLA-4 (**Fig. 1C**). Already low levels of Roquin deletion triggered maximum derepression of OX40 and CTLA-4 in CD4$^+$ T cells lacking only Roquin-1. All other mRNA targets remained repressed up until additional inactivation of Roquin-2 alleles indicating a broad dynamic range of regulation with potential avidity effects (**Fig. 1B, C**). Hence, these data indicate that the amount of Roquin in resting CD4$^+$ T cells is 2-5 times higher than it is required for full repression of its direct mRNA targets which showed variable responses with respect to graded inactivation of Roquin paralogs.

The in-house produced 3F12 anti-Roquin antibody recognized both paralogs similarly, despite three amino acid exchanges being present in or close to the epitope in Roquin-2 (epitope mapping in Fig. 2A was performed by Laura Selina de Jonge). Distinct amino acid changes of Roquin-1 and Roquin-2 are highlighted (**Fig. 2A, B**) and HEK cells transfected with either GFP-Roquin-1^{WT} or GFP-Roquin-1$^{mut\ (62/63/68)}$ were checked for 3F12-dependent recognition of ectopic Roquin expression (**Fig. 2C, D**).
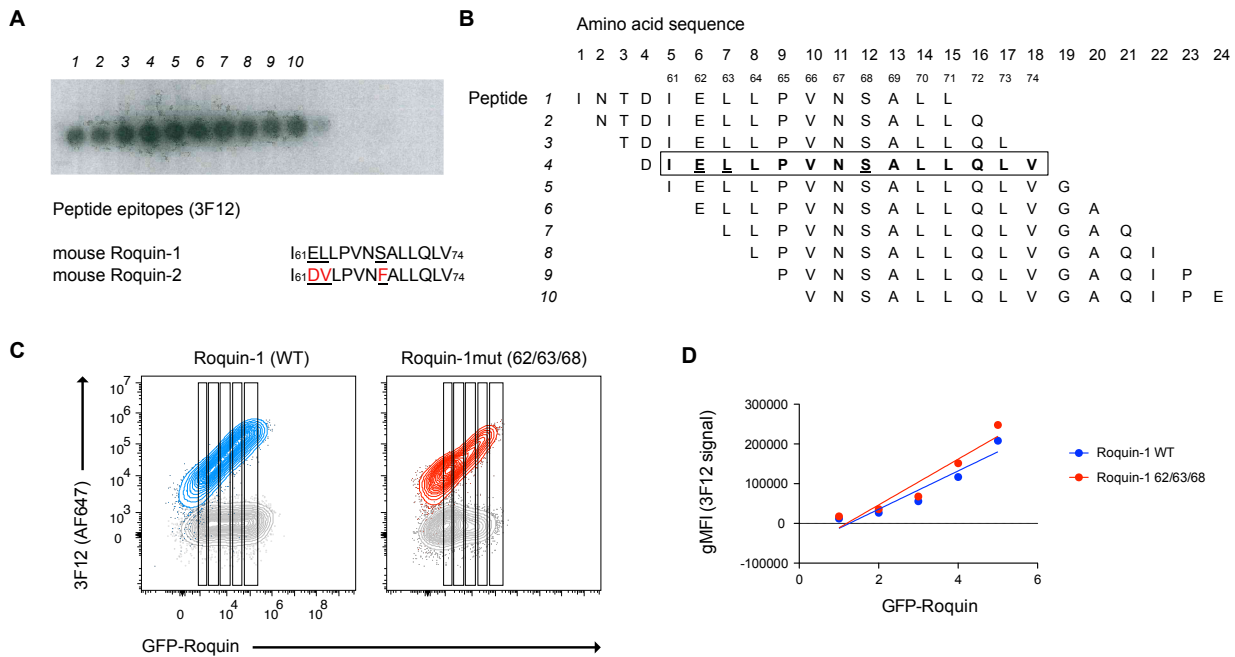
Fig. 2: Epitope mapping for the 3F12 monoclonal anti-Roquin-1/2 antibody. (**A**) Epitope mapping of the Roquin-1 binding site for the rat 3F12 monoclonal antibody. 10 different peptides (amino acids 61-74 of mouse Roquin-1) with the indicated 15 amino acid sequences (**B**) were immobilized on a nitrocellulose membrane and tested as possible binding epitopes. Detection of 3F12 binding was performed with an HRP-conjugated anti-rat secondary antibody, and altered amino acids 62, 63 and 68 in the Roquin-2 epitope sequence are underlined. (**C**) Intracellular detection of Roquin-1 with the 3F12 mAb in HEK293 cells transfected with constructs for GFP-Roquin-1^{WT} (blue) or GFP-Roquin-1$^{mut\ (62/63/68)}$ (red) changing amino acids E62D, L63V and S68F of the 3F12 antigen into the corresponding Roquin-2 epitope showing an overlay of transfected cells with untransfected cells (grey). (**D**) Quantification of (C) as linear regression fit using 5 gates (shown in C) of differential GFP-Roquin expression to analyze graded increase in 3F12 antibody signals.

Expression levels of IκB$_{NS}$ were evaluated using a new monoclonal antibody (mAb) detecting mouse IκB$_{NS}$ in immunoblots and flow cytometry that was established in collaboration with the group of Prof. Ingo Schmitz (**Fig. 3**). The 4C1 mAb recognized ectopic expression of FLAG-tagged mouse IκB$_{NS}$ in HEK293T cells (**Fig. 3A**) and was specific for the recognition of endogenous IκB$_{NS}$ induction following P/I stimulation of lymphocytes or A20 B cells (**Fig. 3B, C**) and following OVA peptide-dependent activation of OT-II T cells (**Fig. 3D**).
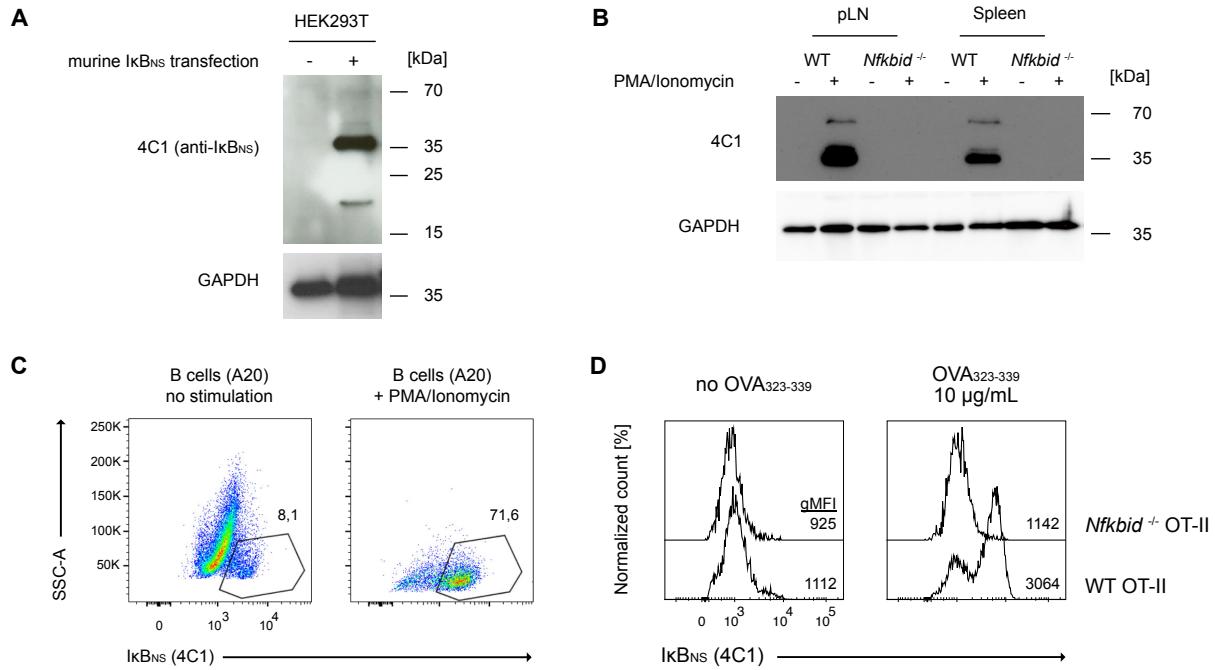
Fig. 3: Characterization of the 4C1 monoclonal anti-IκB_NS antibody. (**A**) Western blot analysis of IκB_NS using the monoclonal antibody 4C1 on extracts from HEK293T cells with and without transfection with a pcDNA3.1-IκB_NS-Flag construct. (**B**) Lymph node cells and splenocytes from WT or *Nfkbid* kockout mice were stimulated with PMA/ionomycin for 2.5 hours or left untreated and extracts were analyzed for IκB_NS expression with the 4C1 primary antibody in Western blotting as in (A). (**C**) The murine B cell line A20, endogenously expressing IκB_NS, was stimulated or not with PMA/ionomycin for 2.5 hours. Intracellular FACS stainings were performed using the primary 4C1 monoclonal antibody with a FITC-conjugated anti-rat secondary antibody. (**D**) Co-culture of WT or *Nfkbid*^{-/-} OT-II transgenic T cells with OVA$_{323-339}$ peptide-loaded BMDCs to test activation-dependent induction of IκB_NS in WT cells compared to kockout controls with 4C1 stainings against IκB_NS; a representative of 3 replicates is shown.

3.1.2. Functional ROQ-CDE avidities guide target regulation

In view of variable target mRNA regulation according to decreased amounts of Roquin levels, it was hypothesized that the molecular basis for graded target derepression is shaped by the binding site affinities of mRNA 3'-UTRs and their individual recognition by the RNA-binding domain of Roquin (ROQ domain). For this, site-directed mutagenesis of residues in the ROQ domain of Roquin-1 (K220A, K239A, Y250A and R260A) was analyzed with respect to functional relevance for mRNA regulation contributing to binding of CDE-, ADE- and LBE-type motifs. Indeed, mutations within the RNA-binding ROQ domain of Roquin-1, which are invariantly present in Roquin-2, substantially affected the affinity/avidity of particular mRNA-ROQ interactions.

Retroviral reconstitution assays were carried out in CD4^{+} T cells derived from Cd4-Cre-ERT2 mice (Sledzinska et al., 2013). Floxed alleles of both Roquin-1 and Roquin-2 were deleted by *in vitro* treatment with 4'OH-tamoxifen (iDKO T cells) and retroviral vectors encoding either GFP-Roquin-1[WT] or single, double or triple ROQ domain mutants were transduced to reexpress

Roquin-1 variants in a doxycycline-inducible manner (experimental outline depicted in **Fig. 4A**). Prior to flow cytometric target analysis, Roquin deletion was checked by intracellular staining with the 3F12 mAb indicating CD4$^+$ iDKO^T cells lacking endogenous Roquin expression (**Fig. 4B**).
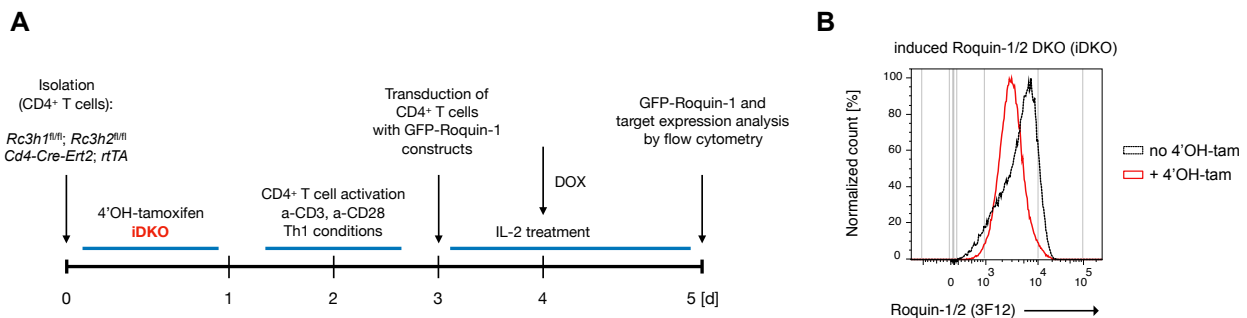
Fig. 4: Workflow of retroviral reconstitutions with GFP-Roquin-1 and *in vitro* deletion of Roquin-1/2 by 4'OH-tamoxifen. (**A**) Representative scheme illustrating the workflow of all reconstitution experiments. (**B**) 24-hour *in vitro* treatment of *Rc3h1/2*$^{fl/fl}$; *CD4-Cre-Ert2*; *rtTA* CD4$^+$ T cells with 4'OH-tamoxifen induces deletion of both Roquin-1/2 proteins (iDKO). The histogram shows intracellular anti-Roquin stainings using the 3F12 monoclonal antibody.

All GFP-Roquin-1 mutants were expressed equally well and they partially retained mRNA target-specific repressive capacities (**Fig. 5A**). The induction of Roquin-1/2 knockouts (iDKO) indeed led to maximum upregulation of target expression while CD4$^+$ T cells reconstituted with increasing amounts of GFP-Roquin-1^{WT} gradually repressed targets back to endogenous wildtype levels (**Fig. 5A**). In reconstitutions with ROQ mutants, however, these repressive effects on target expression were attenuated if not even completely absent as in the case of the triple alanine mutant (K220A; K239A; R260A). Target-specific affinities were revealed in these reconstitutions. It became evident that especially OX40 expression was only genuinely repressed by GFP-Roquin-1^{WT} but not any other mutant variants while particularly IκB$_{NS}$ remained repressed by all single and the double (K220A; R260A) mutants (**Fig. 5A**).

Target expression was additionally analyzed in eight intervals of increasing GFP expression, with individual target signals normalized to target levels in GFP-negative iDKO cells (**Fig. 6**). Each gate represents increasing expression of a particular GFP-Roquin-1 variant which allowed to characterize target repression according to qualitative changes in the mRNA-ROQ interaction. Both OX40 and IκB$_{NS}$ were not repressed by the triple alanine mutant, while effects on ICOS and Regnase-1 were intermediate (**Fig. 5B**). The double mutant (K220A; R260A) as well partially repressed ICOS and Regnase-1, was fully active to repress IκB$_{NS}$ but almost inactive to repress OX40. Moreover, comparing all single mutants, the R260A mutant was intermediate for OX40 and ICOS, while Regnase-1 and IκB$_{NS}$ remained repressed. Interestingly, the Y250A mutation that is involved in the interaction with ADE stem-loops identified in the Ox40 3'-UTR, indeed majorly affected OX40 regulation almost independent of reconstitution levels (**Fig. 5B**). The other targets ICOS, Regnase-1 and IκB$_{NS}$ still showed repression with single mutant reconstitutions, although ICOS was only partially repressed by the Y250A mutant (**Fig. 6B**).
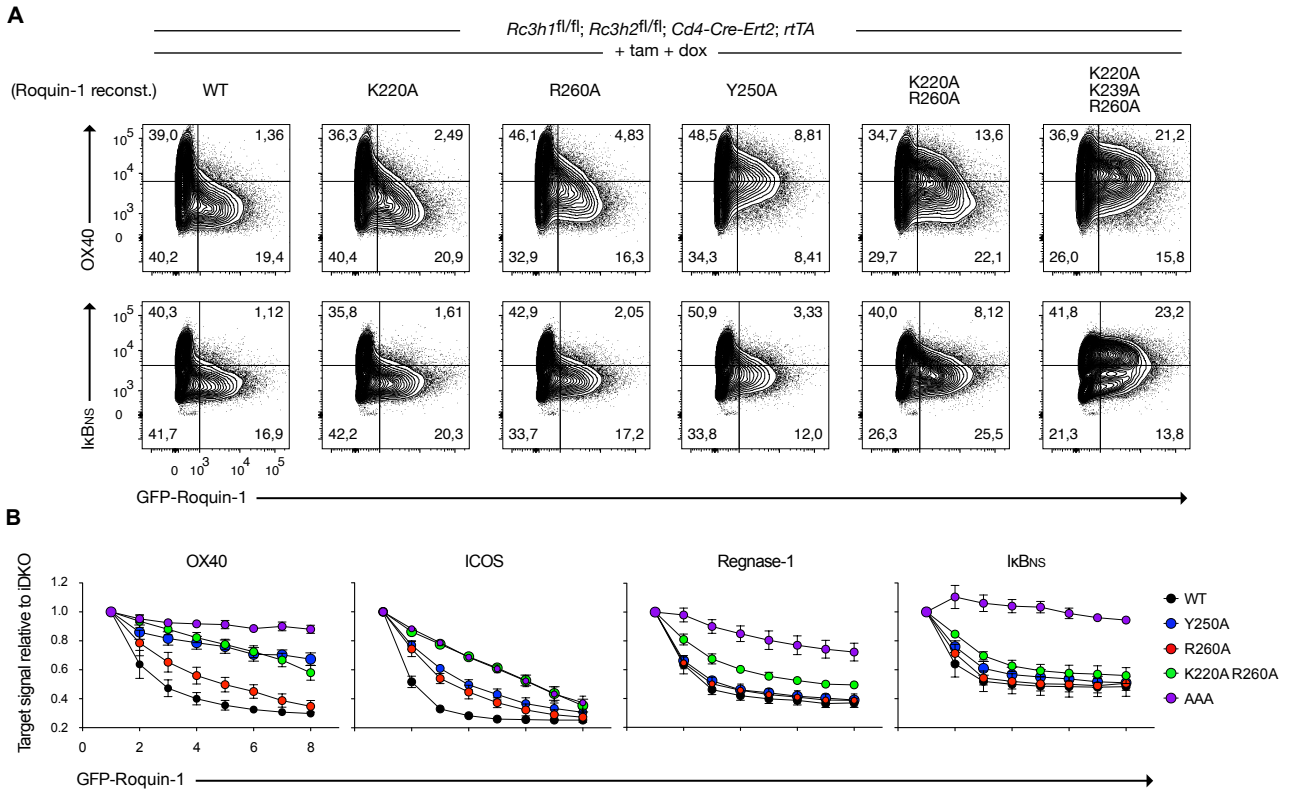
Fig. 5: Decreased RNA affinity of Roquin-1 leads to differential derepression of target mRNAs. (**A**) Contour plots of OX40 and IκB$_{NS}$ expression in iDKO CD4$^+$ T cells retrovirally reconstituted with WT or mutant GFP-Roquin-1 constructs. Knockout of Roquin-1/2 proteins in CD4-Cre-Ert2 CD4$^+$ T cells was induced by *in vitro* 4'OH-tamoxifen and GFP-Roquin-1 constructs were overexpressed in a doxycycline-inducible manner. (**B**) Relative quantification of target expression as in (A) in GFP$^-$ cells and 7 gates of cells with increasing GFP-Roquin-1 expression. WT and mutant GFP-Roquin-1 constructs are color-coded and individual gMFI values (per target) were normalized to maximum levels in iDKO CD4$^+$ T cells without retroviral transduction. Error bars represent ± SEM of 3-4 experiments.
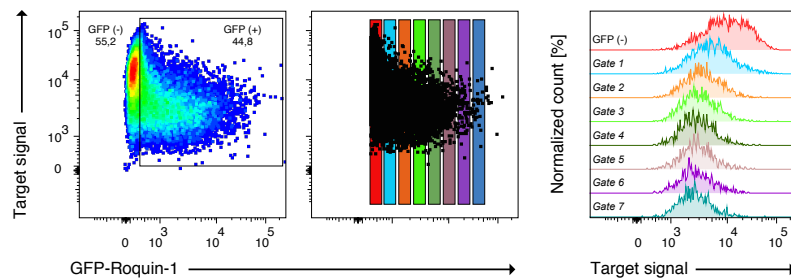
Fig. 6: Gating strategy for individual normalization of target signals according to increasing GFP-Roquin-1 expression. iDKO CD4$^+$ T cells expressing GFP-Roquin-1 were separated from cells without transduction (GFP$^-$). Eight individual gate slices (color-coded) were used to analyze target repression (APC-conjugated antibodies) in distinct increments of increasing GFP-Roquin-1 levels, a representative gating strategy is shown. Target gMFI values per gate slice were normalized to maximum levels in GFP (-) cells.

The mutational analysis suggested an increasing functional avidity from the low avidity target OX40 to the intermediate targets ICOS and Regnase-1 and to the high avidity target IκB$_{NS}$ (i.e. OX40 < ICOS < Regnase-1 < IκB$_{NS}$).

In summary, these data indicate that Roquin targets can be classified as (i) low avidity 3'-UTR targets including OX40 and CTLA-4 being already derepressed at low levels of Roquin-1/2 deletion or at minimal mutational changes in the ROQ domain. On the other hand, the analysis identified (ii) targets of particularly high susceptibility to repression by Roquin including ICOS, IRF4 and Regnase-1 but especially IκB$_{NS}$ as derepression of these required higher rates of Roquin deletion or accumulated site-directed mutations.

3.1.3. Graded deletion of Roquin promotes Th17 cell fate

Peripheral T cell differentiation is antigen dose- as well as cytokine milieu-dependent and the combined deletion of Roquin paralogs in CD4$^+$ T cells promotes Th17 fates. Since antigen-mediated TCR ligation and downstream MALT1 proteolytic activity determine Roquin-1/2 expression levels and graded inactivation in CD4$^+$ T cells, the genetic titration of Roquin alleles was analyzed for differential effects on Th1 and Th17 fate decisions.

Loss of Roquin availability or its partial inactivation did not significantly affect frequencies of *in vitro* CD4$^+$ T cells producing IFN-γ under Th1 conditions (**Fig. 7A**). Despite tendencies of decreased Th1 commitment in DKO^T cells, heterozygous or homozygous deletion the *Rc3h1* and *Rc3h2* were associated with IFN-γ$^+$ CD4$^+$ T cells in the range of 60-85% (**Fig. 7A, B**).
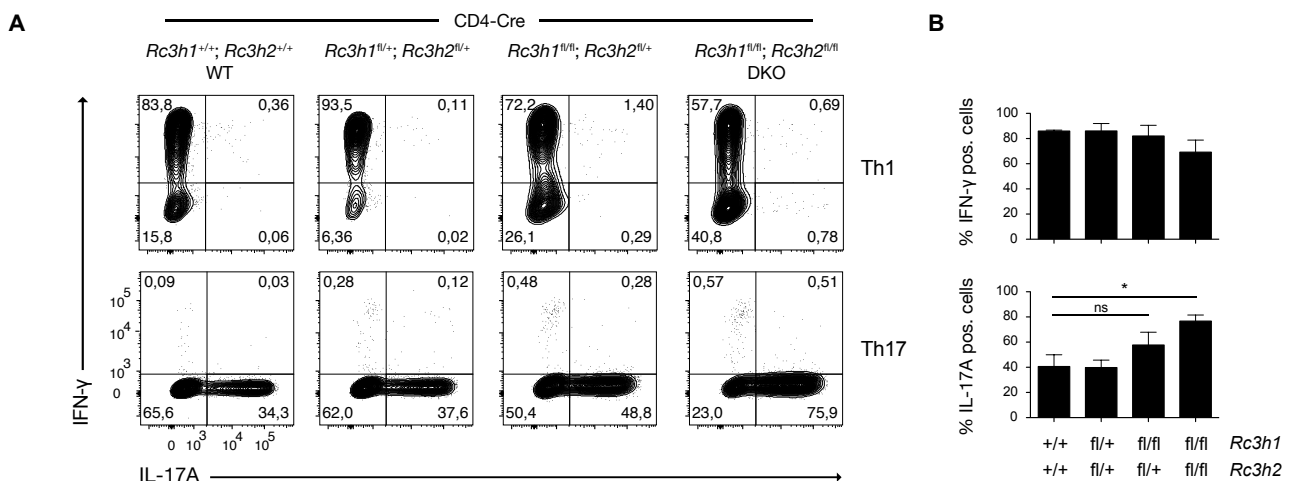
Fig. 7: Loss of Roquin-1/2 expression promotes Th17 but not Th1 differentiation. (**A**) Naive CD4$^+$ T cells of WT, heterozygous *Rc3h1*$^{fl/+}$; *Rc3h2*$^{fl/+}$; CD4-Cre, *Rc3h1*$^{fl/fl}$; *Rc3h2*$^{fl/+}$; CD4-Cre or *Rc3h1*$^{fl/fl}$; *Rc3h2*$^{fl/fl}$; CD4-Cre (i.e. DKO) mice were activated by anti-CD3 and anti-CD28 antibodies and cultivated for 3.5 days *in vitro* under Th1- or Th17-polarizing conditions. T helper cell differentiation was assessed by i.c. cytokine stainings of IFN-γ or IL-17A production after PMA/ionomycin stimulation as shown in contour plots (A) or quantifications (**B**). Statistical analysis was performed by One-Way ANOVA and Dunnett's Multiple Comparison test. Error bars represent ± SEM of 4 replicates; *p* value *< 0.05.

In contrast, Th17 differentiation measured by the frequency of IL-17A producing CD4$^+$ T cells was significantly enhanced in the double knockout (DKO) of both Roquin paralogs (**Fig. 7A**). Importantly, only complete inactivation of Roquin but not heterozygosity strongly facilitated Th17 commitment and already the expression of only one allele of wildtype *Rc3h2* reduced IL-17A production close to wildtype levels (**Fig. 7A, B**). In line with graded effects on Th17-specific target regulation, i.e. IκB$_{NS}$ and IRF4 which required complete loss of Roquin proteins for a maximum fold-induction (see Fig. 1C), Th17 differentiation was balanced at minimum expression levels of Roquin-2 that was approximately 5-times lower expressed in CD4$^+$ T cells.

3.1.4. TCR signal strength determines T cell differentiation

TCR-induced MALT1 paracaspase activity tailors the dynamic expression profiles of Roquin-1 and Roquin-2 during CD4$^+$ T cell activation. Pronounced cleavage of Roquin along T cell activation could lead to minimum expression levels of functional Roquin proteins resembling DKO^T-like mRNA target derepression that facilitates the Th17 fate. Thus, OT-II TCR transgenic co-cultures have been employed to elucidate whether Th1 and Th17 fate choice also differently respond to the amount of antigen-dependent TCR ligation.

When co-cultured with OVA$_{323-339}$-loaded BMDCs, full OT-II T cell differentiation towards IFN-γ producing Th1 cells was already observed at low OVA$_{323-339}$ peptide concentrations of 0.1 µg/mL (**Fig. 8A**). The production of IFN-γ also did not increase at higher peptide loading concentration (1.0 - 10.0 µg/mL) but rather reached a plateau with approximately 80% of IFN-γ$^+$ OT-II T cells (**Fig. 8B**). In contrast, Th17 differentiation was restricted to much higher OVA$_{323-339}$ peptide concentrations of 10.0 µg/mL with an estimated 2.5-fold increase between the two highest concentrations of OVA$_{323-339}$ peptide to a maximum of approx. 25% of IL-17A$^+$ OT-II T cells (**Fig. 8A, B**). Noteworthy, the extent of Th17 commitment was systematically reduced compared to Th1 responses, highlighting favorable low antigen concentrations for Th1 differentiation. In correlation with the pattern of cytokine regulation, low antigen concentrations were observed to induce the Th1 transcription factor T-bet, while higher antigen concentrations were necessary for a stepwise induction of the Th17 transcription factor RORγt (**Fig. 8C, D**).
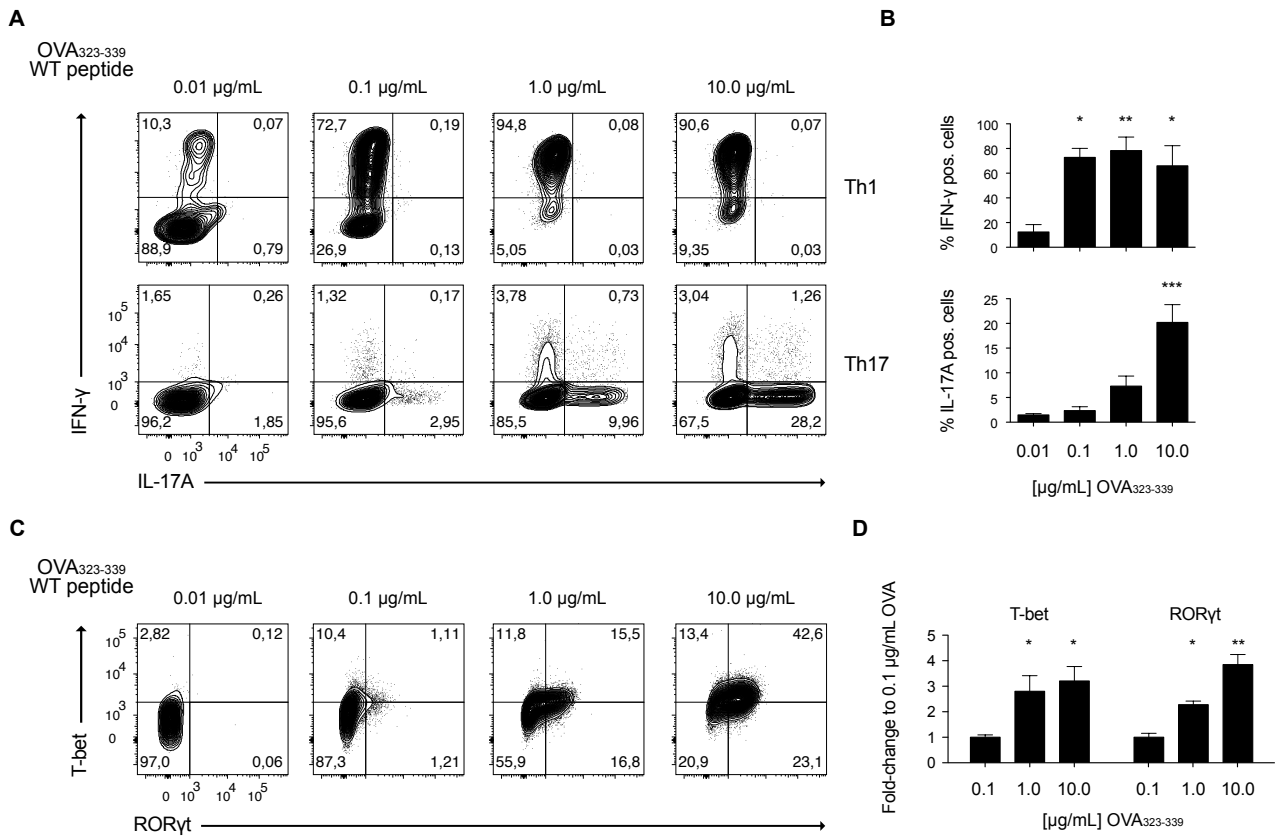
Fig. 8: Strong TCR signals promote Th17 differentiation. (**A**) Co-culture of naive WT OT-II transgenic T cells with OVA$_{323-339}$ peptide-loaded bone marrow-derived dendritic cells (BMDCs) for 3.5 days *in vitro* under Th1- or Th17-polarizing conditions. OT-II T cell differentiation (pre-gated on Vα2/Vβ5 TCR) in response to increasing concentrations of peptides is shown in contour plots (A) or quantifications (**B**) of IFN-γ- or IL-17A-producing OT-II T cells after restimulation with PMA/ionomycin. Error bars represent ± SEM of 3-7 replicates from 5 experiments. (**C**) OT-II co-cultured cells (Th0 conditions) were analyzed for T-bet and RORγt expression by i.c. stainings as shown in contour plots or quantifications of fold-changes in geometric mean fluorescence intensities (gMFI) normalized to individual low-dose expression at 0.1 µg/mL OVA$_{323-339}$ (**D**). Statistical analysis in (B, D) was performed by One-Way ANOVA and Dunnett's Multiple Comparison test. Error bars represent ± SEM of 5 replicates from 3 experiments; *p* values *< 0.05, **< 0.01, ***< 0.001.

In total, these experiments delineate a pronounced dependence of Th17 fate choice on a specific and highly TCR signal strength-dependent induction of factors involved in T cell differentiation. In comparison, Th1 commitment appeared as a transcriptional program triggered at low antigen dose that does not require as high thresholds of TCR strength and Roquin inactivation as shown for Th17 polarization. The data suggested that Th17 differentiation is orchestrated by a fine-tuned cascade of TCR strength-induced Roquin inactivation followed by specific target set derepression that enables a suitable gene expression program for Th17 fate decisions.

3.1.5. Cleavage of Roquin-1 correlates to TCR signal strength

In CD4^{+} T cells, TCR signal transduction and MALT1 protease activity are linked to loss of functional Roquin expression and, reciprocally, to the accumulation of Roquin-1 cleavage fragments. To detect Roquin-1 cleavage on the single cell level, a new monoclonal antibody (clone 5F6) was established that recognizes the N-terminal Roquin-1 1-510 cleavage fragment allowing dose-response analyses relative to TCR signal strength.

In collaboration with Dr. Regina Feederle, an ovalbumin-coupled peptide (OVA-TVTQLIPR) that represents the free carboxy (COOH)-terminus of truncated Roquin-1 (1-510) was used for immunization of rats. Thereof, hybridoma supernatants were screened for antibodies specifically recognizing the free carboxy (COOH)-terminus of the immobilized peptide epitope (biot-TVTQLIPR) but not the similar epitope lacking the carboxy (COOH) binding motif. Candidates were validated in transfected HEK cells to ectopically express full-length GFP-Roquin-1 or the truncated GFP-Roquin-1aa1-510 fragment. The hybridoma supernatant clone 5F6 was confirmed to specifically detect Roquin-1aa1-510 and lacking off-target binding of full-length GFP-Roquin-1 (**Fig. 9A**).
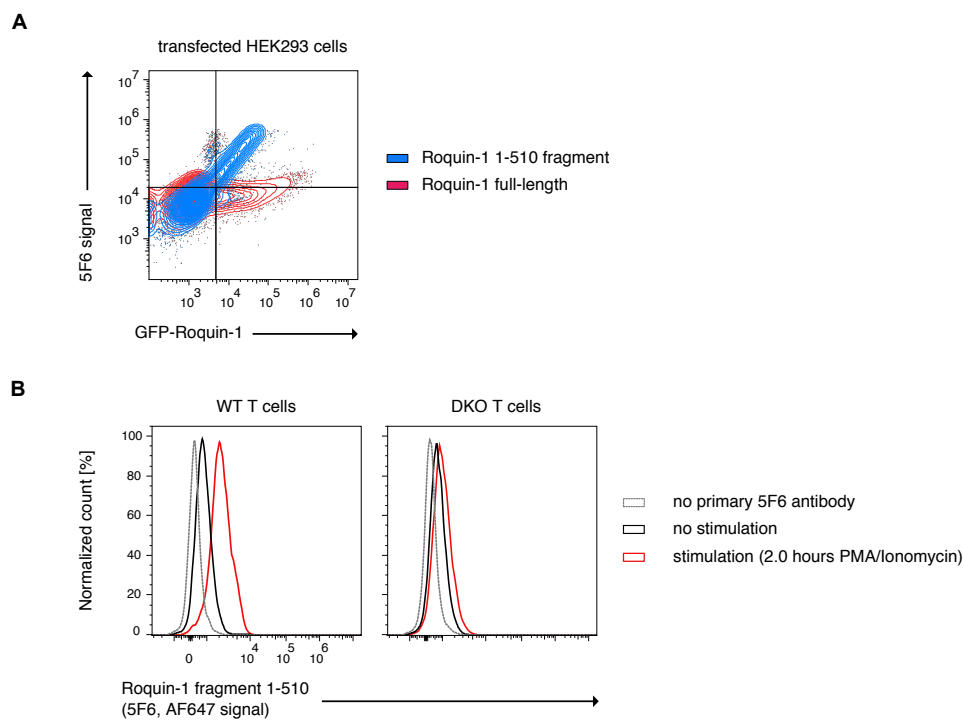
Fig. 9: Characterization of the 5F6 rat anti-Roquin-1 cleavage-specific antibody. (**A**) Overexpression of pRetro-GFP-Roquin-1WT or pRetro-GFP-Roquin-1aa1-510 constructs in HEK293 cells was analyzed by intracellular stainings with the 5F6 mAb that recognizes Roquin-1aa1-510 in a dose-dependent manner (blue) but not Roquin-1WT (full-length, red). A representative of 3 experiments is shown. (**B**) The rat monoclonal Roquin-1 cleavage-specific antibody was used in i.c. stainings of WT or Roquin-DKO T cells that were stimulated (red) or not (black) for 2 hours with PMA/ionomycin. The grey lines indicate cells without stimulation and without primary antibody staining.

Moreover, the 5F6 antibody supernatant recognized endogenous levels of cleaved Roquin-1 protein after stimulation of WT CD4$^+$ T cells with PMA/ionomycin for 2 hours. Importantly, increased signals in intracellular stainings of Roquin-1 cleavage were specific, since the 5F6 antibody did not show off-target intracellular stainings in P/I-stimulated Roquin-deficient (DKO^T) T cells (**Fig. 9B**). Unfortunately, and due to instability, the 5F6 hybridoma could not be established for unlimited monoclonal antibody production and multiple rounds of new immunizations are ongoing to generate another Roquin-1 cleavage antibody.

Fortunately, however, Roquin-1 cleavage could be investigated in *in vitro* activation assays employing titrations of anti-CD3/anti-CD28 antibodies and correlating stainings with the primary 5F6 supernatant to induction of the TCR-inducible Nur77-GFP reporter. Analyzing Nur77-GFP upregulation in stimulated naive CD4$^+$ T cells indicated that fine-tuned induction of the Nur77-GFP reporter required co-stimulation by anti-CD28 incubation along titrations of anti-CD3 antibodies crosslinked to anti-hamster IgG-coated wells (**Fig. 10A**). Including anti-CD28 co-stimulation, induction of Nur77-GFP signals started at low 0.005 µg/mL anti-CD3 concentrations and maximum responses required 100-fold higher concentrations of anti-CD3 (0.05 µg/mL), while only high concentrations of anti-CD3 (1.0 µg/mL) were sufficient to upregulate Nur77-GFP when lacking co-stimulation via anti-CD28 antibodies (**Fig. 10A**). Intracellular analysis of Roquin-1 cleavage after 18 hours of incubation with anti-CD3 and anti-CD28 antibodies correlated with Nur77-GFP induction in mixtures of all indicated anti-CD3 titration increments and the majority of CD4$^+$ T cells were double-positive (5F6$^+$ Nur77-GFP$^+$) (**Fig. 10B**). A smaller but significant proportion of cells was identified as single-positive (5F6$^+$) without TCR-induced Nur77-GFP upregulation, suggesting basal MALT1 activity in CD4$^+$ T cells or loss of GFP signals due to fixation and intracellular 5F6 stainings (**Fig. 10B**). Importantly, CD69 expression similarly increased in mixtures of anti-CD3 stimulations but correlated to Nur77-GFP induction, without showing reporter-independent single-positive (CD69$^+$) cells (**Fig. 10B**). Of note, mixtures of anti-CD3 titrations together with co-stainings for Roquin-1 cleavage (5F6), CD69 expression and the analysis of Nur77-GFP were required as these proof-of-concept assays were performed with the very last amounts available of the primary 5F6 supernatant. Thus, a more detailed titration analysis showcasing Roquin-1 cleavage signals at individual concentrations of anti-CD3 antibodies was not possible but will be addressed utilizing the next generation of upcoming Roquin-1 cleavage hybridoma supernatants.
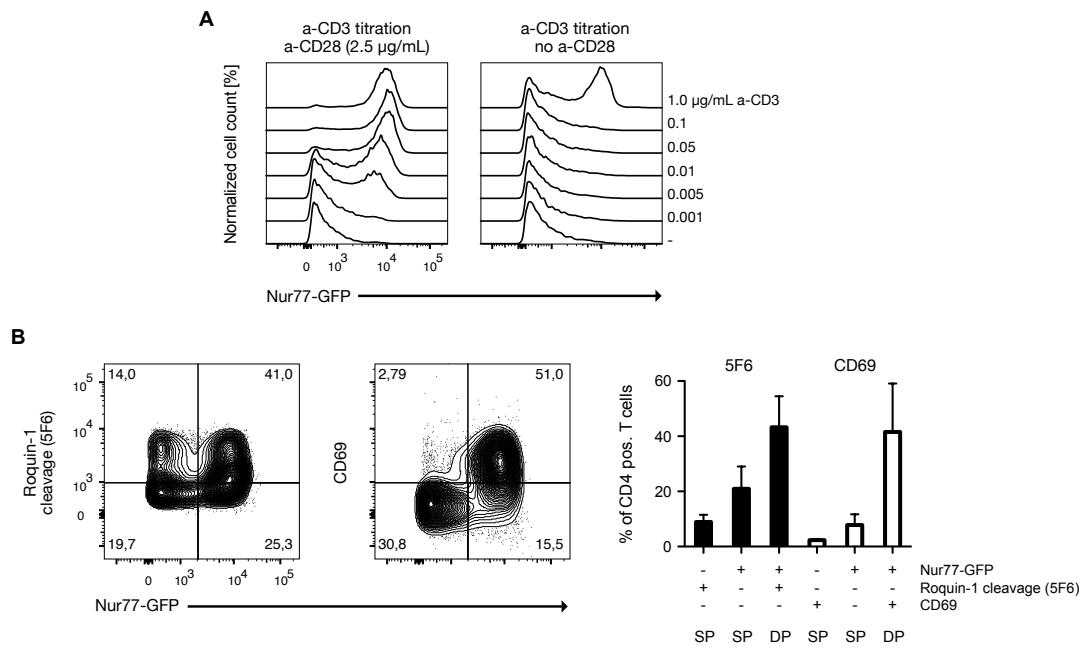
Fig. 10: Roquin-1 cleavage correlates with Nur77-GFP induction upon stimulation with anti-CD3/28.
(**A**). Histogram analysis of Nur77-GFP induction in CD4^{+} T cells *in vitro* stimulated for 18 hours with indicated concentrations of hamster IgG-crosslinked anti-CD3 and anti-CD28 antibodies in coated 96-wells. Nur77-GFP signals were directly measured after fixation comparing stimulation with or without co-stimulation via anti-CD28. A representative of 3 replicates is shown. (**B**). Contour plots of Nur77-GFP induction in CD4^{+} T cells after 18 hours incubation in a mixture of all anti-CD3 titrations depicted in (A) and co-stained with the monoclonal anti-Roquin-1 cleavage antibody (5F6) and CD69. Single-positive (SP) or double-positive (DP) gates for 5F6 or CD69 stainings represent cells of different anti-CD3 concentrations. Quantification of single- (5F6^{+}, CD69^{+} or Nur77-GFP^{+}) or double-positive (5F6^{+} Nur77-GFP^{+} or CD69^{+} Nur77-GFP^{+}) cells is shown for 3 individual replicates and error bars are ± SEM.

Moreover, the primary 5F6 supernatant could be utilized to delineate antigen-induced cleavage of Roquin-1 in OT-II cells co-cultured with WT OVA$_{323-339}$ peptide-loaded BMDCs. In those OT-II co-cultures, increased amounts of WT OVA$_{323-339}$ peptide were accompanied by concentration-dependent Roquin-1 cleavage that correlated with CD69 surface expression and thus T cell activation (**Fig. 11A**). Roquin-1 cleavage was particularly increased starting at OVA$_{323-339}$ concentrations of 0.1 µg/mL (0.056 µM) that are below the described EC$_{50}$ values of 0.2 µM for half-maximal OT-II T cell proliferation (**Fig. 11B**) (Robertson et al., 2000). Of note, a small percentage of OT-II T cells (approx. 7%) were positive for cleaved Roquin-1 at minimum levels of OVA$_{323-339}$ or even in its absence which fitted to moderate basal MALT1 protease activity in Th1 cells or observations from anti-CD3 titrations (**Fig. 1A, 10B, 11A**). MALT1-induced Roquin-1 cleavage was shown to correlate with TCR-peptide:MHC engagement and it increased by 2-3-fold after 18 hours of OVA$_{323-339}$ co-culture. Additionally, an altered peptide mutant H331R (OVA$_{R9}$) of lower OT-II TCR affinity and requiring 10-fold higher EC$_{50}$ in proliferation assays (Cho et al., 2017) was compared to WT OVA$_{323-339}$. OVA$_{R9}$ was of approximately 100-fold lower potency in triggering TCR-induced Roquin-1 cleavage and only elicited minimum responses compared to WT OVA$_{323-339}$ at optimal concentrations (1.0 µg/mL), underscoring that Roquin depletion is indeed governed by TCR strength and TCR affinity (**Fig. 11B**).
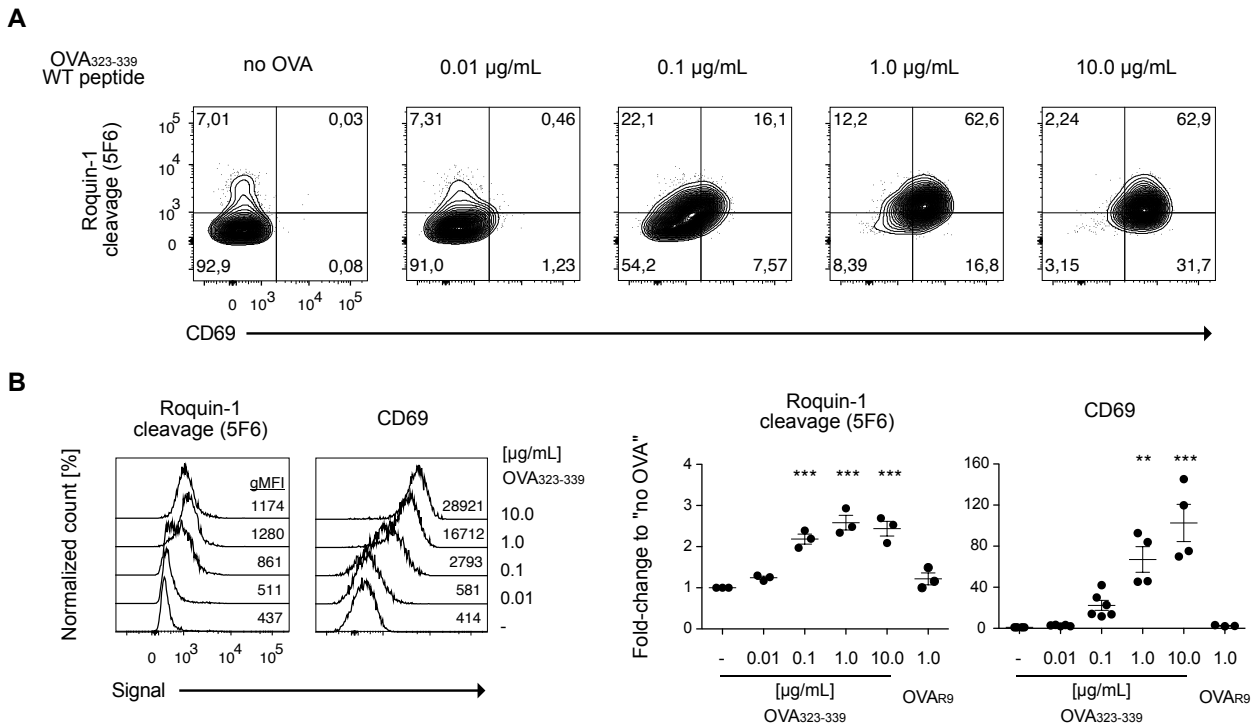
Fig. 11: Roquin cleavage correlates to TCR strength and T cell activation. (**A**) *In vitro* co-culture of naive WT OT-II T cells with WT OVA$_{323-339}$ peptide-loaded BMDCs for 18 hours followed by i.c. staining for Roquin-1 cleavage (mAb 5F6) in OT-II T cells (pre-gated for Vα_2/Vβ_5). Cleavage and surface activation marker CD69 expression were analyzed at increasing concentrations of WT OVA$_{323-339}$ peptides. (**B**) Representative flow cytometric histograms of Roquin-1 cleavage and CD69 upregulation in OT-II co-cultures from (A) and fold-change quantifications of gMFI of Roquin-1 cleavage 5F6 or CD69 signals normalized to OT-II T cells without peptide stimulus. The R9 mutant OVA peptide was compared to WT OVA$_{323-339}$. Error bars represent ± SEM of 3-4 replicates and statistical analysis was performed by One-Way ANOVA and Dunnett's Multiple Comparison test; *p* values *< 0.05, **< 0.01, ***< 0.001.

3.1.6. Antigen-induced targets align with Roquin-1 cleavage

BMDC/OT-II T cell co-cultures were as well tested for OVA$_{323-339}$-induced and Roquin-specific target regulation during T cell activation to link TCR strength to differential dynamics of target derepression. Herein, upregulation of mRNA targets including OX40 and IκB$_{NS}$ appeared in a dose-dependent manner which correlated with CD69 induction (**Fig. 12A**). In line with our previous findings, regulation of the low avidity target OX40 again showed a maximum response at low-range OVA$_{323-339}$ concentrations of 0.1 µg/mL, whereas maximum fold-induction of IκB$_{NS}$ required 10-fold higher OVA$_{323-339}$ concentrations of at least 1.0 µg/mL. Importantly, upregulation of the medium or high avidity targets ICOS, IRF4 and IκB$_{NS}$ increased similarly to CD69, while OX40 responses plateaued independent of increasing CD69 expression (**Fig. 12A, B**). Together, these OT-II co-cultures demonstrated that differential TCR strength deciphers target derepression by identifying sets of low (OX40) or high (IκB$_{NS}$) avidity binding site targets. Low avidity binding sites were derepessed at weak TCR signal strength and targets of high functional avidity required maximum antigen-derived OT-II TCR stimulation.
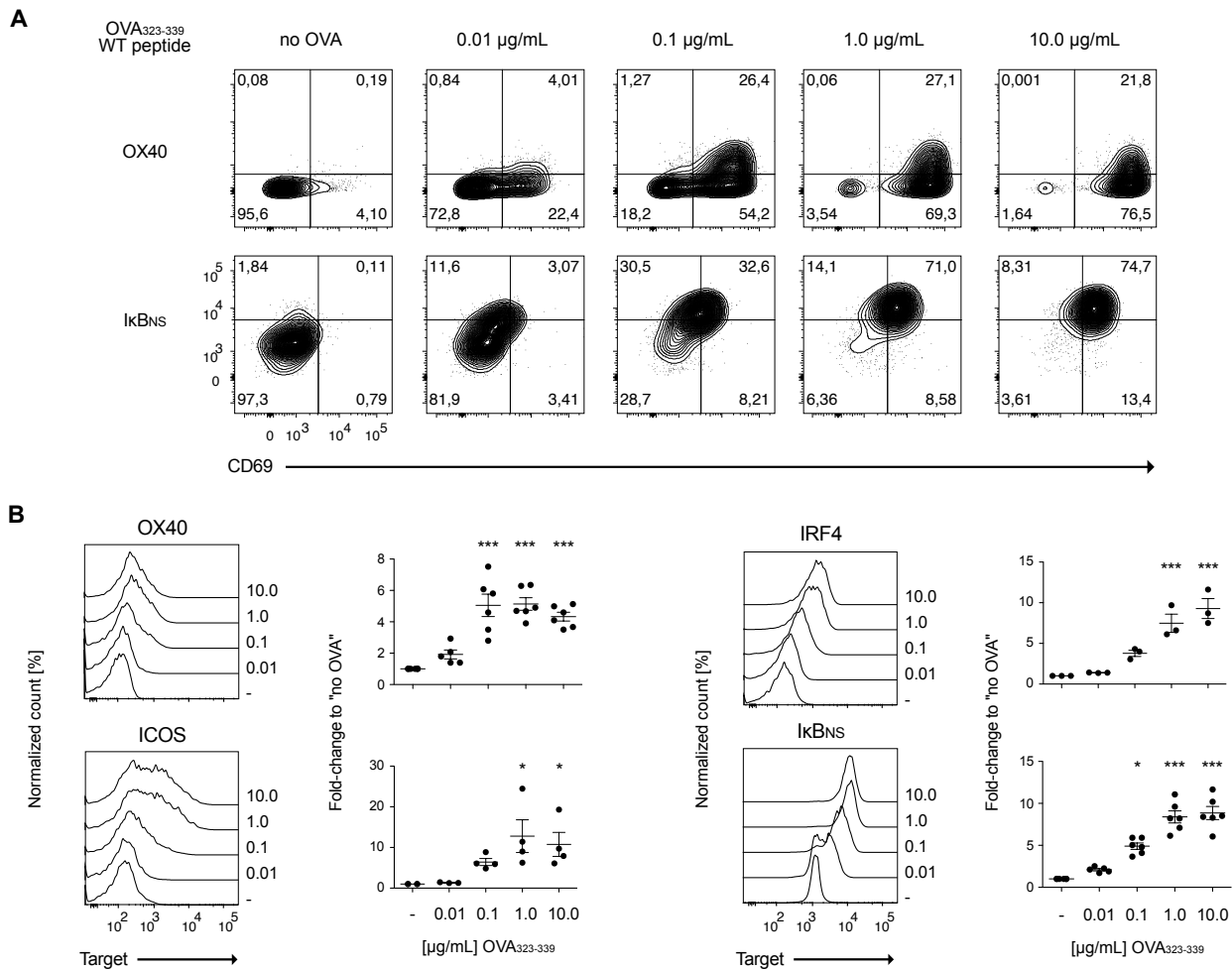
Fig. 12: Dose-dependent derepression of Roquin targets during OT-II T cell activation. (**A**) Contour plots for OX40 and IκB$_{NS}$ target regulation compared to CD69 in *in vitro* OT-II co-cultures as described in Fig. 9. (**B**) Representative histograms of Roquin target upregulation in OT-II T cells from (A) with fold-change quantification of gMFI target signals normalized to OT-II T cells without peptide stimulus (no OVA; as in A). Error bars represent ± SEM of 3-6 replicates from 6 experiments and statistical analysis was performed by One-Way ANOVA and Dunnett's Multiple Comparison test; *p* values *< 0.05, **< 0.01, ***< 0.001.

Noteworthy, these data highlight how the amount of Roquin-1 cleavage is balanced between OVA$_{323-339}$ concentrations of 0.1 to 1.0 µg/mL which appear to determine whether or not a target of low or high avidity binding sites remained repressed. Thus, Roquin-1 cleavage at 0.1 µg/mL OVA$_{323-339}$ might not reach a necessary threshold for derepression of high-affinity targets. e.g. IκB$_{NS}$ (*Nfkbid*).

In total, loss of Roquin availability due to either targeted deletion or TCR signal strength-dependent cleavage released mRNA targets from post-transcriptional repression. Mechanistically, target derepression of differential kinetics aligned with well-known and conserved CDE- or ADE-containing 3'-UTR structures, e.g. of low-affinity *Ox40* and high-avidity *Nfkbid* mRNAs. Finally, this also supported the idea of a general role of Roquin as a dynamic integrator of TCR signal strength since prolonged repression of the Th17 fate-promoting transcriptional modulator IκB$_{NS}$ would limit pathogenic T cell differentiation and thus mitigate potential autoimmune dysbalance.

3.2. Uncoupling Roquin-1 and MALT1 paracaspase activities

3.2.1. Generation of a MALT1-insensitive *Rc3h1*^{Mins} model

The TCR-induced dual function of MALT1 both as scaffold for NF-κB activation and as proteolytic enzyme for different cleavage substrates underlines its crucial role for T cell activation, differentiation and immune homeostasis. While deficiency in MALT1 (*Malt1*^{-/-}) and the protease dead mutant C472A (*Malt1*^{PD/PD}) have been reported to affect Treg differentiation in the thymus and Th1, Th17 and iTreg commitment in the periphery, substrate-specific physiological effects of MALT1-executed cleavage have remained elusive. Hence, models of knockin mice expressing non-cleavable mutant substrates have been suggested to examine the molecular basis of CBM-tailored T cell differentiation or even of IPEX-like diseased *Malt1*^{PD/PD} mice (Demeyer et al., 2016). In order to generate a MALT1-insensitive model of Roquin-1 and in collaboration with Dr. Florian Giesert, CRISPR/Cas9 genome-editing was conducted in the mouse germline creating a novel Roquin-1 encoding allele (*Rc3h1*^{Mins}). For this, two point mutations in exons 10 and 11 of the *Rc3h1* gene were introduced by homology-directed repair (HDR) generating mutant *Rc3h1*^{Mins} knockin mice. The mutations exchanged codons of both MALT1-targeted arginine residues R510 and R579 to alanines (R510A; R579A), intending to rescue the Roquin-1 protein from its negative regulation by blocking cleavage sites of the TCR-induced MALT1 protease (**Fig. 13A**).
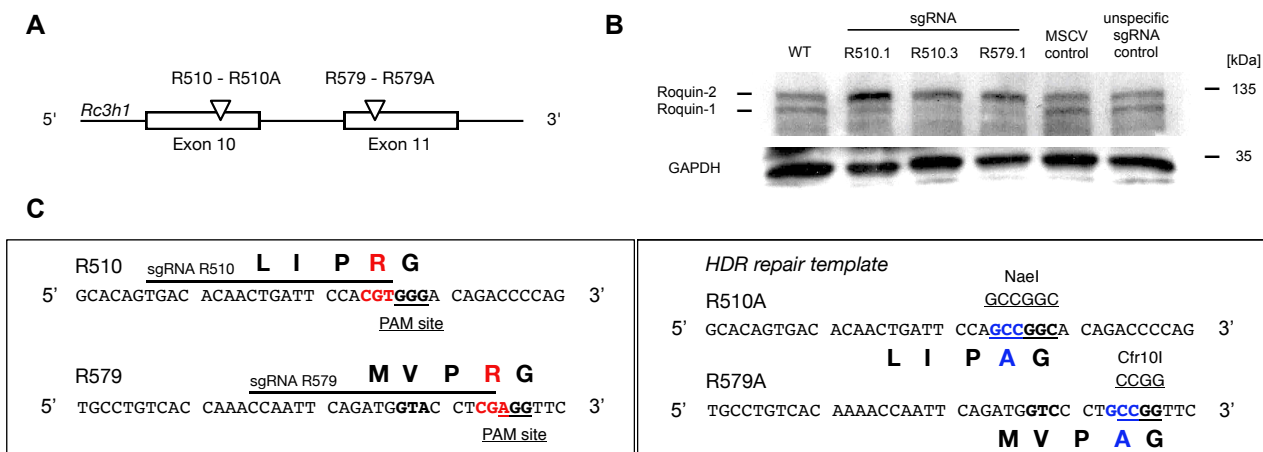
Fig. 13: Targeting strategy for *Rc3h1*^{Mins} and sgRNA efficiency screening. (**A**) Scheme of the targeting strategy for the CRISPR/Cas9-guided generation of the *Rc3h1*^{Mins} mouse model exchanging the codons of arginines 510 and 579 of Roquin-1 to alanines in exons 10 and 11 of the *Rc3h1* gene. (**B**) Efficiency of single guide (sg)RNAs and cleavage of *Rc3h1* was analyzed by Roquin-1/2 immunoblotting of Cas9⁺ MEF cells that were transduced with different sgRNA encoding MSCV constructs. (**C**) The detailed targeting strategy for the CRISPR/Cas9-guided generation of *Rc3h1*^{Mins} mice shows the main and alternative cleavage sites of Roquin-1, R510 and R579, as well as selected sgRNAs next to PAM sites used to target Roquin-1 exons 10/11 and using an homology-directed repair (HDR) template introducing knockin-specific restriction sites for NaeI and Cfr10I enzymes.

Single guide RNAs (sgRNAs) were designed to recruit the Cas9 protein to protospacer-adjacent motif (PAM) sites close to codons of either R510 or R579. Using Cas9^{+} MEF cells *in vitro*, selected sgRNA candidates were screened for efficient induction of Roquin-1 deletion in immunoblots showing a specific reduction of Roquin-1 without affecting Roquin-2 (**Fig. 13B**). The final targeting strategy for the MALT1-insensitive *Rc3h1*[Mins] model utilizing two independent sgRNAs (R510.1 and R579.1) is depicted in **Fig. 13C** and a repair template encoding for both R510A and R579A was provided for homology-directed repair introducing the knockin transgene *Rc3h1*[Mins]. Of note, R510A and R579A mutations (Roquin-1[Mins]) did not affect Roquin-1-mediated repression of targets in flow cytometric assays using reconstituted iDKO CD4^{+} T cells (**Fig. 14**).
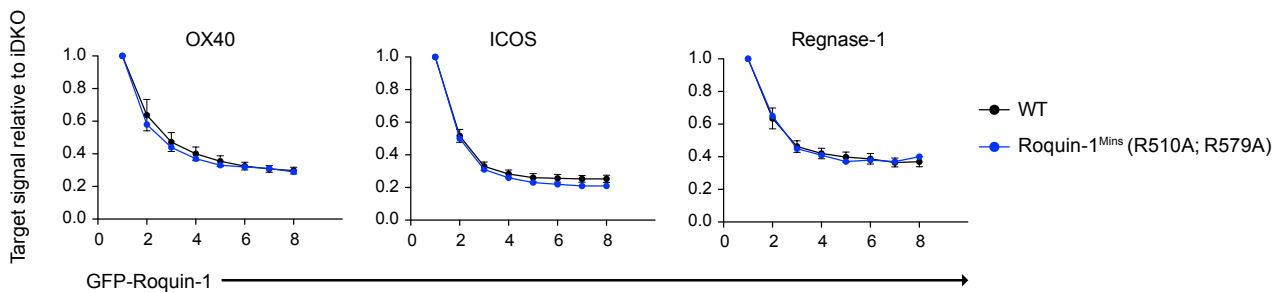
Fig. 14: Roquin-1[Mins] (R510A; R579A) is functional. Relative quantification of target expression as in Fig. 5 in GFP^{−} cells and 7 gates of cells with increasing GFP-Roquin-1[WT] (black) or GFP-Roquin-1[Mins] (blue) expression. Individual gMFI values (per target) were normalized to maximum levels in iDKO CD4^{+} T cells without retroviral transduction. Error bars represent ± SEM of one representative experiment.

The founder and all backcrossed *Rc3h1*[Mins/+] and *Rc3h1*[Mins/Mins] mice were identified by High Resolution Melting (HRM) amplification of genomic DNA and specific PCR amplicon restriction (NaeI, CfrI10). Moreover, a robust protocol for *Rc3h1*[Mins/Mins] genotyping was established to dissect wildtype, *Rc3h1*[Mins/+] and *Rc3h1*[Mins/Mins] gDNA. *Rc3h1*[Mins/Mins] mice appeared normal, were born at Mendelian ratio and, different from *Malt1*[PD/PD] mice, there were no signs of lymphocyte infiltration into tissues (data not shown).

Importantly, *in vitro* stimulation with P/I of Th1-polarized CD4^{+} T cells of wildtype, *Rc3h1*[Mins/+] and *Rc3h1*[Mins/Mins] mice revealed, as a proof-of-concept, an insensitivity of the Roquin-1[Mins/Mins] variant to MALT1-induced proteolysis (**Fig. 15A**). The amounts of Roquin-1 expression were similar to WT Th1 cells, yet WT Th1 cells accumulated cleaved Roquin-1 after stimulation and heterozygous *Rc3h1*[Mins/+] T cells already maintained full-length Roquin-1 (**Fig. 15A**). Besides, both Roquin-2 and Regnase-1, known targets of MALT1, we were still cleaved along T cell activation, thus indicating specificity of the manipulated *Rc3h1*[Mins] system. Being a target of Roquin, Regnase-1 was enriched in DKO[T] cells but its P/I-induced cleavage occured independently of Roquin (**Fig. 15A**).
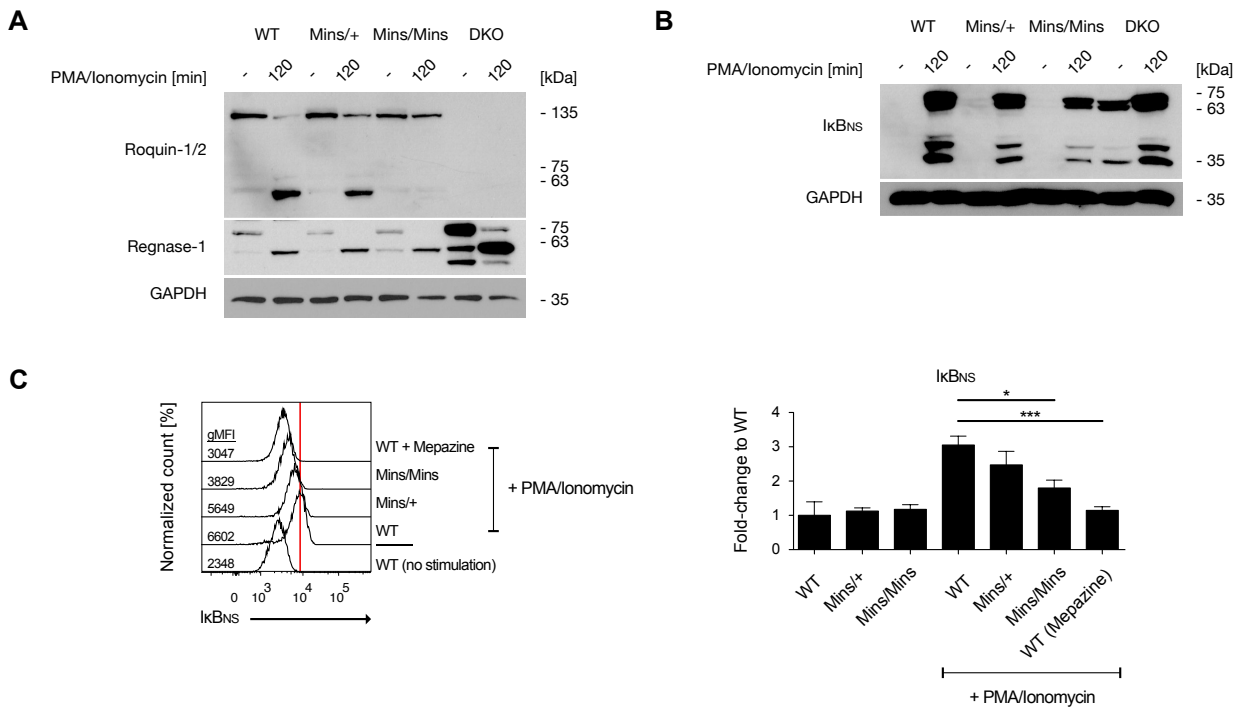
Fig. 15: MALT1-insensitive Roquin-1 impairs TCR-induced target derepression. (**A**) Western blot analysis for Roquin-1/2 cleavage in CD4+ T cells stimulated for 120 minutes *in vitro* with PMA/ionomycin. Roquin-1/2 and Regnase-1 proteins were analyzed for TCR-induced and MALT1-executed cleavage in WT (*Rc3h1*+/+), heterozygous Mins/+ (*Rc3h1*Mins/+), homozygous Mins/Mins (*Rc3h1*Mins/Mins) or Roquin-1/2-deficient T cells (DKO), showing a representative out of 5 independent experiments. (**B**) Western blot analysis as in (A) testing activation-induced upregulation of IκBNS showing a representative of 4 experiments. (**C**) Histograms of IκBNS upregulation in CD4+ T cells from WT, *Rc3h1*Mins/+ or *Rc3h1*Mins/Mins mice stimulated or not with PMA/ionomycin for 2 hours and stained with the antibody for IκBNS (4C1). The stainings and IκBNS induction were compared to WT CD4+ T cells pretreated with the MALT1 protease inhibitor mepazine for 180 min and absolute gMFI values are depicted. The quantification of fold-change values compared to WT CD4+ T cells without stimulation is shown. Error bars represent ± SEM of 3-5 replicates and statistical analysis was performed by One-Way ANOVA and Dunnett's Multiple Comparison test; *p* values *< 0.05, **< 0.01, ***< 0.001.

The *Rc3h1*Mins model allowed to analyze Roquin function from a highly dynamic perspective as full-length Roquin-1 expression was maintained during T cell activation, thus retaining its binding site activity to promote target mRNA degradation. Indeed, *in vitro* stimulations of CD4+ T cells with P/I confirmed Roquin-1Mins gain-of-function as *Rc3h1*Mins/Mins showed reduced induction of the high-avidity target *Nfkbid* (IκBNS) compared to wildtype counterparts, while endogenous levels in resting Th1 cells were equal (**Fig. 15B**). Gradual effects of impaired IκBNS induction were as well observed in heterozygous *Rc3h1*Mins/+ T cells and its partial impairment suggested TCR/MALT1/Roquin-dependent and -independent IκBNS regulation. This was in line with IκBNS upregulation in DKOT cells that endogenously expressed detectable amounts of IκBNS but further increased in IκBNS levels during stimulation (**Fig. 15B**).

Similarly, flow cytometric analyses confirmed impaired IκBNS induction in *Rc3h1*Mins/Mins and intermediate reduction in *Rc3h1*Mins/+, respectively, with reductions of almost 3-fold in *Rc3h1*Mins/Mins CD4+ T cells compared to wildtype counterparts (**Fig. 15C, D**). In addition, effects on IκBNS-specific

repression appeared equivalent to WT CD4^{+} T cells pretreated for 180 minutes with mepazine, an allosteric small molecule inhibitor of MALT1 paracaspase activity (**Fig. 15C, D**).

Thus, rendering Roquin-1 insensitive to MALT1 resembled *in vitro* effects observed for the pharmacological inhibition of MALT1 and suggested fine-tuned exclusive regulation of *Nfkbid* (IκB_NS) by Roquin.
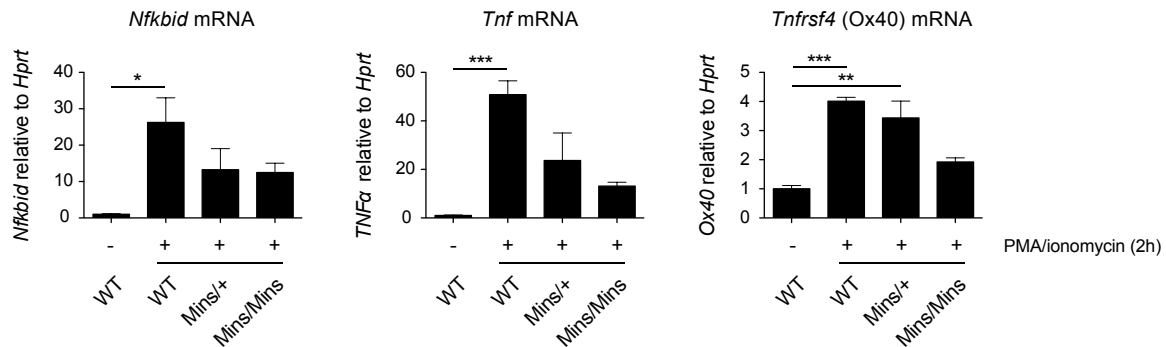

Fig. 16: MALT1-insensitive Roquin-1 acts on the mRNA level. qRT-PCR analysis of indicated Roquin target mRNAs in CD4^{+} T cells that were treated for 120 minutes with PMA/ionomycin or left untreated. The fold-change relative to individual target mRNA without stimulation is displayed with error bars representing ± SEM of 3 individual experiments; statistical analysis was performed by One-Way ANOVA and Dunnett's Multiple Comparison test; *p* values *< 0.05, **< 0.01, ***< 0.001.

The impairment in IκB_NS upregulation was associated to the mRNA level since RT-qPCR revealed that *Nfkbid* mRNA levels and the fold-change induction of *Nfkbid* after stimulation with P/I were reduced in both *Rc3h1*^Mins/+ and *Rc3h1*^Mins/Mins CD4^{+} T cells. Similarly, reduced induction of *Tnfa* and *Tnfrsf4* (*Ox40*) mRNAs were observed for *Rc3h1*^Mins compared to wildtype CD4^{+} T cells (**Fig. 16**). These pronounced effects on IκB_NS and Tnfα in *Rc3h1*^Mins mice were in line with Roquin-RNA-IPs published by Stoecklin and colleagues, suggesting that particularly high-avidity targets remained repressed in Roquin-1^Mins cells during T cell activation (Leppek et al., 2013).

3.2.2. Analyzing TCR-induced target regulation in *Rc3h1*^Mins mice

To test whether *Rc3h1*^Mins/Mins T cells differently respond to physiologically relevant antigen signals, BMDC/OT-II T cell co-cultures were employed for the analysis of target induction. Herein, *Rc3h1*^Mins/Mins OT-II cells revealed attenuated induction of IκB_NS at high OVA_{323-339} antigen doses of 1.0 - 10.0 µg/mL compared to WT OT-II cells (**Fig. 17A-C**). Levels of IκB_NS were similar without OVA_{323-339} stimulation or at low peptide concentration (0.01 µg/mL) but IκB_NS induction segregated at 0.1 µg/mL OVA_{323-339} with an approx. 7-fold induction in WT and only a 3-fold induction in *Rc3h1*^Mins/Mins OT-II cells (**Fig. 17B, C**).
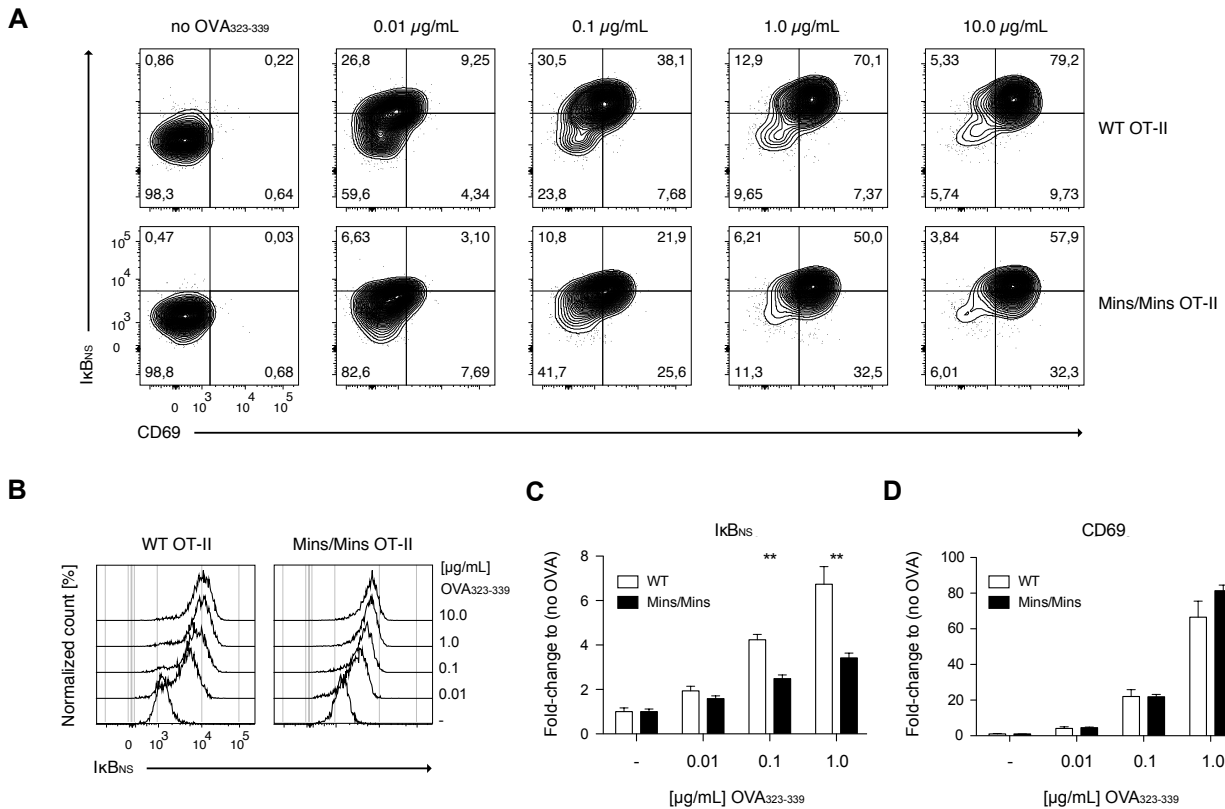
Fig. 17: Roquin-1^{Mins/Mins} restricts antigen-induced IκB_{NS} upregulation. (**A**) Contour plots of IκB_{NS} regulation in WT or *Rc3h1*^{Mins/Mins} OT-II T cells after an 18-hour co-culture with OVA₃₂₃₋₃₃₉-loaded BMDCs; IκB_{NS} upregulation is plotted in comparison to the T cell activation marker CD69. A representative of 5-6 replicates is shown. (**B**) Representative histograms of IκB_{NS} regulation as described in (A). (**C**) Quantification of geometric mean fluorescence intensities (gMFI) as fold-change to controls without OVA stimulation for IκB_{NS}. Error bars represent ± SEM of 5 individual experiments and statistical analysis was performed by Student's *t* test (unpaired, two-tailed); *p* values *< 0.05, **< 0.01, ***< 0.001. (**D**) Quantification of gMFIs as in (C) for CD69 activation marker expression of co-cultures described in (A). Error bars represent ± SEM of 4-5 individual experiments.

The molecular regulation of IκB_{NS} was independent of general effects on T cell activation since CD69 expression was similarly upregulated in OT-II cells from both genotypes (**Fig. 17D**).

Additionally, *Rc3h1*^{Mins/Mins} OT-II cells showed decreased induction of Tnfα and IRF4 levels as measured by absolute gMFI values indicating systematically reduced levels of both Roquin targets, although individual fold-inductions relative to respective low-dose (TNFα) or no OVA₃₂₃₋₃₃₉ (IRF4) controls per genotype were not different from wildtype OT-II cells (**Fig. 18A**). The BMDC/OT-II T cell co-culture assay also confirmed decreased S6 phosphorylation (p-S6) at mid-range OVA₃₂₃₋₃₃₉ concentrations (0.1 µg/mL), suggesting that the gain-of-function Roquin-1^{Mins/Mins} protein exerts stronger inhibiton on direct mRNA targets as well as the Roquin-regulated PI3K/Akt/mTOR pathway (**Fig. 18B**) (Essig et al., 2017).
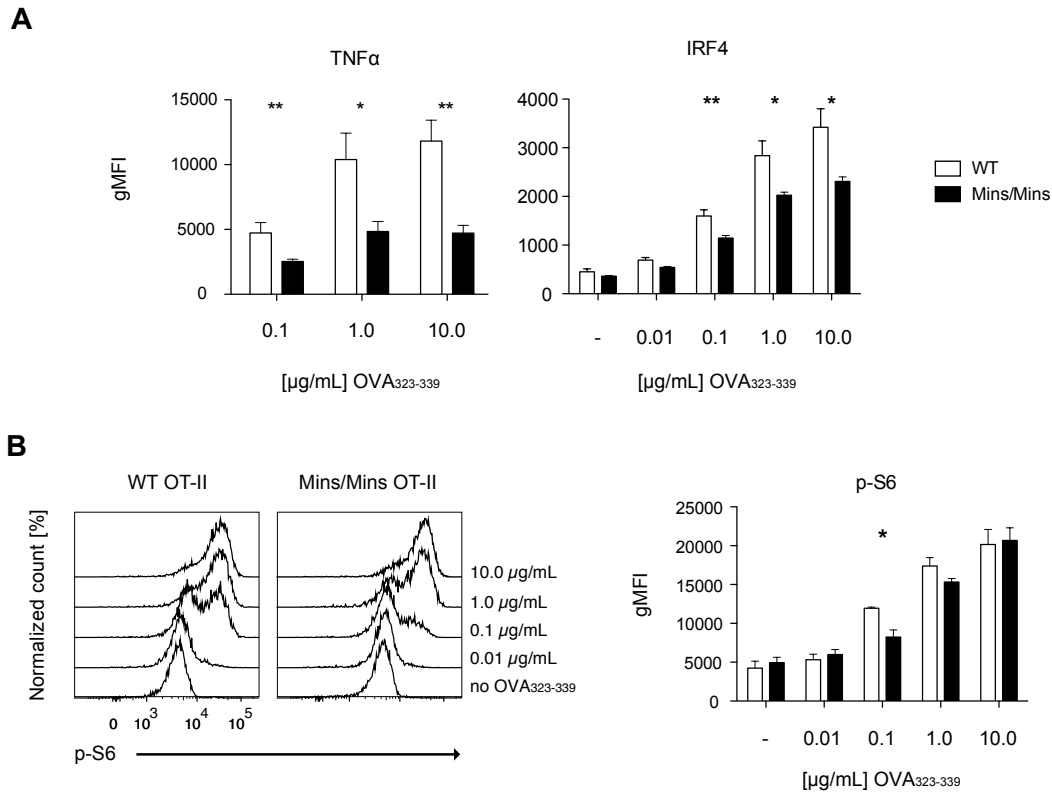
Fig. 17: Roquin-1$^{Mins/Mins}$ restricts antigen-induced IκB$_{NS}$ upregulation. (**A**) Contour plots of IκB$_{NS}$ regulation in WT or *Rc3h1*$^{Mins/Mins}$ OT-II T cells after an 18-hour co-culture with OVA$_{323-339}$-loaded BMDCs; IκB$_{NS}$ upregulation is plotted in comparison to the T cell activation marker CD69. A representative of 5-6 replicates is shown. (**B**) Representative histograms of IκB$_{NS}$ regulation as described in (A). (**C**) Quantification of geometric mean fluorescence intensities (gMFI) as fold-change to controls without OVA stimulation for IκB$_{NS}$. Error bars represent ± SEM of 5 individual experiments and statistical analysis was performed by Student's *t* test (unpaired, two-tailed); *p* values *< 0.05, **< 0.01, ***< 0.001. (**D**) Quantification of gMFIs as in (C) for CD69 activation marker expression of co-cultures described in (A). Error bars represent ± SEM of 4-5 individual experiments.

The molecular regulation of IκB$_{NS}$ was independent of general effects on T cell activation since CD69 expression was similarly upregulated in OT-II cells from both genotypes (**Fig. 17D**).

Additionally, *Rc3h1*$^{Mins/Mins}$ OT-II cells showed decreased induction of Tnfα and IRF4 levels as measured by absolute gMFI values indicating systematically reduced levels of both Roquin targets, although individual fold-inductions relative to respective low-dose (TNFα) or no OVA$_{323-339}$ (IRF4) controls per genotype were not different from wildtype OT-II cells (**Fig. 18A**). The BMDC/OT-II T cell co-culture assay also confirmed decreased S6 phosphorylation (p-S6) at mid-range OVA$_{323-339}$ concentrations (0.1 µg/mL), suggesting that the gain-of-function Roquin-1$^{Mins/Mins}$ protein exerts stronger inhibiton on direct mRNA targets as well as the Roquin-regulated PI3K/Akt/mTOR pathway (**Fig. 18B**) (Essig et al., 2017).

A

B

Fig. 18: Gain-of-function Roquin-1^{Mins} interferes with mRNA target induction and exerts inhibition on S6 phosphorylation. (A) OVA$_{323-339}$ peptide co-culture as in Fig. 17 for the analysis of TNFα and IRF4. A quantification of gMFIs with error bars representing ± SEM of 4-7 replicates from 5 experiments is shown. (**B**) Histograms of intracellular p-S6 (Ser235/236) in OT-II transgenic WT or *Rc3h1*$^{Mins/Mins}$ T cells analyzed at different OVA peptide concentrations (0.01 - 10.0 µg/mL) as in (A). Quantification of p-S6 upregulation was performed as in (A) and error bars represent ± SEM of 3-4 replicates from 2 experiments. Statistical analysis was performed by two-tailed Student's *t* test; *p* values *< 0.05, **< 0.01.

In summary, these results confirmed Roquin-1^{Mins} gain-of-function and highlighted the crucial role of Roquin cleavage in controlling factors involved in T cell activation and differentiation. Strong (TNFα, IκB$_{NS}$) or partial (OX40, IRF4) effects on target inhibition hinted towards attenuated inflammatory programs and reduced abilities to commit to pathogenic T helper cell fates.

3.2.3. Phenotypic analysis of *Rc3h1*^{Mins} mice

Phenotypically, *Rc3h1*^{Mins/Mins} mice did not show any signs of inflammation or lymphocytic tissue infiltrations as reported for mutant *Malt1*^{PD/PD} mice. Thymic T cell development in *Rc3h1*^{Mins/Mins} mice appeared unchanged with normal frequencies of double-negative (DN), double-positive (DP) and single-positive CD4$^+$ or CD8$^+$ thymocytes (**Fig. 19A**). Likewise, assessing β chain rearrangements by CD69 and TCRβ co-stainings and developmental stages during thymic selection did not reveal obvious changes in *Rc3h1*^{Mins/Mins} mice (**Fig. 19B**). Apart from conventional thymic development, frequencies of thymic CD4-SP Foxp3$^+$ Treg cells were reduced, yet absolute numbers appeared normal due to slightly increased thymocytes in *Rc3h1*^{Mins/Mins} mice (**Fig. 19C**). Similar to *Malt1*^{PD/PD} mice, there were no changes in thymic selection but reduced frequencies of natural Tregs in thymi of *Rc3h1*^{Mins/Mins} mice, although effects in *Malt1*^{-/-} or *Malt1*^{PD/PD} models were much more pronounced (Bornancin et al., 2015; Jaworski et al., 2014; Gewies et al., 2014).
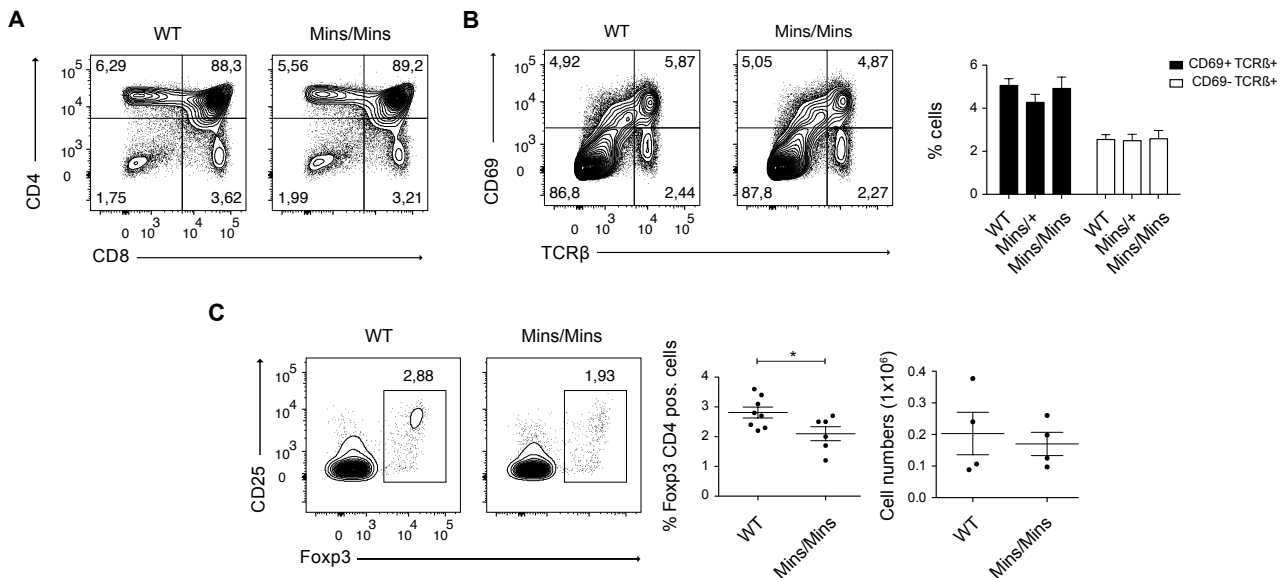
Fig. 19: Thymic development of CD4/CD8 T cells in *Rc3h1*^{Mins/Mins} mice. (**A**) Flow cytometric analysis of thymic CD4 and CD8 single- or double-positive populations from WT or *Rc3h1*^{Mins/Mins} mice. Plots are representatives of 7 replicates. (**B**) Thymic T cell development assessed by CD69 and TCRβ stainings of thymocyte single cell suspensions from WT, *Rc3h1*^{Mins/+} or *Rc3h1*^{Mins/Mins} mice. Bar diagrams are quantifications of 7 replicates and error bars represent ± SEM. (**C**) Identification of CD4-SP CD25$^+$ Foxp3$^+$ thymocytes from WT or *Rc3h1*^{Mins/Mins} mice showing 1 representative out of 6 analyses as well as the quantification of frequencies and numbers of thymic Tregs. Error bars represent ± SEM and statistical analysis was performed by two-tailed Student's *t* test; *p* value *< 0.05.

In the periphery, *Rc3h1*^{Mins/Mins} mice showed normal frequencies and numbers of CD4$^+$ and CD8$^+$ populations similar to wildtype counterparts (**Fig. 20A**). Both CD4$^+$ and CD8$^+$ T cells did not show any signs of altered activation states assessed by CD62L and CD44 co-stainings dissecting naive (N), effector memory (EM) and central memory (CM) T cells (**Fig. 20B**). In view of reduced thymic Treg frequencies, *Rc3h1*^{Mins/Mins} mice did yet not show lower frequencies of peripheral Treg cells as

measured by approx. 8% of CD25 and Foxp3 expressing CD4$^+$ T cells for both genotypes (**Fig. 20C**). Peripheral Treg cells from lymph nodes, however, were reduced in frequencies but splenic compartments were normal indicating variations in specific lymph node Treg populations.
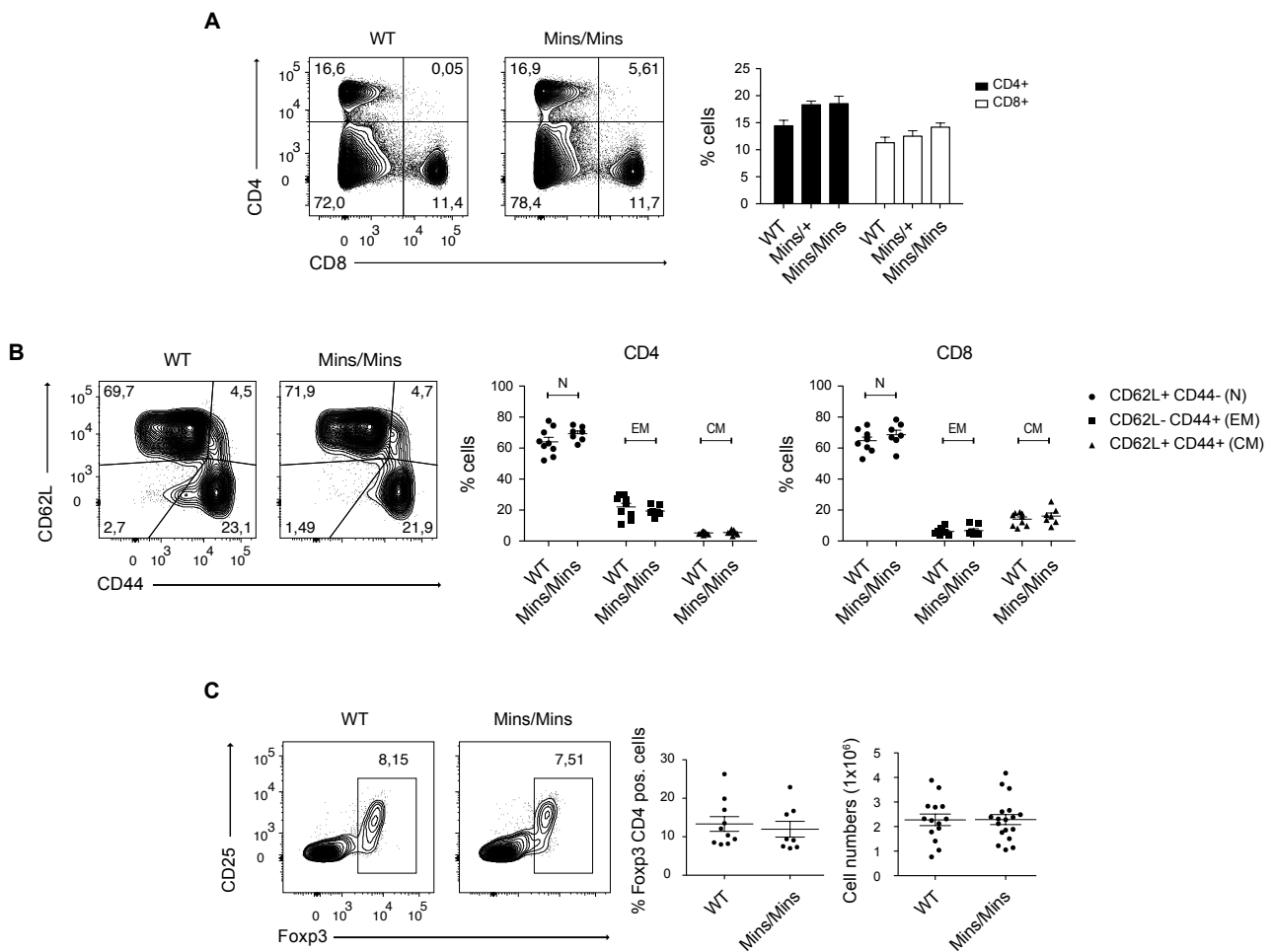
Fig. 20: Peripheral CD4/CD8 T cell populations in *Rc3h1*Mins/Mins mice. (**A**) Analysis of peripheral CD4 and CD8 populations from spleens of WT, *Rc3h1*Mins/+ or *Rc3h1*Mins/Mins mice. Error bars represent ± SEM of 7 replicates. (**B**) Analysis of peripheral CD4$^+$ T lymphocyte activation from spleens of WT or *Rc3h1*Mins/Mins mice; a representative of naive (CD62L$^+$ CD44$^-$), central memory (CD62L$^+$ CD44$^+$) and effector memory (CD62L$^-$ CD44$^+$) cells from 7 replicates is shown. Quantified activation of splenic WT, *Rc3h1*Mins/+ or *Rc3h1*Mins/Mins CD4 and CD8 populations grouped into naive (N), effector memory (EM) or central memory (CM) categories for 7-9 replicates from 7 experiments is shown. Error bars represent ± SEM. (**C**) Identification of splenic CD4$^+$ Foxp3$^+$ T cells of WT or *Rc3h1*Mins/Mins mice showing a representative experiment with frequencies and numbers from 8-10 replicates.

Analyzing Roquin-specific targets in both splenic and lymph node Treg populations from WT or *Rc3h1*Mins/Mins mice, Foxp3$^+$ OX40$^+$ and Foxp3$^+$ CTLA-4$^+$ Treg cells appeared reduced compared to wildtype controls (**Fig. 21A**) since there was a reduced expression of OX40 and CTLA-4 in these cells (**Fig. 21B**). Interestingly, *Rc3h1*Mins/Mins Treg cells revealed a tendency to increased IFN-γ but clearly reduced TNFα production after *ex vivo* stimulation with P/I (**Fig. 21C**). IFN-γ production in *Rc3h1*Mins/Mins Treg cells was increased to approximately 5% compared to only 2% of wildtype

IFN-γ⁺ Foxp3⁺ CD4⁺ Tregs (**Fig. 21C**). As a target of Roquin, TNFα was reduced 4-fold to levels below 5% in spleen-derived Tregs compared to >20% of wildtype TNFα⁺ Foxp3⁺ CD4⁺ Tregs, indicating that the Roquin-1$^{Mins/Mins}$ protein maintained low target levels not only in *in vitro* cultivated CD4⁺ T cells but also in specific functional T cell subsets.
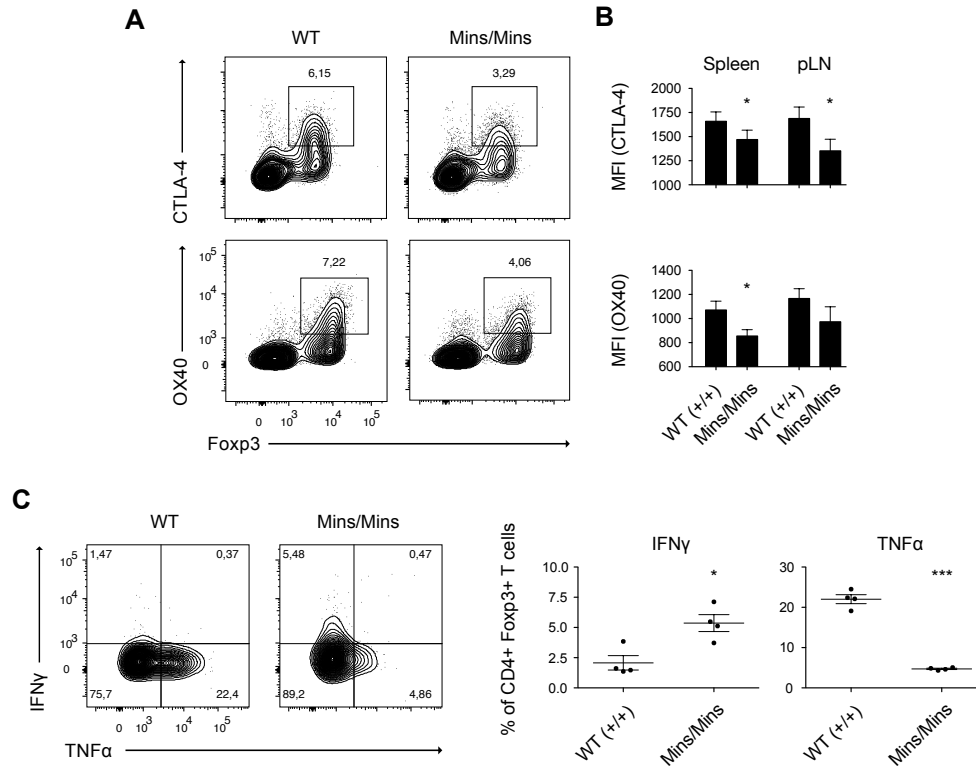
Fig. 21: Characterization of peripheral Tregs of *Rc3h1*^{Mins} mice. (**A**) Representative contour plots of CTLA-4 and OX40 expression in splenic CD4⁺ Foxp3⁺ Treg cells from WT or *Rc3h1*$^{Mins/Mins}$ mice. (**B**) Quantification of mean fluorescence intensities (MFI) of CTLA-4 and OX40 expression in Tregs as shown in (A) for 4-6 replicates. Error bars represent ± SEM. (**C**) Representative contour plots of intracellular IFN-γ and IL-17A detection in splenic CD4⁺ Foxp3⁺ Treg cells from WT or *Rc3h1*$^{Mins/Mins}$ mice. Splenocytes were stimulated with PMA/ionomycin and cytokine production was quantified for 4 replicates. Error bars represent ± SEM. Statistical analysis was performed by two-tailed Student's *t* test; p values * < 0.05, ** < 0.01, *** < 0.001.

In line with the described inhibitory function of Roquin proteins in follicular helper T cell (Tfh) differentiation, the gain-of-function in *Rc3h1*$^{Mins/Mins}$ mice caused reduced frequencies and numbers of Tfh and regulatory Tfh (Tfr) cells in the spleen (**Fig. 22A, B**). Tfh (CD4⁺ PD-1^{hi} CXCR5^{hi}), Tfh among CD44^{hi} as well as Tfr (CD4⁺ Foxp3⁺ PD-1^{hi} CXCR5^{hi}) cells were decreased in *Rc3h1*$^{Mins/Mins}$ mice.
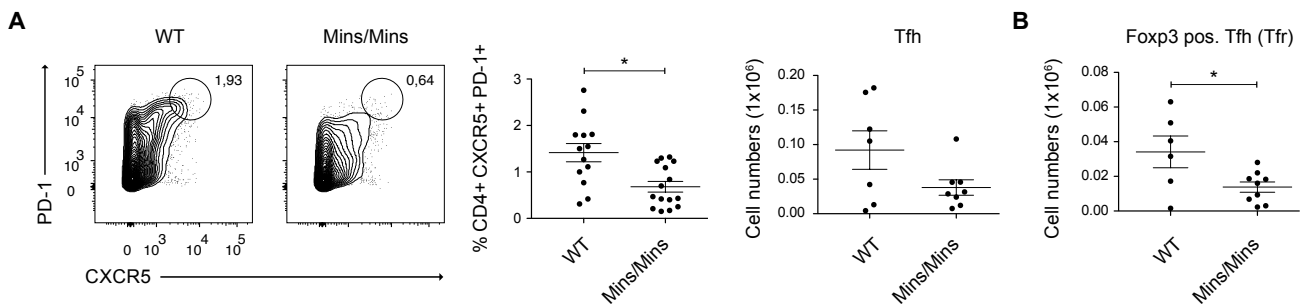
Fig. 22: Reduced Tfh cell differentiation in *Rc3h1*Mins mice. (**A**) Stainings of CD4+ PD-1hi CXCR5hi Tfh cells from splenocytes of WT or *Rc3h1*Mins/Mins mice. A representative and quantifications of frequencies and total numbers is shown. Error bars represent ± SEM of 13-15 replicates. (**B**) Total numbers of CD4+ Foxp3+ PD-1hi CXCR5hi Tfr cells from splenocytes of WT or *Rc3h1*Mins/Mins mice. Error bars represent ± SEM of 6-9 replicates. Statistical analysis was performed by two-tailed Student's *t* test; *p* value *< 0.05.

Accordingly, germinal center (GC) B cells were analyzed in spleens and Peyer's patches (PP) of both genotypes indicating no changes in GC B cell frequencies (8-9% of B220+ CD95+ GL-7+ cells in PP) which was consistent to maintained normal ratios of Tfh to Tfr cells (**Fig. 23A**). Absolute numbers of peripheral B cells determined by either CD19 or B220 stainings were not changed in *Rc3h1*Mins/Mins mice (**Fig. 23B**). In contrast to *Malt1*PD/PD and *Malt1*-/- mice, however, the Roquin-1Mins/Mins protein did also not affect splenic marginal zone (MZ) or follicular (FO) B cell development with approx. 5-7% of CD19+ CD21hi CD23dim MZ B cells in spleens of both genotypes (**Fig. 23C**).
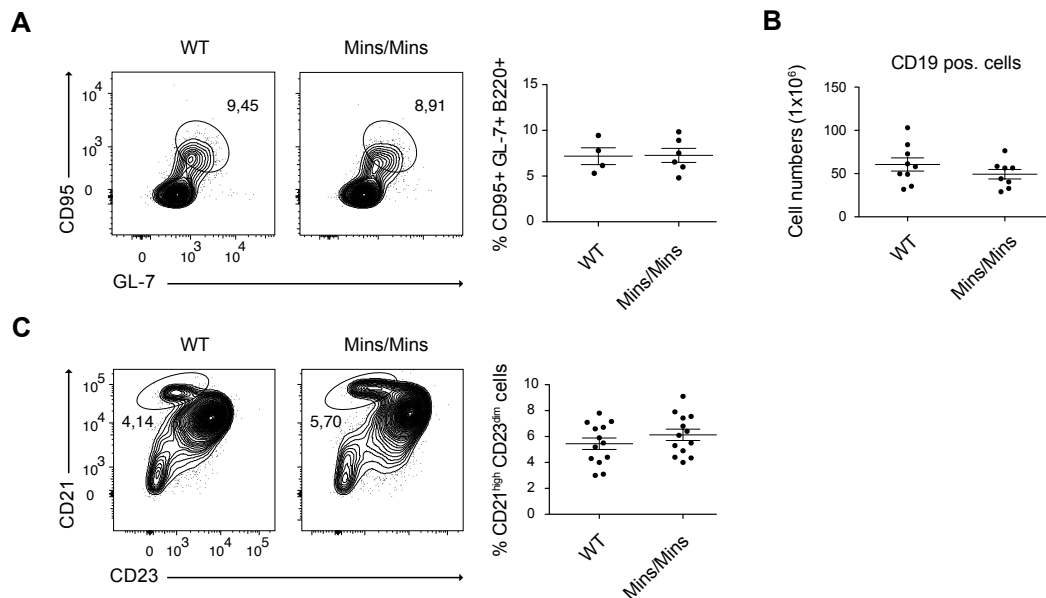
Fig. 23: Roquin-1[Mins/Mins] does not affect germinal center (GC) or marginal zone (MZ) B cell development. (**A**) Identification of B220$^+$ CD95^{hi} GL-7^{hi} GC B cells from Peyer's Patches (PP) of WT or *Rc3h1*[Mins/Mins] mice. A representative out of 4 experiments is shown with frequencies and error bars representing ± SEM of 4-6 replicates. (**B**) Total numbers of CD19$^+$ B cells from spleens of WT or *Rc3h1*[Mins/Mins] mice. Error bars represent ± SEM of 8-9 replicates from 8 experiments. (**C**) Contour plots of CD19$^+$ CD21^{hi} CD23^{dim} marginal zone B cells from spleens of WT or *Rc3h1*[Mins/Mins] mice showing a representative experiment out of 12 and a quantification of frequencies. Error bars represent ± SEM of 13 replicates.

In total, the phenotypic analysis of *Rc3h1*[Mins] mice described mild effects on immune homeostasis that largely focused on the somewhat reduced frequency or functionality of thymic or peripheral Treg cells. The Treg-specific cytokine profiles in *Rc3h1*[Mins/Mins] mice with diminished TNFα production surprisingly increased in Th1-specific IFN-γ production, of which increased IFN-γ was similar to observed effects in *Malt1*[PD/PD] mice harboring excessive IFN-γ production in conventional T and Treg cells that were strongly reduced in absolute numbers (Bornancin et al., 2015). Lastly, reduced Tfh differentiation in *Rc3h1*[Mins/Mins] mice was consistent with Tfh/Tfr-biased DKO^T cells from Roquin-deficient mice (Vogel et al., 2013). Hence, these observations place Roquin function downstream of CBM complex formation and imply that TCR signal-dependent post-transpripctional control by Roquin plays a dynamic role in immune homeostasis and inflammatory disease scenarios.

3.2.4. Th17 fate requires cleavage of Roquin-1 and IκB$_{NS}$ induction

Loss of Roquin-1/2 expression is associated with the accumulation of IL-17A$^+$ CD4$^+$ T cells but it has remained unclear which of the released mRNA targets specifically directs this pathogenic Th17 fate decision in DKO^T cells. Additionally, minimum amounts of wildtype Roquin-2 expression in CD4$^+$ T cells were enough to inhibit Th17 commitment suggesting that high avidity interactions of Th17-relevant mRNA CDE motifs and the ROQ domain account for the full TCR strength-induced Th17 differentiation (see section 3.1.3.).

Investigating T helper cell differentiation for the *Rc3h1*^{Mins} model showed that Th1 fates measured by IFN-γ producing CD4$^+$ T cells was not significantly increased in *Rc3h1*$^{Mins/+}$ or *Rc3h1*$^{Mins/Mins}$ mice but the small increase in IFN-γ matched *ex vivo* stainings of elevated IFN-γ production in splenic *Rc3h1*$^{Mins/Mins}$ Treg cells (**Fig. 24A** and see Fig. 20).
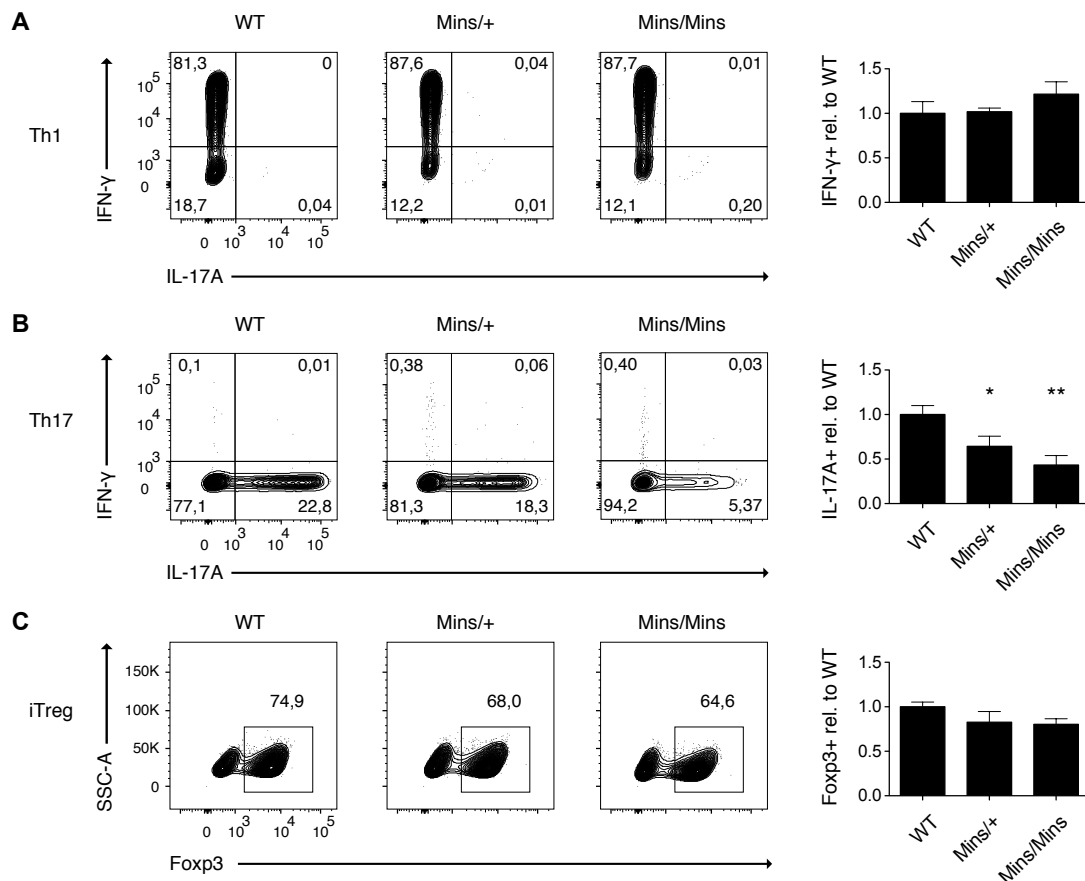
Fig. 24: Roquin-1 cleavage by MALT1 is required for Th17 cell fate decisions. (**A**) *In vitro* Th1 cell differentiation of naive WT, *Rc3h1*$^{Mins/+}$ or *Rc3h1*$^{Mins/Mins}$ CD4$^+$ T cells was analyzed by i.c. cytokine stainings after 4 hours of PMA/ionomycin treatment. Representative contour plots and quantifications as fold-change differences of IFN-γ production compared to WT counterparts from 4 replicates is shown; error bars represent ± SEM. (**B**) *In vitro* differentiation as in (A) but under Th17-polarizing conditions. Error bars represent ± SEM of 4 replicates. (**C**) *In vitro* differentiation as in (A) but utilizing iTreg-polarizing conditions and analyzing intracellular Foxp3 expression. A representative of 3 experiments and quantification as fold-change to WT counterparts is shown; error bars represent ± SEM. Statistical analysis was performed by One-Way ANOVA and Dunnett's Multiple Comparison test; *p* values *< 0.05, **< 0.01, ***< 0.001 of 3 individual replicates.

The opposite was observed upon *in vitro* Th17 differentiation as heterozygous and homozygous *Rc3h1*^{Mins} CD4+ T cells were impaired in IL-17A production by approx. 3-fold with 20% IL-17A+ CD4+ T cells from wildtype and only 6% IL-17A+ CD4+ T cells from *Rc3h1*^{Mins/Mins} mice (**Fig. 24B**). Effects of *Rc3h1*^{Mins} were gradual as Th17 commitment was already impaired in *Rc3h1*^{Mins/+} T cells. Importantly, *Rc3h1*^{Mins} CD4+ T cells did not shift towards Foxp3 expression under Th17 conditions and the induction of iTregs by *in vitro* differentiation including TGF-β was unchanged in both *Rc3h1*^{Mins} genotypes (**Fig. 24C**).

In order to examine whether impaired Th17 differentiation of the *Rc3h1*^{Mins/Mins} genotype was caused by the observed reduction in TCR-induced IκB_{NS}, *Nfkbid*-deficient CD4+ T cells were analyzed in collaboration with the group of Prof. Ingo Schmitz. The atypical inhibitor of NF-κB signaling, *Nfkbid* (IκB_{NS}), has been shown to play pivotal roles in thymic Treg development and peripheral Th17 differentiation (Schuster et al., 2012; Annemann et al., 2015).
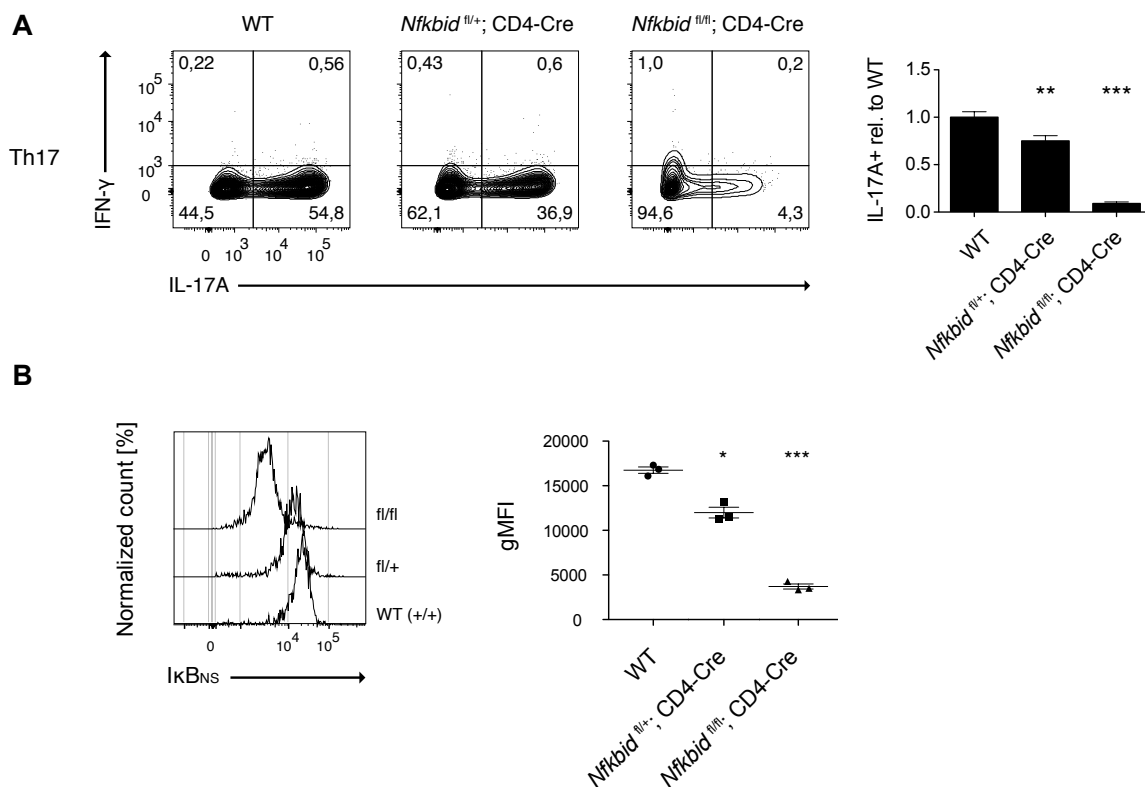
Fig. 25: Induction of IκB_{NS} is essential for Th17 differentiation. (**A**) *In vitro* Th17 cell differentiation as in Fig. 24 but of naive CD4+ T cells from WT, *Nfkbid*^{fl/+}; CD4-Cre or *Nfkbid*^{fl/fl}; CD4-Cre mice. CD4+ T cell fate was assessed as in Fig. 24B, showing 1 representative out of 2 experiments with 3-6 mice per group and quantifications of IL-17A positive cells as compared to WT counterparts. Error bars represent ± SEM. (**B**) Representative histograms of IκB_{NS} induction in CD4+ T cells from mice in (A) after treatment with PMA/ ionomycin. The quantification of IκB_{NS} levels is shown as gMFI of 3 replicates per group and error bars represent ± SEM. Statistical analysis was performed by One-Way ANOVA and Dunnett's Multiple Comparison test; *p* values *< 0.05, **< 0.01, ***< 0.001.

Indeed, *in vitro* differentiation assays using CD4^{+} T cells of homo- or heterozygous *Nfkbid*^{fl/fl}; CD4-Cre and *Nfkbid*^{fl/+}; CD4-Cre mice confirmed impaired Th17 commitment in the absence of IκB$_{NS}$ (**Fig. 25A**). Already the heterozygous deletion of *Nfkbid* remarkably decreased the frequencies of IL-17A producing T cells and the fold-change reduction compared to wildtype controls (*Nfkbid*^{+/+}; CD4-Cre) was very similar to effects observed for *Rc3h1*[Mins/Mins] mice (compare with **Fig. 24B**). The homozygous knockout of *Nfkbid* in T cells resulted in an even stronger impairment of Th17 differentiation suggesting that the quantity of IκB$_{NS}$ expression resembles a crucial determinant of Th17 fate regulation likely explaining decreased Th17 induction in the *Rc3h1*[Mins] model (**Fig. 25A**). Of note, gradual deletion of *Nfkbid* expression was confirmed by flow cytometric detection of IκB$_{NS}$ utilizing the monoclonal antibody supernatant 4C1 (**Fig. 25B**).

Together, these data suggest that Roquin-1[Mins/Mins] limits Th17 differentiation in an IκB$_{NS}$-dependent manner. Impaired induction of this atypical inhibitor of NF-κB signaling appears to be insufficient to reach a necessary TCR-dependent threshold of IκB$_{NS}$ to facilitate Th17 fate decisions. Thus, the *Rc3h1*[Mins/Mins] model not only phenocopied aspects of *Malt1*[PD/PD] but also of *Nfkbid*-deficient genotypes in steady-state *ex vivo* analyses as well as in *in vitro* assays of T cell differentiation.

3.2.5. γδ T and iNKT cells in *Rc3h1*[Mins] mice

The previous sections described effects of Roquin-deficient and Roquin-1[Mins] models on Th17 differentiation of conventional αβ-TCR[+] T helper cells. Apart from conventional T helper cells, Roquin-deficiency has been reported to affect the development and differentiation of thymic invariant natural killer T cells (iNKT) which represent a specialized subset of the unconventional T cell compartment (Drees et al., 2017). Thymic iNKT cells differentiate into iNKT1, iNKT2 and iNKT17 subsets and RORγt^{+} iNKT17 cells were shown to be highly enriched among Roquin-deficient thymic iNKT cells that were reduced in abundance (Drees et al., 2017). IL-17A-associated γδ-TCR^{+} T cells resemble another thymic subset of the unconventional T cell compartment and γδ T cells have been described as TCR strength-dependent and major producers of IL-17A (Haks et al. 2005; Hayes et al., 2005).

The impaired Th17 differentiation of *Rc3h1*[Mins/Mins] CD4^{+} T cells, however, was unique to the αβ-TCR^{+} T helper cells since there were no changes in neither abundance nor differentiation of iNKT and γδ T cell subsets (**Fig. 26, 27**). In more detail, frequencies and numbers of peripheral γδ T cells in *Rc3h1*[Mins/Mins] mice were similar to wildtype controls and the differentiation averaged at normal ratios of approx. 10% γδTCR^{+} CD44^{hi} CD122^{dim} γδT17 and 15-20% γδTCR^{+} CD44^{dim} CD122^{hi} γδT1 cells in both genotypes (**Fig. 26A, B**). Likewise, CD1d-PBS57 tetramer stainings of thymic iNKT cells showed equal frequencies and numbers of CD1d^{+} iNKTs, and iNKT subsets analyzed by RORγt and PLZF co-stainings (Savage et al., 2008) resulted in similar numbers of 2-3 x10^{5} iNKT1 and 4-10 x10^{3} iNKT2 and iNKT17 cells from both genotypes (**Fig. 27A, B**).
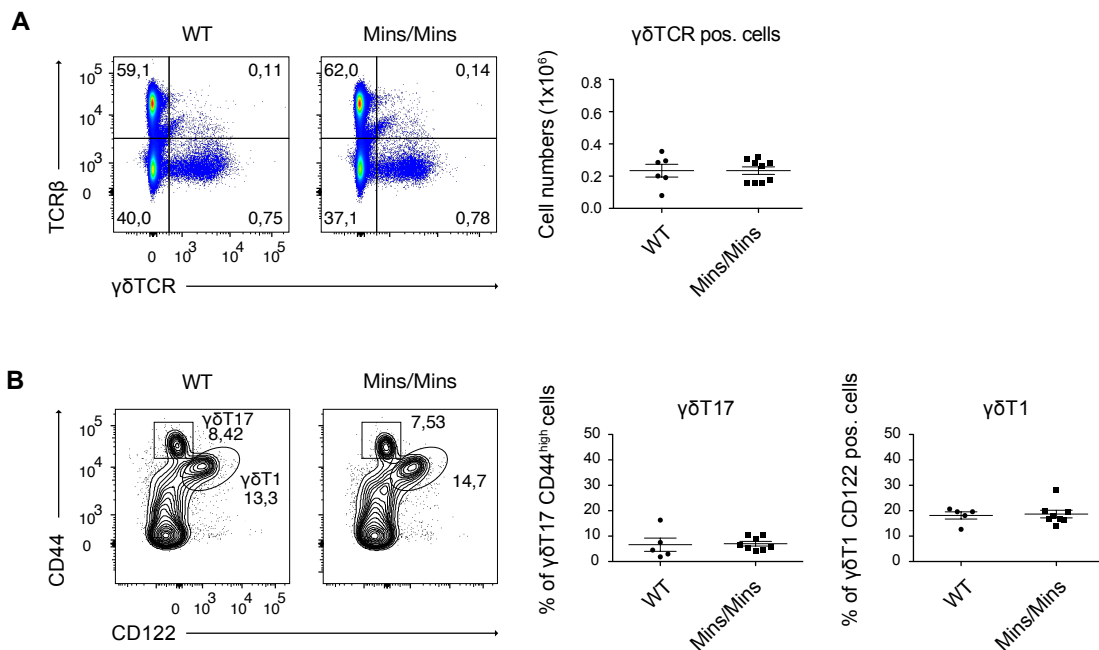
Fig. 26: Differentiation of γδ T cells in *Rc3h1*^Mins mice. (**A**) Flow cytometric analysis of γδ T cell populations from peripheral lymph nodes of WT or *Rc3h1*^Mins/Mins mice. γδ TCR-positive cells were quantified as total numbers of live cells and error bars represent ± SEM of 6-9 replicates from 6 experiments. (**B**) γδ T cell differentiation into γδT1 or γδT17 subsets was assessed by additional surface stainings of CD44 and CD122. The cell subsets were quantified from γδ TCR-positive cells (A). Error bars represent ± SEM of 5-8 replicates.
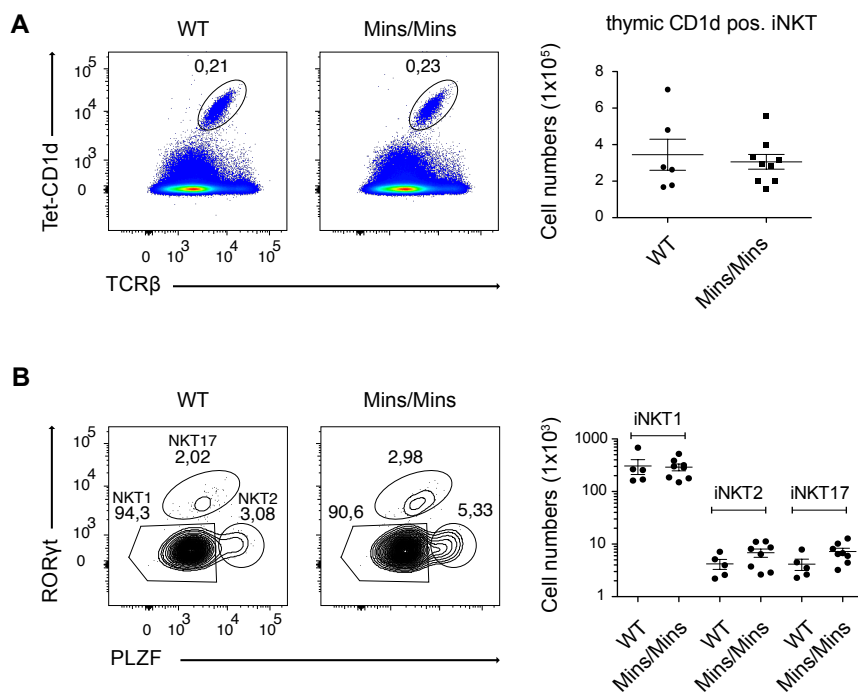
Fig. 27: Differentiation of iNKT cells in *Rc3h1*^Mins mice. (**A**) *Ex vivo* PBS57-CD1d-PE tetramer stainings of thymic iNKT cells from WT or *Rc3h1*^Mins/Mins mice. Quantification of total numbers (1 x10^5 cells) of thymic Tet-CD1d^+ TCRβ^+ iNKT cells is shown. Error bars represent ± SEM of 6-9 replicates of 5 experiments. (**B**) Analysis of thymic Tet-CD1d^+ iNKT1, NKT2 and NKT17 cell differentiation via RORγt and PLZF stainings. Total cell numbers (1 x10^3 cells) are quantified and error bars represent ± SEM of 5-8 replicates.

3.2.6. Gain-of-function Roquin-1^{Mins} protects from EAE *in vivo*

In view of the impaired Th17 differentiation in *Rc3h1*$^{Mins/+}$ and *Rc3h1*$^{Mins/Mins}$ CD4$^+$ T cells, *Rc3h1*$^{Mins/Mins}$ and wildtype control mice were challenged *in vivo* by induction of experimental autoimmune encephalomyelitis (EAE), which is a Th17-specific experimental model of autoimmune disease that affects the central nervous system (CNS) and resembles in many aspects human multiple sclerosis (MS) disease. Mice of both groups were tracked for 15 days and scored starting at day 9 post immunization with myelin oligodendrocyte glycoprotein (MOG$_{35-55}$) and pertussis toxin (PTX), investigating whether the gain-of-function of Roquin-1$^{Mins/Mins}$ proved relevant in Th17 responses *in vivo*.

Indeed, the onset and severity of EAE disease was restrained in *Rc3h1*$^{Mins/Mins}$ mice and reduced average clinical scores of less than 0.5 according to the EAE scoring procedure were determined compared to wildtype counterparts (**Fig. 28A**). In fact, only two *Rc3h1*$^{Mins/Mins}$ mice developed mild symptoms of EAE disease. The number of CNS-infiltrating CD4$^+$ T cells in both groups indicated pronounced infiltration in wildtype mice (10-15 x10^4 CD4$^+$ T cells), while there were variable amounts of T cell infiltrates in the CNS of *Rc3h1*$^{Mins/Mins}$ mice (**Fig. 28B**).
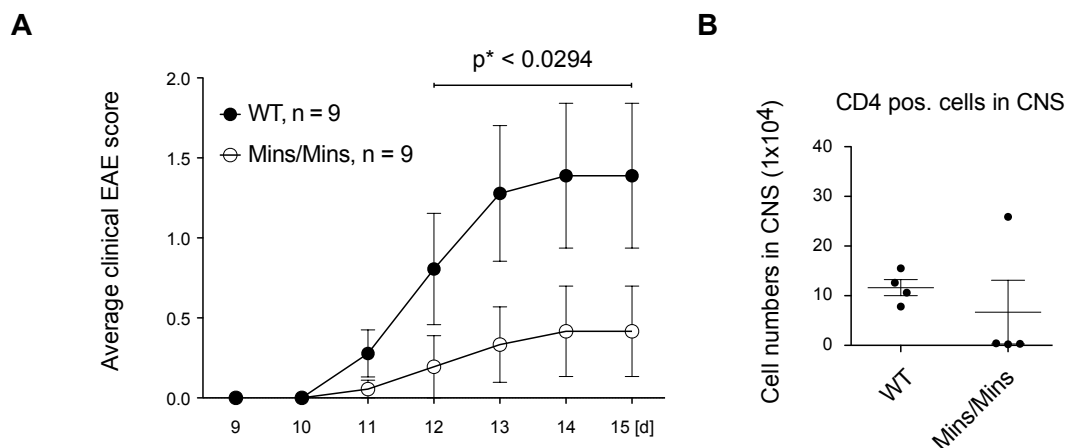
Fig. 28: Roquin-1$^{Mins/Mins}$ protects from severe onset of EAE. (**A**) Average clinical EAE scores from day 9 to day 15 of WT and *Rc3h1*$^{Mins/Mins}$ mice immunized with MOG peptide (s.c.) and injected with Pertussis toxin (PTX, i.v.) on day 0 and day 2. Error bars represent ± SEM of scores from 9 mice per group. Statistical analysis was performed by Mann-Whitney test; *p* value *< 0.05. (**B**) Quantification of total numbers of CNS-infiltrating CD4$^+$ T lymphocytes in WT and *Rc3h1*$^{Mins/Mins}$ mice at day 15 (peak) of EAE in 4 mice per group with active disease, isolated from spinal cords and brains (pooled per mouse). Error bars represent ± SEM.

Analyzing infiltrating CD4$^+$ T cells upon *ex vivo* P/I stimulation showed unaltered frequencies of 40-50% of IFN-γ producing cells in the CNS of both genotypes (**Fig. 29A, B**). In contrast, CNS-derived CD4$^+$ T cells of *Rc3h1*$^{Mins/Mins}$ mice showed greatly reduced frequencies of only 5-10% of IL-17A$^+$ single-positive or IFN-γ$^+$ IL-17A$^+$ double-positive CD4$^+$ T cells compared to approx. 25% of IL-17A$^+$ CD4$^+$ T cells in wildtype controls (**Fig. 29A, B**).

In addition, CD4+ T cells within the CNS of *Rc3h1*Mins/Mins mice demonstrated normal expression of T-bet but low levels of RORγt expression resulting in attenuated frequencies of RORγt+ IL-17A+ double-positive CD4+ T cells in the CNS of *Rc3h1*Mins/Mins mice (**Fig. 29C, D**).
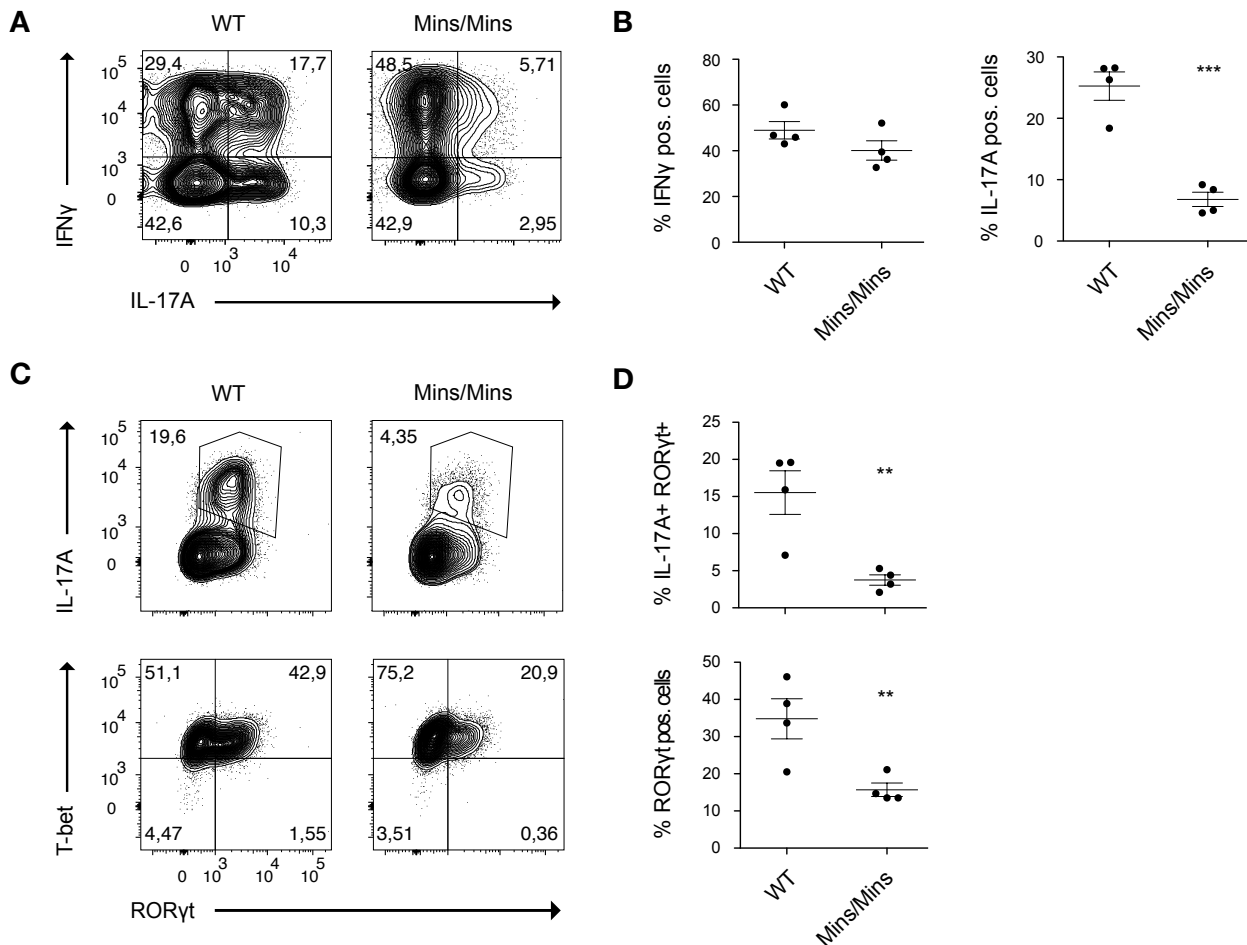

Fig. 29: Roquin-1 Mins/Mins **controls Th17-specific IL-17A and RORγt *in vivo*.** (**A**) Representative contour plots of cytokine production by CD4+ T cell infiltrates in the CNS of WT and *Rc3h1*Mins/Mins mice at day 15 (peak) of EAE analyzing IFN-γ and IL-17A after 4 hours of restimulation with PMA/ionomycin. (**B**) Quantification of IFN-γ and IL-17A positive CNS-infiltrating CD4+ T cells shown in (A); error bars represent ± SEM of 4 mice per group. (**C**) Representative contour plots of IL-17A+ RORγt+ or T-bet+ RORγt+ CD4+ T cells from infiltrates in the CNS at day 15 (peak) of EAE. (**D**) Quantification of IL-17A+ RORγt+ double-positive or RORγt+ CNS-infiltrating CD4+ T cells shown in (E) for WT and *Rc3h1*Mins/Mins mice at day 15 (peak) of EAE. Error bars represent ± SEM of 4 mice per group and statistical analysis was performed by two-tailed Student's *t* test; *p* values *< 0.05, **< 0.01, ***< 0.001.

Conclusively, these data supported the notion of Roquin-1 as one of the best-known post-transcriptional regulators of Th17 fate choice. The *in vivo* EAE model proved Roquin-1 gain-of-function relevant as a central molecular determinant regulating and restricting Th17-derived immunopathology. Hence, Roquin-1 represents the first substrate of proteolytic MALT1 activity that limits Th17 fate and presumably protects from autoimmune disorders such as multiple sclerosis (MS). These findings revealed the physiologic importance of TCR-induced and MALT1-executed cleavage of Roquin-1 for the development of autoimmune disease.

In summary, the data promoted the concept in which TCR signal strength causes a certain degree of Roquin inactivation. Interfering with this distinct TCR strength integrating CBM signalosome pathway is able to specifically mitigate Th17-mediated immunopathology. Finally, the mechanistic concept implies that exceeding a specific threshold enables sufficient induction of $I\kappa B_{NS}$ as a prerequisite for Th17 differentiation.

4. Discussion

The *in vitro* and *in vivo* data presented in this doctoral thesis have described TCR strength-mediated cleavage of Roquin as a dynamic integrator of TCR signals causing selective mRNA target derepression to control Th17 cell fate decisions. Antigen signals of increasing avidity were converted into graded cleavage of Roquin and the MALT1-insensitive Roquin-1$^{Mins/Mins}$ mutant proved its crucial involvement in controlling the transcriptional modulator IκB$_{NS}$ (*Nfkbid*) and protecting from severe Th17-driven EAE disease *in vivo*.

The following sections will discuss how expression of different amounts of Roquin expression or its mutational inactivation affect target derepression (4.1. Molecular control of Roquin targets) and CD4$^+$ T cell fate decisions will be evaluated according to loss of Roquin expression and antigen-dependent TCR signals mediating Roquin cleavage (4.2. TCR signal-dependent Roquin cleavage in T cell differentiation). Finally, target-specific effects of the novel *Rc3h1*^{Mins} model will be summarized in respect to T cell differentiation (4.3. The MALT1-insensitive Roquin-1 model) and compared to phenotypes of previously published CBM mutant models to deduce Roquin-specific effects of MALT1 cleavage on physiologic immune regulation (4.4. Comparing *Rc3h1*^{Mins} with CBM-associated mutant models).

4.1. Molecular control of Roquin targets

Multiple amino acid residues within the ROQ domain of Roquin-1 contribute to high-affinity interactions with target mRNA-associated CDE and ADE type binding motifs. Initially identified for the 3'-UTR of *Tnf* mRNA (Tan et al., 2014), these ROQ domain residues (K220, K239, Y250, R260) have been shown to be integral sites of mRNA/ROQ interactions (Schlundt et al., 2014). Single or combined mutations of the ROQ domain differentially affected target expression suggesting a low to high avidity target ranking, i.e. Ox40 < Icos < Regnase-1 < Nfkbid (IκB$_{NS}$). Accordingly, CD4$^+$ T cell reconstitutions with single ROQ domain mutants (Y250A and R260A) already led to partial derepression of the low avidity target Ox40 and double (K239A; R260A) or triple (K220A; K230A; R260A) mutants were inactive to repress Ox40 expression (**Fig. 5, 6**). This aligns well with previous observations of only two CDE-like (K$_d$ ~ 1.5 µM) or ADE-like (K$_d$ ~ 0.08 µM) binding motifs described for the 3'-UTR of Ox40 mRNA, although the ADE-like motif represents a single high affinity binding site majorly interacting with Y250 in the ROQ domain (Janowski et al., 2016). Both Icos and Regnase-1 showed intermediate responses as single and double ROQ mutants were still able to repress these targets, however, Regnase-1 was no longer repressed by the triple mutant (**Fig. 5**). Importantly, reconstitutions revealed high functional avidity of the ROQ-CDE (*Nfkbid*) interaction as all single and double but not the triple alanine mutant were able to repress IκB$_{NS}$ expression (**Fig. 5**). This observation may support the idea of multivalent binding events with several ROQ residues being involved in binding one or more similar or different CDE motifs within the *Nfkbid* 3'-UTR. In more detail, additional domains adjacent to the ROQ domain, i.e. RING,

CCCH and HEPN domains, might dynamically contribute to RNA-Roquin interactions once the first mRNA CDE motif is bound and this might as well involve perturbations in secondary stem-loop structures facilitating access to additional binding motifs. Indeed, multiple stem-loop motifs have been identified for the *Nfkbid* 3'-UTR to allow mRNA target recognition by Roquin (Essig et al., 2018). The pronounced functional avidity of the *Nfkbid* mRNA involves the high affinity binding of individual CDE and ADE type binding sites as well as high numbers of at least seven Roquin-recognized stem-loops and linear binding elements in its 3'-UTR (Leppek et al., 2013; Essig et al., 2018). These interactions are proposed to embrace accessory, cooperative or redundant functions but also enable translational inhibition of $I\kappa B_{NS}$ as its 3'-UTR is enriched in ≥ 4 individual or additive Roquin binding sites allowing increased recruitment of downstream effectors (Essig et al., 2018). Similarly, pronounced ROQ-CDE (*Nfkbid*) interactions have been well-described by RNA-immunoprecipitation analyses in macrophages that also included the conserved CDE-containing *Tnf* 3'-UTR of maximum enrichment scores (Leppek et al., 2013).

On the other hand, different dose-response kinetics of target derepression or upregulation were investigated by the genetic titration of Roquin alleles and OVA antigen co-cultures (**Fig. 1, 12**). Gradual deletion of *Rc3h1* and *Rc3h2* wildtype alleles in CD4$^+$ T cells as well as antigen-mediated OT-II T cell activation helped to characterize OX40 and CTLA-4 receptors as low-avidity targets already responding to a maximum by Roquin-1 deletion or low TCR signal strength, while maximum expression of intermediate to high avidity targets such as IRF4 and $I\kappa B_{NS}$ required deletion of both Roquin paralogs or high TCR strength (≥ 1.0 μg/mL $OVA_{323-339}$) to become fully derepressed or upregulated, respectively (**Fig. 1, 12**). In CD4$^+$ T cells, Roquin-1 expression outcompeted Roquin-2 levels by approx. 5-6-fold and heterozygous deletion of *Rc3h1* had no effects on target derepression with OX40 and CTLA-4 requiring at least full deletion of *Rc3h1* for maximum derepression (Heissmeyer and Jeltsch, 2016). Hence, Roquin-1 expression appeared to be at least 5-times higher than required as the expression of Roquin-2 alleles only was still sufficient to repress Roquin targets of particularly high binding avidities, i.e. *Icos*, *Zc3h12a* (Regnase-1), *Irf4* and *Nfkbid*.

All three experimental setups highlighted increased functional avidity as the major mechanism of *Nfkbid* ($I\kappa B_{NS}$) regulation and thus prioritization of target repression according to the quantity of high-affinity 3'-UTR binding sites still being recognized during TCR-dependent Roquin cleavage and inactivation. Apart from Th17 promoting $I\kappa B_{NS}$ regulation, other intermediate affinity targets like *Nfkbiz*, *Irf4* and *Icos* may - derepressed at intermediate TCR strength - additionally promote Th17 commitment (Annemann et al., 2016; Bauquet et al., 2009; Paulos et al., 2010; Okamoto et al., 2010). However, effects observed for *Nfkbiz* and *Irf4* derepression in DKO^T cells were minor compared to responses of *Nfkbid* ($I\kappa B_{NS}$). Besides, the endonuclease Regnase-1 is a well-known regulator of *Nfkbiz* mRNA stability and therefore likely cross-regulates *Nfkbiz* expression in DKO^T cells in which endogenous Regnase-1 expression was elevated (**Fig. 1**). Conversely, also low avidity targets such as OX40 and CTLA-4 might shape the TCR-dependent Th17 threshold since OX40 was demonstrated to inhibit Th17 differentiation via activation of RelB-dependent recruitment of epigenetic repressors (G9a, SETDB1) to the *Il17* locus and CTLA-4 was involved in constraining T cell differentiation by antagonizing CD28-mediated co-stimulation (Li et al., 2008; Xiao et al.,

2016; Wang et al., 2015; Wei et al., 2019). In OT-II co-culture, OX40 and CTLA-4 were fully induced at low TCR signal strength or intermediate levels of Roquin inactivation and could therefore prevent Th17 commitment in response to T cell stimulations inducing only suboptimal levels of $I\kappa B_{NS}$.

4.2. TCR-dependent Roquin cleavage and T cell differentiation

T cell-specific Roquin-1 cleavage was detected upon stimulation with anti-CD3/CD28 antibodies or OVA peptide-loaded BMDCs in OT-II co-cultures using the novel monoclonal antibody 5F6 (**Fig. 10, 11**). Both *in vitro* assays provided evidence for graded TCR activation-induced cleavage of Roquin-1 and Roquin-1$^{aa1-510}$ fragment accumulation correlated well with anti-CD3/CD28-dependent *Nr4a1*-Nur77-GFP reporter upregulation (Moran et al., 2011). Since surface expression of CD69 can be induced by non-specific homeostatic or inflammatory stimuli such as type I interferons or LPS, the analysis of Nur77-GFP was TCR-specific and as well evaluated with respect to antigen-derived upregulation of CD69 and Roquin-1 cleavage in OVA$_{323-339}$ co-cultures (**Fig. 11**). Interestingly, small but significant frequencies of T cells harboring Roquin-1 cleavage without antigen/TCR ligation indicated low basal MALT1 activity which was especially prominent in immunoblots of the genetic Roquin titration (**Fig. 1**), in correlations of 5F6 signals with Nur77-GFP (**Fig. 10**) and OT-II T cells from co-cultures without OVA peptide loading of BMDCs (**Fig. 11**). In view of antigen/TCR-independent Roquin-1 cleavage, it is tempting to speculate that MALT1 substrate specificities have been previously underestimated. Roquin-1, yet not Roquin-2, harbors two independent MALT1 cleavage sites (LIPR$_{510}$, MVPR$_{579}$) possibly rendering Roquin-1 particularly susceptible to MALT1 cleavage and it remains elusive to which extent secondary allosteric- or exosite-driven mechanisms remote from the active catalytic site may enhance cleavage activity translating average into highly efficient cleavage sites targeted by the MALT1 protease (Hachmann et al., 2012). Apart from technical issues due to fixation/permeabilization, T cells positive for Roquin-1 cleavage but lacking Nur77-GFP induction likely describe effects of either basal tonic TCR signaling in absence of foreign antigen or even self-pMHC-independent basal activity of MALT1. Moreover, Roquin-1 cleavage positive T cells might showcase altered half-lives/stabilities of the Roquin-1$^{aa1-510}$ fragment or the Nur77-GFP reporter signals resulting in Roquin-1$^{aa1-510}$ positive ex-Nur77-GFP$^+$ T cells after approx. 18 hours of *in vitro* stimulation. Of note, among *Nr4a* paralogs *Nr4a1* is the most sensitive to TCR signals responding to tonic signaling and requiring only minimum antigen concentrations for upregulation in T cells but accumulating GFP reporter expression has been described persistent and TCR dwell time-dependent (Jennings et al., 2020). In OT-II T cells co-cultured with BMDCs, 5F6 Roquin-1$^{aa1-510}$ signals increased with OVA$_{323-339}$ concentrations obtaining a dose-response peak at peptide loading concentrations of 1.0 µg/mL (**Fig. 11**). Comparing the WT OVA$_{323-339}$ peptide to the R331 mutant (OVA$_{R9}$) at concentrations optimal for OVA$_{WT}$ responses (1.0 µg/mL), the OVA$_{R9}$ mutant peptide of approx. 10-fold lower affinity for the OT-II TCR was insufficient to induce similar CD69 expression or Roquin-1 cleavage (**Fig. 11** and Cho et al., 2017). Together, this strongly supported

the concept in which both single TCR affinity (OVA_{WT} or OVA_{R9}) as well as the amount of antigen-dependent TCR ligations (OVA titration) determine the strength of TCR signals that quantitatively mediate CBM complex formation, MALT1 activity and dynamic Roquin cleavage.

Investigating T cell fate decisions, full deletion of Roquin encoding alleles (*Rc3h1* and *Rc3h2*) in $CD4^+$ T cells as well as maximum antigen doses in $OVA_{323-339}$ co-cultures promoted Th17 differentiation, yet already heterozygous Roquin-2 expression restricted Th17 fates and intermediate concentrations of $OVA_{323-339}$ were not sufficient to foster TCR strength-responsive Th17 but Th1 commitment (**Fig. 7, 8**). In addition to Th17-specific IL-17A production, the induction of RORγt similarly required maximum OVA concentrations upon Th0 conditions to drive the transcriptional program inducing Th17 fates. In contrast, Th1 promoting T-bet expression was differentially sensitive to the strength of TCR stimulation requiring 10-fold lower concentrations (1.0 µg/mL) for full induction (**Fig. 8**). The dynamic onset of Th17-associated target derepression and Th17 fate choice align well with previous reports on EC_{50} values for OT-II proliferation of 0.2 µM ($OVA_{323-339}$) which is covered by $OVA_{323-339}$ concentrations of 0.1 - 1.0 µg/mL (0.056 - 0.56 µM) used in this work (Robertson et al., 2000). In fact, Th1 commitment accompanies OT-II T cell proliferation at peptide loading concentrations of 0.056 - 0.56 µM rather resembling a default T effector fate decision during clonal expansion *in vitro*. However, EC_{50} peptide concentrations for half-maximal OT-II proliferation were insufficient for Th17 differentiation which required elevated concentrations beyond the threshold of ≥ 5.6 µM (10 µg/mL $OVA_{323-339}$ and **Fig. 7, 8**). Besides, the comparison of OVA_{WT} (H331) and OVA_{R9} (R331) mutant peptides with an estimated 100-fold difference in its potency to drive OT-II T cell activation (CD69 expression) resembles findings for *in vivo* OVA-CFA immunizations identifying TCR signal quality to instruct OT-II T cell fate behavior and OT-I proliferation triggered by $LCMV-GP_{33-41}$-derived M/C-peptides of altered affinities (Henrickson et al., 2008; Cho et al., 2017).

Previously, TCR strength has been reported to outcompete qualitative effects of adjuvants/cytokines in polarizing T cell differentiation (van Panhuys et al., 2016). Furthermore, the extent of TCR ligation is directly linked to graded IRF4 induction coordinating T effector and Tfh cell fate trajectories. Preceding CD25 receptor signaling via IL-2, IRF4-mediated DNA element recognition is associated with Blimp-1 upregulation activating the Bcl6-Blimp-1 antagonistic transcription factor module (Johnston et al., 2009; Krishnamoorthy et al., 2017). Mechanistically, Irf4-deficient models have been employed together with antigen immunizations to link increased IRF4 expression to binding of low affinity ISRE DNA recognition elements promoting the Teff program via Blimp-1. In addition, transcriptional activities of cooperating BATF and IRF4 correlate with induction of TCR-sensitive target genes caused by pronounced binding of AICE motifs which integrates TCR strength-guided transcription factor activity to distinct gene signatures of T cell differentiation (Iwata et al., 2017). The IL-2-inducible Tec family kinase (ITK) has been identified as another "sensor" of TCR strength whose deficiency leads to reduced Th17 differentiation via enhanced p-STAT5 to p-STAT3 signaling ratios and $Itk^{-/-}$ models are directly connected to reduced TCR signal strength involving impaired upregulation of IRF4 and altered memory formation in $CD8^+$ T cells (Gomez-Rodriguez et al., 2009; Conley et al., 2020; Solouki et al., 2020). Comparing $CD4^+$ helper T cell differentiation, strong TCR signals are assumed to promote effector Th1 over Th2 as well as Th17

over iTreg fates and conflicting data suggested either Th1 over Tfh commitment at high TCR signals or pronounced Tfh accumulation due to persistent antigen-TCR interactions (Milner et al., 2010; Jorritsma et al., 2003; Gomez-Rodriguez et al., 2014; Keck et al. 2014; Baumjohann et al., 2013). Moreover, recent work by Bartleson and colleagues proposes a pivotal role of tonic signaling strength experienced by polyclonal populations with a diverse repertoire of TCR affinities which tailors T effector versus Tfh cell decisions. Herein, the well-established IL-2-Blimp-1 axis correlating to TCR activation and antagonizing Tfh-specific Bcl6 regulation has been supposed to represent a model of T effector versus Tfh cell decisions with low tonic signaling promoting Tfh cell fates (Bartleson et al., 2020). However, the reports described above mostly focused on T effector or Tfh fate decisions and technical variations analyzing TCR avidity for antigen peptide:MHC interactions have promoted controversial findings: Groups concluding increased TCR signal strength promotes T effector responses used altered peptide ligand systems increasing tonic signaling and TCR activation strength *in vivo* (Krishnamoorthy et al., 2017; Snook et al., 2018; Kotov et al., 2019), while others characterized high antigenic TCR affinity essential for Tfh cell development utilizing either TCR-transgenic models or pMHC-tetramer binding readouts (Fazilleau et al., 2009; Tubo et al., 2013; DiToro et al., 2018). Finally, biophysical determinants of different TCR-peptide:MHC II systems such as ligand binding on/off-rates (K_{on}/K_{off}), dissociation constants (K_d), EC_{50} values and interaction dwell times (half-lives, $t_{1/2}$) appear to account for individual antigen/TCR-specific signal intensities that dissect alternative Th cell fate programs and it remains contentious to directly compare APL systems of multiple different parameters (Aleksic et al. 2010; Govern et al., 2010).

Importantly, and apart from Tfh or Treg commitment, it has remained elusive how effects of TCR strength enable to resolve the bifurcation of Th1 from Th17 cells within the T effector compartment. *In vitro* OT-II T cell experiments described in this doctoral thesis highlight the crucial effects of TCR-induced Roquin cleavage as a specific integrator/regulator of Th17 effector differentiation and illustrate side-by-side the crucial involvement of high antigen dose to promote Th17 but not Th1 effector cell fates. Conclusively, the interplay of TCR-induced MALT1 activity and Roquin function defines a post-transcriptional threshold of TCR strength in Th17 differentiation and the model strongly suggests a pivotal involvement of Roquin-based control of the transcriptional modulators IRF4 and IκB$_{NS}$ to foster gene regulatory programs specific for Th17 fates.

4.3. MALT1-insensitive Roquin-1 (*Rc3h1*[Mins])

The CRISPR/Cas9-based model of MALT1-insensitive Roquin-1 (*Rc3h1*[Mins]) has uncovered that repression of IκB$_{NS}$ represents a major mechanism of preferential Roquin activity to integrate TCR signaling into the modulation of NF-κB activation and Th17 cell fate control. Both Roquin-1[Mins/+] and Roquin-1[Mins/Mins] restricted IκB$_{NS}$ upregulation during P/I- or OVA peptide-induced activation to limit Th17 cell differentiation *in vitro.* Importantly, gain-of-function Roquin-1[Mins/Mins] as well protected from Th17-driven EAE disease *in vivo.*

Gene editing by CRISPR/Cas9-guided homology-directed repair was employed to create the *Rc3h1*[Mins] knockin in the mouse germline (**Fig. 13**). Constitutive gene expression of *Rc3h1*[Mins] was verified in immunoblots of CD4^{+} T cells stimulated with P/I to induce cleavage of Roquin paralogs and to test MALT1 insensitivity of *Rc3h1*[Mins/+] and *Rc3h1*[Mins/Mins] T cells (**Fig. 15**). Heterozygous *Rc3h1*[Mins/+] was already sufficient to maintain half of full-length Roquin-1 expression during T cell activation, while homozygous *Rc3h1*[Mins/Mins] T cells completely lacked Roquin-1 cleavage fragments. Notably, independent of Roquin-1[Mins] both Roquin-2 and Regnase-1 were still targeted by MALT1 cleavage (**Fig. 15**). *Rc3h1*[Mins] mice did not show apparent immunological phenotypes under homeostatic conditions and Roquin-specific direct targets were expressed at endogenous levels similar to wildtype controls. Upon *in vitro* stimulation, however, maintained presence of full-length Roquin-1 in *Rc3h1*[Mins/+] and *Rc3h1*[Mins/Mins] T cells selectively attenuated TCR-dependent induction of targets including TNFα, *Nfkbid* (IκB$_{NS}$), OX40 and IRF4 (**Fig. 15-18**). Strongest target repression in *Rc3h1*[Mins/Mins] T cells was observed for protein and mRNA levels of TNFα and *Nfkbid* (IκB$_{NS}$) that showed attenuated induction in both P/I stimulations of CD4^{+} T cells and antigen-induced OT-II co-cultures (**Fig. 15-18**). In more detail, TCR strength-dependent induction of IκB$_{NS}$ relative to cells without antigen stimulus and its individual mean fluorescence intensities were reduced in *Rc3h1*[Mins/Mins] OT-II cells which was not the case for IRF4 that was only reduced in absolute expression levels but not in its fold-induction. These target-specific effects in *Rc3h1*[Mins] T cells align well with Roquin-RNA-IP analyses conducted in LPS-stimulated RAW264.7 macrophages that revealed 475-fold enrichment of the *Nfkbid* mRNA target containing multiple binding sites including a unique tandem CDE and 192-fold enrichment of the proinflammatory cytokine *Tnfa* mRNA (Leppek et al., 2013). Importantly, both 3'-UTR CDE sequences are conserved across multiple (≥ 10) vertebrate species providing evidence of mRNA CDE motifs as the primary Roquin targets (Leppek et al., 2013). In total, six cooperative stem-loop structures and a linear sequence element (LBE) have been identified to account for robust post-transcriptional regulation of the *Nfkbid* 3'-UTR, requiring at least three stem-loops for strongest regulation mediated by decapping, deadenylation and translational inhibition (Essig et al., 2018). In line with potential high avidity binding of multiple stem-loops, the unique repression of IκB$_{NS}$ induction by Roquin-1[Mins/Mins] was even comparable to mepazine-pretreated Roquin-1[WT] T cells in which pharmacological inhibiton of the MALT1 protease mirrored maintained Roquin-1 expression during P/I stimulation (**Fig. 15**).

Together, these data established an important functional connection of the Th17 determining factors MALT1, Roquin and IκB$_{NS}$ as *Rc3h1*[Mins/Mins] T cells were specifically impaired in Th17 differentiation (**Fig. 24**). The MALT1/Roquin/IκB$_{NS}$ axis sets a unique post-transcriptional threshold of TCR strength in Th17 differentiation because blocking Roquin-1 cleavage by MALT1 did not shift cell fates towards iTreg differentiation as previously observed for TCR strength- and ITK-dependent control of Th17 differentiation (Gomez-Rodriguez et al., 2009; Gomez-Rodriguez et al., 2014). Likewise, already the heterozygous knockout of *Nfkbid*, thus altered expression levels of IκB$_{NS}$, significantly reduced the frequencies of Th17 cells (**Fig. 25**). This supports the idea that defined thresholds of IκB$_{NS}$ expression and its transcriptional activity determine Th17 fate commitment. IκB$_{NS}$-dependent defects in Th17 differentiation of *Rc3h1*[Mins] T cells were similar to

effects observed for graded knockout of *Nfkbid* alleles and low levels of IκB$_{NS}$ induction in *Rc3h1*$^{Mins/Mins}$ T cells were equivalent to attenuated IκB$_{NS}$ expression in *Nfkbid*$^{fl/+}$; CD4-Cre T cells (**Fig. 15, 17, 25**). These results reciprocally confirm the current view on Roquin-regulated Th17 fates as increased Th17 differentiation in Roquin-deficient CD4$^+$ T cells could be partially normalized back to WT levels by knockdown experiments utilizing *Nfkbid*-specific shRNA that did not affect IFN-γ producing Th1 cells (Jeltsch et al., 2014). Similarly, deficiency in *Nfkbid* (IκB$_{NS}$) has been associated with impaired thymic Treg development, reduced peripheral Treg cells and both *in vitro* iTreg-specific Foxp3 as well as Th17-specific IL-17A induction have been reported impaired (Annemann et al., 2015; Schuster et al., 2012). These effects have been explained by IκB$_{NS}$ binding to the *Foxp3* promotor and the κB site CNS3, interaction of IκB$_{NS}$ with c-Rel and p50 as well as reduced IL-2Rα (CD25) and IL-2Rβ (CD122) expression leading to an accumulation of thymic Foxp3$^-$ precursor Treg cells in *Nfkbid*$^{-/-}$ mice (Schuster et al., 2012; Schuster et al., 2017). However, dual effects on IL-2R and Foxp3 expression were not observed for *Rc3h1*^{Mins} mice whose Foxp3 expression appeared similar to wildtype counterparts, thus suggesting lacking MALT1 inducibility of Foxp3 under homeostatic conditions (**Fig. 24**). Of note, no differences in Treg-specific signaling via STAT5 phosphorylation have been observed for *Nfkbid*-deficient T cells which is as well different from *Itk*$^{-/-}$ T cells that have increased IL-2-dependent p-STAT5 but impaired IL-6/TGF-β-dependent p-STAT3 signaling and thus promote Foxp3$^+$ iTreg fates at the expense of Th17 differentiation (Gomez-Rodriguez et al., 2009; Gomez-Rodriguez et al., 2014). Putting the observed defects of *in vitro* Th17 differentiation to the test, *Rc3h1*$^{Mins/Mins}$ mice prevented the severe onset of Th17-driven *in vivo* EAE disease which correlated with impaired Th17 commitment and reduced EAE symptoms reported for *Nfkbid*$^{-/-}$ mice (**Fig. 28, 29** and Kobayashi et al., 2014).

To further strengthen the mechanistic understanding of Roquin-1-mediated suppression of IκB$_{NS}$ during T cell stimulation, future studies should as well focus on CD4$^+$ T cell proliferation kinetics, IL-2R expression as well as IL-2, IL-6 or TGF-β responsiveness. Likewise, and with respect to shRNA knockdowns of *Nfkbid* in DKO^T cells, reexpression of IκB$_{NS}$ in *Rc3h1*$^{Mins/Mins}$ T cells by viral reconstitution represents another elegant strategy to provide mechanistic evidence for the unique Roquin-specific regulation of *Nfkbid* mRNA relevant for Th17 control. Eventually, these data strongly suggest Roquin-dependent repression of IκB$_{NS}$ as an inverse readout of TCR strength or MALT1 activity, respectively, and indicate that limited upregulation of IκB$_{NS}$ in *Rc3h1*^{Mins} mice phenocopies deficiency in *Nfkbid* and its effects on Th17 fate decisions.

4.4. Comparing *Rc3h1*^{Mins} with CBM-associated mutant models

The Carma1/CARD11-Bcl10-MALT1 (CBM) signalosome is a central regulator of T cell signaling that drives transcriptional NF-κB activation and the MALT1 protease employs direct cleavage of substrate proteins to modify TCR-inducible NF-κB signaling and post-transcriptional gene regulation. Unexpectedly, *Malt1*$^{PD/PD}$ mice revealed overt pathologies compared to otherwise healthy *MALT1*-deficient models. The *Malt1*$^{PD/PD}$ mice showed multiorgan T/B cell

infiltrations, lymphadenopathy accompanied by abnormal cellularity of B220^{+} B cells, CD4^{+}/CD8^{+} cells, enhanced peripheral activation of CD4^{+}/CD8^{+} T cells, elevated IgG1 and IgE antibody titers and increased production of IFN-γ and IL-4 cytokines (Bornancin et al., 2015). In total, *Malt1*[PD/PD] pathologies were majorly assigned to an IPEX syndrome-like phenotype, showing defective Treg and innate-like B cell development concomitant to their relative dysbalance to increased IFN-γ-mediated autoinflammation. Similar to *Malt1*^{-/-} mice, inactivation of MALT1 protease was associated with reductions in peritoneal B1 B cells, PP-localized GC B cells, splenic MZ B cells, follicular helper T cells, natural Treg cells and impaired production of TNFα, IL-10 and IL-2 cytokines. Interestingly, both c-Rel and p50, known interactors of the Roquin top target *Nfkbid* (IκB_{NS}), revealed impaired upregulation upon anti-CD3/CD28-guided T cell activation together with defective proliferative responses and impaired induction of IL-2 (Bornancin et al., 2015; Gewies et al., 2014). Notably, c-Rel is specifically targeted by the MALT1 substrate Regnase-1 and thus c-Rel expression is possibly controlled by maintained Regnase-1 activity in *Malt1*[PD/PD] T cells (Uehata et al., 2013). Likewise, rendering Roquin-1 insensitive to MALT1 appears to maintain control over IκB_{NS} expression levels and it supports the idea that IκB_{NS} induction represents a potential reporter of MALT1 activity. In fact, concerted action of both factors c-Rel and IκB_{NS} could affect IL-2 induction or proliferation of T cells and determine development and expansion of iTreg/Th17 cells found reduced in both *cRel*- and *Nfkbid*-deficient models (Chen et al., 2011; Grinberg-Bleyer et al., 2017; Schuster et al., 2017). Both MALT1 models were less capable of *in vitro* Th17 induction and protected mice from EAE disease, yet *Malt1*[PD/PD] but not heterozygous *Malt1*[PD/WT] was necessary to limit Th17-specific CNS infiltration (Brüstle et al., 2012; Jaworski et al., 2014; Bornancin et al., 2015).

Rc3h1[Mins/Mins] mice appeared normal but shared some milder phenotypes with *Malt1*[PD/PD] mice including the reduced thymic Treg frequencies without affecting iTreg development *in vitro* (**Fig. 19, 24** and Bornancin et al., 2015; Gewies et al., 2014; Jaworski et al., 2014). Consistent with a gain of Roquin-1 function in the *Rc3h1*[Mins] model frequencies and numbers of splenic Tfh and Tfr cells were reduced in *Rc3h1*[Mins/Mins] mice, which is opposite to accumulation of these cells and the loss of Roquin function in DKO[T] mice but similar to the MALT1-deficient or C472A mutant models (**Fig. 22** and Essig et al., 2017; Vogel et al., 2013; Bornancin et al., 2015). Mechanistically, reduced S6 phosphorylation (p-S6) at low TCR strength or basal signaling *in vivo* as well as improved repression of *Icos* target mRNA could be responsible for low Tfh cell frequencies in *Rc3h1*[Mins/Mins] mice in which Tfh-promoting PI3K/Akt/mTOR signaling and *Pten* regulation should be explored in more detail (Essig et al., 2017). Intriguingly, similar effects on mTORC1-dependent S6 phosphorylation and thus T cell metabolism have been observed for Carma1, Bcl10 and MALT1 knockouts or MALT1 protease inhibition and Treg cell development has been associated with TCR/IL-2-dependent mTORC1 activation to program suppressive CTLA-4/ICOS-mediated Treg functions (Zeng et al., 2013; Nakaya et al., 2014; Hamilton et al., 2015). Yet, an inverse relationship to Roquin-deficient mice was neither observed for the development of thymic iNKT cells nor for biased commitment to iNKT17 cells in *Rc3h1*[Mins/Mins] mice (**Fig. 27** and Drees et al., 2017). Despite minor phenotypic changes in decreased thymic Treg and splenic Tfh cell populations, *Rc3h1*[Mins/Mins] mice appeared unchanged to wildtype counterparts with normal B cell

development and peripheral CD4/CD8 activation (**Fig. 20, 21, 23**). These findings suggest that different from Tfh and Tfr cells the development of Treg cells, B cells, NKT cells and probably also γδ T cells does not respond to the gain of Roquin-1 function or does not depend on TCR-induced inactivation of Roquin-1, respectively. However, analyzing stimulation-dependent effects in T cells derived from *Rc3h1*[Mins/Mins] mice, T cell-intrinsic levels of enhanced IFN-γ but reduced TNFα cytokines and a defect in Th17 differentiation *in vitro* were comparable to *Malt1*[PD/PD] T cells (**Fig. 21, 25** and Bornancin et al., 2015; Gewies et al., 2014; Jaworski et al., 2014). Both *ex vivo* Tregs and *in vitro* CD4+ Th1 cells from *Rc3h1*[Mins/Mins] mice showed increased IFN-γ levels, which recapitulated mild effects observed for different CBM mutants utilizing either Cd4-Cre or Foxp3-IRES-YFP-Cre (FIC) knockout models for Carma1 (CARD11) or Bcl10, respectively (Di Pilato et al., 2019; Rosenbaum et al., 2019). Similar to *Carma1*^{-/-} or *Bcl10*^{-/-} models, *Rc3h1*[Mins/Mins] Tregs expressed low levels of the Roquin targets OX40 and CTLA-4 indicating T cell-specific gain of Roquin-1 function as well as a failure of effector (e)Tregs to express relevant suppressive signature genes rendering them Th1-like producers of IFN-γ (Rosenbaum et al., 2019). Lastly, mice treated with the MALT1 inhibitor mepazine also showed increased IFN-γ production and both Carma or Bcl10 deficiencies and MALT1 paracaspase inhibition improved tumor suppression most likely caused by activated IFN-γ+ Treg cells in the tumor microenvironment.

Of note, also other targets of MALT1 in the NF-κB pathway can be crucial for phenotypic changes in *Malt1*[PD/PD] mice that are not shared with *Rc3h1*[Mins/Mins] mice. Additionally, the lack of Roquin-1 cleavage could be compensated by cleavage of the functionally redundant Roquin-2 protein or the functionally related Regnase-1 protein (Vogel et al., 2013; Jeltsch et al., 2014). Conclusively, the data indicate that the impact of the MALT1 protease activity on Th17 differentiation and Th1/Th17-driven autoimmunity segregates with cleavage of the Roquin-1 substrate, and different from pharmacologic or genetic MALT1 paracaspase inhibition no development of IPEX-like pathologies was observed in *Rc3h1*[Mins/Mins] mice (Gewies et al., 2014; Demeyer et al., 2019; Martin et al., 2019).

4.5. Implications, model and perspective

Implications. The discovery of TCR-induced proteolytic activity of MALT1 stimulated efforts to establish specific inhibitors of MALT1 function to treat diffuse large B-cell lymphoma (DLBCL) whose growth kinetics heavily depend on *Carma1* mutations identified by shRNA library screens and general downstream NF-κB activation (Ngo et al., 2006; Jaworski et al., 2016). In 2009, the first tetrapeptide MALT1 inhibitor, z-VRPR-fmk, was validated for having preferential cytotoxicity on cells derived from activated B cell-like (ABC) subtype DLBCL, which suggested essential roles of MALT1 paracaspase activation in the survival and malignant proliferation of B cell-like DLBCL (Ferch et al., 2009). Since then several other phenothiazine-based inhibtors of MALT1, namely mepazine, thioridazine and promazine, as well as allosteric small molecule inhibitors, e.g. MI-2 or MLT-747, MLT-748 and MLT-943, have been evaluated to block MALT1 proteolytic function and to treat ABC-DLBCL *in vitro* and *in vivo* (Nagel et al., 2012; Fontan et al., 2012; Quancard et al.,

2019; Martin et al., 2020). However, these preclinical strategies have been challenged by studies showing that gene-edited MALT1 protease-dead knockin mice (systemic, conditional T cell-specific or Treg-specific *Malt1*[PD/PD]) suffer from autoimmune disease including dysbalanced immune function and also pharmacological MALT1 inhibition led to dose-response reduction of peripheral Tregs which resulted in progressive immune abnormalities and clinical manifestations of IPEX-like pathology (Cheng et al., 2019; Demeyer et al., 2019; Martin et al., 2020). Conditional *Malt1*[PD/PD] expression in CD4^{+} T cells, i.e. *MALT1*-PDT mice (*Malt1*[PD/fl]; CD4-Cre), only partially phenocopies systemic *Malt1*[PD/PD] mice indicating that other cell types, i.e. B cells, myeloid cells, NK cells and epithelial cells, may contribute to Treg induction in a MALT1 paracaspase-dependent manner (Ruland et al., 2018; Demeyer et al., 2019). In addition, loss-of-function CBM protein mutations have been described for human immunodeficient (CID) patients lacking appropriate MALT1 expression or displaying dysfunctional MALT1 which caused reduced Treg numbers, compromised T/B cell receptor signaling or low B cell numbers (Jabara et al., 2013; McKinnon et al., 2014; Punwani et al., 2015; Quancard et al., 2019). Placed at the crossroads of fatal autoimmunity and therapeutic potential for antitumor immunity, genetic or pharmacological manipulation of CBM complex effector pathways majorly affects lymphocyte homeostasis and activation governed by proper activation of gene expression, yet the T cell-intrinsic role of substrate-specific cleavage by MALT1 activity has remained elusive.

Model. This doctoral thesis describes *Rc3h1*[Mins] (Roquin-1[Mins/Mins]) as the first MALT1-insensitive substrate that, at least in parts, recapitulates *in vitro* and *in vivo* effects of genetic or pharmacological inhibition of the mouse MALT1 paracaspase. The data suggest Roquin-1 as a target of TCR-induced MALT1 in CD4^{+} T cells with particularly high susceptibility to cleavage owing to two individual arginine cleavage motifs at R510 and R579. Loss of Roquin activity is critical for high TCR signal strength to release the robust repression of the high avidity target *Nfkbid* (IκB$_{NS}$) inducing Th17 gene expression programs via the TCR-MALT1-Roquin-IκB$_{NS}$ axis (**Figure 30**).
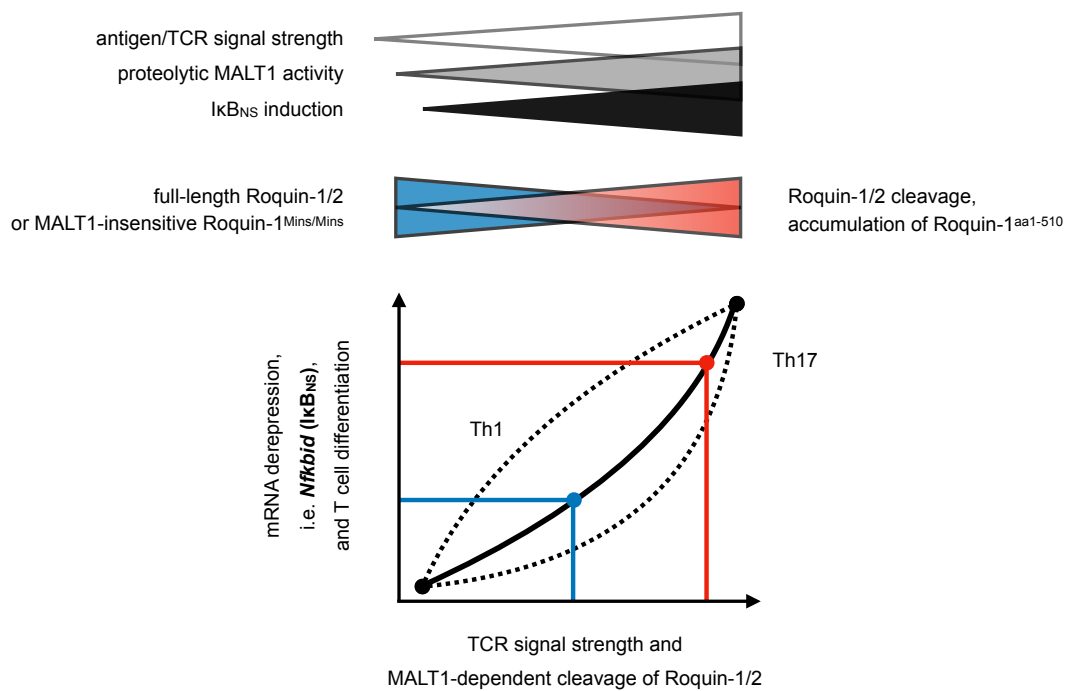
Fig. 30: TCR/MALT1-induced Roquin cleavage to control IκB$_{NS}$-specific Th17 cells. Antigen/TCR ligation and TCR signaling induce CBM complex formation and MALT1 paracaspase activity. MALT1-dependent cleavage of Roquin paralogs reduces functional Roquin levels which gradually derepresses low- or high avidity mRNA targets at differential TCR signal strengths. Derepression and induction of the high-avidity Roquin target *Nfkbid* (IκB$_{NS}$) requires maximum TCR strength, quantitative cleavage of Roquin and aligns with Th17 fate decisions (red). Low TCR strength is insufficient to induce IκB$_{NS}$ and Roquin-1$^{Mins/Mins}$ restricts IκB$_{NS}$ expression to suboptimal levels inappropriate for Th17 but not Th1 differentiation (blue).

It is tempting to speculate that MALT1 activity is guided in an affinity- and substrate-specific manner. The susceptibility of Roquin to MALT1-dependent cleavage may be compensated by overall increased Roquin-1 expression in CD4$^+$ T cells (5-fold higher than Roquin-2) to ensure Roquin-1 threshold levels at low TCR signal strength that still inhibit Th17-relevant mRNA targets. With this, even at reduced Roquin expression due to MALT1-driven depletion, high-affinity mRNA targets such as *Nfkbid* with multiple CDE motifs would be kept in check to prevent excessive Th17 differentiation, maintaining suboptimal levels of Th17 promoting factors. Both antigen-induced and TCR strength-dependent *in vitro* assays of Th17 differentiation and target upregulation as well as the *Rc3h1*^{Mins} model specifically restricting IκB$_{NS}$ induction confirm this hypothesis and contribute a mechanistic understanding from multiple perspectives. Upregulation of IκB$_{NS}$ can be envisioned as a direct readout for antigen/TCR-induced MALT1 activity that inversely correlates with Roquin function. Conclusively, Roquin-1 integrates TCR strength in a MALT1-dependent proteolytic cascade and employs post-transcriptional repression of *Nfkbid* (IκB$_{NS}$) as the major mechanism for the prevention of excessive Th17 polarization.

Perspective. In view of the observed effects of *Rc3h1*^Mins it will be of importance to combine the current model with MALT1-insensitive Roquin-2 (*Rc3h2*) to not only elucidate target-specific contributions of Roquin-1/2 cleavage products but also to exclude contributions of Roquin cleavage to general *Malt1*^PD/PD phenotypes not observed for *Rc3h1*^Mins/Mins mice. Future work will answer these questions by generating MALT1-insensitive Roquin-2 (*Rc3h2*) or also Regnase-1 (*Zc3h12a*) alleles and combining them with *Rc3h1*^Mins/Mins alleles. Selectively rendering MALT1 substrates insensitive to TCR-induced cleavage will allow comprehensive analyses of exclusive, redundant or cooperative contributions of MALT1 substrates to the observed dysregulation of lymphocyte homeostasis in *Malt1*^PD/PD mice or mice treated with long/short-term doses of pharmacological MALT1 inhibitors. Utilizing fluorophore-conjugated anti-IκB$_{NS}$ and anti-Roquin-1^aa1-510 cleavage antibodies, cell subset-specific effects of enhanced IκB$_{NS}$ and pronounced cleavage of Roquin-1 may be deciphered in autoimmune disease models or diseased human samples from patients suffering from Th17-mediated multiple sclerosis, systemic lupus erythematosus (SLE), psoriasis or rheumatoid arthritis (RA). Mechanistically, in-depth analyses of TCR-induced gene expression changes in *Rc3h1*^Mins or wildtype T cells may be addressed by RNA sequencing (RNA-seq) and RNA/protein interaction kinetics may be further elucidated by various CLIP techniques (UV cross-linking and immunoprecipitation, i.e. CLIP, iCLIP, CLIP-seq, HITS-CLIP, KIN-CLIP) indicating how Roquin-1^Mins maintains interactions with high-affinity CDE or ADE motifs such as in the *Nfkbid* 3'-UTR during antigen/TCR-mediated lymphocyte activation (Hafner et al., 2010; Lee et al., 2018; Sharma et al., 2021).

Analyzing T cell fate decisions, the consequences of reduced peripheral Tfh cells in *Rc3h1*^Mins mice may be further tested by either NP-OVA peptide immunizations of OT-II T cell recipients or by acute infections of SMα-TCR T cell recipients with LCMV (Armstrong) to analyze the *in vivo* polarization of Th1/Tfh and GC B cells. Apart from specific immune challenges, T cell metabolism and calcium signaling are a well-known drivers of helper T cell differentiation and mitochondrial oxidative phosphorylation (OXPHOS) as well as increased calcium influx promote pathogenic Th17 fates (Kaufmann et al., 2019). Of note, pharmacological blockade of OXPHOS reduced BATF-dependent Th17 differentiation and promoted IL-2/STAT5-dependent Foxp3 induction in CD4⁺ T cells (Shin et al., 2020). This aligns well with similar observations for *Itk*-deficient T cells instructing only reduced IRF4 induction and favoring iTreg over Th17 fates (Gomez-Rodriguez et al., 2014), yet a reciprocal relationship of iTreg over Th17 fates was not observed for the *Rc3h1*^Mins model. Metabolic changes also including CTLA-4/Treg-relevant mTORC1 signaling may additionally contribute to altered T cell fate decisions described for *Malt1*^PD/PD and *Rc3h1*^Mins/Mins mice (Zeng et al., 2013).

Finally, with respect to Treg-specific downregulation of CTLA-4 and OX40 signature genes and cytokine profiles shifted towards IFN-γ production, Treg identity markers as well as proliferation and IL-2 signaling of *Rc3h1*^Mins T cells will be of interest to describe cell cycle progression or expansion of *Rc3h1*^Mins T cells in which MALT1 function is selectively blocked to disable Roquin-specific post-transcriptional control of gene expression. Intratumoral alterations of Treg identity and function have been described for Treg-specific deficiencies in Carma1 and Bcl10 expression associated with therapeutic potential to elicit intratumoral Th1 autoimmune responses driven by IFN-γ producing Tregs. Together with PD-1/PD-L1-targeted immune checkpoint therapy (ICT), both

mouse models of inhibited CBM complex function and also pharmacological MALT1 inactivation mediated destabilization of Treg cells towards self-reactive pro-inflammatory contributors of local antitumor responses restricting tumor growth in melanoma models (Di Pilato et al., 2019; Rosenbaum et al., 2019). Since mouse models of *cRel* deficiency and its chemical inhibition by pentoxifylline (PTXF) treatment as well increased IFN-γ-mediated antitumor responses by affecting Treg identity and suppressive function, it will be of great interest to similarly compare *Nfkbid*-deficient and *Rc3h1*[Mins/Mins] models in B16-, D4M.3A- or MC38-induced tumor experiments to explore which CBM-dependent transcriptional factors and modulators of T cell differentiation determine altered Treg performance relevant for cancer immunotherapy approaches (Grinberg-Bleyer et al., 2017). Strikingly, targeted deletion of the endoribonuclease Regnase-1 (iKO) was reported to program long-lived CD8^{+} effector cells for improved cancer therapy and its ribonucleolytic activity was linked to regulation of the transcriptional modulator BATF whose enhanced expression fuels mitochondrial fitness and promotes pro-inflammatory effector responses (Wei et al., 2019). Hence, it will be necessary to selectively combine genetic mouse models and pharmacological inhibitors of CBM or NF-κB function to decipher individual, redundant, cooperative or even antagonistic modulators of antitumor responses that appear to strongly depend on fine-tuned iTreg/Th1/Th17 cell fate decisions and its involved metabolic changes. For this, CRISPR/Cas-based technologies make it possible to modulate genomes with relative ease allowing to combine multiple transgenic models. Advanced gene editing strategies will be helpful to link genetic variation to precise phenotypic outcomes and to answer long-standing questions of fine-tuned immunological reactivity and peripheral T cell tolerance.

Importantly, the *Rc3h1*[Mins] mouse model shows that the impact of the MALT1 protease activity on Th17 differentiation and Th17-driven autoimmunity but not insufficient Treg function and IPEX-like pathologies segregates with Roquin-1 substrate cleavage. This suggests that strengthening the function or specifically rendering Roquin-1 insensitive to MALT1 cleavage rather than systemically inhibiting the MALT1 paracaspase activity would represent a preferred therapeutic avenue for the treatment of Th17-mediated autoimmunity. Conclusively, the development of a Roquin-specific small molecule inhibitor targeting the interaction with the MALT1 paracaspase would resemble an elegant approach to circumvent the described IPEX-like pathologies in protease-dead *Malt1*[PD/PD] mice but to selectively mitigate Th17 cell pathogenicity in autoimmune diseases.

5. Bibliography

Afkarian, M., Sedy, J.R., Yang, J., Jacobson, N.G., Cereb, N., Yang, S.Y., Murphy, T.L., and Murphy, K.M. (2002). T-bet is a STAT1-induced regulator of IL-12R expression in naïve CD4+ T cells. Nature Immunology 3, 549-557.

Akira, S., Uematsu, S., and Takeuchi, O. (2006). Pathogen recognition and innate immunity. Cell 124, 783-801.

Aleksic, M., Dushek, O., Zhang, H., Shenderov, E., Chen, J.L., Cerundolo, V., Coombs, D., and van der Merwe, P.A. (2010). Dependence of T cell antigen recognition on T cell receptor-peptide MHC confinement time. Immunity 32, 163-174.

Alterauge, D., Bagnoli, J.W., Dahlström, F., Bradford, B.M., Mabbott, N.A., Buch, T., Enard, W., and Baumjohann, D. (2020). Continued Bcl6 Expression Prevents the Transdifferentiation of Established Tfh Cells into Th1 Cells during Acute Viral Infection. Cell Reports 33, 108232.

Annemann, M., Wang, Z., Plaza-Sirvent, C., Glauben, R., Schuster, M., Ewald Sander, F., Mamareli, P., Kühl, A.A., Siegmund, B., Lochner, M., et al. (2015). IκBNS Regulates Murine Th17 Differentiation during Gut Inflammation and Infection. The Journal of Immunology 194, 2888-2898.

Annemann, M., Plaza-Sirvent, C., Schuster, M., Katsoulis-Dimitriou, K., Kliche, S., Schraven, B., and Schmitz, I. (2016). Atypical IκB proteins in immune cell differentiation and function. Immunology Letters 171, 26-35.

Ansel, K.M., Greenwald, R.J., Agarwal, S., Bassing, C.H., Monticelli, S., Interlandi, J., Djuretic, I.M., Lee, D.U., Sharpe, A.H., Alt, F.W., et al. (2004). Deletion of a conserved Il4 silencer impairs T helper type 1–mediated immunity. Nature Immunology 5, 1251-1259.

Athanasopoulos, V., Barker, A., Yu, D., Tan, A.H.M., Srivastava, M., Contreras, N., Wang, J., Lam, K.-P., Brown, S.H.J., Goodnow, C.C., et al. (2010). The ROQUIN family of proteins localizes to stress granules via the ROQ domain and binds target mRNAs. FEBS Journal 277, 2109-2127.

Bachmann, M.F., Sebzda, E., Kündig, T.M., Shahinian, A., Speiser, D.E., Mak, T.W., and Ohashi, P.S. (1996). T cell responses are governed by avidity and co-stimulatory thresholds. Eur J Immunol 26, 2017-2022.

Balamuth, F., Leitenberg, D., Unternaehrer, J., Mellman, I., and Bottomly, K. (2001). Distinct Patterns of Membrane Microdomain Partitioning in Th1 and Th2 Cells. Immunity 15, 729-738.

Bartleson, J.M., Viehmann Milam, A.A., Donermeyer, D.L., Horvath, S., Xia, Y., Egawa, T., and Allen, P.M. (2020). Strength of tonic T cell receptor signaling instructs T follicular helper cell–fate decisions. Nature Immunology.

Baumjohann, D., Preite, S., Reboldi, A., Ronchi, F., Ansel, K.M., Lanzavecchia, A., and Sallusto, F. (2013). Persistent Antigen and Germinal Center B Cells Sustain T Follicular Helper Cell Responses and Phenotype. Immunity 38, 596-605.

Bauquet, A.T., Jin, H., Paterson, A.M., Mitsdoerffer, M., Ho, I.C., Sharpe, A.H., and Kuchroo, V.K. (2009). The costimulatory molecule ICOS regulates the expression of c-Maf and IL-21 in the development of follicular T helper cells and TH-17 cells. Nature Immunology 10, 167-175.

Beelman, C. A., Stevens, A., Caponigro, G., LaGrandeur, T. E., Hatfield, L., Fortner, D. M., and Parker, R. (1996). An essential component of the decapping enzyme required for normal rates of mRNA decay in yeast. Nature 382, 642-646.

Bertossi, A., Aichinger, M., Sansonetti, P., Lech, M., Neff, F., Pal, M., Wunderlich, F.T., Anders, H.J., Klein, L., and Schmidt-Supprian, M. (2011). Loss of Roquin induces early death and immune deregulation but not autoimmunity. J Exp Med 208, 1749-1756.

Bettelli, E., Carrier, Y., Gao, W., Korn, T., Strom, T.B., Oukka, M., Weiner, H.L., and Kuchroo, V.K. (2006). Reciprocal developmental pathways for the generation of pathogenic effector TH17 and regulatory T cells. Nature 441, 235-238.

Blonska, M., Pappu, B.P., Matsumoto, R., Li, H., Su, B., Wang, D., and Lin, X. (2007). The CARMA1-Bcl10 Signaling Complex Selectively Regulates JNK2 Kinase in the T Cell Receptor-Signaling Pathway. Immunity 26, 55-66.

Bogin, Y., Ainey, C., Beach, D., and Yablonski, D. (2007). SLP-76 mediates and maintains activation of the Tec family kinase ITK via the T cell antigen receptor-induced association between SLP-76 and ITK. Proceedings of the National Academy of Sciences 104, 6638-6643.

Bornancin, F., Renner, F., Touil, R., Sic, H., Kolb, Y., Touil-Allaoui, I., Rush, J.S., Smith, P.A., Bigaud, M., Junker-Walker, U., et al. (2015). Deficiency of MALT1 paracaspase activity results in unbalanced regulatory and effector T and B cell responses leading to multiorgan inflammation. J Immunol 194, 3723-3734.

Brenner, S., Jacob, F., and Meselson, M. (1961). An Unstable Intermediate Carrying Information From Genes to Ribosomes For Protein Synthesis. Nature 190, 576-581.

Bretscher, P., and Cohn, M. (1970). A theory of self–nonself discrimination. Science 169, 1042-1049.

Brunkow, M.E., Jeffery, E.W., Hjerrild, K.A., Paeper, B., Clark, L.B., Yasayko, S.-A., Wilkinson, J.E., Galas, D., Ziegler, S.F., and Ramsdell, F. (2001). Disruption of a new forkhead/winged-helix protein, scurfin, results in the fatal lymphoproliferative disorder of the scurfy mouse. Nature Genetics 27, 68-73.

Bruno, L., Mazzarella, L., Hoogenkamp, M., Hertweck, A., Cobb, B.S., Sauer, S., Hadjur, S., Leleu, M., Naoe, Y., Telfer, J.C., et al. (2009). Runx proteins regulate Foxp3 expression. Journal of Experimental Medicine 206, 2329-2337.

Brüstle, A., Heink, S., Huber, M., Rosenplänter, C., Stadelmann, C., Yu, P., Arpaia, E., Mak, T.W., Kamradt, T., and Lohoff, M. (2007). The development of inflammatory TH-17 cells requires interferon-regulatory factor 4. Nature Immunology 8, 958-966.

Brüstle, A., Brenner, D., Knobbe, C.B., Lang, P.A., Virtanen, C., Hershenfield, B.M., Reardon, C., Lacher, S.M., Ruland, J., Ohashi, P.S., et al. (2012). The NF-kappaB regulator MALT1 determines the encephalitogenic potential of Th17 cells. J Clin Invest 122, 4698-4709.

Burchill, M.A., Yang, J., Vang, K.B., Moon, J.J., Chu, H.H., Lio, C.-W.J., Vegoe, A.L., Hsieh, C.-S., Jenkins, M.K., and Farrar, M.A. (2008). Linked T Cell Receptor and Cytokine Signaling Govern the Development of the Regulatory T Cell Repertoire. Immunity 28, 112-121.

Chakrabarti, S., Jayachandran, U., Bonneau, F., Fiorini, F., Basquin, C., Domcke, S., Le Hir, H., and Conti, E. (2011). Molecular Mechanisms for the RNA-Dependent ATPase Activity of Upf1 and Its Regulation by Upf2. Molecular Cell 41, 693-703.

Chan, A.C., Iwashima, M., Turck, C.W., and Weiss A. (1992). ZAP-70: a 70 kd protein-tyrosine kinase that associates with the TCR zeta chain. Cell 71, 649-662.

Chaudhry, A., Samstein, Robert M., Treuting, P., Liang, Y., Pils, Marina C., Heinrich, J.-M., Jack, Robert S., Wunderlich, F.T., Brüning, Jens C., Müller, W., et al. (2011). Interleukin-10 Signaling in Regulatory T Cells Is Required for Suppression of Th17 Cell-Mediated Inflammation. Immunity 34, 566-578.

Chen, G., Hardy, K., Pagler, E., Ma, L., Lee, S., Gerondakis, S., Daley, S., and Shannon, M.F. (2011). The NF-κB Transcription Factor c-Rel Is Required for Th17 Effector Cell Development in Experimental Autoimmune Encephalomyelitis. The Journal of Immunology 187, 4483-4491.

Chen, L., and Flies, D.B. (2013). Molecular mechanisms of T cell co-stimulation and co-inhibition. Nature Reviews Immunology 13, 227-242.

Cheng, L., Deng, N., Yang, N., Zhao, X., and Lin, X. (2019). Malt1 Protease Is Critical in Maintaining Function of Regulatory T Cells and May Be a Therapeutic Target for Antitumor Immunity. The Journal of Immunology 202, 3008-3019.

Chinen, T., Kannan, A.K., Levine, A.G., Fan, X., Klein, U., Zheng, Y., Gasteiger, G., Feng, Y., Fontenot, J.D., and Rudensky, A.Y. (2016). An essential role for the IL-2 receptor in Treg cell function. Nature Immunology 17, 1322-1333.

Cho, Y.-L., Flossdorf, M., Kretschmer, L., Höfer, T., Busch, D.H., and Buchholz, V.R. (2017). TCR Signal Quality Modulates Fate Decisions of Single CD4 + T Cells in a Probabilistic Manner. Cell Reports 20, 806-818.

Choi, Youn S., Kageyama, R., Eto, D., Escobar, Tania C., Johnston, Robert J., Monticelli, L., Lao, C., and Crotty, S. (2011). ICOS Receptor Instructs T Follicular Helper Cell versus Effector Cell Differentiation via Induction of the Transcriptional Repressor Bcl6. Immunity 34, 932-946.

Choi, J., Diao, H., Faliti, C.E., Truong, J., Rossi, M., Bélanger, S., Yu, B., Goldrath, A.W., Pipkin, M.E., and Crotty, S. (2020). Bcl-6 is the nexus transcription factor of T follicular helper cells via repressor-of-repressor circuits. Nature Immunology 21, 777-789.

Ciofani, M., and Zúñiga-Pflücker, J.C. (2010). Determining γδ versus αβ T cell development. Nature Reviews Immunology 10, 657-663.

Ciofani, M., Madar, A., Galan, C., Sellars, M., Mace, K., Pauli, F., Agarwal, A., Huang, W., Parkurst, C.N., Muratet, M., et al. (2012). A Validated Regulatory Network for Th17 Cell Specification. Cell 151, 289-303.

Codarri, L., Gyülvészi, G., Tosevski, V., Hesske, L., Fontana, A., Magnenat, L., Suter, T., and Becher, B. (2011). RORγt drives production of the cytokine GM-CSF in helper T cells, which is essential for the effector phase of autoimmune neuroinflammation. Nature Immunology 12, 560-567.

Conley, J.M., Gallagher, M.P., Rao, A., and Berg, L.J. (2020). Activation of the Tec Kinase ITK Controls Graded IRF4 Expression in Response to Variations in TCR Signal Strength. The Journal of Immunology 205, 335-345.

Constant, S., Pfeiffer, C., Woodard, A., Pasqualini, T., and Bottomly, K. (1995). Extent of T Cell Receptor Ligation Can Determine the Functional Differentiation of Naive CD4+ T Cells. J Exp Med 182, 1591-1596.

Coornaert, B., Baens, M., Heyninck, K., Bekaert, T., Haegman, M., Staal, J., Sun, L., Chen, Z.J., Marynen, P., and Beyaert, R. (2008). T cell antigen receptor stimulation induces MALT1 paracaspase–mediated cleavage of the NF-κB inhibitor A20. Nature Immunology 9, 263-271.

Coudronniere, N., Villalba, M., Englund, N., and Altman, A. (2000). NF-kappa B activation induced by T cell receptor/CD28 costimulation is mediated by protein kinase C-theta. Proceedings of the National Academy of Sciences 97, 3394-3399.

Cretney, E., Xin, A., Shi, W., Minnich, M., Masson, F., Miasari, M., Belz, G.T., Smyth, G.K., Busslinger, M., Nutt, S.L., et al. (2011). The transcription factors Blimp-1 and IRF4 jointly control the differentiation and function of effector regulatory T cells. Nature Immunology 12, 304-311.

Croft, M. (2010). Control of Immunity by the TNFR-Related Molecule OX40 (CD134). Annual Review of Immunology 28, 57-78.

Crotty, S. (2011). Follicular Helper CD4 T Cells (TFH). Annual Review of Immunology 29, 621-663.

Crotty, S. (2019). T Follicular Helper Cell Biology: A Decade of Discovery and Diseases. Immunity 50, 1132-1148.

Cua, D.J., Sherlock, J., Chen, Y., Murphy, C.A., Joyce, B., Seymour, B., Lucian, L., To, W., Kwan, S., Churakova, T., Zurawski, S., Wiekowski, M., Lira, S.A., Gorman, D., Kastelein, R.A., and Sedgwick, J.D. (2003). Interleukin-23 rather than interleukin-12 is the critical cytokine for autoimmune inflammation of the brain. Nature 421, 744-748.

David, L., Li, Y., Ma, J., Garner, E., Zhang, X., and Wu, H. (2018). Assembly mechanism of the CARMA1-BCL10-MALT1-TRAF6 signalosome. Proc Natl Acad Sci U S A 115, 1499-1504.

D'Cruz, L.M., and Klein, L. (2005). Development and function of agonist-induced CD25+Foxp3+ regulatory T cells in the absence of interleukin 2 signaling. Nature Immunology 6, 1152-1159.

Decker, C. J. and Parker, R. (1993). A turnover pathway for both stable and unstable mRNAs in yeast: evidence for a requirement for deadenylation. Genes Dev. 7, 1632-1643.

Deenick, E.K., Chan, A., Ma, C.S., Gatto, D., Schwartzberg, P.L., Brink, R., and Tangye, S.G. (2010). Follicular Helper T Cell Differentiation Requires Continuous Antigen Presentation that Is Independent of Unique B Cell Signaling. Immunity 33, 241-253.

Demeyer, A., Staal, J., and Beyaert, R. (2016). Targeting MALT1 Proteolytic Activity in Immunity, Inflammation and Disease: Good or Bad? Trends in Molecular Medicine 22, 135-150.

Demeyer, A., Skordos, I., Driege, Y., Kreike, M., Hochepied, T., Baens, M., Staal, J., and Beyaert, R. (2019). MALT1 Proteolytic Activity Suppresses Autoimmunity in a T Cell Intrinsic Manner. Frontiers in Immunology 10.

Di Pilato, M., Kim, E.Y., Cadilha, B.L., Prussmann, J.N., Nasrallah, M.N., Seruggia, D., Usmani, S.M., Misale, S., Zappulli, V., Carrizosa, E., et al. (2019). Targeting the CBM complex causes Treg cells to prime tumours for immune checkpoint therapy. Nature 570, 112-116.

Diehn, M., Alizadeh, A.A., Rando, O.J., Liu, C.L., Stankunas, K., Botstein, D., Crabtree, G.R., and Brown, P.O. (2002). Genomic expression programs and the integration of the CD28 costimulatory signal in T cell activation. Proc Natl Acad Sci U S A 99, 11796-11801.

DiToro, D., Winstead, C.J., Pham, D., Witte, S., Andargachew, R., Singer, J.R., Wilson, C.G., Zindl, C.L., Luther, R.J., Silberger, D.J., et al. (2018). Differential IL-2 expression defines developmental fates of follicular versus nonfollicular helper T cells. Science 361, eaao2933.

Dower, N. A., Stang, S. L., Bottorff, D. A., Ebinu, J. O., Dickie, P., Ostergaard, H. L., and Stone, J. C. (2000). RasGRP is essential for mouse thymocyte differentiation and TCR signaling. Nature 4, 317-321.

Drees, C., Vahl, J.C., Bortoluzzi, S., Heger, K.D., Fischer, J.C., Wunderlich, F.T., Peschel, C., and Schmidt-Supprian, M. (2017). Roquin Paralogs Differentially Regulate Functional NKT Cell Subsets. J Immunol 198, 2747-2759.

Dudziak, D., Kamphorst, A.O., Heidkamp, G.F., Buchholz, V.R., Trumpfheller, C., Yamazaki, S., Cheong, C., Liu, K., Lee, H.W., Park, C.G., et al. (2007). Differential antigen processing by dendritic cell subsets in vivo. Science 315, 107-111.

Dunkelberger, J.R., and Song, W.C. (2010). Complement and its role in innate and adaptive immune responses. Cell Res 20, 34-50.

Düwel, M., Welteke, V., Oeckinghaus, A., Baens, M., Kloo, B., Ferch, U., Darnay, B.G., Ruland, J., Marynen, P., and Krappmann, D. (2009). A20 Negatively Regulates T Cell Receptor Signaling to NF-κB by Cleaving Malt1 Ubiquitin Chains. The Journal of Immunology 182, 7718-7728.

Eberle, A.B., Lykke-Andersen, S., Mühlemann, O., and Jensen, T.H. (2008). SMG6 promotes endonucleolytic cleavage of nonsense mRNA in human cells. Nature Structural & Molecular Biology 16, 49-55.

Egawa, T., and Littman, D. R. (2008). The transcription factor ThPOK acts late in helper T cell lineage specification and suppresses Runx-mediated commitment to the cytotoxic T cell lineage. Nat Immunol 9, 1131-1139.

El-Behi, M., Ciric, B., Dai, H., Yan, Y., Cullimore, M., Safavi, F., Zhang, G.-X., Dittel, B.N., and Rostami, A. (2011). The encephalitogenicity of TH17 cells is dependent on IL-1- and IL-23-induced production of the cytokine GM-CSF. Nature Immunology 12, 568-575.

Essig, K., Hu, D., Guimaraes, J.C., Alterauge, D., Edelmann, S., Raj, T., Kranich, J., Behrens, G., Heiseke, A., Floess, S., et al. (2017). Roquin Suppresses the PI3K-mTOR Signaling Pathway to Inhibit T Helper Cell Differentiation and Conversion of Treg to Tfr Cells. Immunity 47, 1067-1082 e1012.

Essig, K., Kronbeck, N., Guimaraes, J.C., Lohs, C., Schlundt, A., Hoffmann, A., Behrens, G., Brenner, S., Kowalska, J., Lopez-Rodriguez, C., et al. (2018). Roquin targets mRNAs in a 3'-UTR-specific manner by different modes of regulation. Nat Commun 9, 3810.

Evavold, B. D. and Allen, P. M. (1991). Separation of IL-4 Production from Th Cell Proliferation by an Altered T Cell Receptor Ligand. Science 252.

Falk, S., Weir, John R., Hentschel, J., Reichelt, P., Bonneau, F., and Conti, E. (2014). The Molecular Architecture of the TRAMP Complex Reveals the Organization and Interplay of Its Two Catalytic Activities. Molecular Cell 55, 856-867.

Fazilleau, N., McHeyzer-Williams, L.J., Rosen, H., and McHeyzer-Williams, M.G. (2009). The function of follicular helper T cells is regulated by the strength of T cell antigen receptor binding. Nature Immunology 10, 375-384.

Ferch, U., Kloo, B., Gewies, A., Pfänder, V., Düwel, M., Peschel, C., Krappmann, D., and Ruland, J. (2009). Inhibition of MALT1 protease activity is selectively toxic for activated B cell–like diffuse large B cell lymphoma cells. Journal of Experimental Medicine 206, 2313-2320.

Feske, S. (2007). Calcium signalling in lymphocyte activation and disease. Nature Reviews Immunology 7, 690-702.

Fiorini, E., Schmitz, I., Marissen, W.E., Osborn, S.L., Touma, M., Sasada, T., Reche, P.A., Tibaldi, E.V., Hussey, R.E., Kruisbeek, A.M., et al. (2002). Peptide-Induced Negative Selection of Thymocytes Activates Transcription of an NF-KB Inhibitor. Molecular Cell 9, 637-648.

Fraser, J.D., Newton, M.E., and Weiss, A. (1992). CD28 and T Cell Antigen Receptor Signal Transduction Coordinately Regulate Interleukin 2 Gene Expression In Response to Superantigen Stimulation. J Exp Med 175, 1131-1134.

Fontan, L., Yang, C., Kabaleeswaran, V., Volpon, L., Osborne, Michael J., Beltran, E., Garcia, M., Cerchietti, L., Shaknovich, R., Yang, Shao N., et al. (2012). MALT1 Small Molecule Inhibitors Specifically Suppress ABC-DLBCL In Vitro and In Vivo. Cancer Cell 22, 812-824.

Fontenot, J.D., Gavin, M.A., and Rudensky, A.Y. (2003). Foxp3 programs the development and function of CD4+CD25+ regulatory T cells. Nature Immunology 4, 330-336.

Fontenot, J.D., Rasmussen, J.P., Gavin, M.A., and Rudensky, A.Y. (2005). A function for interleukin 2 in Foxp3-expressing regulatory T cells. Nature Immunology 6, 1142-1151.

Francisco, L.M., Salinas, V.H., Brown, K.E., Vanguri, V.K., Freeman, G.J., Kuchroo, V.K., and Sharpe, A.H. (2009). PD-L1 regulates the development, maintenance, and function of induced regulatory T cells. Journal of Experimental Medicine 206, 3015-3029.

Frentzel, S., Katsoulis–Dimitriou, K., Jeron, A., Schmitz, I., and Bruder, D. (2019). Essential role of IκBNS for in vivo CD4+ T–cell activation, proliferation, and Th1–cell differentiation during Listeria monocytogenes infection in mice. European Journal of Immunology *49*, 1391-1398.

Fu, G., Casas, J., Rigaud, S., Rybakin, V., Lambolez, F., Brzostek, J., Hoerter, J.A., Paster, W., Acuto, O., Cheroutre, H., et al. (2013). Themis sets the signal threshold for positive and negative selection in T-cell development. Nature 504, 441-445.

Fu, G., Rybakin, V., Brzostek, J., Paster, W., Acuto, O., and Gascoigne, N.R.J. (2014). Fine-tuning T cell receptor signaling to control T cell development. Trends in Immunology 35, 311-318.

Fu, M., and Blackshear, P.J. (2016). RNA-binding proteins in immune regulation: a focus on CCCH zinc finger proteins. Nature Reviews Immunology 17, 130-143.

Garg, A.V., Amatya, N., Chen, K., Cruz, J.A., Grover, P., Whibley, N., Conti, H.R., Mir, G.H., Sirakova, T., Childs, E.C., et al. (2015). MCPIP1 Endoribonuclease Activity Negatively Regulates Interleukin-17-Mediated Signaling and Inflammation. Immunity 43, 475-487.

Gascoigne, N.R.J., Rybakin, V., Acuto, O., and Brzostek, J. (2016). TCR Signal Strength and T Cell Development. Annual Review of Cell and Developmental Biology 32, 327-348.

Gehring, T., Seeholzer, T., and Krappmann, D. (2018). BCL10 – Bridging CARDs to Immune Activation. Frontiers in Immunology 9.

Germain, R.N. (2002). T-cell development and the CD4-CD8 lineage decision. Nat Rev Immunol 2, 309-322.

Gett, A.V., Sallusto, F., Lanzavecchia, A., and Geginat, J. (2003). T cell fitness determined by signal strength. Nature Immunology 4, 355-360.

Gewies, A., Gorka, O., Bergmann, H., Pechloff, K., Petermann, F., Jeltsch, K.M., Rudelius, M., Kriegsmann, M., Weichert, W., Horsch, M., et al. (2014). Uncoupling Malt1 threshold function from paracaspase activity results in destructive autoimmune inflammation. Cell Rep 9, 1292-1305.

Gibson, S., Truitt, K., Lu, Y., Lapushin, R., Khan, H., Imboden, J.B., and Mills, G.B. (1998). Efficient CD28 signalling leads to increases in the kinase activities of the TEC family tyrosine kinase EMT/ITK/TSK and the SRC family tyrosine kinase LCK. Biochem J 330, 1123-1128.

Glasmacher, E., Hoefig, K.P., Vogel, K.U., Rath, N., Du, L., Wolf, C., Kremmer, E., Wang, X., and Heissmeyer, V. (2010). Roquin binds inducible costimulator mRNA and effectors of mRNA decay to induce microRNA-independent post-transcriptional repression. Nat Immunol 11, 725-733.

Glasmacher, E., Agrawal, S., Chang, A.B., Murphy, T.L., Zeng, W., Vander Lugt, B., Khan, A.A., Ciofani, M., Spooner, C.J., Rutz, S., et al. (2012). A Genomic Regulatory Element That Directs Assembly and Function of Immune-Specific AP-1-IRF Complexes. Science 338, 975-980.

Gomez-Rodriguez, J., Sahu, N., Handon, R., Davidson, T.S., Anderson, S.M., Kirby, M.R., August, A., and Schwartzberg, P.L. (2009). Differential Expression of Interleukin-17A and -17F Is Coupled to T Cell Receptor Signaling via Inducible T Cell Kinase. Immunity 31, 587-597.

Gomez-Rodriguez, J., Wohlfert, E.A., Handon, R., Meylan, F., Wu, J.Z., Anderson, S.M., Kirby, M.R., Belkaid, Y., and Schwartzberg, P.L. (2014). Itk-mediated integration of T cell receptor and cytokine signaling regulates the balance between Th17 and regulatory T cells. J Exp Med 211, 529-543.

Ghoreschi, K., Laurence, A., Yang, X.-P., Tato, C.M., McGeachy, M.J., Konkel, J.E., Ramos, H.L., Wei, L., Davidson, T.S., Bouladoux, N., et al. (2010). Generation of pathogenic TH17 cells in the absence of TGF-β signalling. Nature 467, 967-971.

Gosh, P., Tan., T.-H., Rice, N.R., Sica, A., and Young, H.A. (1993). The interleukin 2 CD28-responsive complex contains at least three members of the NFkB family: c-Rel, p50, and p65. Proc Natl Acad Sci U S A, 90, 1696-1700.

Govern, C.C., Paczosa, M.K., Chakraborty, A.K., and Huseby, E.S. (2010). Fast on-rates allow short dwell time ligands to activate T cells. Proc Natl Acad Sci U S A 107, 8724-8729.

Gross, O., Grupp, C., Steinberg, C., Zimmermann, S., Strasser, D., Hannesschläger, N., Reindl., W., Jonsson, H., Huo, H., Littman, D.R., Peschel, C., Yokoyama, W.M., Krug, A., and Ruland, J. (2008). Multiple ITAM-coupled NK-cell receptors engage the Bcl10/Malt1 complex via Carma1 for NF-B and MAPK activation to selectively control cytokine production. Blood 12 (6), 2421-2428.

Grinberg-Bleyer, Y., Oh, H., Desrichard, A., Bhatt, D.M., Caron, R., Chan, T.A., Schmid, R.M., Klein, U., Hayden, M.S., and Ghosh, S. (2017). NF-κB c-Rel Is Crucial for the Regulatory T Cell Immune Checkpoint in Cancer. Cell 170, 1096-1108.e1013.

Gunzer, M., Schäfer, A., Borgmann, S., Grabbe, S., Zänker, K. S., Bröcker, E.-B., Kämpgen, E. and Friedl, P. (2000). Antigen Presentation in Extracellular Matrix: Interactions of T Cells with Dendritic Cells Are Dynamic, Short Lived, and Sequential. Immunity 13, 323-332.

Hachmann, J., Snipas, Scott J., van Raam, Bram J., Cancino, Erik M., Houlihan, Emily J., Poreba, M., Kasperkiewicz, P., Drag, M., and Salvesen, Guy S. (2012). Mechanism and specificity of the human paracaspase MALT1. Biochemical Journal 443, 287-295.

Hafner, M., Landthaler, M., Burger, L., Khorshid, M., Hausser, J., Berninger, P., Rothballer, A., Ascano, M., Jungkamp, A.-C., Munschauer, M., et al. (2010). Transcriptome-wide Identification of RNA-Binding Protein and MicroRNA Target Sites by PAR-CLIP. Cell 141, 129-141.

Hailfinger, S., Lenz, G., Ngo, V., Posvitz-Fejfar, A., Rebeaud, F., Guzzardi, M., Murga Penas, E.-M., Dierlamm, J., Chan, W.C., Staudt, L.M., and Thome, M. (2009). Essential role of MALT1 protease activity in activated B cell-like diffuse large B-cell lymphoma. Proc Natl Acad Sci U S A 106 (47), 19946-19951.

Hailfinger, S., Nogai, H., Pelzer, C., Jaworski, M., Cabalzar, K. Charton, J.-E., Guzzardi, M., Décaillet, C., Grau, M., Dörken, B., Lenz, P., Lenz, G. and Thome, M. (2011). Malt1-dependent RelB cleavage promotes canonical NF-kB activation in lymphocytes and lymphoma cell lines. Proc Natl Acad Sci U S A 108, 14596-14601.

Halbach, F., Reichelt, P., Rode, M., and Conti, E. (2013). The Yeast Ski Complex: Crystal Structure and RNA Channeling to the Exosome Complex. Cell 154, 814-826.

Hamilton, K.S., Phong, B., Corey, C., Cheng, J., Gorentla, B., Zhong, X., Shiva, S., and Kane, L.P. (2014). T cell receptor-dependent activation of mTOR signaling in T cells is mediated by Carma1 and MALT1, but not Bcl10. Sci Signal 7, ra55.

Haks, M.C., Lefebvre, J.M., Lauritsen, J.P.H., Carleton, M., Rhodes, M., Miyazaki, T., Kappes, D.J., and Wiest, D.L. (2005). Attenuation of γδTCR Signaling Efficiently Diverts Thymocytes to the αβ Lineage. Immunity 22, 595-606.

Hara, H., Wada, T., Bakal, C., Kozieradzki, I., Suzuki, S., Suzuki, N., Nghiem, M., Griffiths, E.K., Krawczyk, C., Bauer, B., et al. (2003). The MAGUK Family Protein CARD11 Is Essential for Lymphocyte Activation. Immunity 18, 763-775.

Hardtke, S., Ohl, L., and Förster, R. (2005). Balanced expression of CXCR5 and CCR7 on follicular T helper cells determines their transient positioning to lymph node follicles and is essential for efficient B-cell help. Blood 106, 1924-1931.

Harrington, L.E., Hatton, R.D., Mangan, P.R., Turner, H., Murphy, T.L., Murphy, K.M., and Weaver, C.T. (2005). Interleukin 17–producing CD4+ effector T cells develop via a lineage distinct from the T helper type 1 and 2 lineages. Nature Immunology 6, 1123-1132.

Hayden, M.S., and Ghosh, S. (2012). NF- B, the first quarter-century: remarkable progress and outstanding questions. Genes & Development 26, 203-234.

Hayes, S.M., Li, L., and Love, P.E. (2005). TCR Signal Strength Influences αβ/γδ Lineage Fate. Immunity 22, 583-593.

He, X., He, X., Dave, V. P., Zhang, Y., Hua, X., Nicolas, E., Xu, W., Roe, B. A., and Kappes, D. J. (2005). The zinc finger transcription factor Th-POK regulates CD4 versus CD8 T-cell lineage commitment. Nature 433, 826-833.

Heink, S., Yogev, N., Garbers, C., Herwerth, M., Aly, L., Gasperi, C., Husterer, V., Croxford, A.L., Möller-Hackbarth, K., Bartsch, H.S., et al. (2016). Trans-presentation of IL-6 by dendritic cells is required for the priming of pathogenic TH17 cells. Nature Immunology 18, 74-85.

Heissmeyer, V., and Vogel, K.U. (2013). Molecular control of Tfh-cell differentiation by Roquin family proteins. Immunol Rev 253, 273-289.

Henrickson, S.E., Mempel, T.R., Mazo, I.B., Liu, B., Artyomov, M.N., Zheng, H., Peixoto, A., Flynn, M.P., Senman, B., Junt, T., et al. (2008). T cell sensing of antigen dose governs interactive behavior with dendritic cells and sets a threshold for T cell activation. Nature Immunology 9, 282-291.

Hochedlinger, K., Yamada, Y., Beard, C., and Jaenisch, R. (2005). Ectopic Expression of Oct-4 Blocks Progenitor-Cell Differentiation and Causes Dysplasia in Epithelial Tissues. Cell 121, 465-477.

Hogquist, K.A., Jameson, S.C., Heath, W.R., Howard, J.L., Bevan, M.J., and Carbone, F.R. (1994). T cell receptor antagonist peptides induce positive selection. Cell 76, 17-27.

Hogquist, K.A., and Jameson, S.C. (2014). The self-obsession of T cells: how TCR signaling thresholds affect fate 'decisions' and effector function. Nat Immunol 15, 815-823.

Holdorf, A.D., Green, J.M., Levin, S.D., Denny, M.F., Straus, D.B., Link, V., Changelian, P.S., Allen, P.M., and Shaw, A.S. (1999). Proline Residues in CD28 and the Src Homology (SH)3 Domain of Lck Are Required for T Cell Costimulation. J Exp Med 190 (3), 375-384.

Hörber, S., Hildebrand, D.G., Lieb, W.S., Lorscheid, S., Hailfinger, S., Schulze-Osthoff, K., and Essmann, F. (2016). The Atypical Inhibitor of NF-κB, IκBζ, Controls Macrophage Interleukin-10 Expression. Journal of Biological Chemistry 291, 12851-12861.

Hori, S., Nomura, T., and Sakaguchi, S. (2003). Control of Regulatory T Cell Development by the Transcription Factor Foxp3. Science 299, 1057-1061.

Hosken, N.A., Shibuya, K., Heath, A.W., Murphy, K.M., and O'Garra, A. (1995). The Effect of Antigen Dose on CD4+ T Helper Cell Phenotype Development in a T Cell Receptor-αβ-transgenic Model. J Exp Med 182, 1579-1584.

Huntzinger, E., and Izaurralde, E. (2011). Gene silencing by microRNAs: contributions of translational repression and mRNA decay. Nature Reviews Genetics 12, 99-110.

Huxford, T., Huang, D.-B., Malek, S., and Gosh, G. (1998). The Crystal Structure of the IκBα/NF-κB Complex Reveals Meachnisms of NF-κB Inactivation. Cell 95, 759-770.

Ichiyama, K., Yoshida, H., Wakabayashi, Y., Chinen, T., Saeki, K., Nakaya, M., Takaesu, G., Hori, S., Yoshimura, A., and Kobayashi, T. (2008). Foxp3 Inhibits RORγt-mediatedIL-17AmRNA Transcription through Direct Interaction with RORγt. Journal of Biological Chemistry 283, 17003-17008.

Iezzi, G., Sonderegger, I., Ampenberger, F., Schmitz, N., Marsland, B.J., and Kopf, M. (2009). CD40–CD40L cross-talk integrates strong antigenic signals and microbial stimuli to induce development of IL-17-producing CD4+ T cells. Proceedings of the National Academy of Sciences 106, 876-881.

Ivanov, I.I., McKenzie, B.S., Zhou, L., Tadokoro, C.E., Lepelley, A., Lafaille, J.J., Cua, D.J., and Littman, D.R. (2006). The Orphan Nuclear Receptor RORγt Directs the Differentiation Program of Proinflammatory IL-17+ T Helper Cells. Cell 126, 1121-1133.

Iwata, A., Durai, V., Tussiwand, R., Briseno, C.G., Wu, X., Grajales-Reyes, G.E., Egawa, T., Murphy, T.L., and Murphy, K.M. (2017). Quality of TCR signaling determined by differential affinities of enhancers for the composite BATF-IRF4 transcription factor complex. Nat Immunol 18, 563-572.

Jabara, H.H., Ohsumi, T., Chou, J., Massaad, M.J., Benson, H., Megarbane, A., Chouery, E., Mikhael, R., Gorka, O., Gewies, A., et al. (2013). A homozygous mucosa-associated lymphoid tissue 1 (MALT1) mutation in a family with combined immunodeficiency. Journal of Allergy and Clinical Immunology 132, 151-158.

Jacobs Anderson, J. S. and Parker, R. (1998). The 3′ to 5′ degradation of yeast mRNAs is a general mechanism for mRNA turnover that requires the SKI2 DEVH box protein and 3′ to 5′ exonucleases of the exosome complex. EMBO J. 17, 1497-1506.

Janowski, R., Heinz, G.A., Schlundt, A., Wommelsdorf, N., Brenner, S., Gruber, A.R., Blank, M., Buch, T., Buhmann, R., Zavolan, M., et al. (2016). Roquin recognizes a non-canonical hexaloop structure in the 3'-UTR of Ox40. Nat Commun 7, 11032.

Jaworski, M., Marsland, B., Gehrig, J., Held, W., Favre, S., Luther, S., Perroud, M., Golshayan, D., Gaide, O. & Thome, M. (2014). Malt1 protease inactivation efficiently dampens immune responses but causes spontaneous autoimmunity. EMBO.

Jeltsch, K.M., and Heissmeyer, V. (2016). Regulation of T cell signaling and autoimmunity by RNA-binding proteins. Curr Opin Immunol 39, 127-135.

Jeltsch, K.M., Hu, D., Brenner, S., Zoller, J., Heinz, G.A., Nagel, D., Vogel, K.U., Rehage, N., Warth, S.C., Edelmann, S.L., et al. (2014). Cleavage of roquin and regnase-1 by the paracaspase MALT1 releases their cooperatively repressed targets to promote T(H)17 differentiation. Nat Immunol 15, 1079-1089.

Jenner, R.G., Townsend, M.J., Jackson, I., Sun, K., Bouwman, R.D., Young, R.A., Glimcher, L.H., and Lord, G.M. (2009). The transcription factors T-bet and GATA-3 control alternative pathways of T-cell differentiation through a shared set of target genes. Proceedings of the National Academy of Sciences 106, 17876-17881.

Jennings, E., Elliot, T.A.E., Thawait, N., Kanabar, S., Yam-Puc, J.C., Ono, M., Toellner, K.-M., Wraith, D.C., Anderson, G., and Bending, D. (2020). Nr4a1 and Nr4a3 Reporter Mice Are Differentially Sensitive to T Cell Receptor Signal Strength and Duration. Cell Reports 33, 108328.

Jiang, S.H., Shen, N., and Vinuesa, C.G. (2015). Posttranscriptional T cell gene regulation to limit Tfh cells and autoimmunity. Current Opinion in Immunology 37, 21-27.

Johnston, R. J., Poholek, A. C., DiToro, D., Yusuf, I., Eto, D., Barnett, B., Dent, A. L., Craft, J., and Crotty, S. (2009). Bcl6 and Blimp-1 Are Reciprocal and Antagonistic Regulators of T Follicular Helper Cell Differentiation. Science 325, 1006-1010.

Joller, N., Lozano, E., Burkett, Patrick R., Patel, B., Xiao, S., Zhu, C., Xia, J., Tan, Tze G., Sefik, E., Yajnik, V., et al. (2014). Treg Cells Expressing the Coinhibitory Molecule TIGIT Selectively Inhibit Proinflammatory Th1 and Th17 Cell Responses. Immunity 40, 569-581.

Jordan, M. S., Boesteanu, A., Reed, A. J., Petrone, A. L., Holenbeck, A. E., Lerman, M. A., Naji, A., and Caton, A. J. (2001). Thymic selection of CD4+ CD25+ regulatory T cells induced by an agonist self-peptide. Nat Immunol 2, 301-306.

Jorritsma, P. J., Brogdon, J. L., and Bottomly, K. (2003). Role of TCR-Induced Extracellular Signal-Regulated Kinase Activation in the Regulation of Early IL-4 Expression in Naive CD4 T Cells. J Immunol 170, 2427-2434.

June, C. H., Ledbetter, J. A., Gillespie, M. M., Lindsten, T., and Thompson, C. B. (1987). T-Cell Proliferation Involving the CD28 Pathway Is Associated with Cyclosporine-Resistant Interleukin 2 Gene Expression. Mol Cell Biol 7 (12), 4472-4481.

Kafasla, P., Skliris, A., and Kontoyiannis, D.L. (2014). Post-transcriptional coordination of immunological responses by RNA-binding proteins. Nature Immunology 15, 492-502.

Kanhere, A., Hertweck, A., Bhatia, U., Gökmen, M.R., Perucha, E., Jackson, I., Lord, G.M., and Jenner, R.G. (2012). T-bet and GATA3 orchestrate Th1 and Th2 differentiation through lineage-specific targeting of distal regulatory elements. Nature Communications 3.

Kaufmann, U., Kahlfuss, S., Yang, J., Ivanova, E., Koralov, S.B., and Feske, S. (2019). Calcium Signaling Controls Pathogenic Th17 Cell-Mediated Inflammation by Regulating Mitochondrial Function. Cell Metabolism 29, 1104-1118.

Keck, S., Schmaler, M., Ganter, S., Wyss, L., Oberle, S., Huseby, E.S., Zehn, D., and King, C.G. (2014). Antigen affinity and antigen dose exert distinct influences on CD4 T-cell differentiation. Proc Natl Acad Sci U S A 111, 14852-14857.

Kim, C., Wilson, T., Fischer, K.F., and Williams, M.A. (2013). Sustained interactions between T cell receptors and antigens promote the differentiation of CD4(+) memory T cells. Immunity 39, 508-520.

King, C.G., Koehli, S., Hausmann, B., Schmaler, M., Zehn, D., and Palmer, E. (2012). T cell affinity regulates asymmetric division, effector cell differentiation, and tissue pathology. Immunity 37, 709-720.

Klein, T., Fung, S.-Y., Renner, F., Blank, M.A., Dufour, A., Kang, S., Bolger-Munro, M., Scurll, J.M., Priatel, J.J., Schweigler, P., et al. (2015). The paracaspase MALT1 cleaves HOIL1 reducing linear ubiquitination by LUBAC to dampen lymphocyte NF-κB signalling. Nature Communications 6.

Kobayashi, S., Hara, A., Isagawa, T., Manabe, I., Takeda, K., and MaruYama, T. (2014). The Nuclear IκB Family Protein IκBNS Influences the Susceptibility to Experimental Autoimmune Encephalomyelitis in a Murine Model. PLoS ONE 9, e110838.

Korn, T., Bettelli, E., Oukka, M., and Kuchroo, V.K. (2009). IL-17 and Th17 Cells. Annual Review of Immunology 27, 485-517.

Kotov, D.I., Mitchell, J.S., Pengo, T., Ruedl, C., Way, S.S., Langlois, R.A., Fife, B.T., and Jenkins, M.K. (2019). TCR Affinity Biases Th Cell Differentiation by Regulating CD25, Eef1e1, and Gbp2. J Immunol 202, 2535-2545.

Kovalovsky, D., Uche, O.U., Eladad, S., Hobbs, R.M., Yi, W., Alonzo, E., Chua, K., Eidson, M., Kim, H.-J., Im, J.S., et al. (2008). The BTB–zinc finger transcriptional regulator PLZF controls the development of invariant natural killer T cell effector functions. Nature Immunology 9, 1055-1064.

Kreslavsky, T., Garbe, A.I., Krueger, A., and von Boehmer, H. (2008). T cell receptor–instructed αβ versus γδ lineage commitment revealed by single-cell analysis. Journal of Experimental Medicine 205, 1173-1186.

Krishnamoorthy, V., Kannanganat, S., Maienschein-Cline, M., Cook, S.L., Chen, J., Bahroos, N., Sievert, E., Corse, E., Chong, A., and Sciammas, R. (2017). The IRF4 Gene Regulatory Module Functions as a Read-Write Integrator to Dynamically Coordinate T Helper Cell Fate. Immunity 47, 481-497 e487.

Kündig, T.M., Shahinian, A., Kawai, K., Mittrücker, H.-W., Sebzda, E., Bachmann, M.F., Mak, T.W., and Ohashi, P.S. (1996) Duration of TCR Stimulation Determines Costimulatory Requirement of T Cells. Immunity 5, 41-52.

Lafferty, K.J., and Cunningham, A.J. (1975). A new analysis of allogeneic interactions. Aust. J. Exp. Biol. Med. Sci. 53, 27–42.

Lazarevic, V., Chen, X., Shim, J.-H., Hwang, E.-S., Jang, E., Bolm, A.N., Oukka, M., Kuchroo, V.K., and Glimcher, L.H. (2010). T-bet represses TH17 differentiation by preventing Runx1-mediated activation of the gene encoding RORγt. Nature Immunology 12, 96-104.

Lee, H.J., Takemoto, N., Kurata, H., Kamogawa, Y., Miyatake, S., O'Garra, A., and Arai, N. (2000). GATA-3 Induces T Helper Cell Type 2 (Th2) Cytokine Expression and Chromatin Remodeling in Committed Th1 Cells. J Exp Med 192, 105-115.

Lee, F.C.Y., and Ule, J. (2018). Advances in CLIP Technologies for Studies of Protein-RNA Interactions. Molecular Cell 69, 354-369.

Lee, P.P., Fitzpatrick, D.R., Beard, C., Jessup, H.K., Lehar, S., Makar, K.W., Pérez-Melgosa, M., Sweetser, M.T., Schlissel, M.S., Nguyen, S., Cherry, S.R., Tsai, J.H., Tucker, S.M., Weaver, W.M., Kelso, A., Jaenisch, R., and Wilson, C.B. (2001). A Critical Role for Dnmt1 and DNA Methylation in T Cell Development, Function, and Survival. Immunity 15, 763-774.

Lee, S.K., Silva, D.G., Martin, J.L., Pratama, A., Hu, X., Chang, P.-P., Walters, G., and Vinuesa, C.G. (2012). Interferon-γ Excess Leads to Pathogenic Accumulation of Follicular Helper T Cells and Germinal Centers. Immunity 37, 880-892.

Lee, S.K., Rigby, R.J., Zotos, D., Tsai, L.M., Kawamoto, S., Marshall, J.L., Ramiscal, R.R., Chan, T.D., Gatto, D., Brink, R., et al. (2011). B cell priming for extrafollicular antibody responses requires Bcl-6 expression by T cells. Journal of Experimental Medicine 208, 1377-1388.

Lee, Y.K., Turner, H., Maynard, C.L., Oliver, J.R., Chen, D., Elson, C.O., and Weaver, C.T. (2009). Late Developmental Plasticity in the T Helper 17 Lineage. Immunity 30, 92-107.

Leitenberg, D., Boutin, Y., Constant, S. and Bottomly, K. (1998). CD4 Regulation of TCR Signaling and T Cell Differentiation Following Stimulation with Peptides of Different Affinities for the TCR. J Immunol 161, 1194-1203.

Lenz, G., Davis, R.E., Ngo, V.N., Lam, L., George, T.C., Wright, G.W., Dave, S.S., Zhao, H., Xu, W., Rosenwald, A., Ott, G., Muller-Hermelink, H.K., Gascoyne, R.D., Connors, J.M., Rimsza, L.M., Campo, E., Jaffe, E.S., Delabie, J., Smeland, E.B., Fisher, R.I., Chan, W.C., and Staudt, L.M. (2008). Science 319, 1676-1679.

Leppek, K., Schott, J., Reitter, S., Poetz, F., Hammond, M.C., and Stoecklin, G. (2013). Roquin promotes constitutive mRNA decay via a conserved class of stem-loop recognition motifs. Cell 153, 869-881.

Li, Q.J., Chau, J., Ebert, P.J., Sylvester, G., Min, H., Liu, G., Braich, R., Manoharan, M., Soutschek, J., Skare, P., et al. (2007). miR-181a is an intrinsic modulator of T cell sensitivity and selection. Cell 129, 147-161.

Li, J., Li, L., Shang, X., Benson, J., Merle Elloso, M., Schantz, A., Bracht, M., Orlovsky, Y., and Sweet, R. (2008). Negative regulation of IL-17 production by OX40/OX40L interaction. Cellular Immunology 253, 31-37.

Linterman, M.A., Rigby, R.J., Wong, R., Silva, D., Withers, D., Anderson, G., Verma, N.K., Brink, R., Hutloff, A., Goodnow, C.C., et al. (2009). Roquin Differentiates the Specialized Functions of Duplicated T Cell Costimulatory Receptor Genes Cd28 and Icos. Immunity 30, 228-241.

Liu, J., Carmell, M. A., Rivas, F. V., Marsden, C. G., Thomson, J. M., Song, J.-J., Hammond, S. M., Joshua-Tor, L., and Hannon, G. J. (2004). Argonaute2 Is the Catalytic Engine of Mammalian RNAi. Science 305, 1437-1441.

Long, M., Park, S.-G., Strickland, I., Hayden, M.S., and Ghosh, S. (2009). Nuclear Factor-κB Modulates Regulatory T Cell Development by Directly Regulating Expression of Foxp3 Transcription Factor. Immunity 31, 921-931.

Lykke-Andersen, S., Brodersen, D.E., and Jensen, T.H. (2009). Origins and activities of the eukaryotic exosome. Journal of Cell Science 122, 1487-1494.

Madaan, A., Verma, R., Singh, A.T., Jain, S.K., and Jaggi, M. (2014). A stepwise procedure for isolation of murine bone marrow and generation of dendritic cells. Journal of Biological Methods 1.

Magram, J., Connaughton, S.E., Warrier, R.R., Carvajal, D.M., Wu, C., Ferrante, J., Stewart, C., Sarmiento, U., Faherty, D.A., and Gately, M.K. (1996). IL-12-Deficient Mice Are Defective in IFNγ Production and Type 1 Cytokine Responses. Immunity 4, 471-481.

Malek, T.R., Yu, A., Vincek, V., Scibelli, P., and Kong, L. (2002). CD4 Regulatory T Cells Prevent Lethal Autoimmunity in IL-2R-Deficient Mice: Implications for the Nonredundant Function of IL-2. Immunity 17, 167-178.

Marengère, L.E., Okkenhaug, K., Clavreul, A., Couez, D., Gibson, S., Mills, G.B., Mak, T.W., and Rottapel., R. (1997). The SH3 domain of Itk/Emt binds to proline-rich sequences in the cytoplasmic domain of T cell costimulatory receptor CD28. J Immunol 159, 3220-3229.

Martin, K., Touil, R., Kolb, Y., Cvijetic, G., Murakami, K., Israel, L., Duraes, F., Buffet, D., Glück, A., Niwa, S., et al. (2019). Malt1 Protease Deficiency in Mice Disrupts Immune Homeostasis at Environmental Barriers and Drives Systemic T Cell–Mediated Autoimmunity. The Journal of Immunology 203, 2791-2806.

Martin, K., Junker, U., Tritto, E., Sutter, E., Rubic-Schneider, T., Morgan, H., Niwa, S., Li, J., Schlapbach, A., Walker, D., et al. (2020). Pharmacological Inhibition of MALT1 Protease Leads to a Progressive IPEX-Like Pathology. Frontiers in Immunology 11.

Masuda, K., Ripley, B., Nishimura, R., Mino, T., Takeuchi, O., Shioi, G., Kiyonari, H., and Kishimoto, T. (2013). Arid5a controls IL-6 mRNA stability, which contributes to elevation of IL-6 level in vivo. Proceedings of the National Academy of Sciences 110 (23), 9409-9414.

Matsumoto, R., Wang, D., Blonska, M., Li, H., Kobayashi, M., Pappu, B., Chen, Y., Wang, D., and Lin, X. (2005). Phosphorylation of CARMA1 Plays a Critical Role in T Cell Receptor-Mediated NF-κB Activation. Immunity 23, 575-585.

Matsushita, K., Takeuchi, O., Standley, D.M., Kumagai, Y., Kawagoe, T., Miyake, T., Satoh, T., Kato, H., Tsujimura, T., Nakamura, H., et al. (2009). Zc3h12a is an RNase essential for controlling immune responses by regulating mRNA decay. Nature 458, 1185-1190.

McKinnon, M.L., Rozmus, J., Fung, S.-Y., Hirschfeld, A.F., Del Bel, K.L., Thomas, L., Marr, N., Martin, S.D., Marwaha, A.K., Priatel, J.J., et al. (2014). Combined immunodeficiency associated with homozygous MALT1 mutations. Journal of Allergy and Clinical Immunology 133, 1458-1462.

Mempel, T. R., Henrickson, S. E. and van Andrian, U. H. (2004). T-cell priming by dendritic cells in lymph nodes occurs in three distinct phases. Nature 427, 154-159.

Michel, F., Mangino, G., Attal-Bonnefoy, G., Tuosto, L., Alcover, A., Roumier, A., Olive, D., and Acuto, O. (2000). CD28 Utilizes Vav-1 to Enhance TCR-Proximal Signaling and NF-AT Activation. J Immunol 165, 3820-3829.

Michel, F., Attal-Bonnefoy, G., Mangino, G., Mise-Omata, S., and Acuto, O. (2001). CD28 as a Molecular Amplifier Extending TCR Ligation and Signaling Capabilities. Immunity 15, 935-945.

Michel, M.L., Mendes-da-Cruz, D., Keller, A.C., Lochner, M., Schneider, E., Dy, M., Eberl, G., and Leite-de-Moraes, M.C. (2008). Critical role of ROR- t in a new thymic pathway leading to IL-17-producing invariant NKT cell differentiation. Proceedings of the National Academy of Sciences 105, 19845-19850.

Milner, J.D., Fazilleau, N., McHeyzer-Williams, M., and Paul, W. (2010). Cutting edge: lack of high affinity competition for peptide in polyclonal CD4+ responses unmasks IL-4 production. J Immunol 184, 6569-6573.

Mino, T., Murakawa, Y., Fukao, A., Vandenbon, A., Wessels, H.H., Ori, D., Uehata, T., Tartey, S., Akira, S., Suzuki, Y., et al. (2015). Regnase-1 and Roquin Regulate a Common Element in Inflammatory mRNAs by Spatiotemporally Distinct Mechanisms. Cell 161, 1058-1073.

Mitchell, P., Petfalski, E., Shevchenko, A., Mann, M., and Tollervey, D. (1997). The exosome: a conserved eukaryotic RNA processing complex containing multiple 3′–5′ exoribonucleases. Cell 91, 457-466.

Moran, A.E., and Hogquist, K.A. (2012). T-cell receptor affinity in thymic development. Immunology 135, 261-267.

Moran, A.E., Holzapfel, K.L., Xing, Y., Cunningham, N.R., Maltzman, J.S., Punt, J., and Hogquist, K.A. (2011). T cell receptor signal strength in Treg and iNKT cell development demonstrated by a novel fluorescent reporter mouse. J Exp Med 208, 1279-1289.

Muhlrad, D., Decker, C. J., and Parker, R. (1994). Deadenylation of the unstable mRNA encoded by the yeast MFA2 gene leads to decapping followed by 5′-3′ digestion of the transcript. Genes Dev. 8, 855-866.

Murakawa, Y., Hinz, M., Mothes, J., Schuetz, A., Uhl, M., Wyler, E., Yasuda, T., Mastrobuoni, G., Friedel, C.C., Dolken, L., et al. (2015). RC3H1 post-transcriptionally regulates A20 mRNA and modulates the activity of the IKK/NF-kappaB pathway. Nat Commun 6, 7367.

Murphy, K.M., and Reiner, S.L. (2002). The lineage decisions of helper T cells. Nature Reviews Immunology 2, 933-944.

Nagel, D., Spranger, S., Vincendeau, M., Grau, M., Raffegerst, S., Kloo, B., Hlahla, D., Neuenschwander, M., Peter von Kries, J., Hadian, K., et al. (2012). Pharmacologic inhibition of MALT1 protease by phenothiazines as a therapeutic approach for the treatment of aggressive ABC-DLBCL. Cancer Cell 22, 825-837.

Nakaya, M., Xiao, Y., Zhou, X., Chang, J.H., Chang, M., Cheng, X., Blonska, M., Lin, X., and Sun, S.C. (2014). Inflammatory T cell responses rely on amino acid transporter ASCT2 facilitation of glutamine uptake and mTORC1 kinase activation. Immunity 40, 692-705.

Nakayamada, S., Kanno, Y., Takahashi, H., Jankovic, D., Lu, Kristina T., Johnson, Thomas A., Sun, H.-w., Vahedi, G., Hakim, O., Handon, R., et al. (2011). Early Th1 Cell Differentiation Is Marked by a Tfh Cell-like Transition. Immunity 35, 919-931.

Ngo, V.N., Davis, R.E., Lamy, L., Yu, X., Zhao, H., Lenz, G., Lam, L.T., Dave, S., Yang, L., Powell, J., et al. (2006). A loss-of-function RNA interference screen for molecular targets in cancer. Nature 441, 106-110.

Oeckinghaus, A., and Ghosh, S. (2009). The NF- B Family of Transcription Factors and Its Regulation. Cold Spring Harbor Perspectives in Biology 1, a000034.

Okamoto, K., Iwai, Y., Oh-hora, M., Yamamoto, M., Morio, T., Aoki, K., Ohya, K., Jetten, A.M., Akira, S., Muta, T., et al. (2010). IκBζ regulates TH17 development by cooperating with ROR nuclear receptors. Nature 464, 1381-1385.

Okkenhaug, K., and Rottapel, R. (1998). Grb2 Forms an Inducible Protein Complex with CD28 through a Src Homology 3 Domain-Proline Interaction. J Biol Chem 273 (33), 21194-21202.

Oppmann, B., Lesley, R., Blom, B., Timans, J. C., Xu, Y., Hunte, B., Vega, F., Yu, N., Wang, J., Singh, K., Zonin, F. et al. (2000). Novel p19 Protein Engages IL-12p40 to Form a Cytokine, IL-23, with Biological Activities Similar as Well as Distinct from IL-12. Immunity 13, 715-725.

O'Shea, J.J., and Paul, W. E. (2010). Mechanisms Underlying Lineage Commitment and Plasticity of Helper CD4+ T Cells. Science 327, 1098-1102.

Pagès, F., Ragueneau, M., Rottapel, R., Truneh, A., Nunes, J., Imbert, J., and Olive, D. (1994). Binding of phosphatidyl-inositol-3-OH kinase to CD28 is required for T-cell signalling. Nature 369, 327-329.

Pandiyan, P., Zheng, L., Ishihara, S., Reed, J., and Lenardo, M.J. (2007). CD4+CD25+Foxp3+ regulatory T cells induce cytokine deprivation–mediated apoptosis of effector CD4+ T cells. Nature Immunology 8, 1353-1362.

Park, A.Y., Hondowicz, B.D., and Scott, P. (2000). IL-12 Is Required to Maintain a Th1 Response During Leishmania major Infection. The Journal of Immunology 165, 896-902.

Parker, R., and Song, H. (2004). The enzymes and control of eukaryotic mRNA turnover. Nature Structural & Molecular Biology 11, 121-127.

Paulos, C.M., Carpenito, C., Plesa, G., Suhoski, M.M., Varela-Rohena, A., Golovina, T.N., Carroll, R.G., Riley, J.L., and June, C.H. (2010). The Inducible Costimulator (ICOS) Is Critical for the Development of Human TH17 Cells. Science Translational Medicine 2, 55ra78.

Pelzer, C., Cabalzar, K., Wolf, A., Gonzalez, M., Lenz, G., and Thome, M. (2013). The protease activity of the paracaspase MALT1 is controlled by monoubiquitination. Nature Immunology 14, 337-345.

Pepper, M., Pagán, Antonio J., Igyártó, Botond Z., Taylor, Justin J., and Jenkins, Marc K. (2011). Opposing Signals from the Bcl6 Transcription Factor and the Interleukin-2 Receptor Generate T Helper 1 Central and Effector Memory Cells. Immunity 35, 583-595.

Ploquin, M.J.Y., Eksmond, U., and Kassiotis, G. (2011). B Cells and TCR Avidity Determine Distinct Functions of CD4+T Cells in Retroviral Infection. The Journal of Immunology 187, 3321-3330.

Punwani, D., Wang, H., Chan, A.Y., Cowan, M.J., Mallott, J., Sunderam, U., Mollenauer, M., Srinivasan, R., Brenner, S.E., Mulder, A., et al. (2015). Combined Immunodeficiency Due to MALT1 Mutations, Treated by Hematopoietic Cell Transplantation. Journal of Clinical Immunology 35, 135-146.

Quancard, J., Klein, T., Fung, S.-Y., Renatus, M., Hughes, N., Israël, L., Priatel, J.J., Kang, S., Blank, M.A., Viner, R.I., et al. (2019). An allosteric MALT1 inhibitor is a molecular corrector rescuing function in an immunodeficient patient. Nature Chemical Biology 15, 304-313.

Qiao, Q., Yang, C., Zheng, C., Fontán, L., David, L., Yu, X., Bracken, C., Rosen, M., Melnick, A., Egelman, Edward H., et al. (2013). Structural Architecture of the CARMA1/Bcl10/MALT1 Signalosome: Nucleation-Induced Filamentous Assembly. Molecular Cell 51, 766-779.

Radtke, F., Wilson, A., Stark, G., Bauer, M., van Meerwijk, J., MacDonald, H. R., and Aguet, M. (1999). Deficient T Cell Fate Specification in Mice with an Induced Inactivation of Notch1. Immunity 10, 547-558.

Rebeaud, F., Hailfinger, S., Posevitz-Fejfar, A., Tapernoux, M., Moser, R., Rueda, D., Gaide, O., Guzzardi, M., Iancu, E.M., Rufer, N., et al. (2008). The proteolytic activity of the paracaspase MALT1 is key in T cell activation. Nature Immunology 9, 272-281.

Rehage, N., Davydova, E., Conrad, C., Behrens, G., Maiser, A., Stehklein, J.E., Brenner, S., Klein, J., Jeridi, A., Hoffmann, A., et al. (2018). Binding of NUFIP2 to Roquin promotes recognition and regulation of ICOS mRNA. Nat Commun 9, 299.

Ricón, M. and Flavell, R.A. (1994). AP-1 transcriptional activity requires both T-cell receptor-mediated and co-stimulatory signals in primary T lymphocytes. EMBO Journal 13 (18), 4370-4381.

Robertson, J.M., Jensen, P.E., and Evavold, B.D. (2000). DO11.10 and OT-II T Cells Recognize a C-Terminal Ovalbumin 323–339 Epitope. The Journal of Immunology 164, 4706-4712.

Rogers, P.R., and Croft, M. (2000). CD28, Ox-40, LFA-1, and CD4 Modulation of Th1/Th2 Differentiation Is Directly Dependent on the Dose of Antigen. J Immunol 164, 2955-2963.

Rosenbaum, M., Gewies, A., Pechloff, K., Heuser, C., Engleitner, T., Gehring, T., Hartjes, L., Krebs, S., Krappmann, D., Kriegsmann, M., et al. (2019). Bcl10-controlled Malt1 paracaspase activity is key for the immune suppressive function of regulatory T cells. Nat Commun 10, 2352.

Ruby, C.E., Montler, R., Zheng, R., Shu, S., and Weinberg, A.D. (2008). IL-12 Is Required for Anti-OX40-Mediated CD4 T Cell Survival. The Journal of Immunology 180, 2140-2148.

Rudd, C.E., and Schneider, H. (2003). Unifying concepts in CD28, ICOS and CTLA4 co-receptor signalling. Nature Reviews Immunology 3, 544-556.

Ruland, J., Duncan, G.S., Elia, A., del Barco Barrantes, I., Nguyen, L., Plyte, S., Millar, D.G., Bouchard, D., Wakeham, A., Ohashi, P.S., and Mak, T.W. (2001). Bcl10 Is a Positive Regulator of Antigen Receptor–Induced Activation of NF-κB and Neural Tube Closure. Cell 104, 33-42.

Ruland, J., Duncan, G. S, Wakeham, A., and Mak, T. W. (2003). Differential Requirement for Malt1 in T and B Cell Antigen Receptor Signaling. Immunity 19, 749-758.

Ruland, J., and Hartjes, L. (2018). CARD-BCL-10-MALT1 signalling in protective and pathological immunity. Nat Rev Immunol 19, 118-134.

Savage, A.K., Constantinides, M.G., Han, J., Picard, D., Martin, E., Li, B., Lantz, O., and Bendelac, A. (2008). The Transcription Factor PLZF Directs the Effector Program of the NKT Cell Lineage. Immunity 29, 391-403.

Sawada, S., Scarborough, J.D., Killeen, N., and Littman, D.R. (1994). A lineage-specific transcriptional silencer regulates CD4 gene expression during T lymphocyte development. Cell 77 (6), 917-929.

Schairer, R., Hall, G., Zhang, M., Cowan, R., Baravalle, R., Muskett, F.W., Coombs, P.J., Mpamhanga, C., Hale, L.R., Saxty, B., et al. (2020). Allosteric activation of MALT1 by its ubiquitin-binding Ig3 domain. Proc Natl Acad Sci U S A 117, 3093-3102.

Schaerli, P., Willimann, K., Lang, A.B., Lipp, M., Loetscher, P., and Moser, B. (2000). CXC Chemokine Receptor 5 Expression Defines Follicular Homing T Cells with B Cell Helper Function. J Exp Med 192 (11), 1553-1562.

Schlauderer, F., Lammens, K., Nagel, D., Vincendeau, M., Eitelhuber, A.C., Verhelst, S.H.L., Kling, D., Chrusciel, A., Ruland, J., Krappmann, D., et al. (2013). Structural Analysis of Phenothiazine Derivatives as Allosteric Inhibitors of the MALT1 Paracaspase. Angewandte Chemie International Edition 52, 10384-10387.

Schlauderer, F., Seeholzer, T., Desfosses, A., Gehring, T., Strauss, M., Hopfner, K.P., Gutsche, I., Krappmann, D., and Lammens, K. (2018). Molecular architecture and regulation of BCL10-MALT1 filaments. Nat Commun 9, 4041.

Schlundt, A., Heinz, G.A., Janowski, R., Geerlof, A., Stehle, R., Heissmeyer, V., Niessing, D., and Sattler, M. (2014). Structural basis for RNA recognition in roquin-mediated post-transcriptional gene regulation. Nat Struct Mol Biol 21, 671-678.

Schmitz, M.L., and Krappmann, D. (2006). Controlling NF-κB activation in T cells by costimulatory receptors. Cell Death & Differentiation 13, 834-842.

Schuster, M., Glauben, R., Plaza-Sirvent, C., Schreiber, L., Annemann, M., Floess, S., Kühl, Anja A., Clayton, Linda K., Sparwasser, T., Schulze-Osthoff, K., et al. (2012). IκBNS Protein Mediates Regulatory T Cell Development via Induction of the Foxp3 Transcription Factor. Immunity 37, 998-1008.

Schuster, M., Annemann, M., Plaza-Sirvent, C., and Schmitz. I. (2013). Atypical IκB proteins - nuclear modulators of NF-κB signaling. Cell Communication and Signaling, 11:23.

Schuster, M., Plaza-Sirvent, C., Matthies, A.-M., Heise, U., Jeron, A., Bruder, D., Visekruna, A., Huehn, J., and Schmitz, I. (2017). c-REL and IκBNS Govern Common and Independent Steps of Regulatory T Cell Development from Novel CD122-Expressing Pre-Precursors. The Journal of Immunology 199, 920-930.

Schuster, S.L., and Hsieh, A.C. (2019). The Untranslated Regions of mRNAs in Cancer. Trends in Cancer 5, 245-262.

Schuetz, A., Murakawa, Y., Rosenbaum, E., Landthaler, M., and Heinemann, U. (2014). Roquin binding to target mRNAs involves a winged helix-turn-helix motif. Nature Communications 5.

Setoguchi, R., Hori, S., Takahashi, T., and Sakaguchi, S. (2005). Homeostatic maintenance of natural Foxp3+ CD25+ CD4+ regulatory T cells by interleukin (IL)-2 and induction of autoimmune disease by IL-2 neutralization. Journal of Experimental Medicine 201, 723-735.

Sharma, D., Zagore, L.L., Brister, M.M., Ye, X., Crespo-Hernández, C.E., Licatalosi, D.D., and Jankowsky, E. (2021). The kinetic landscape of an RNA-binding protein in cells. Nature.

Shimizu, K., Sugiura, D., Okazaki, I.-m., Maruhashi, T., Takegami, Y., Cheng, C., Ozaki, S., and Okazaki, T. (2020). PD-1 Imposes Qualitative Control of Cellular Transcriptomes in Response to T Cell Activation. Molecular Cell 77, 937-950.

Shin, B., Benavides, G.A., Geng, J., Koralov, S.B., Hu, H., Darley-Usmar, V.M., and Harrington, L.E. (2020). Mitochondrial Oxidative Phosphorylation Regulates the Fate Decision between Pathogenic Th17 and Regulatory T Cells. Cell Reports 30, 1898-1909.

Śledzińska, A., Hemmers, S., Mair, F., Gorka, O., Ruland, J., Fairbairn, L., Nissler, A., Müller, W., Waisman, A., et al. (2013). TGF-β Signalling Is Required for CD4+ T Cell Homeostasis But Dispensable for Regulatory T Cell Function. PLoS Biology 11, e1001674.

Smith-Garvin, J.E., Koretzky, G.A., and Jordan, M.S. (2009). T Cell Activation. Annual Review of Immunology 27, 591-619.

Snook, J.P., Kim, C., and Williams, M.A. (2018). TCR signal strength controls the differentiation of CD4(+) effector and memory T cells. Sci Immunol 3.

Solouki, S., Huang, W., Elmore, J., Limper, C., Huang, F., and August, A. (2020). TCR Signal Strength and Antigen Affinity Regulate CD8+ Memory T Cells. The Journal of Immunology 205, 1217-1227.

Sommer, K., Guo, B., Pomerantz, J.L., Bandaranayake, A.D., Moreno-García, M.E., Ovechkina, Y.L., and Rawlings, D.J. (2005). Phosphorylation of the CARMA1 Linker Controls NF-κB Activation. Immunity 23, 561-574.

Srivastava, M., Duan, G., Kershaw, N.J., Athanasopoulos, V., Yeo, J.H.C., Ose, T., Hu, D., Brown, S.H.J., Jergic, S., Patel, H.R., et al. (2015). Roquin binds microRNA-146a and Argonaute2 to regulate microRNA homeostasis. Nature Communications 6.

Staal, J., Driege, Y., Bekaert, T., Demeyer, A., Muyllaert, D., Van Damme, P., Gevaert, K., and Beyaert, R. (2011). T-cell receptor-induced JNK activation requires proteolytic inactivation of CYLD by MALT1. The EMBO Journal 30, 1742-1752.

Stoecklin, G., Lu, M., Rattenbacher, B., and Moroni, C., (2003). A Constitutive Decay Element Promotes Tumor Necrosis Factor Alpha mRNA Degradation via an AU-Rich Element-Independent Pathway. Mol Cell Biol 23 (10), 3506-3515.

Stoecklin, G., Stubbs, T., Kedersha, N., Wax, S., FC Rigby, W., Blackwell, T.K., and Anderson, P. (2004). MK2-induced tristetraprolin:14-3-3 complexes prevent stress granule association and ARE-mRNA decay. EMBO J 23, 1313-1324.

Strasser, D., Neumann, K., Bergmann, H., Marakalala, Mohlopheni J., Guler, R., Rojowska, A., Hopfner, K.-P., Brombacher, F., Urlaub, H., Baier, G., et al. (2012). Syk Kinase-Coupled C-type Lectin Receptors Engage Protein Kinase C-δ to Elicit Card9 Adaptor-Mediated Innate Immunity. Immunity 36, 32-42.

Sun, L., Deng, L., Ea, C.-K., Xia, Z.-P., and Chen, Z.J. (2004). The TRAF6 Ubiquitin Ligase and TAK1 Kinase Mediate IKK Activation by BCL10 and MALT1 in T Lymphocytes. Mol Cell 14, 289-301.

Szabo, S.J., Kim, S.T., Costa, G.L., Zhang, X., Garrison Fathman, C., and Gilmcher, L.H. (2000). A Novel Transcription Factor, T-bet, Directs Th1 Lineage Commitment. Cell 100, 655-669.

Tafuri, A., Shahinian, A., Bladt, F., Yoshinaga, S.K., Jordana, M., Wakeham, A., Boucher, L.-M., Bouchard, D., Chan, V.S.F., Duncan, G., Odermatt, B., Ho, A., Itie, A., Horan, T., Whoriskey, J.S., Pawson, T., Penninger, J.M., Ohashi, P.S., and Mak., T.W. (2001). ICOS is essential for effective T-helper-cell responses. Nature 409, 105-109.

Tai, X., Cowan, M., Feigenbaum, L., and Singer, A. (2005). CD28 costimulation of developing thymocytes induces Foxp3 expression and regulatory T cell differentiation independently of interleukin 2. Nature Immunology 6, 152-162.

Tan, D., Zhou, M., Kiledjian, M., and Tong, L. (2014). The ROQ domain of Roquin recognizes mRNA constitutive-decay element and double-stranded RNA. Nat Struct Mol Biol 21, 679-685.

Tarun, S. Z. and Sachs, A. B. (1996). Association of the yeast poly(A) tail binding protein with translation initiation factor eIF-4G. EMBO J. 15, 7168-7177.

Tavernier, S.J., Athanasopoulos, V., Verloo, P., Behrens, G., Staal, J., Bogaert, D.J., Naesens, L., De Bruyne, M., Van Gassen, S., Parthoens, E., et al. (2019). A human immune dysregulation syndrome characterized by severe hyperinflammation with a homozygous nonsense Roquin-1 mutation. Nat Commun 10, 4779.

Teng, M.W.L., Bowman, E.P., McElwee, J.J., Smyth, M.J., Casanova, J.-L., Cooper, A.M., and Cua, D.J. (2015). IL-12 and IL-23 cytokines: from discovery to targeted therapies for immune-mediated inflammatory diseases. Nature Medicine 21, 719-729.

Tharun, S. and Parker, R. (2001). Targeting an mRNA for decapping: displacement of translation factors and association of the Lsm1p-7p complex on deadenylated yeast mRNAs. Mol. Cell 8, 1075-1083.

Thome, M., Charton, J.E., Pelzer, C., and Hailfinger, S. (2010). Antigen Receptor Signaling to NF-kB via CARMA1, BCL10, and MALT1. Cold Spring Harbor Perspectives in Biology 2, a003004.

Touma, M., Antonini, V., Kumar, M., Osborn, S.L., Bobenchik, A.M., Keskin, D.B., Connolly, J.E., Grusby, M.J., Reinherz, E.L., and Clayton, L.K. (2007). Functional Role for IκBNS in T Cell Cytokine Regulation As Revealed by Targeted Gene Disruption. The Journal of Immunology 179, 1681-1692.

Tubo, N.J., Pagan, A.J., Taylor, J.J., Nelson, R.W., Linehan, J.L., Ertelt, J.M., Huseby, E.S., Way, S.S., and Jenkins, M.K. (2013). Single naive CD4+ T cells from a diverse repertoire produce different effector cell types during infection. Cell 153, 785-796.

Tuosto, L., and Acuto, O. (1998). CD28 affects the earliest signaling events generated by TCR engagement. Eur J Immunol 28, 2131-2142.

Uehata, T., Iwasaki, H., Vandenbon, A., Matsushita, K., Hernandez-Cuellar, E., Kuniyoshi, K., Satoh, T., Mino, T., Suzuki, Y., Standley, Daron M., et al. (2013). Malt1-Induced Cleavage of Regnase-1 in CD4+ Helper T Cells Regulates Immune Activation. Cell 153, 1036-1049.

Uren, A. G., O'Rourke, K., Aravind, L., Pisabarro, M. T., Seshagiri, S., Koonin, E. V., and Dixit, V. M. (2000). Identification of Paracaspases and Metacaspases: Two Ancient Families of Caspase-like Proteins, One of which Plays a Key Role in MALT Lymphoma. Molecular Cell 6, 961-967.

Valitutti, S., Müller, S., Cella, M., Padovan, E., and Lanzavecchia, A. (1995). Serial triggering of many T-cell receptors by a few peptide-MHC complexes. Nature 375, 148-151.

van Panhuys, N., Klauschen, F., and Germain, R.N. (2014). T-cell-receptor-dependent signal intensity dominantly controls CD4(+) T cell polarization In Vivo. Immunity 41, 63-74.

van Panhuys, N. (2016). TCR Signal Strength Alters T–DC Activation and Interaction Times and Directs the Outcome of Differentiation. Frontiers in Immunology 7.

Veldhoen, M., Hocking, R.J., Atkins, C.J., Locksley, R.M., and Stockinger, B. (2006). TGFβ in the Context of an Inflammatory Cytokine Milieu Supports De Novo Differentiation of IL-17-Producing T Cells. Immunity 24, 179-189.

Vinuesa, C.G., Cook, M.C., Angelucci, C., Athanasopoulos, V., Rui, L., Hill, K.M., Yu, D., Domaschenz, H., Whittle, B., Lambe, T., et al. (2005). A RING-type ubiquitin ligase family member required to repress follicular helper T cells and autoimmunity. Nature 435, 452-458.

Viola, A., and Lanzavecchia, A. (1996). T cell activation determined by T cell receptor number and tunable thresholds. Science 273, 104-106.

Vogel, K.U., Edelmann, S.L., Jeltsch, K.M., Bertossi, A., Heger, K., Heinz, G.A., Zoller, J., Warth, S.C., Hoefig, K.P., Lohs, C., et al. (2013). Roquin paralogs 1 and 2 redundantly repress the Icos and Ox40 costimulator mRNAs and control follicular helper T cell differentiation. Immunity 38, 655-668.

von Moeller, H., Basquin, C., and Conti, E. (2009). The mRNA export protein DBP5 binds RNA and the cytoplasmic nucleoporin NUP214 in a mutually exclusive manner. Nature Structural & Molecular Biology 16, 247-254.

Wang, D., You, Y., Case, S.M., McAllister-Lucas, L.M., Wang, L., DiStefano, P.S., Nuñez, G., Bertin, J., and Lin, X. (2002). A requirement for CARMA1 in TCR-induced NF-κB activation. Nature Immunology 3, 830-835.

Wang, V.Y.-F., Huang, W., Asagiri, M., Spann, N., Hoffmann, A., Glass, C., and Ghosh, G. (2012). The Transcriptional Specificity of NF-κB Dimers Is Coded within the κB DNA Response Elements. Cell Reports 2, 824-839.

Wang, C.J., Heuts, F., Ovcinnikovs, V., Wardzinski, L., Bowers, C., Schmidt, E.M., Kogimtzis, A., Kenefeck, R., Sansom, D.M., and Walker, L.S.K. (2015). CTLA-4 controls follicular helper T-cell differentiation by regulating the strength of CD28 engagement. Proceedings of the National Academy of Sciences 112, 524-529.

Wei, J., Long, L., Zheng, W., Dhungana, Y., Lim, S.A., Guy, C., Wang, Y., Wang, Y.-D., Qian, C., Xu, B., et al. (2019). Targeting REGNASE-1 programs long-lived effector T cells for cancer therapy. Nature 576, 471-476.

Wei, S.C., Sharma, R., Anang, N.-A.A.S., Levine, J.H., Zhao, Y., Mancuso, J.J., Setty, M., Sharma, P., Wang, J., Pe'er, D., et al. (2019). Negative Co-stimulation Constrains T Cell Differentiation by Imposing Boundaries on Possible Cell States. Immunity 50, 1084-1098.

Wing, K., Onishi, Y., Prieto-Martin, P., Yamaguchi, T., Miyara, M., Fehervari, Z., Nomura, T., and Sakaguchi, S. (2008). CTLA-4 Control Over Foxp3+ Regulatory T Cell Function. Science 322, 271-275.

Winter, J., Jung, S., Keller, S., Gregory, R. I., and Diedrichs, S. (2009). Many roads to maturity: microRNA biogenesis pathways and their regulation. Nature Cell Biology 11, 3.

Wülfing, C., Rabinowitz, J.D., Beeson, C., Sjaastad, M.D., McConnell, H.M., and Davis, M. (1997). Kinetics and Extent of T Cell Activation as Measured with the Calcium Signal. J Exp Med 10, 1815-1825.

Xiao, X., Shi, X., Fan, Y., Wu, C., Zhang, X., Minze, L., Liu, W., Ghobrial, Rafik M., Lan, P., and Li, Xian C. (2016). The Costimulatory Receptor OX40 Inhibits Interleukin-17 Expression through Activation of Repressive Chromatin Remodeling Pathways. Immunity 44, 1271-1283.

Xing, Y., and Hogquist, K.A. (2012). T-Cell Tolerance: Central and Peripheral. Cold Spring Harbor Perspectives in Biology 4, a006957.

Yamane, H., and Paul, W.E. (2013). Early signaling events that underlie fate decisions of naive CD4+ T cells toward distinct T-helper cell subsets. Immunological Reviews 252, 12-23.

Yamasoba, D., Sato, K., Ichinose, T., Imamura, T., Koepke, L., Joas, S., Reith, E., Hotter, D., Misawa, N., Akaki, K., Uehata, T., Mino, T., Miyamoto, S., Noda, T., Yamashita, A., Standley, D.M., Kirchhoff, F., Sauter, D., Koyanagi, Y., and Takeuchi, O. (2019). N4BP1 restricts HIV-1 and its inactivation by MALT1 promotes viral reactivation. Nat Microbiol 4, 1532-1544.

Yang, X.O., Nurieva, R., Martinez, G.J., Kang, H.S., Chung, Y., Pappu, B.P., Shah, B., Chang, S.H., Schluns, K.S., Watowich, S.S., et al. (2008). Molecular Antagonism and Plasticity of Regulatory and Inflammatory T Cell Programs. Immunity 29, 44-56.

Yu, D., Tan, A.H., Hu, X., Athanasopoulos, V., Simpson, N., Silva, D.G., Hutloff, A., Giles, K.M., Leedman, P.J., Lam, K.P., et al. (2007). Roquin represses autoimmunity by limiting inducible T-cell co-stimulator messenger RNA. Nature 450, 299-303.

Yu, J.W., Jeffrey, P.D., Ha, J.Y., Yang, X., and Shi, Y. (2011). Crystal structure of the mucosa-associated lymphoid tissue lymphoma translocation 1 (MALT1) paracaspase region. Proceedings of the National Academy of Sciences 108, 21004-21009.

Yu, X., Harden, K., C Gonzalez, L., Francesco, M., Chiang, E., Irving, B., Tom, I., Ivelja, S., Refino, C.J., Clark, H., et al. (2008). The surface protein TIGIT suppresses T cell activation by promoting the generation of mature immunoregulatory dendritic cells. Nature Immunology 10, 48-57.

Zeng, H., Yang, K., Cloer, C., Neale, G., Vogel, P., and Chi, H. (2013). mTORC1 couples immune signals and metabolic programming to establish Treg-cell function. Nature 499, 485-490.

Zhang, D.-H., Cohn, L., Ray, P., Bottmly, K., and Ray, A. (1997). Transcription Factor GATA-3 Is Differentially Expressed in Murine Th1 and Th2 Cells and Controls Th2-specific Expression of the Interleukin-5 Gene. J Biol Chem 272 (34), 21597-21603.

Zhang, W., Sloan-Lancaster, J., Kitchen, J., Trible, R. P., and Samelson, L. (1998). LAT: The ZAP-70 Tyrosine Kinase Substrate that Links T Cell Receptor to Cellular Activation. Cell 92, 83-92.

Zhang, F., Meng, G., and Strober, W. (2008). Interactions among the transcription factors Runx1, RORγt and Foxp3 regulate the differentiation of interleukin 17–producing T cells. Nature Immunology 9, 1297-1306.

Zhang, X., Xiao, X., Lan, P., Li, J., Dou, Y., Chen, W., Ishii, N., Chen, S., Xia, B., Chen, K., et al. (2018). OX40 Costimulation Inhibits Foxp3 Expression and Treg Induction via BATF3-Dependent and Independent Mechanisms. Cell Reports 24, 607-618.

Zhou, L., Lopes, J.E., Chong, M.M.W., Ivanov, I.I., Min, R., Victora, G.D., Shen, Y., Du, J., Rubtsov, Y.P., Rudensky, A.Y., et al. (2008). TGF-β-induced Foxp3 inhibits TH17 cell differentiation by antagonizing RORγt function. Nature 453, 236-240.

Zhu, J., Yamane, H., and Paul, W.E. (2010). Differentiation of Effector CD4 T Cell Populations. Annual Review of Immunology 28, 445-489.

6. Appendix

6.1. List of figures

6.2. List of tables

Acknowledgements

I would like to express my gratitude to everyone involved in this doctoral thesis contributing to my research project by experimental support and stimulating discussions in meetings, data presentations and multiple poster sessions. Sharing ideas and receiving recommendations helped me to progress with my research and to dynamically implement valuable new feedback into the design of the very next experimental setup.

Firstly, I am thankful to Prof. Dr. Vigo Heissmeyer for his dedicated supervision starting in 2017 and the opportunity to involve myself in discovering such an exciting research project. His expertise and pronounced interest in my project has always been a great motivation that fostered my experimental ambition and also helped me to finalize this manuscript.

I cordially thank Prof. Dr. Alla Skapenko for evaluating this dissertation as the second reviewer. Moreover, I thank Prof. Dr. Ludger Klein and Prof. Dr. Dietmar Zehn for their scientific discussions and experimental input during thesis advisory committee (TAC) meetings.

I am glad to acknowledge all collaborations that contributed to the peer-reviewed manuscript, special thanks go to Dr. Florian Giesert and Prof. Dr. Wolfgang Wurst for generating the CRISPR/Cas9-mediated $Rc3h1^{Mins}$ model, Dr. Carlos Plaza-Sirvent and Prof. Dr. Ingo Schmitz for providing conceptual support and $Nfkbid$ knockout models, Dr. Regina Feederle and Andrew Flatley for their development of monoclonal antibodies against cleaved Roquin-1 as well as $I\kappa B_{NS}$ and Dr. Andreas Muschaweckh and Prof. Dr. Thomas Korn for their expertise and valuable support during the $in\ vivo$ EAE experiment.

I would like to thank all former colleagues at the Institute for Immunology and especially my group members also from the Helmholtz center for providing feedback during data presentations and experimental expertise in laboratories. I am very grateful to Dr. Gesine Behrens for her outstanding technical support and her ideas throughout my research that as well shaped the trajectories of my project. Besides, I would like to thank Dr. Taku Ito-Kureha, Timsse Raj and Dr. Kai P. Höfig for their interest in my scientific project and for discussing critical aspects of experiments.

I thank Claudia Keplinger and Lena Esser for providing great help concerning all issues of lab maintenance, genotyping and the organization of the mouse data base. Likewise, I thank Michael Hagemann, Franziska Liebel and their team members at the Hemholtz center for their courageous management and organization of all relevant mouse colonies.

Finally - and last but not least - I would like to express my gratitude to my friends as well as my parents, Angelika and Bernd Schmidt, for their advice, support and unceasing interest in my studies during the last years. It is my greatest pleasure to acknowledge their appreciation, empathy and guidance throughout my doctoral research.